FLOW FIELD AND STABILITY OF THE FAR WAKE BEHIND CYLINDERS AT HYPERSONIC SPEEDS

Thesis by

Wilhelm Behrens

In Partial Fulfillment of the Requirements

For the Degree of

Doctor of Philosophy

California Institute of Technology

Pasadena, California

1966

(Submitted May 12, 1966)

ACKNOWLEDGEMENTS

The author wishes to express his sincere thanks and deep appreciation to Professor Lester Lees for his guidance and support throughout this research and to Professor Toshi Kubota who always was available to give invaluable advice.

The author is grateful to Mrs. T. Van Harreveld for her conscientious and painstaking numerical and graphical work; the staff of the GALCIT Hypersonic Wind Tunnel, P. Baloga, G. Van Halewyn, S. Roman, J. Van Dijk and H. Mazurowski for their able assistance during the wind tunnel tests; the staff of the Aeronautics Shop under G. Carlson for manufacturing the models and probes; Dr. K. Jacob and Miss K. Matsumoto for writing the IBM 7094 computer programs; Dr. H. Gold for providing the computer program for the stability calculations; and Mrs. V. Conner for her expert typing of this thesis.

Special thanks go to Professor E. Truckenbrodt from the Technical University in München who sparked the author's first enthusiasm for fluid mechanics and for his continued interest and support of the author's further studies. The author acknowledges the receipt of a NATO-Graduate Fellowship from the "Deutscher Akademischer Austauschdienst" for the academic years 1961-1963 and the receipt of a Graduate Research Assistantship from the California Institute of Technology for the years 1963-1966.

The author wishes to thank his wife Sondra for her inspiration and encouragement which was essential for the completion of this work.

ABSTRACT

An experimental study of the mean wake flow field and its stability has been carried out in the far wake of circular cylinders at a Mach number of 6. The Reynolds numbers ranged from 200 to 4000 with a few measurements at higher Reynolds numbers. Pitot pressure, static pressure and mean flow hot wire measurements were done at many axial stations behind cylinders up to (x/d) = 2400.

The inner wake formed from the cylinder boundary layers is laminar and loses its identity within the first 60 diameters or less depending on the Reynolds numbers so that only the outer wake, caused by the bow shock, has to be considered. Within a certain region the experimental results compare well with linear laminar theory, but the wake profiles are not similar up to the farthest downstream station (x/d = 2400). At four Reynolds numbers strong deviations from steady laminar behavior were observed far behind the cylinder, indicating breakdown of the flow because of non-linear instability effects.

In the instability study hot wire fluctuation measurements were made over the whole frequency range (f = 1 - 320 KC) and also at particular frequencies in a band width of 1 KC up to x/d = 12000 at the lowest Reynolds number. Two instability regions were found and investigated: the linear growth region and the non-linear region. In the linear region there is quite a close correspondence with linear stability theory. The onset of non-linearity is characterized by the

ABSTRACT (Cont'd)

simultaneous strong deviation of the mean flow from laminar steady behavior, the increase of the fundamental frequency fluctuation component on the wake axis and the sudden rise of the first harmonic frequency component. The non-linear region is compared with the non-linear wake region at low speeds behind a flat plate. On the basis of these measurements a tentative picture is given of the onset of non-linearity and/or transition in the inner and outer wake behind blunt bodies at hypersonic speeds.

TABLE OF CONTENTS

TABLE OF CONTENTS (Cont'd)

TABLE OF CONTENTS (Cont'd)

LIST OF FIGURES, PART I

LIST OF FIGURES, PART I (Cont'd)

LIST OF FIGURES, PART II

LIST OF FIGURES, PART II (Cont'd)

LIST OF FIGURES, PART II (Cont'd)

LIST OF TABLES, PART II

LIST OF SYMBOLS, PART I

a	speed of sound
b_u, b_T	half wake width, based on velocity and temperature profiles and measured at the positions where $\frac{u_e - u}{u_e - u_\ell} = 0.5$ and $\frac{T - T_e}{T_\ell - T_e} = 0.5$
C	Chapman-Rubesin factor $\left(= \frac{\mu_e \rho_e}{\mu \rho}\right)$
C_D	drag coefficient
c_p	specific heat
d	diameter
h	heat transfer coefficient $\left(= \frac{q}{T_w - T_{aw}}\right)$
i	hot wire current
k	air thermal conductivity
k_w	wire thermal conductivity
K_n	Knudsen number $\left(= \sqrt{\frac{\pi \gamma}{2}}\, \frac{M}{Re_\infty}\right)$
ℓ	hot wire length
M	Mach number
Nu_m	Nusselt number, measured $\left(= \frac{h_m d}{k_o}\right)$
Nu_o	Nusselt number $\left(= \frac{h d}{k_o}\right)$
p	static pressure
p_o	stagnation or total pressure in the free stream
p_p	Pitot pressure
Pr	Prandtl number
q	heat transfer rate per unit area
R	hot wire resistance or gas constant
Re	Reynolds number

LIST OF SYMBOLS, PART I (Cont'd)

Re_d	free stream Reynolds number of cylinder $\left(= \frac{\rho_\infty u_\infty d}{\mu_\infty}\right)$
Re_o	stagnation Reynolds number $\left(= \frac{\rho u d}{\mu_o}\right)$
T	static temperature
ΔT	static temperature excess $(= T - T_e)$
T_o	stagnation or total temperature
u	velocity
Δu	velocity defect $(= u_e - u)$
V	hot wire voltage
x	distance in the flow direction measured from the center of the cylinder
y	normal distance from the center of the wake
$\bar{y}$	Howarth-Dorodnitsyn variable $\left(= \int_o^y \frac{\rho}{\rho_e}\, dy\right)$
a_r	temperature resistivity coefficient, $\left[\frac{R_w}{R_r} = 1 + a_r (T_w - T_r)\right]$
γ	ratio of specific heats
δ^*	displacement thickness
Δ	difference of two quantities
η	nondimensional temperature $\left[= \frac{T}{T_o}\ (\text{recovery factor})\right]$
θ	wake momentum thickness $\left[= \int_o^{y_e} \frac{\rho u}{\rho_e u_e}\left(1 - \frac{u}{u_e}\right) dy\right]$
μ	viscosity
ρ	density
$\bar{\chi}$	hypersonic viscous interaction parameter
ψ	stream function
ψ_N, ψ_R	end loss correction factors

LIST OF SYMBOLS, PART II

a	speed of sound
b	wake half width based on the mean velocity profile, measured from centerline to position at which $\frac{\Delta u}{\Delta u_{\mathfrak{L}}} = 0.5$
$\overline{b}$	transformed (Howarth-Dorodnitsyn) wake half width $\left(= \int_o^b \frac{\rho}{\rho_e} dy\right)$
b_1	wake width based on mean square fluctuation profile (see Figure 9)
c	complex wave velocity
c_g	group velocity
c_I	temporal amplification coefficient
Δc_I	normalized amplification coefficient $\left(= \frac{c_I}{\Delta u_{\mathfrak{L}}}\right)$
c_R	phase velocity
Δc_R	relative normalized phase velocity $\left(= \frac{c_R - u_e}{\Delta u_{\mathfrak{L}}}\right)$
d	diameter of model (if not noted otherwise)
e'	fluctuation component of hot wire voltage
$\tilde{e}_f'$	root mean square voltage fluctuation at given frequency
$\overline{e'^2}$	mean square fluctuation voltage (whole frequency range of 1 KC - 320 KC)
Δe_m	hot wire mass flux sensitivity coefficient
Δe_T	hot wire total temperature sensitivity coefficient
f	frequency
ℓ	hot wire length
ℓ/d	hot wire aspect ratio
m	mass flux $\left[\Delta m = \left(\overline{\rho}\,\overline{u}\right)_e - \left(\overline{\rho}\,\overline{u}\right)_{\mathfrak{L}}\right]$

LIST OF SYMBOLS, PART II (Cont'd)

M	Mach number
ΔM	relative Mach number in the wake $\left(= \frac{u_e - u_\ell}{a_e}\right)$
p_o	supply or total free stream pressure
$Q(\vec{r}, t)$	quantity of total flow
Q'	fluctuating component of flow quantity
$\overline{Q}$	mean component of flow quantity
ΔQ	$= \lvert Q_\ell - Q_e \rvert$
$q'(y)$	amplitude of fluctuating quantity
R	hot wire resistance
Re	Reynolds number
Re_d	free stream Reynolds number based on cylinder diameter
T	static temperature
T_o	total temperature
ΔT	static temperature excess $\left(= T - T_e\right)$
u	velocity
Δu	velocity defect $\left(= u_e - u\right)$
x	distance along wake centerline measured from model center
y	normal distance from the centerline of the wake
$\bar{y}$	transformed (Howarth-Dorodnitsyn) distance from the centerline of the wake $\left(= \int_o^y \frac{\rho}{\rho_e}\, dy\right)$
α	complex wave number
α_R	wave number (when the timewise amplification is considered $\alpha = \alpha_R$ and the subscript R is dropped)
α_I	spatial damping rate
β	complex frequency

LIST OF SYMBOLS, PART II (Cont'd)

β_R	frequency $\left(= \alpha_R c_R\right)$
$\beta_I = \alpha_R c_I$	timewise rate of amplification $(= \alpha c_I$ in general)
γ	ratio of specific heats
λ	wave length
ρ	density
$\Delta\rho$	density defect $\left(= \rho_e - \rho\right)$

SUBSCRIPTS

$\mathfrak{L}$	wake centerline
e	wake edge
f	quantity determined at a given frequency
i	initial station
N	noise
N. L.	onset of nonlinearity
n	normalized quantity
T	total signal
∞	free stream

SUPERSCRIPTS

$\sim$	root mean square value of a fluctuating quantity
$'$	fluctuation component of a quantity
$\overline{\quad}$	mean value of a fluctuating quantity

PART I. FLOW FIELD OF THE FAR WAKE BEHIND CYLINDERS AT HYPERSONIC SPEEDS

1. INTRODUCTION

The flow field about a blunt body at hypersonic speeds is characterized by a strong bow shock which produces most of the drag of the body and generates the "outer" wake (Figure 1). The boundary layer separates from the body at some point, and the coalescing free shear layers form the "inner" wake. Recompression in the near inner wake just behind the body produces the wake shock, which also compresses and heats the outer wake. As shown by Feldman (1), in the first hundred diameters downstream of the body the static pressure drops back to the free stream level. The outer wake is expansion-controlled in this region, and it can be considered "inviscid" in comparison to the inner viscous wake. Far downstream, however, viscosity and thermal conductivity play a dominant role.

The laminar flow in the outer wake has been studied theoretically by Feldman (1) and Lykoudis (2). In the work of Lees and Hromas (3) the main interest lies in the swallowing of the outer wake by a turbulent inner wake, while in the present study we are concerned with the case of a laminar inner wake. Most of the theoretical work in the literature is concerned with base flow and inner wake problems.

Relatively few thorough experimental investigations have been done. Experiments behind blunt bodies have concentrated on the base and inner wake regions. Besides some specialized measurements

[References (4) to (7)]detailed flow field studies in these regions have been carried out by McCarthy (8), Dewey (9) and Herzog (10). In ballistic ranges gross wake properties have been obtained by photographic and microwave techniques [(11)-(14)], involving mainly wake growth and laminar-turbulent transition data.

There are no detailed flow field measurements in the far wake beyond x/d = 100, and this region is the one which is emphasized in the present study. The objectives of Part I of this study are as follows: (1) to define the region of steady, laminar flow in the outer wake experimentally; (2) to observe any departures in mean flow quantities from the steady laminar flow theory as the first gross indicators of instability; (3) to furnish accurate mean flow measurements as the necessary input for linear laminar instability theory. The flow field was measured in detail behind circular cylinders at M = 6 in a Reynolds number range of Re_d = 320 to 3840, and to a downstream distance of x/d = 2400 and 600, respectively. Figure 2 shows all test conditions and measuring positions. In this Reynolds number range the inner wake is laminar as found by Kendall (5) and the author (see Part II of this thesis).

The experimental techniques and calibration procedures are described in Section 2. The mean flow was defined by making static pressure, Pitot pressure and hot wire measurements. When used as a mean flow measuring device the hot wire measures essentially the total temperature and mass flux, as described by Dewey (15). The experimental results exhibit the bow shock and wake shock positions and strength in the Reynolds number range of $Re_d \cong 200$ to 40,000,

the decay of static pressure at various Reynolds numbers, and the development of the inner laminar wake.

Because corrections and iterative calculations are necessary in order to reduce the hot wire data, the data reduction was done on an IBM 7094 computing machine. In the far wakes the Mach number $M \geq 2.5$ everywhere. For this case a relatively simple data reduction procedure is developed which converges in 3 to 5 iterations. Its main features are explained in Section 3; the calculation procedures and formulae are stated in Appendix A.

Experimental profiles, measured at the end of the expansion region, are compared with theoretical prediction, using Lykoudis' model (2). These experimental profiles are then utilized as initial data for Kubota's linear laminar theory (16). The integral-solution of this theory obtained by Gold (17) for arbitrary initial profiles is evaluated numerically on the IBM 7094. The experimentally determined far wake flow is compared with this theory in Section 4. Departures from the steady laminar theory are also observed, and these results lead naturally into Part II of this thesis.

2. EXPERIMENTAL EQUIPMENT AND TECHNIQUES

2.1. Wind Tunnel and Models

The experiments were done in the GALCIT Hypersonic Wind Tunnel Leg I, which is a closed return, continuous flow wind tunnel with a 5 x 5 square inch cross section and a nominal Mach number of 6. Because of the growth of the nozzle wall boundary layer the Mach number varies somewhat with stagnation pressure, as shown in Figure 3. The stagnation pressure can be changed from 0 psig ($\cong$ 1 atm) to 100 psig ($\cong$ 8.5 atm), corresponding to a Reynolds number range of about 30,000 per inch to 230,000 per inch, for a reservoir temperature of 275° F ($\cong$ 408° K). For the present experiments the reservoir temperature was kept at this value to be sure that condensation effects would not invalidate measured results. Condensation effects were observed by the author at lower reservoir temperatures (18). The supply pressure was maintained at a constant value to $\pm$ 0.02 psi and the supply temperature to $\pm$ 1° F.

The models were located 23 inches downstream of the throat of the nozzle in its horizontal centerplane. Most measurements were made in the vertical centerplane (normal to the model centerplane) of the test-section within a region 12 inches long and 2 inches wide starting from the model. Data were taken at each axial station within $\pm$ 1 inch from the nozzle centerline (compare Figure 2). There was a small gradient in the free stream flow direction, as shown by the free stream static pressure and Mach number plotted along the centerline of the test section (Figure 4). An attempt was made to correct for

this gradient in the data reduction of the wake measurements. Because of non-uniformities in part of the test-section at pressures lower than 20 psig and higher than 90 psig, tests were made at or in between those pressures. At these pressure levels the variation of the free stream static pressure at a given vertical cross-section was at most ± 3% (Figure 5).

The models were cylindrical tungsten or steel wires with diameters ranging from 0.005 inch to 0.064 inch; a steel tube was employed for the 0.1 inch cylinder. The models spanned the tunnel and tension was applied by means of a spring outside the tunnel in order to prevent oscillations. Actually, there was no noticeable model vibration, as deduced from the fact that a variation in tension, which changes frequency and amplitude, did not result in any change of the wake flow field. The models also were insulated electrically from the tunnel walls in order to be able to heat them electrically and to position measuring probes with respect to the models by touching them and thus closing an electrical circuit.

For the larger cylinders ($d \geq 0.04$ inch) slender double wedges were soldered to the models; the wedges extended from the wall into the flow about 0.80 inch as shown in Figure 6. This precaution was necessary because waves emanated from the intersection of the model with the wind tunnel side walls. These waves were felt at the center of the wake at a distance of about 3.5 inches behind the cylinder. As shown by static pressure measurements on the wake centerline (Figure 7), the flow disturbances were reduced in strength by end wedges. In order to amplify the effect of the observed disturbances

cylindrical end pieces 0.2 inch in diameter extending also 0.80 inch into the flow were mounted on the 0.064 inch cylinder, and the static pressure was measured. As expected, a large jump in static pressure occurred at a distance of about 3.5 inches behind the model (Figure 7). For smaller models ($d \leqq 0.02$ in.) only a very weak wave was detected in the wake at about 6 inches downstream of the cylinder (Figure 7). In wakes behind these small cylinders ($d \leqq 0.02$ in.) the flow in the center plane of the nozzle is considered two-dimensional (except for minor disturbances mentioned), since the aspect ratio AR (spanwise uniform flow over cylinder diameter) is $\geqq 150$. Dewey (19) detected a small change in cylinder base pressures when $AR \cong 10$.

2.2. Measuring Techniques

In order to specify a steady flow field, three independent quantities have to be measured. As shown by Dewey (15), with the Pitot probe, static pressure probe and the hot wire probe, four independent quantities can be determined. The hot wire measures two quantities; resistance at zero current, which depends on the total temperature of the flow; heat transfer rate to the gas, which is proportional to the mass flux.

The probes were mounted in the center of the test section on a rigid sting which could be moved 14 inches in the free stream flow direction and 4 inches normal to the flow by means of an electro-mechanical system. The pressure tubes were constructed out of steel (Dia. = 0.083 in.) and were led out of the tunnel downstream of the second throat. These steel tubes had enough stiffness to slide in

and out of the tunnel when the probe was moved, and at the same time to resist the non-steady forces of the downstream flow field.

For these same reasons the electrical leads of the hot wire system were enclosed in steel tubes of the same diameter. The probes were positioned to within ± 0.001 inch with respect to the model by establishing contact before each experiment between the model and a little plate soldered to the probe, which closed an electrical circuit.

2.3. Pitot Pressure Measurements

The Pitot pressure was measured with a straight steel Pitot tube which was aligned with the centerline of the test section. The flow is not necessarily parallel to the test section centerline, yet McCarthy (8) found no effect of Pitot probe angularity within ± 10 degrees with respect to the flow; in the present experiments the probe angularity is well within ± 5 degrees. In order to obtain good resolution in the wake of the smallest model, the probe had a very small flat tip. Its outside dimensions were 0.0525 x 0.005 square inch, and about 0.04 x 0.002 square inch inside (Figure 8). The pressure was measured with a Statham PA 208 EC (0-5 psia) pressure transducer with its reference side kept at 0.5 μHg. In order to avoid hysteresis the transducer pressure was maintained below 5 psia during the whole test program. Since the response time of the Pitot probe is several seconds, the measurements had to be taken point by point and recorded on an X-Y plotter. The recording system has been described by Herzog (10) in detail.

The absolute accuracy of the Pitot pressures was estimated to be better than 2%. The viscous effects on the probe were at most 1% for all Reynolds and Mach numbers encountered when compared with viscous effects on round probes of equal cross section, as measured by Mathews (20) and Sherman (21) at various Mach numbers. Since this comparison is not completely satisfactory, measurements were done with a larger probe. The results were as good as the repeatability of measurements with the same probe, which was better than 1%. Therefore, no attempt was made to correct for viscous effects.

2.4. Static Pressure Measurements

The static pressure experiments were done with small cone-cylinder probes as shown in Figure 8, and the pressures (1-6 mm Hg) were measured with a U-tube Silicone manometer, maintained at a pressure of 0.5 μ Hg. on the reference side. For the smallest pressures encountered the repeatability of measurements was within 1.3%.

The measured pressures had to be corrected for viscous interaction effects as described previously by the author (22). The calibration curves of the probes are shown in Figure 9. Note that the viscous interaction decreases somewhat with decreasing diameter of the probe, suggesting that the transverse curvature of the probe is of significance, as discussed in (22). It is assumed that the calibration at a Mach number of 6 is valid also at the lower Mach numbers encountered in the wakes. This assumption was made because of lack of data at other Mach numbers. It should be pointed out here that

the viscous interaction relation changes somewhat when the free-stream Mach number cannot be considered large compared to unity. In this case, following Lees and Probstein's analysis [see Hayes and Probstein (23)] the relation for the induced pressure on a flat plate becomes [expanding the oblique shock relation for small angle (24)]:

$$\frac{p}{p_\infty} = 1 + \frac{\gamma M_\infty^2}{\sqrt{M_\infty^2 - 1}} \frac{d\delta^*}{dx} + \frac{\gamma M_\infty^2 \left[(M_\infty^2 - 2)^2 + \gamma M_\infty^4 \right]}{4 (M_\infty^2 - 1)^2} \left(\frac{d\delta^*}{dx} \right)^2 + \cdots$$

where $\frac{d\delta^*}{dx} = (0.865 + 0.223\, M_\infty^2) \frac{\sqrt{C_\infty}}{\sqrt{Re_{x,\infty}}}$

instead of

$$\frac{p}{p_\infty} = 1 + 0.223\, \gamma\, \bar{\chi} + 0.050\, \frac{\gamma(\gamma+1)}{4}\, \bar{\chi}^2 + \cdots$$

where $\bar{\chi} = \frac{M_\infty^3 \sqrt{C_\infty}}{\sqrt{Re_{x,\infty}}}$; $Pr = 0.725$

and $C_\infty = \frac{\mu_w}{\mu_\infty} \frac{T_\infty}{T_w}$;

the subscripts "∞" and "w" signify freestream and wall conditions. Thus, if the assumed analogy between the viscous interaction of the flat plate and cone-cylinder still holds at low Mach numbers (in the wake $M \cong 3$) the viscous interaction correction is somewhat underestimated (of the order of 30% of the correction which is up to 6% of the measured pressure at $M = 3$) using $\bar{\chi}$ as independent parameter. Any further conclusions have to be left to a future experimental investigation of the cone-cylinder probe viscous interaction at a series of Mach numbers.

2.5. Hot Wire Measurements

The hot wire technique for steady state measurements was applied to hypersonic flow by Dewey (15). The method is briefly described as follows: The resistance, R, of the hot wire varies as the flow conditions and thus the wire temperature change while the current, i, is kept constant. The voltage drop across the wire and the current are measured directly, and the resistance is then

$$R = V/i.$$

These measurements are made for at least two currents in order to determine the straight line plot of R versus i^2R. The zero intercept of this line gives the adiabatic hot wire resistance, R_{aw}, which is a function of the adiabatic hot wire temperature, T_{aw}. The slope of this line $\left[\frac{d(Ri^2)}{dR}\right]_{i \Rightarrow 0}$ is proportional to the Nusselt number, Nu_o. These quantities can be reduced to the total temperature, T_o, and the mass flux, ρu. In the technique described by Dewey (15), and discussed in detail by Herzog (10), the Mach number M is involved, since the recovery factor is a function of Knudsen number. However, it was found that the hot wire recovery factor, $\eta = T_{aw}/T_o$, is a function only of the local stagnation Reynolds number $Re_o = \frac{\rho u d}{\mu_o}$ (based on total temperature) for $M \geq 2$ (Figure 10). Sherman (25) pointed out that for $2 < M < 6$ the ratio of Kn and $1/Re_o$ varies only $\pm 6\%$ around a constant average value using the viscosity law: $\frac{\mu_\infty}{T_o} = \left(\frac{T_\infty}{T_o}\right)^{0.75}$. When Sutherland's viscosity law is utilized, this ratio varies about $\pm 17\%$ for the same Mach number range. The scatter of the experimental data with $1/Re_o$ as independent variable

is not larger than with Kn as independent variable as long as $M > 2$ [compare Figure 8 in (11) with Figure 10]. Since the Mach number independence principle (hypersonic freezing) applies, the stagnation Reynolds number, Re_o, is the more significant parameter. The empirical relation for the recovery factor η in terms of $1/Re_o$ is

$$\eta = 1.167 - \frac{0.217}{1 + \frac{1}{(0.335\, Re_o)^{1.33}}}$$

It fits the experimental data well for $M > 2$. The continuum limit is approached for large Re_o ($\eta = 0.95$) and the free molecule limit for small Re_o ($\eta = 1.167$ as $M \Rightarrow \infty$ and changes little for $2 < M \leq \infty$; at $M = 2$, $\eta = 1.150$). The results obtained by Vrebalovich (26) at $M = 1.6$ show a Mach number effect as expected. In this case the free molecule limit is $\eta = 1.135$.

The second empirical relation essential for the data reduction becomes for $M \geq 2$:

$$Re_o = 5.26\, Nu_o + 5.74\, Nu_o^2$$

This expression was suggested by Kubota (private communication). It fits the experimental data (15) well and shows the two limits directly. For continuum flow the Reynolds number is proportional to the square of the Nusselt number (large Re_o), and for free molecule flow (small Re_o) the Reynolds number is proportional to the Nusselt number. A comparatively simple data reduction scheme based on these empirical relations will be discussed in the next chapter.

The hot wire probe employed in the present experiments was a straight brass probe with two thin needle tips to which the hot wire was soft soldered (Figure 11). The hot wire itself was of Platinum-10% Rhodium, 0.0001 inch in diameter and with an aspect ratio (length/diameter) of 230 to 250. Before using a hot wire it was annealed and calibrated in an oven to find its temperature-resistivity coefficient, α_r. In order to prevent breakage the positioning plate on the probe was mounted in such a way that the hot wire did not cross the bow shock of the model when measuring the probe position. Under these conditions the most critical times for the survival of the hot wire were the starting and shutdown periods of the wind tunnel flow. No consistency in breaking of hot wires was observed. Some could be used for days, while others broke when the tunnel was started. A few hot wires broke during measurements, probably when hit by a dust particle. In the present experiments hot wire measurements at each station were performed for two currents, i = 1 mAmp. and 4 mAmp. The measured data were transformed into digital form and recorded on IBM cards in order to use them directly in a computer program. To check the data at once they were also plotted on an X-Y plotter. The details of the recording system, designed and built by Herzog, are described in (10).

As measured by Dewey, the recovery factor of the hot wire needle tips is $\eta_s = \frac{T_s}{T_o} = 0.903$ in the freestream at $M_\infty \cong 6$. Because of the Mach number independence principle (hypersonic freezing), one expects this value to be correct also in the far wake where $M_\infty > 2$.

3. DATA REDUCTION

3.1. Discussion of Data Reduction Procedure

From experiments by McCarthy (8) it is known that the Mach number in the far wake behind a cylinder at M = 6 is at least as large as 2.5. Accordingly, the assumptions made in the data reduction were based on this fact. The data reduction consisted of several parts: (1) raw data reduction; (2) Pitot and static pressure corrections; (3) final data reduction. Because of the large number of data points and the many calculations, most of the data reduction was done on an IBM 7094.

In the raw data reduction the measured hot wire currents and voltages were reduced to adiabatic wall temperature, T_{awm}, and slope $\left[\frac{d(i^2R)}{dR}\right]_{i \Rightarrow 0}$, and plotted with the Pitot pressure in order to compare results at corresponding stations. For example, the shock positions were identifiable in all three measurements. In case of poor correspondence between these measurements and/or large scatter of data the measurements could be redone without going through the complete data reduction. The formulae and details of the raw data reduction are described in Appendix A. For both the Pitot and the static pressure there are, in general, three corrections required:

(1) viscous interaction;

(2) free stream Mach number variation with total pressure change;

(3) free stream flow non-uniformities.

The effect of viscous interaction on the Pitot pressure probe was negligible; all other corrections were typically a few percent. The correction calculations are discussed in Appendix A.

For the final data reduction four independent quantities are available: p, p_p, T_{awm} and $\left[\frac{d(Ri^2)}{dR}\right]_{i \Rightarrow 0}$. One of these quantities is redundant, since three quantities define a steady state flow field. In the actual data reduction the first three variables, p, p_p, T_{awm} were used. The hot wire end loss corrections were taken into account. The essential features of the calculation, which is described in detail in Appendix A, are as follows: The Mach number is directly obtained from (p/p_p). By use of the hot wire calibration formulae for the recovery factor, η, and the Nusselt number, Nu_o, as functions of the Reynolds number, Re_o, (see Section 2.5), an iteration scheme allows the calculation of the stagnation temperature. Any other flow variable can then be calculated directly.

In order to compare two possible schemes, the static pressure was replaced by the slope $\left[\frac{d(Ri^2)}{dR}\right]_{i \to 0}$. This scheme also requires iterations [Appendix A]; there were no difficulties such as Dewey (15) had reported, but he used a different approach involving the Mach number. In his data reduction scheme the recovery factor, η, was taken to be a function of the Knudsen number $\left(K_n \sim \frac{M}{Re}\right)$ and not of the stagnation Reynolds number, Re_o, as in the present calculations (compare Section 2.5). The Mach number is therefore necessary for the calculation of the total temperature and is obtained from the equation

$$\frac{\left(1+\frac{\gamma-1}{2}M^2\right)^{\frac{1}{2}}\left[\frac{2\gamma M^2-(\gamma-1)}{(\gamma+1)}\right]^{\frac{1}{(\gamma-1)}}}{\left(\frac{\gamma+1}{2}M^2\right)^{\frac{\gamma+1}{2(\gamma-1)}}} = \frac{Re_o\mu}{d\,p_p}\sqrt{\frac{\gamma+1}{2\gamma}RT_o}$$

For Mach numbers $M \geq 3$ this relation is very insensitive to Mach number (hypersonic freezing) and a small error in the right hand side of the equation yields a larger error in M. This difficulty is removed in the present scheme since $\eta = \eta(1/Re_o)$. Nevertheless, the comparison between the results of the two schemes was poor, because of the limitations of the second scheme. One of the reasons for the inaccuracy of this scheme in hypersonic flow is that two large quantities, T_o and $\frac{u^2}{2c_p}$, have to be subtracted from each other to yield a small quantity, T. Other difficulties and improvements of this data reduction procedure will be discussed by R. Batt in a forthcoming thesis.

3.2 Discussion of Accuracy of Final Results

There are two types of errors which affect the accuracy of the results: The systematic error and the random error. The systematic error is of significance only when it changes with flow conditions. The random error can be determined by repeating the measurements several times.

The factors on which the accuracy of the final results depend are:

(1) accuracy of measurements

(2) accuracy of measuring probe dimensions

(3) accuracy of calibration curves

(4) accuracy of probe positioning

(5) disturbance of flow caused by probe

(6) uniformity of the free stream

(7) disturbance of wake generated by intersection of model and tunnel walls

(8) accuracy of data reduction scheme.

These factors will now be discussed separately and a cumulative error estimated for the final results.

(1) The accuracy of measured data is discussed in Section 2.

(2) The Pitot and static pressure probe dimensions could be measured within 10^{-3} inches, and furthermore do not enter critically into the data reduction. However, the aspect ratio, ℓ/d, and the diameter of the hot wire probe, d, are important for the data reduction. These quantities could not be determined accurately. The diameter of the hot wire ($d = 10^{-4}$ inches) was taken from supplier specifications. The cross-section area is correct to ± 5%. The determination of the hot wire length was done by optical means and also computed from the measured resistance and the resistance per length as given by the supplier. For all hot wires the calculated length was about 6% shorter than the measured one. This difference might be caused by annealing of the hot wire, inaccuracy of measurement, inaccuracy of resistance per length given or the solder on the wire ends. To insure consistency in the measurements the hot wires were made from the same roll of wire for the complete test program.

(3) The empirical calibration relations used for the hot wire data reduction are a mean of the measured calibration points, for which

the scatter is about ± 10%. The repeatability of the measurement of temperature resistivity coefficient, α_r, was ± 0.5%.

The hot wire support temperature was taken to be 0.903 T_o across the wake, as measured by Dewey (15) in the free stream. This value seemed reasonable for a straight probe aligned with the tunnel centerline and very little or no inclination with the wake flow. The measured adiabatic wall temperatures were symmetric about the wake centerline, which means that only the local total temperature was important and not the history of probe position. An uncertainty of a few percent in the recovery factor $\eta_s = \frac{T_s}{T_o}$ was introduced by the shape of the support and the position of the junction of support and hot wire.

(4) The probes could be positioned to within ± 10^{-3} inches; the error introduced under most unfavorable conditions (steepest gradients of smallest cylinder wake) is about 3% in static temperature.

(5) Measuring probes immersed in shear flows give rise to streamline displacements because of their finite size. This effect has been studied carefully by Dewey (19) for Pitot probes and found to be negligible in cases where the ratio of free shear layer thickness to probe size was larger than 2. In the present experiments this ratio is larger than 20.

The distance from the tip of the static probe to the measuring taps is 0.28 inch. Especially close to the bow shock in regions of relatively strong gradients the accuracy of measurements is limited because of the finite length of the probe. However, the measurements on the centerline of the wake, (from x/d = 15 downstream) did not

show any size effect, since measurements at the same condition with two probes of different sizes (d_1 = 0.022, d_2 = 0.042 inch) yielded the same results.

(6) The free stream flow non-uniformity is a source of error of uncertain magnitude. The correction applied could only be an estimate.

(7) Another disturbance is introduced by the intersection of the model with the tunnel side walls. It was found for the larger cylinders ($d \geq 0.04$ inch) that there was a disturbance emanating from this region which could be decreased by mounting slender double wedges on the cylinders extending from the wall into the flow 0.80 inch (Section 2). The waves were felt in the center of the wake about 3.5 to 6 inches behind the model. The smaller the model size, the smaller was the effect. The disturbance was estimated to introduce an error up to 4% in static temperature excess. No attempt was made to correct for this effect.

(8) The only errors introduced by the data reduction procedure are caused by interpolation between measured points and numerical integration. However the flow profiles are smooth in the regions of interest. These errors are therefore negligible.

Using the error estimates of all variables employed in the calculation of the static temperature (which is the most sensitive quantity) the error estimate of the static temperature was ± 3%. In comparison, the free stream static temperature for all measurements

varied ± 3.5% around T = 49° K, and for measurements at one test-condition the variation was ± 1.6%.

The qualitative conclusion drawn from this error analysis is that the largest and most uncertain single sources of error are the free stream flow non-uniformity and the waves coming from model-sidewall intersection. There might be a systematic error introduced by the hot wire constants and calibration relations, but it should have nearly the same effect on all measurements and is unimportant for the final results.

4. RESULTS AND DISCUSSION

4.1. General Features of the Flow Field

Wakes behind cylinders were studied at a Mach number of 6 in a Reynolds number range from 200 to 20,000. Detailed flow field measurements were made at four Reynolds numbers (Re_d = 320, 960, 2400, 3840) in a region from x/d = 50 to x/d = 2400 at the two lowest Reynolds numbers (Figure 2 gives a complete survey of test conditions). From these measurements two essential features of the flow field become apparent. First, there is a distinct bow shock down to a Reynolds number of 200 (Knudsen number = 0.045), which gives rise to the outer wake. Second, there are two different characteristic length scales for the inner and the outer wake. The inner viscous wake stemming from the boundary layer is laminar up to $Re_d \cong 10,000$. It is distinguishable from the outer wake at $M \cong 6$ up to about 60 diameters or less, depending on the Reynolds number. Qualitatively, this fast diffusion of the inner wake is attributed to the smaller wake width (characteristic length scale) and the lower density. In order to estimate the magnitude of the wake decay rate it is assumed that both the inner wake and the outer wake profiles are Gaussian. McCarthy's data for the inner wake (8) and the present outer wake measurements indicate that this assumption is a reasonable first approximation. The pressure gradient is also neglected.

Then the velocity profile for the inner as well as outer wake is of the form:

$$\frac{u_e - u}{u_e} = \bar{u}(X, Y) = \bar{u}_{\ell o} \left(\frac{A}{4X+A}\right)^{\frac{1}{2}} e^{-\frac{Y^2}{(4X+A)}} \qquad (4.1)$$

where X is measured from some arbitrary "initial" wake position and

$$A(\ell n 2) = \left(\frac{\bar{b}_{u_o}}{d}\right)^2 Re_d C \left(\frac{\rho_e u_e}{\rho_\infty u_\infty}\right)^2$$

$\bar{b}_{u_o}$ = half width of wake in transformed coordinates at X=0

$\left(b_u\right.$ = half width of wake at location where $\frac{\bar{u}}{\bar{u}_{\ell}} = 0.5\Big)$

$$Y = \frac{\rho_e u_e}{\rho_\infty u_\infty} \left(Re_d C\right)^{\frac{1}{2}} \int_o^y \frac{\rho}{\rho_e} \, d\left(\frac{y}{d}\right)$$

$$X = \int_o^x \frac{\rho_e \mu_e u_e}{\rho_\infty \mu_\infty u_\infty} \, d\left(\frac{x}{d}\right) \cong \frac{u_e}{u_\infty} \frac{x}{d}$$

The rate of decay at the position X = 0 is:

$$\frac{1}{\bar{u}_{\ell o}} \left(\frac{d\bar{u}_{\ell}}{dX}\right)_o = -\frac{2}{A} = -\frac{2(\ell n 2)}{\left(\bar{b}_{u_o}/d\right)^2 Re_d C} \left(\frac{\rho_\infty u_\infty}{\rho_e u_e}\right)^2$$

The ratio of the decay rates of the velocity defect in the inner and outer wake becomes then:

$$\frac{\left[\frac{1}{\bar{u}_{\ell o}} \frac{d\bar{u}_{\ell}}{u(x/d)}\right]_{i.w.}}{\left[\frac{1}{\bar{u}_{\ell o}} \frac{d\bar{u}_{\ell}}{d(x/d)}\right]_{o.w.}} \cong \frac{\left(\bar{b}_u^2\right)_{o.w.}}{\left(\bar{b}_u^2\right)_{i.w.}} \frac{u_\infty}{u_e} \left(\frac{\rho_\infty}{\rho_e}\right)^2 \qquad (4.2)$$

Here, "e" refers to the edge of the inner wake. The outer wake edge quantities are at the free stream level. Characteristic numbers for the various quantities are: $\frac{u_e}{u_\infty} \cong 0.8$, $\frac{\left(\bar{b}_u\right)_{o.w.}}{\left(\bar{b}_u\right)_{i.w.}} \cong 5$; $\frac{\rho_e}{\rho_\infty} \cong \frac{1}{3}$.

Substituting these numbers into relation (4. 2) shows that the rate of decay of the inner wake is two to three orders of magnitude larger than the rate of decay of the outer wake. It is therefore not surprising that the inner wake has lost its identity within less than 100 diameters, whereas the outer wake is still pronounced 10, 000 diameters behind the cylinder.

One can see this behavior also in terms of a wake length based on the increase of the wake width. Since two dimensional boundary layer equations apply in the wake, the wake grows as follows:

$$\bar{b}_u^2 \sim \frac{4\mu \ell}{u \rho}$$

and the "wake length"

$$\ell \sim \frac{\bar{b}_u^2 \rho u}{4\mu}$$

Applying this relation to the inner and outer wake (characteristic quantities taken at the respective wake edges), one obtains for the ratio of the outer to inner wake length:

$$\frac{\ell_{o.w.}}{\ell_{i.w.}} \cong \frac{\left(\bar{b}_u\right)^2_{o.w.}}{\left(\bar{b}_u\right)^2_{i.w.}} \frac{\rho_\infty}{\rho_e} \frac{u_\infty}{u_e} \frac{\mu_e}{\mu_\infty}$$

but

$$\frac{\mu_e}{\mu_\infty} \cong \frac{\rho_\infty}{\rho_e}$$

As expected the ratio of wake lengths has the inverse form of the ratio of velocity decay rates, namely:

$$\frac{\ell_{o.w.}}{\ell_{i.w.}} \cong \frac{\left(\bar{b}_u^2\right)_{o.w.}}{\left(\bar{b}_u^2\right)_{i.w.}} \left(\frac{\rho_\infty}{\rho_e}\right)^2 \frac{u_\infty}{u_e}$$

The conclusion reached is that the outer wake length is two to three orders of magnitude larger than the inner wake length.

Some detailed properties of the flow field will now be discussed.

The Bow and Wake Shocks

When the cylinder Reynolds number is decreased by almost a factor of 200 from Re_d = 40,000 to Re_d = 230, the bow shock and wake shock positions change slightly in the outward direction as shown in Figure 12. (The shock positions were obtained from Pitot and hot wire measurements.) The bow shock widens because of an increase in boundary layer displacement thickness on the cylinder. The strength of the bow shock at any given downstream position remains nearly constant in the Reynolds number range considered, as indicated by the Pitot pressure traces across the wake taken at x/d = 20 and x/d = 50 (Figures 13 and 14). However, the wake shock strength decreases rapidly with decreasing Reynolds number, and it is not distinguishable any more at x/d = 50 for a Reynolds number of 320. The reasons are as follows: the boundary layer of the cylinder grows thicker as the Reynolds number is decreased. As indicated by Grange's theoretical results (27) the boundary layer thickness at separation is of the order of the body radius for $Re_d \cong 500$ (it should be noted that the validity of Prandtl boundary layer equations on which this analysis is based is questionable at these low Reynolds numbers). Therefore, the expansion of the flow around the base is reduced at these low Reynolds numbers, so the turning angle decreases and the wake shock becomes weaker. Similar results were found experimentally by Trepaud (28) who made Pitot pressure measurements in

the near wake region at $Re_d = 533$ and $M_\infty = 3.85$. This explanation also suggests that the base pressure should reach a minimum at a certain Reynolds number and increase again as the Reynolds number is decreased further.*

Bow Shock Far From the Cylinder

The bow shock far from the body can be closely approximated by a parabola whose axis is in the free stream Mach wave direction, as shown by T. Kubota (private communication). This approximation can be explained as follows: a weak shock wave bisects the angle formed by the Mach wave ahead and behind the shock. Also a parabola bisects the angle formed by the abscissa and the rays originating at the focal point. The focal point of the parabola is taken to be at the location of the body (which appears as a point at a large distance), and the parameter p for $\left(\frac{y'}{d}\right)^2 = 2p\left(\frac{x'}{d}\right)$ is calculated from the data. The parabola compares well with experiment as indicated in Figure 15.

Static Pressure

McCarthy (8) found that the static pressure across the inner wake was nearly constant. The same result was obtained in the present experiments as shown in Figure 16. However, the pressure increases close to the bow shock. This behavior is qualitatively similar to that predicted by blast wave theory as applied to a flow about a hemisphere cylinder by Lees and Kubota (29;30). Feldman (1), who did a characteristic calculation for a hemisphere cylinder at

* Dewey (9) measured decreasing base pressures as the Reynolds number was reduced in a range of Reynolds numbers from $Re_d \cong 2\times10^3$ to 3×10^4.

hypersonic speeds, found similar results. The slight dip in the pressure between about y/d = 4 and 8 even far downstream (x/d = 500) has not been explained as yet.

The static pressure on the centerline of the wake decreases monotonically from the pressure measured at x/d = 16 (this location is as close to the model as measurements could be done), and approaches the free stream pressure to within 3%, as indicated in Figure 17 (the reasons for this 3% discrepancy were not found). The static pressures measured at Reynolds numbers from Re_d = 320 to 3840 were independent of Reynolds number, and they appear to fair smoothly into the pressures measured by Herzog (10) in a region up to x/d = 10 at a Reynolds number of 30,000 (Figure 18). These results suggest that the static pressure development starting at a distance of a few diameters downstream of the rear stagnation point depends only upon the outer inviscid flow field and not upon the inner viscous wake.

It should be pointed out here that the static pressures measured previously by McCarthy in this laboratory (8) do not correspond to the present measurements and appear to be erroneous because of sidewall interference.

Inner and Outer Wake

From the Pitot pressure measurements (Figures 13 and 14) it is apparent that the inner wake becomes less and less distinguishable from the outer wake as the flow moves downstream. [The inner wake remains laminar in the flows considered (see Part II).]

One way to delineate the boundaries between outer and "inner wake" flow far downstream is to heat the cylinder and follow the total temperature decay, since it is different from free stream total temperature only in the inner wake. The temperature is used as a tracer; it does not change the nature of the flow field essentially. The non-dimensional total temperature, $\left(\frac{T_{o_H} - T_{o_A}}{T_{o_e}}\right)$, is the difference of the total temperature, T_{o_H}, for a heated cylinder, and the total temperature, T_{o_A}, at adiabatic conditions, divided by the external total temperature, T_{o_e}, which is equal to the free stream total temperature. The decay of the total temperature is shown in Figure 19. Far downstream the growth of the total temperature wake is nearly the same as the growth of the outer wake, as shown in Figure 20. This behavior seems plausible, because the inner wake as a separate flow region has ceased to exist.

The Far Wake

In the far flow field ($x/d \geq 100$) the wake is now treated as a whole, which was shown to be appropriate if the complete flow field is laminar up to this point. Since this flow is a constant pressure region the momentum thickness should yield the total drag. The momentum thickness, θ, calculated by numerically integrating the measured data, is nearly constant (Figure 21). The variation in θ at different axial positions is considered experimental error. Taking the average of all momentum thicknesses measured for each case, an increase with decreasing Reynolds number is observed. Since the measurements are still in the continuum regime, the result suggests that the drag coefficient ($C_D = 4\ \theta/d$) increases for two reasons:

(1) increasing contribution of skin friction; (2) effectively larger body because of boundary layer displacement effect which increases the "bow shock-drag".

When the drag coefficient is plotted like the recovery factor as a function of the Reynolds number based on stagnation conditions, the present results compare well with the drag measurements by Maslach and Schaaf (31) and Penland (32) at about the same Mach number, as shown in Figure 22. These authors measured the forces on the cylinders directly. The results indicate that only a narrow region close to the wake centerline in which the measurements were done is of importance as far as drag is concerned (compare Figure 2). The contribution to the drag of the rest of the flow field up to the bow shock can at most be a few percent and is, therefore, negligible in the study of the far wake of a blunt body. For example, at a Reynolds number, $Re_d = 3840$ the cylinder wake "edge" $\left(\frac{T-T_e}{T_e} \cong 0.01\right)$ at $x/d = 400$ is at about $y/d = 12$ and the bow shock is at $y/d = 90$.

Another characteristic wake property is the form parameter δ^*/θ. Crocco's relation $c_p T_o = c_p T + \frac{u^2}{2} = au + b$ holds for Prandtl number $Pr = 1$ and $p = p_e = \text{const}$; the form parameter as derived by Lees (private communication) is

$$\frac{\delta^*}{\theta} = \left[1 + \frac{\gamma-1}{2} M_e^2\right] \frac{\delta_i^*}{\theta} + \frac{\gamma-1}{2} M_e^2 + \left(1 + \frac{\gamma-1}{2} M_e^2\right) \frac{\delta_i^*}{\theta} \frac{\left(T_{o\xi} - T_{oe}\right)/T_{oe}}{\left(u_e - u_\xi\right)/u_e}$$

where

$$\delta^* = \int_0^\delta \left(1 - \frac{\rho u}{\rho_e u_e}\right) dy$$

$$\theta = \int_0^\delta \frac{\rho u}{\rho_e u_e} \left(1 - \frac{u}{u_e}\right) dy$$

and

$$\delta_i^* = \int_o^\delta \left(1 - \frac{u}{u_e}\right) \frac{\rho}{\rho_e}\, dy$$

Far away from the body, $\theta \cong \delta_i^*$ and the form parameter becomes

$$\frac{\delta^*}{\theta} = 1 + (\gamma-1)M_e^2 + \left[1 + \left(\frac{\gamma-1}{2}\right)M_e^2\right] \frac{\left(T_{o\ell} - T_{oe}\right)/T_{oe}}{\left(u_e - u_\ell\right)/u_e} \qquad (4.3)$$

Gruschwitz (33) obtained the same result for the adiabatic case $\left(T_{o\ell} = T_{oe}\right)$ under the asumption of $\frac{u_e - u_\ell}{u_e} \ll 1$ and $\frac{\rho}{\rho_e} \cong 1$. As shown in Figure 23, the comparison between theory and experiment is quite good. (Note that the stagnation temperature, T_o, should be replaced by the stagnation enthalpy for very hot wakes.)

In the far wake the velocity is already close to the free stream value, but the temperature is still much higher than T_e. To cite an example, for $Re_d = 3840$, at $x/d = 200$ the centerline velocity is $0.84\ u_\infty$ and the temperature is $2.96\ T_\infty$. Consequently the Mach number is only half the free stream Mach number. For all test cases considered, the Mach number development along the wake axis is displayed in Figure 24. The measured half wake widths, (b_T/d), based on the temperature profiles at the position where $\frac{T - T_e}{T_\ell - T_e} = 0.5$ appear in Figure 25. The velocity wake width, (b_u/d), measured in the same way from the velocity profiles was about $0.91\ b_T$ in almost all measurements. The ratio b_u/b_T started to decrease at $x/d = 1600$ for $Re_d = 960$ until it reached 0.82 at $x/d = 2400$. More will be said about this region in Section 4.3.

A summary of all profile measurements is shown in Figure 26, where the velocity defect is plotted against the normalized coordinate

across the flow; the thickness of the wake, (b_u/d), is measured at the position where $\frac{u_e-u}{u_e-u_\ell} = 0.5$. The profiles are not similar close to the body, but seem to slowly approach a similar Gaussian profile far downstream at a rate that is the faster the lower the Reynolds number. The temperature profiles are of the same shape as the velocity profiles and indicate the same trends.

4.2. The Outer Wake as Determined from Shock Shape

In order to calculate the far wake flow an "initial" wake profile has to be determined. The simplest model--suggested by Lykoudis (2)--is a flow which is compressed by the bow shock and expanded isentropically to free stream pressure, neglecting the inner wake and the wake shock.

The flow quantities on each streamline, ψ, are determined by the free stream Mach number M_∞ and the local shock angle. (In the calculation the shock angle was determined from a Schlieren photograph.) The physical position of these flow variables in the wake is determined from the conservation of mass, i.e.

$$d\psi = \rho_\infty u_\infty dy_\infty = \rho_w u_w dy_w$$

or

$$y_w = \int_0^{y_\infty} \frac{\rho_\infty u_\infty}{\rho_w u_w} dy_\infty$$

$$y_w = \int_0^{y_\infty} \frac{M_\infty^2}{M_w^2} dy_\infty \quad \text{if} \quad \frac{u_\infty - u_w}{u_\infty} \ll 1$$

("w" refers here to the wake.)

The experimental results for various flow variables compare best with the theoretical calculation at x/d = 200 (Figures 27 and 28). At this position in the flow field the expansion has been completed everywhere across the whole wake. There is some deviation in the center of the wake caused by neglecting the inner wake. In the Reynolds number range considered, it appears that the wake shock has little effect on the far wake. Figure 27, in which the bow shock and the velocity wake profiles are plotted at x/d = 200, shows again that only the small strong portion of the bow shock causes most of the outer wake. The drag calculated from the theoretical model is $C_D = 1.06$ compared to $C_D = 1.19$ obtained from the experiments, integrating in both cases up to (y/d = 22).

The result of this calculation in comparison with experiments, together with the Reynolds number independence of the static pressure decrease, suggests that the outer wake is expansion-dominated up to the point where the pressure again reaches the free stream level (for the present measurements $x/d \cong 200$). Feldman (1) already came to the same conclusion on the basis of theoretical considerations.

4.3. Comparison of the Flow Field Measurements with Laminar Linear Theory

4.3.1. Theoretical Solution

The compressible laminar linear wake problem was solved by Kubota (16). The only assumptions necessary are that the velocity defect $\frac{u_e - u}{u_e} \ll 1$ and $\frac{\mu\rho}{\mu_e\rho_e}$ = constant. In the hypersonic far wake of a blunt body the pressure is constant and the wake edge conditions

are at the free stream level (within experimental accuracy). The solution in integral form as obtained by Gold (17), is:

$$\frac{u_e-u}{u_e} = \frac{\left(Re_d C\right)^{\frac{1}{2}}}{2\left(\pi\left(\frac{x-x_i}{d}\right)\right)^{\frac{1}{2}}} \int_{-\infty}^{\infty} \bar{u}_i(\bar{\xi}/d) \exp\left[-\frac{\left(\bar{y}-\bar{\xi}\right)^2\left(Re_d C\right)}{4(x-x_i)d}\right] d\left(\frac{\bar{\xi}}{d}\right) \quad (4.4)$$

The solution for the temperature excess, $\frac{T-T_e}{T_e}$, is of the same form, except that $(x-x_i)$ has to be replaced by $\frac{(x-x_i)}{Pr}$ where Pr is the Prandtl number.

The symbols are

$\bar{u}_i\left(\frac{\bar{\xi}}{d}\right) = \frac{u_e-u}{u_e}$ at the initial wake position where $x = x_i$.

$\bar{\xi} = \int_0^{\xi} \frac{\rho}{\rho_e} d\xi$ Howarth-Dorodnitsyn coordinate at $x = x_i$.

$\bar{y} = \int_0^{y} \frac{\rho}{\rho_e} dy$ Howarth-Dorodnitsyn coordinate at arbitrary x.

In order to compare the theoretical profiles with measurements at various x-stations, the integral was evaluated numerically on the IBM 7094.

The initial profile data, taken from experimental results at four different Reynolds numbers, were $\frac{u_e-u_\xi}{u_e}$ = 0.149, 0.143, 0.122 and 0.104. These numbers actually represent a first estimate of error committed by linearizing the equations, namely $\left(\frac{u_e-u_\xi}{u_e}\right)^2 \Big/ \left(\frac{u_e-u_\xi}{u_e}\right)$ is 15 to 10% at the initial stations. In the present experiments the Chapman-Rubesin factor $C = \frac{\mu_e \rho_e}{\mu \rho}$ changed in each case by less than one percent across the wake. Its mean value was 1.004. This is expected since the viscosity-temperature relation is linear to within 1% from 50°K to 150°K and $\frac{T\rho}{T_e \rho_e} = 1$ across the wake.

4.3.2 Comparison of Theoretical and Experimental Results

The experimental static temperature profiles are compared at four Reynolds numbers (Re_d = 3840, 2400, 960 and 320) with the linear integral solution (4.4), where the experimentally determined profiles were used as initial values. The respective initial stations were $(x/d)_i$ = 300 for the highest Reynolds number (Re_d = 3840), and $(x/d)_i$ = 400 for the other three Reynolds numbers. The results appear in Figures 29 to 32, where the profiles are shown at several axial stations. There are only small deviations of the experimental results from the theoretical integral solution in all cases, except at a Reynolds number Re_d = 960, in the region $x/d > 1600$. The effect of Prandtl number is felt only at large distances from the initial profile, as shown in Figure 32. In order to compare these results with a Gaussian distribution, a Gaussian was fitted to the experimental profiles at the initial station $(x/d)_i$ at two points, i.e. at the centerline of the wake and at the point where $\frac{u_e - u}{u_e - u_c} = 0.5$, and its downstream development calculated. The Gaussian profiles are the broken lines in Figures 29 to 32. Results for the velocity profiles indicate the same trends as the static temperature profiles. One example (Re_d = 320) is shown in Figure 33. From the theoretical temperature and velocity profiles total temperature profiles were calculated and plotted together with the results obtained from experimental measurements in Figure 34. The theoretical results indicate the same trends as experiments. The decay of the static temperature excess and velocity defect along the wake axis, and the growth of the wake widths

based on temperature profiles are compared in Figures 35, 36 and 37.

As the profile results already indicated, the laminar theory agrees reasonably well with experiment, except at $Re_d = 960$ in the region $x/d > 1600$, where the temperature excess starts to decrease much more rapidly and the wake width increases sharply. This behavior indicates that the wake in this region is not a linear laminar flow anymore. From the close correspondence between linear laminar theory and experiments it is concluded that the wake is laminar up to $x/d \cong 1600$ at $Re_d = 960$ ($d = 0.005$ inch), and for the three other Reynolds number cases ($Re_d = 3840$, $d = 0.02$ inch; $Re_d = 2400$, $d = 0.0125$ inch and $Re_d = 320$, $d = 0.005$ inch) in the whole axial range in which experimental results were obtained, i.e. up to $(x/d)_{max.} = 600$, 960 and 2400 respectively. The fact that the rate of growth of the wake increases and the decay of mean flow quantities is more rapid downstream of $x/d = 1600$ at $Re_d = 960$ suggests the possibility of laminar instability or transition to turbulence in the far wake of blunt bodies. This interesting phenomenon will be treated in Part II of this thesis.

REFERENCES

1. Feldman, S.: "Trails of Axi-Symmetric Hypersonic Blunt Bodies Flying Through the Atmosphere, "AVCO-Everett, Research Report 82, Dec. 1959; also J. Aero. Sci. 28, 433-448 (1961).

2. Lykoudis, P. S.: "Theory of Ionized Trails for Bodies at Hypersonic Speeds," Rand RM-2682-1-PR, May 1961, revised Oct. 1961.

3. Lees, L. and L. Hromas: "Turbulent Diffusion in the Wake of a Blunt-Nosed Body at Hypersonic Speeds," J. Aero. Sci., 29, 976-993 (1962).

4. Kingsland, Louis Jr.: "Experimental Study of Helium and Argon Diffusion in the Wake of a Circular Cylinder at M = 5.8," GALCIT Hypersonic Research Project, Memorandum No. 60 (June 1961).

5. Kendall, J. M. Jr.: "Experimental Study of Cylinder and Sphere Wakes at a Mach Number of 3.7," Jet Propulsion Laboratory, Calif. Inst. of Tech. TR 32-363 (Nov. 1962).

6. Brown, A. C., R. L. Kramer and C. E. Smith: "Hypersonic Cylinder Wake Studies at Mach 20," Lockheed Missiles and Space Co., Gas Dynamics RR-9-63-14 (Sept. 1963).

7. Vas, I. E., E. M. Murman and S. M. Bogdonoff: "Studies of Wakes of Support-Free Spheres at M = 16 in Helium," AIAA J. 3, 1237-1244 (July 1965).

8. McCarthy, J. F. Jr.: "Hypersonic Wakes," GALCIT Hypersonic Research Project, Memorandum No. 67 (July 1962).

9. Dewey, C. F. Jr.: "Near Wake of a Blunt Body at Hypersonic Speeds," AIAA J. 3, 1001-1010 (June 1965).

10. Herzog, R. T.: "Nitrogen Injection into the Base Region of a Hypersonic Body," GALCIT Hypersonic Research Project, Memorandum No. 71 (August 1964).

11. Slattery, R. E. and W. G. Clay: "Experimental Measurements of Turbulent Transition, Motion, Statistics and Gross Radial Growth Behind Hypervelocity Objects," Physics Fluids 5, 849-855 (1962).

12. Clay, W. G., M. Labbit and R. E. Slattery: "Measured Transition from Laninar to Turbulent Flow and Subsequent Growth of Turbulent Wakes," AIAA J. 3, 837-841 (May 1965).

13. Wilson, L. N.: "Body Shape Effects on Axisymmetric Wakes," General Motors Defense Research Laboratories, Santa Barbara, Calif., TR 64-02K (Oct. 1964).

14. Knystautas, R.: "Growth of the Turbulent Inner Wake Behind 3"-Diam. Spheres," AIAA J., 2, 1485-1486 (August 1964).

15. Dewey, C. F., Jr.: "Hot Wire Measurements in Low Reynolds Number Hypersonic Flows," ARS J., 1709-1718 (Dec. 1961).

Also, Dewey, C. F., Jr.: "Measurements in Highly Dissipative Regions of Hypersonic Flows. Part I. Hot-Wire Measurements in Low Reynolds Number Hypersonic Flows," Ph. D. Thesis, California Institute of Technology, Pasadena, California (1963).

16. Kubota, T.: "Laminar Wake with Streamwise Pressure Gradient," GALCIT Hypersonic Research Project, Internal Memorandum 9 (April 1962).

17. Gold, H.: "Laminar Wake with Arbitrary Initial Profiles," AIAA J. 2, 948-949 (May 1964).

18. Behrens, W.: "Condensation Effects of Air in Wind Tunnel Leg 1 (M = 6)," GALCIT Hypersonic Research Project, Internal Memorandum No. 13 (1963).

19. Dewey, C. F., Jr.: "Measurements in Highly Dissipative Regions of Hypersonic Flows. Part II. The Near Wake of a Blunt Body at Hypersonic Speeds," Ph. D. Thesis, Calif. Inst. of Tech., Pasadena, Calif. (1963).

20. Mathews, M. L.: "An Experimental Investigation of Viscous Effects on Static and Impact Pressure Probes in Hypersonic Flow," GALCIT Hypersonic Research Project, Memorandum No. 44 (June 1958).

21. Sherman, F. S.: "New Experiments on Impact-Pressure Interpretation in Supersonic and Subsonic Rarefied Air Stream," NACA TN 2995 (1953).

22. Behrens, W.: "Viscous Interaction Effects on a Static Pressure Probe at M = 6," AIAA J. 1: 12, 2864-2366 (1963).

23. Hayes, W. D. and R. F. Probstein: "Hypersonic Flow Theory," (Academic Press, New York and London, 1959), Chap. IX.

24. Ames Research Staff: "Equations, Tables and Charts for Compressible Flow," NACA Rep. 1135 (1953).

25. Sherman, F. S.: "Transition Flow," (A Survey of Experimental Results and Methods for the Transition Region of Rarefied Gas Dynamics), University of California, Institute of Engineering Research, Berkeley, Calif., TR HE-150-201, (August 15, 1962).

26. Vrebalovich, T.: "Heat Loss from Hot Wires in Transonic Flow," JPL Research Summary No. 36-14 (May 1, 1962).

27. Grange, J. M.: "Laminar Boundary Layer Separation and Near Wake Flow for a Smooth Blunt Body at Hypersonic Speeds," Ae.E. Thesis, Calif. Inst. of Tech., Pasadena, Calif. (June 1966).

28. Trepaud, P.: "Etude des Sillages de Cylindres Placés dans un Écoulement de Gaz Raréfié," Rapport No. 65-11, Laboratoire D'Aerothermique, Centre National de la Recherche Scientifique, Faculté des Sciences de Paris, Meudon (Dec. 1965).

29. Lees, L. and T. Kubota: "Inviscid Hypersonic Flow over Blunt-Nosed Slender Bodies," J. Aero. Sci. 24, 195-202 (1957).

30. Kubota, T.: "Investigation of Flow around Simple Bodies in Hypersonic Flow," GALCIT Hypersonic Research Project, Memorandum No. 40 (June 1957).

31. Maslach, G. J. and S. A. Schaaf: "Cylinder Drag in the Transition from Continuum to Free-Molecule Flow," Physics of Fluids 6, 315-321 (March 1963).

32. Penland, J. A.: "Aerodynamic Characteristics of a Circular Cylinder at Mach Number 6.86 and Angles of Attack up to 90°," NACA RM 454A14 (March 11, 1954).

33. Gruschwitz, E.: "Berechnung des Profilwiderstandes in Kompressibler Unterschallströmung aus dem Nachlauf," Z. Flugwiss. 12, Heft 5, 166-169 (1964).

APPENDIX A

PROCEDURE AND FORMULAE OF DATA REDUCTION

1. Raw Data Reduction

Two examples of measured wake data are shown in Figures 38a and 38b. As indicated in Figure 38a there is a good correspondence between hot wire and Pitot pressure data at characteristic points such as the wake and bow shock.

The first steps in the data reduction are the determination of the slope, $\left[\frac{d(i^2R)}{dR}\right]_{i \Rightarrow o}$ and the adiabatic resistance of the hot wire, R_{awm} (calculated at i = o). The data are interpolated so that the output of the hot wire is given at the same stations as the Pitot pressure data. The data reduction formulae are quoted in order of calculations performed by the computer.

(1) Compute the slope $\left[\frac{d(i^2R)}{dR}\right]_{i \Rightarrow o}$

$$\left[\frac{d(i^2R)}{dR}\right]_{i \Rightarrow o} = \frac{i_2^2 R_2 - i_1^2 R_1}{R_2 - R_1}$$

(2) Compute the measured hot wire adiabatic resistance, R_{awm} from the extrapolation formula:

$$R_{awm} = \frac{R_1 R_2 (i_2^2 - i_1^2)}{R_2 i_2^2 - R_1 i_1^2}$$

where i_1 and i_2 are measured and

$$R_j = \frac{V_j}{i_j} = \frac{V_{B_j} + \Delta V_j F_j}{i_j} - R_L$$

V_{B_j} = bucking voltage

ΔV_j = voltage measured

F_j = potentiometer attenuation factor

R_L = resistance of the hot wire leads.

This relation is derived from the equation for a straight line, namely,

$$R_1 = \left(\frac{R_2 - R_1}{i_2^2 R_2 - i_1^2 R_1}\right) i_1^2 R_1 + R_{awm}$$

These first two steps in the data reduction are illustrated in Figures 38b and 39. Three cases marked a, b and c are shown as examples.

(3) Compute y-station and interpolate data for given (y/d) such that hot wire and Pitot measurements are given at same stations.

(4) Take mean values of data for ± (y/d).

(5) Compute the measured adiabatic temperature:

$$T_{awm} - T_r = \left(\frac{R_{awm} - R_r}{R_r}\right) \frac{1}{a_r}$$

where R_r = reference resistance

and a_r = temperature resistivity coefficient.

(6) Plot hot wire data together with Pitot pressure measurements.

(7) Output on IBM-cards and plots:

$$p_p,\ T_{awm},\ \left[\frac{d(Ri^2)}{dR}\right]_{i \Rightarrow o} = f\left(\frac{y}{d}, \frac{x}{d}\right)$$

$$p = p\left(\frac{x}{d}\right)$$

One typical example of the output data is shown in Figure 40.

2. Pitot Pressure Corrections

As discussed in Section 2.3, there are no viscous interaction corrections necessary to the measured Pitot pressure. The free stream Mach number varies somewhat with changes in total pressure (Figure 3). However, it is desirable to compare results at the same Mach number. This correction was made, assuming that the flow is compressed by a bow shock and expanded to free stream static pressure. Calculating the ratio of the Pitot pressures in the wake for two Mach numbers close to M = 6, it was found that this ratio varies only little across the wake and at the edge of the wake it is the same as in the free stream. The correction is, therefore,

$$p_{p_{M_1}} = p_{p_{M_2}} \left(\frac{p_{p_{M_1}}}{p_{p_{M_2}}} \right)_{theor.}$$

where $\left(\frac{p_{p_{M_1}}}{p_{p_{M_2}}} \right)_{theor.}$ is the ratio of Pitot pressures of the flow at the free stream Mach numbers M_1 and M_2.

Another correction was applied because of free stream non-uniformities (Figure 4); this correction was estimated to have the form:

$$p_{p_{corr.}} = p_{p_m} \left[\frac{p_{p\infty(x=o)}}{p_{p\infty}} \right],$$

where $\frac{p_{p\infty(x=o)}}{p_{p\infty}}$ is the ratio of the Pitot pressures of the free stream at the location of the model to that at the location of measurement.

3. Static pressure corrections

The static pressure has to be corrected for viscous interaction effects using the empirical formula obtained from a calibration, as shown in Figure 9:

$$\frac{p_m}{p_{orig}} = 1 + 0.065\,\bar{\chi} + 0.04\,\bar{\chi}^2$$

where

$$\bar{\chi} = \frac{M^3_{orig}\sqrt{C_{orig}}}{\sqrt{Re_{x\,orig}}}$$

$$C_{orig} = \frac{\mu_w}{\mu_{orig}}\,\frac{T_{orig}}{T_w}$$

and the subscripts are

m = measured quantity

orig = inviscid quantity at the station of the pressure taps (x is measured from the tip of the probe).

w = quantity on the probe wall.

For the calculation of this correction T_o was assumed to be the free stream total temperature and the measured quantities were used to determine M. An iteration was not necessary for the present measurements. This formula is a first approximation to the viscous interaction correction in the wake (see remarks in Section 2.4.).

As in the case of the Pitot pressure, a second correction was necessary because of the different free stream Mach numbers at different total pressures. Since the pressure in the far wake is close to the free stream level the ratio of measured pressures is

equal to the ratio of the free stream pressures at different Mach numbers:

$$\frac{p_{m_{M_1}}}{p_{m\ M_2}} = \frac{p_{\infty_{M_1}}}{p_{\infty\ M_2}}$$

Finally, the same type of correction was applied for free stream flow non-uniformities:

$$\frac{p_{m\,corr.}}{p_m} = \frac{p_{\infty(x=o)}}{p_\infty}$$

4. Final Data Reduction Procedure

The input data are the corrected Pitot pressure, p_p, and the adiabatic wall temperature of the hot wire, T_{awm}, both at the same stations for each axial wake position, and the corrected static pressure, p, which is assumed to be constant across the wake. The formulae again are quoted in the sequence of calculations performed by the computer.

(1) Calculate the Mach number, M:

$$M = \sqrt{\frac{p_p}{p\,K} - \frac{5}{14}}$$

where K = 1.2876 for air.

For Mach numbers $M \geq 2.5$ this approximate formula is valid to within 0.2% or better.

(2) Calculate the momentum flux ρu^2:

$$\rho u^2 = \frac{\gamma p_p}{K\left(1+\frac{5}{14M^2}\right)}$$

This expression is of the same degree of accuracy as equation (1).

(3) In the subsequent calculation of the total temperature the hot wire end loss corrections are included as described by Dewey (15). An iteration scheme is required. A first guess for the recovery factor for a wire of finite length is:

$$\eta_m^{(o)} = 1.05$$

(4) $$T_o^{(o)} = \frac{T_{awm}}{\eta_m^{(o)}}$$

(5) $$Re_o^{(o)} \approx \frac{\rho u^2 d}{u_\infty \mu_o^{(o)}}$$

Note: In the far wake $\Delta u/u << 1$ and to obtain the Reynolds number in the first approximation $u \approx u_\infty$. [Without this simplifying approximation, $u^{(o)}$ could have been calculated from M and $T_o^{(o)}$.] By definition:

$$\nu^{a(o)} = \left(\frac{\ell}{d}\right)^2 \frac{k_o^{(o)}}{k_w} Nu_o^{(o)}$$

where $Nu_o^{(o)}$ is calculated from

$$Re_o = 5.26\, Nu_o + 5.74\, Nu_o^2.$$

(6) Calculate the recovery factor for a wire of infinite length:

$$\eta^{(o)} = 1.167 - \frac{0.217}{1 + \left(\frac{1}{0.335 Re_o}\right)^{1.33}}$$

(7) Calculate the finite wire correction factor:

$$\psi_R^{(o)} = \frac{\left(1 - \frac{\eta_s}{\eta_m^{(o)}} \omega\right)}{1 - \omega}$$

where

$$w = \frac{\tanh \nu}{\nu}$$

(8) $$\eta_m^{(1)} = \frac{\eta^{(o)}}{\psi_R^{(o)}}$$

(9) $$T_o^{(1)} = \frac{T_{awm}^{(1)}}{\eta_m^{(1)}}$$

$$T^{(1)} = \frac{T_o^{(1)}}{1 + \frac{\gamma-1}{2} M^2}$$

(10) $$\rho^{(1)} = \frac{p}{R T^{(1)}}$$

(11) $$\left(\frac{\rho u^2}{\rho^{(1)}}\right)^{\frac{1}{2}} = u^{(1)}$$

(12) $$Re_o^{(1)} = \frac{\rho^{(1)} u^{(1)} d}{\mu_o^{(1)}}$$

(13) Return to (5)

Iterate until $T^{(n)} - T^{(n-1)} \leqq 0.1$ [°K].

This iteration scheme converged after four or five iterations. A typical example of final data is shown in Figure 41.

In case the static pressure cannot be measured, the second group of variables p_p, T_{awm}, $\left[\frac{d(R i^2)}{dR}\right]_{i \Rightarrow o}$ can be used to calculate other flow quantities for the derivation of the heat transfer relations, see Dewey (15). For large Mach numbers ($M \geqslant 2.5$) this calculation is quite straightforward. The total temperature, T_o, and the mass flux, ρu, can be calculated from the following formulae:

$$Nu_m = \frac{R_r a_r \left[\frac{d(i^2R)}{dR}\right]_{i=o}}{\pi \ell k_o} \quad \text{(measured Nusselt number)}$$

$$\psi_N = (1-w)\left[1 + \frac{st_s}{2}\,\frac{(2w-1)\,w - \frac{1}{\cosh^2 v}}{(1-w)^2}\right]$$

where

$$st_s = \frac{a_r T_o(\eta_s - \eta_m)}{1+a_r(T_{awm} - T_r)} \quad \text{by definition.}$$

[Note: This formula for ψ_N was not quoted correctly by Dewey (15).]

$$Nu_o = \psi_N\, Nu_m$$

$$Re_o = 5.26\, Nu_o + 5.74\, Nu_o^2$$

$$\frac{T_{aw}}{T_o} = \eta = 1.167 - \frac{0.217}{1 + \left(\frac{1}{0.335 Re_o}\right)^{1.33}}$$

and

$$\rho u = \frac{Re_o \mu_o}{d}$$

This data reduction again requires an iteration, since T_o is not known but is necessary for the calculation of (ρu). The velocity and static temperature are calculated from

$$\rho u^2 = \frac{\gamma P_p}{K\left(1 + \frac{5}{14 M^2}\right)} \quad \text{and } \rho u$$

$$T = T_o - \frac{u^2}{2 c_p}$$

by another iteration. Since it was assumed that $M \geq 2.5$, the error committed, neglecting to iterate, is very small. However, the inherent error committed in subtracting two large quantities, T_o and $\frac{u^2}{2c_p}$, of reasonable accuracy becomes large in calculating a small quantity, i.e. the static temperature.

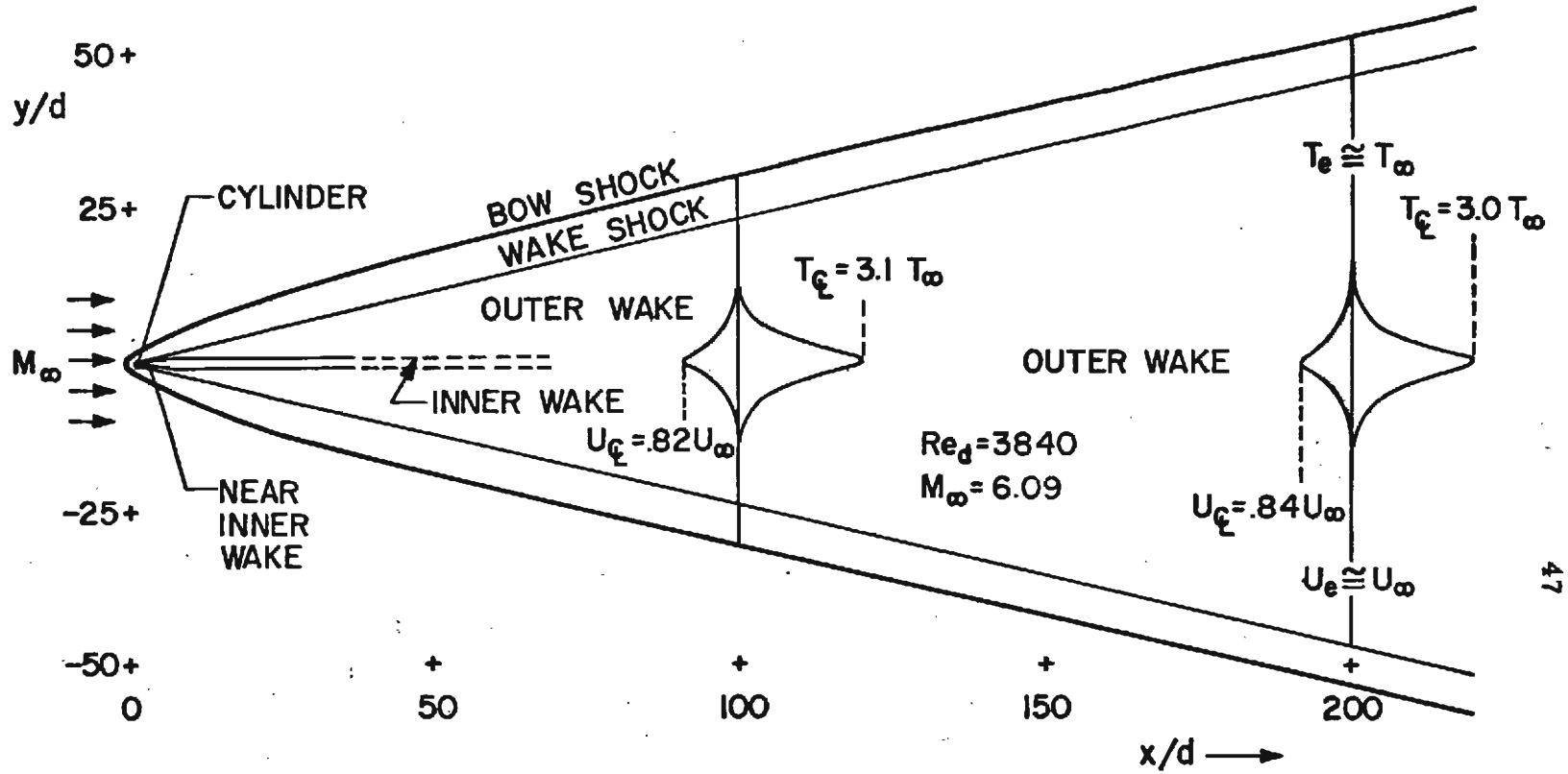

FIG. 1 FLOW FIELD REGIONS BEHIND A CYLINDER AT $M_\infty = 6$

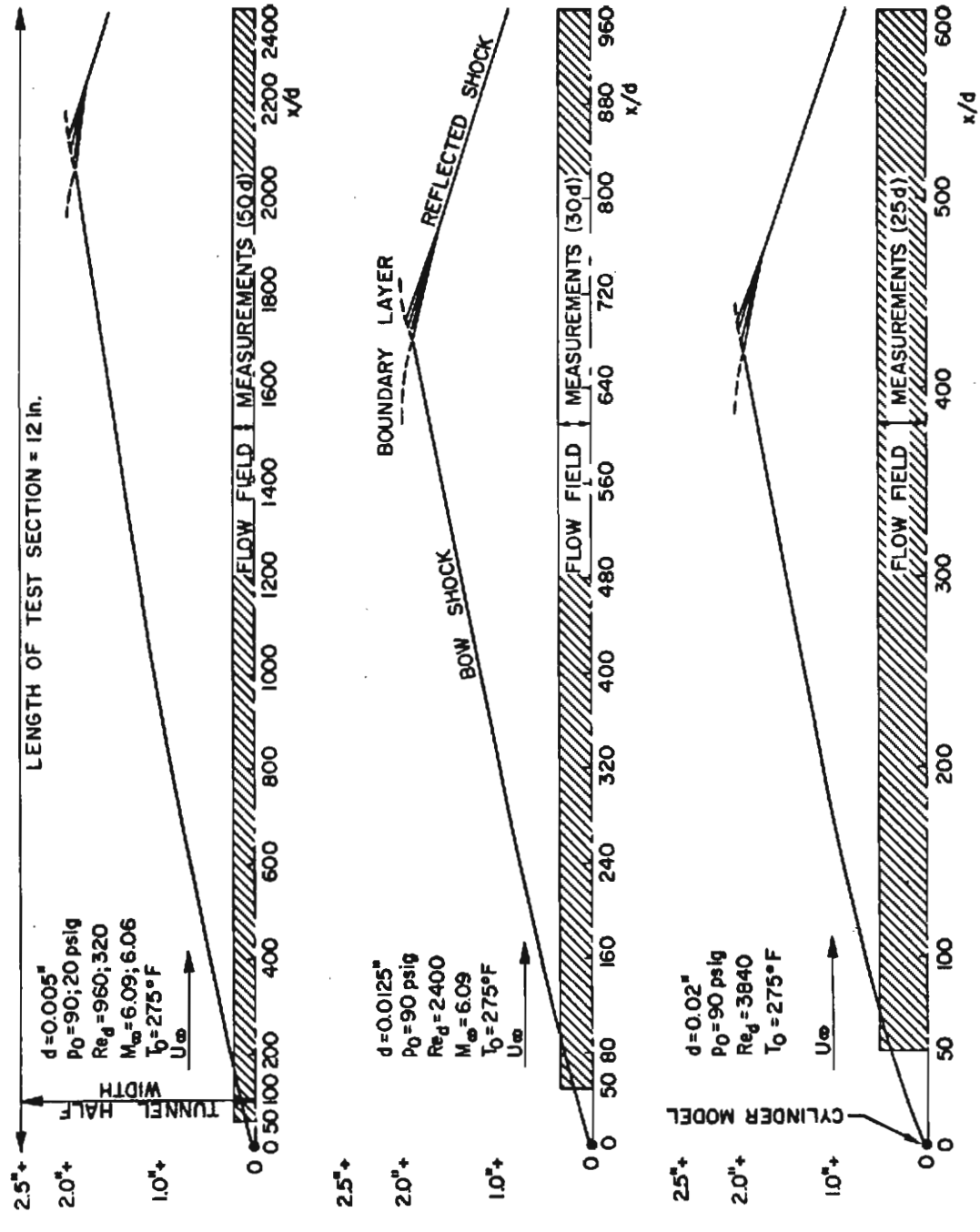

FIG. 2 SURVEY OF TEST CONDITIONS

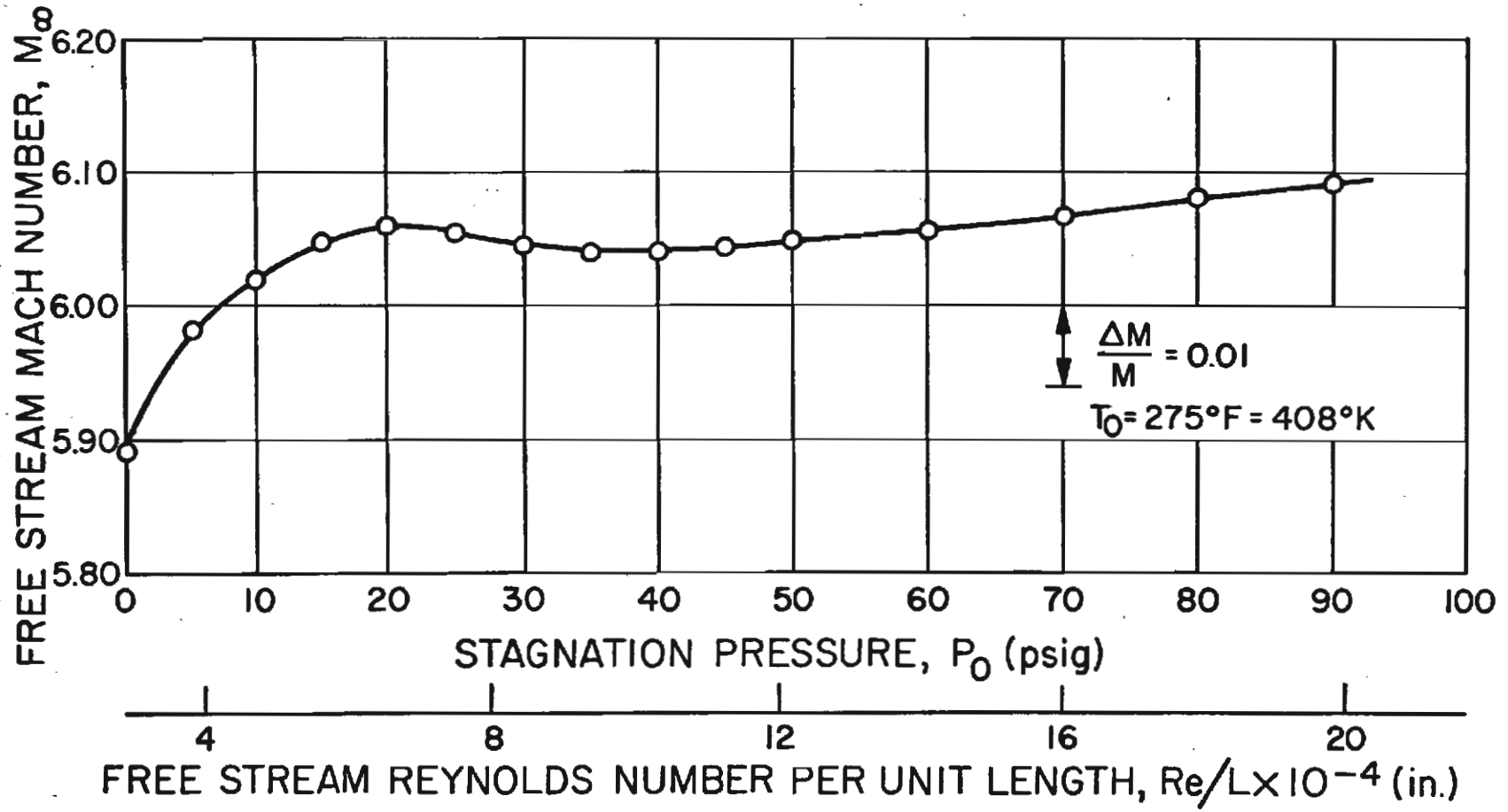

FIG. 3 FREE STREAM MACH NUMBER VERSUS REYNOLDS NUMBER MEASURED AT THE STATION OF THE MODEL

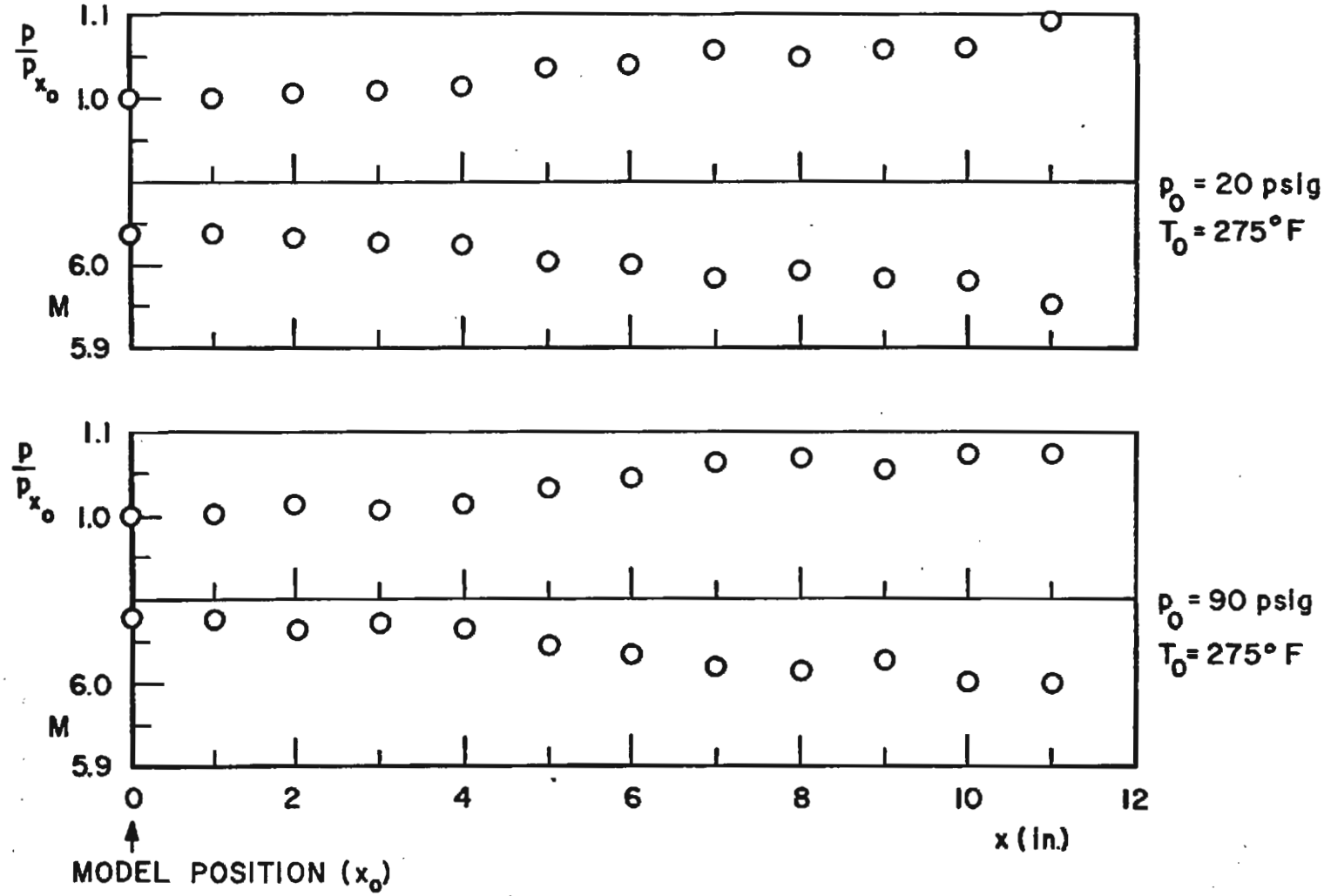

FIG. 4 VARIATION OF FREE STREAM QUANTITIES ALONG TUNNEL CENTERLINE

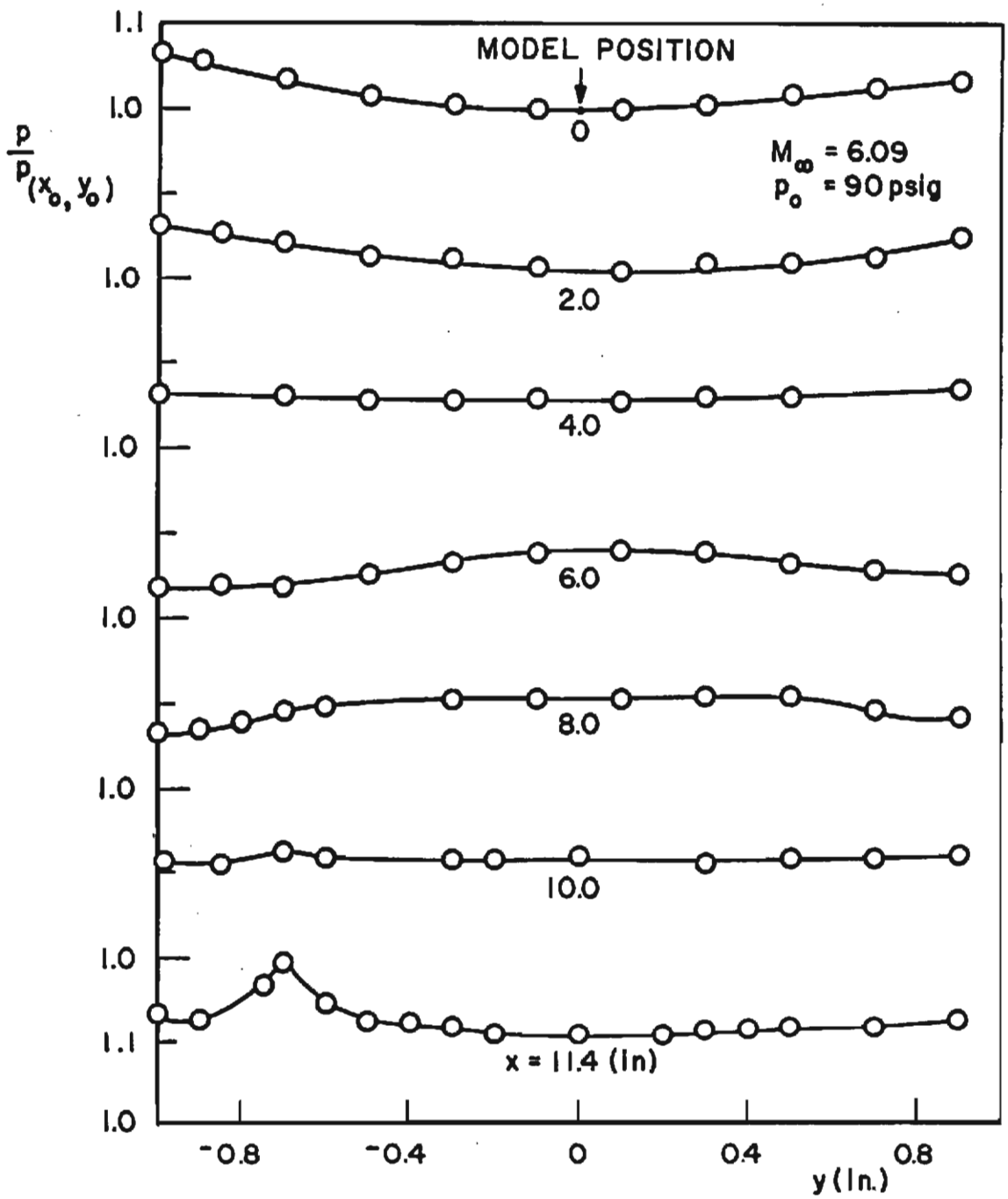

FIG. 5 FREE STREAM STATIC PRESSURE VARIATION IN THE VERTICAL CENTER PLANE OF THE TUNNEL

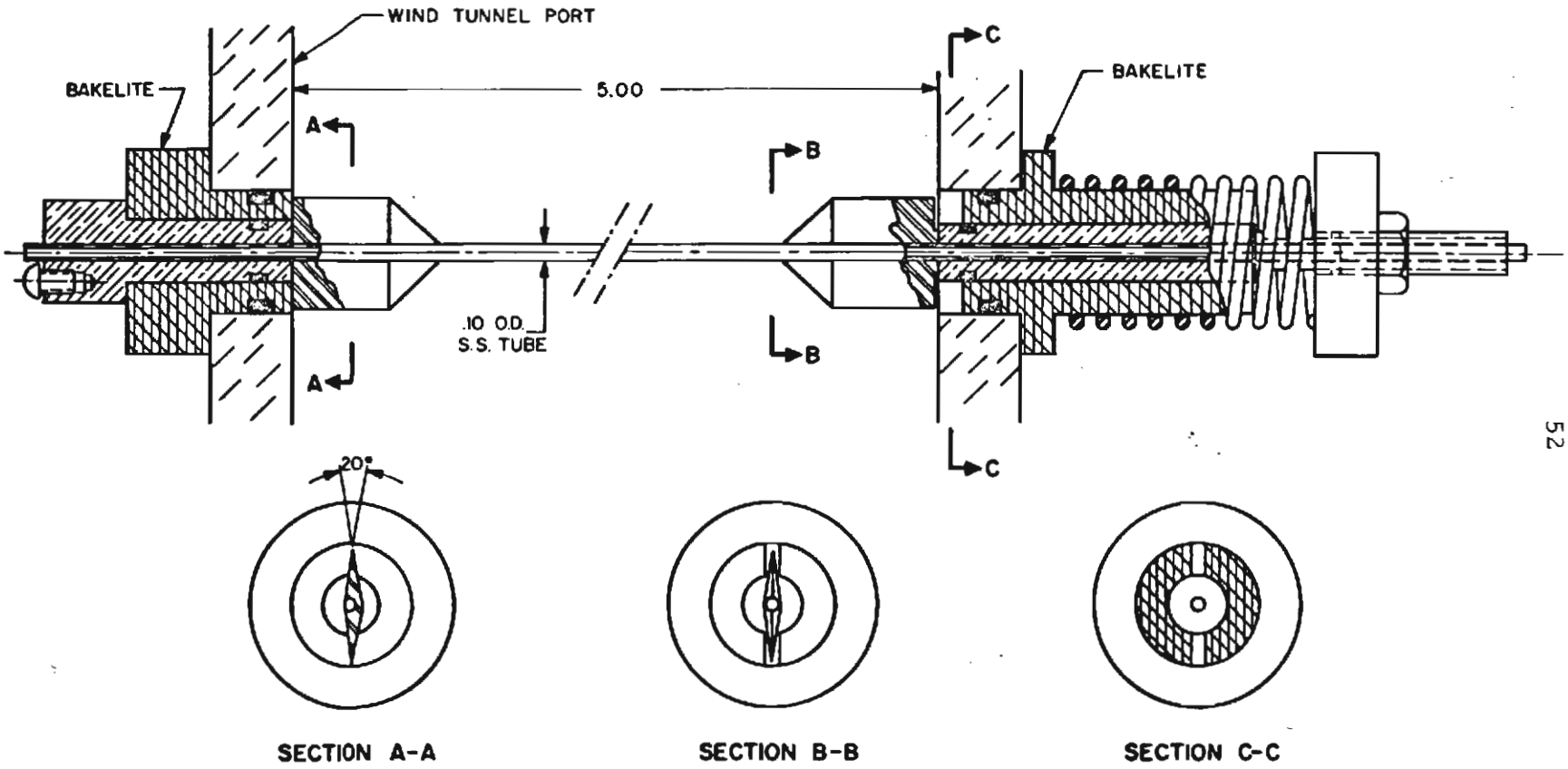

NOTE: DIMENSIONS ARE IN INCHES.

FIG. 6 TYPICAL MODEL

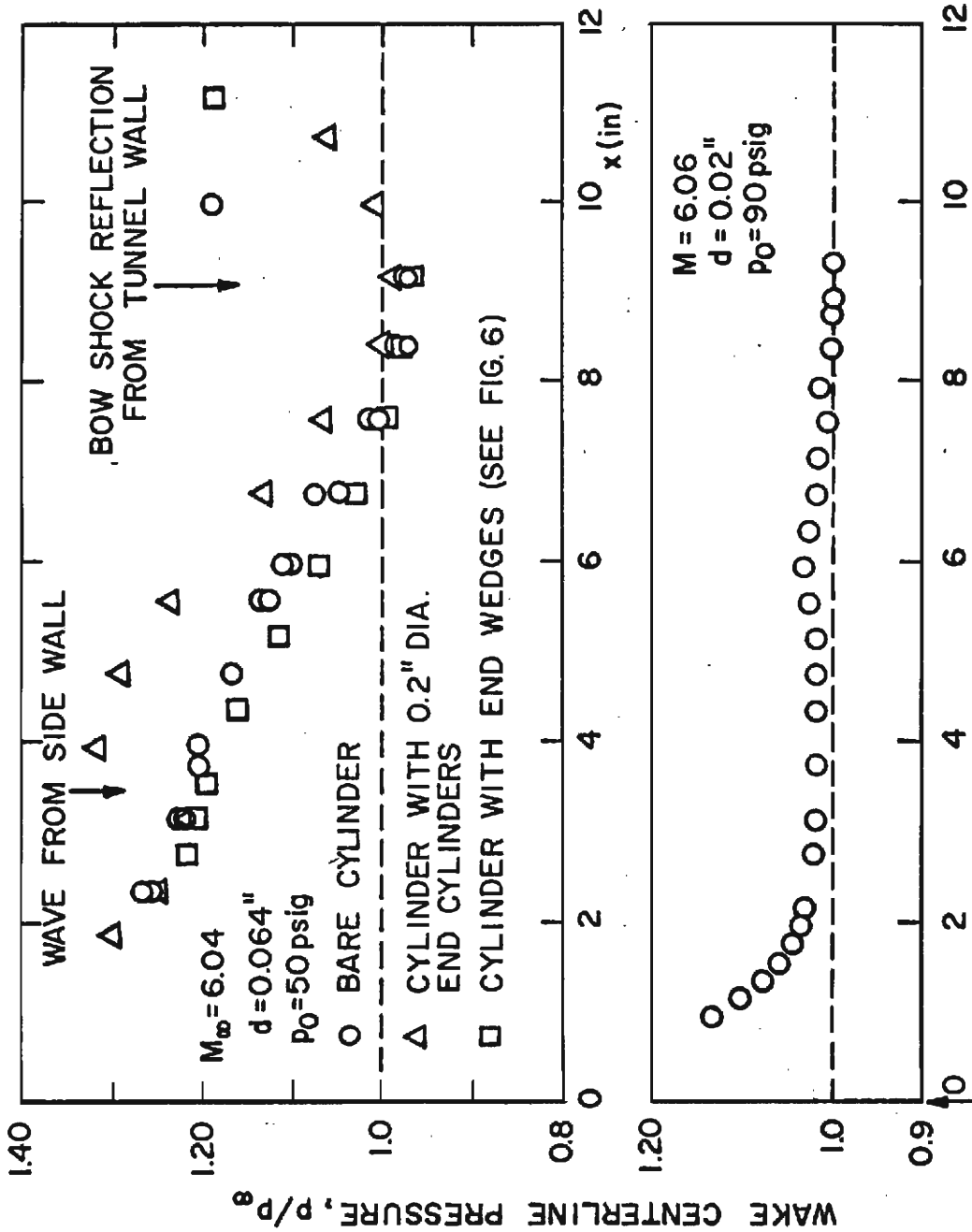

FIG. 7 EFFECT OF MODEL-TUNNEL WALL INTERSECTION ON STATIC PRESSURE

STATIC PRESSURE PROBE (SIDE VIEW)

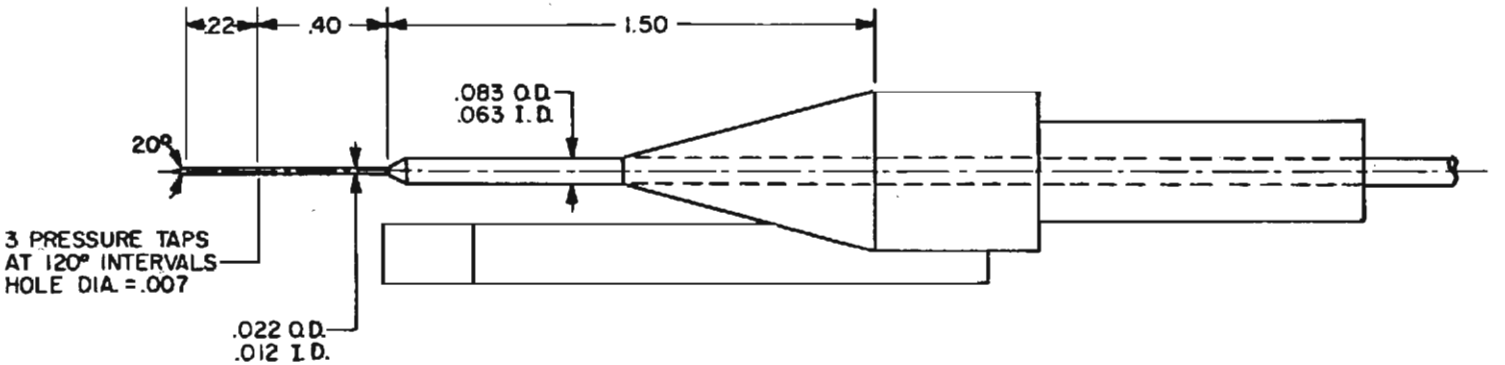

FRONT VIEW
SCALE 20:1

PITOT PRESSURE PROBE (TOP VIEW)

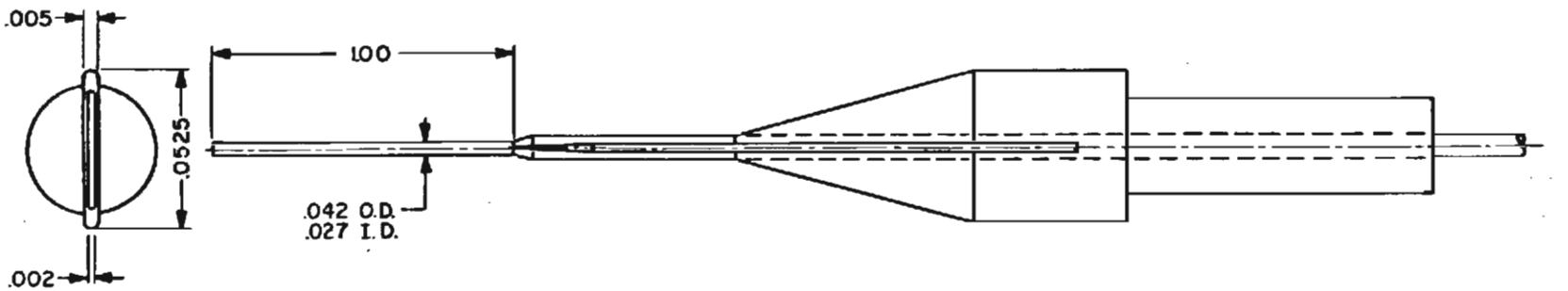

NOTE: DIMENSIONS ARE IN INCHES

FIG. 8 STATIC AND PITOT PRESSURE PROBES

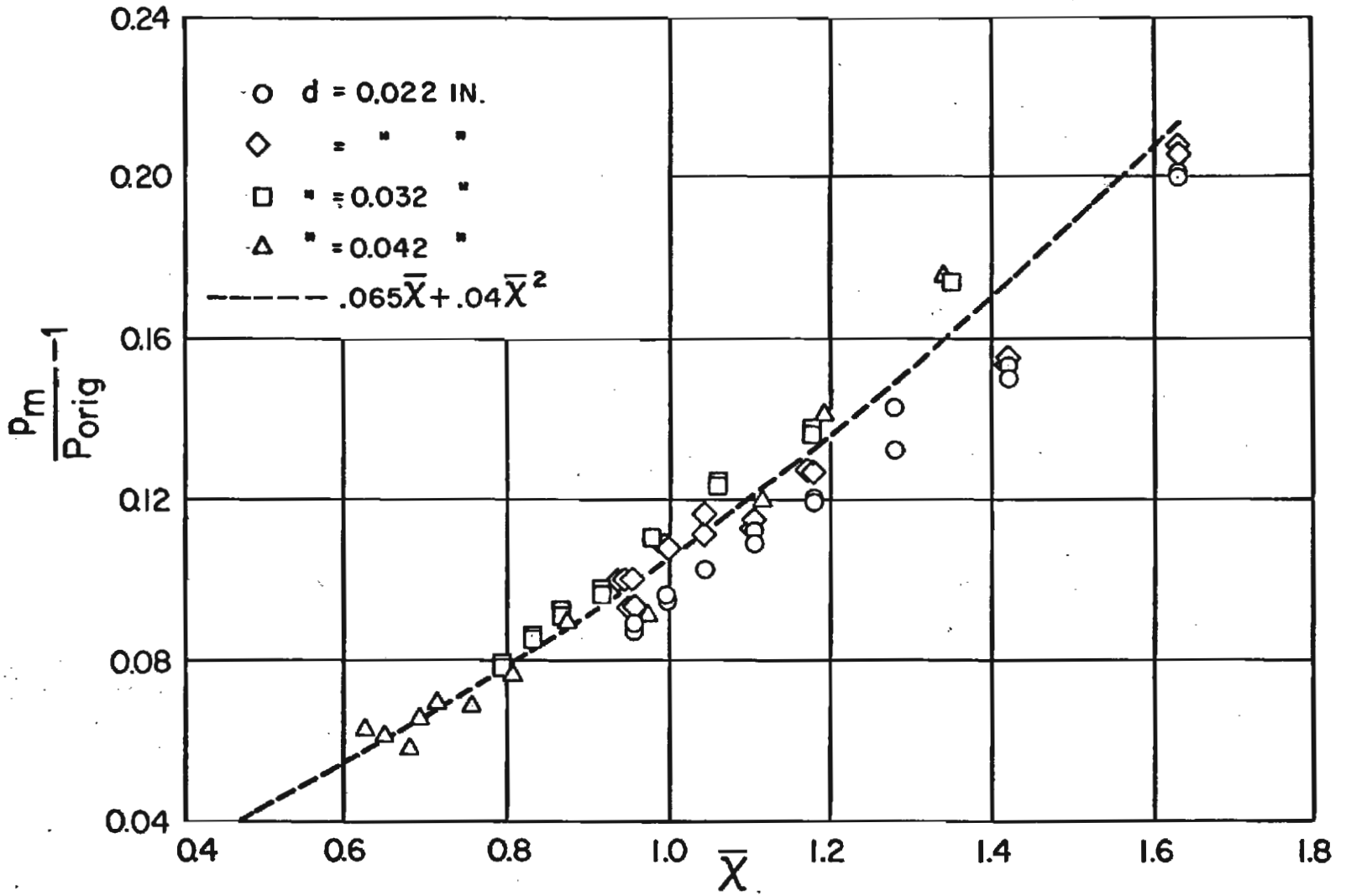

FIG. 9 VISCOUS INTERACTION ON THE STATIC PROBE (CONE-CYLINDER) MEASURED AT $M_\infty = 6.0 - 6.1$

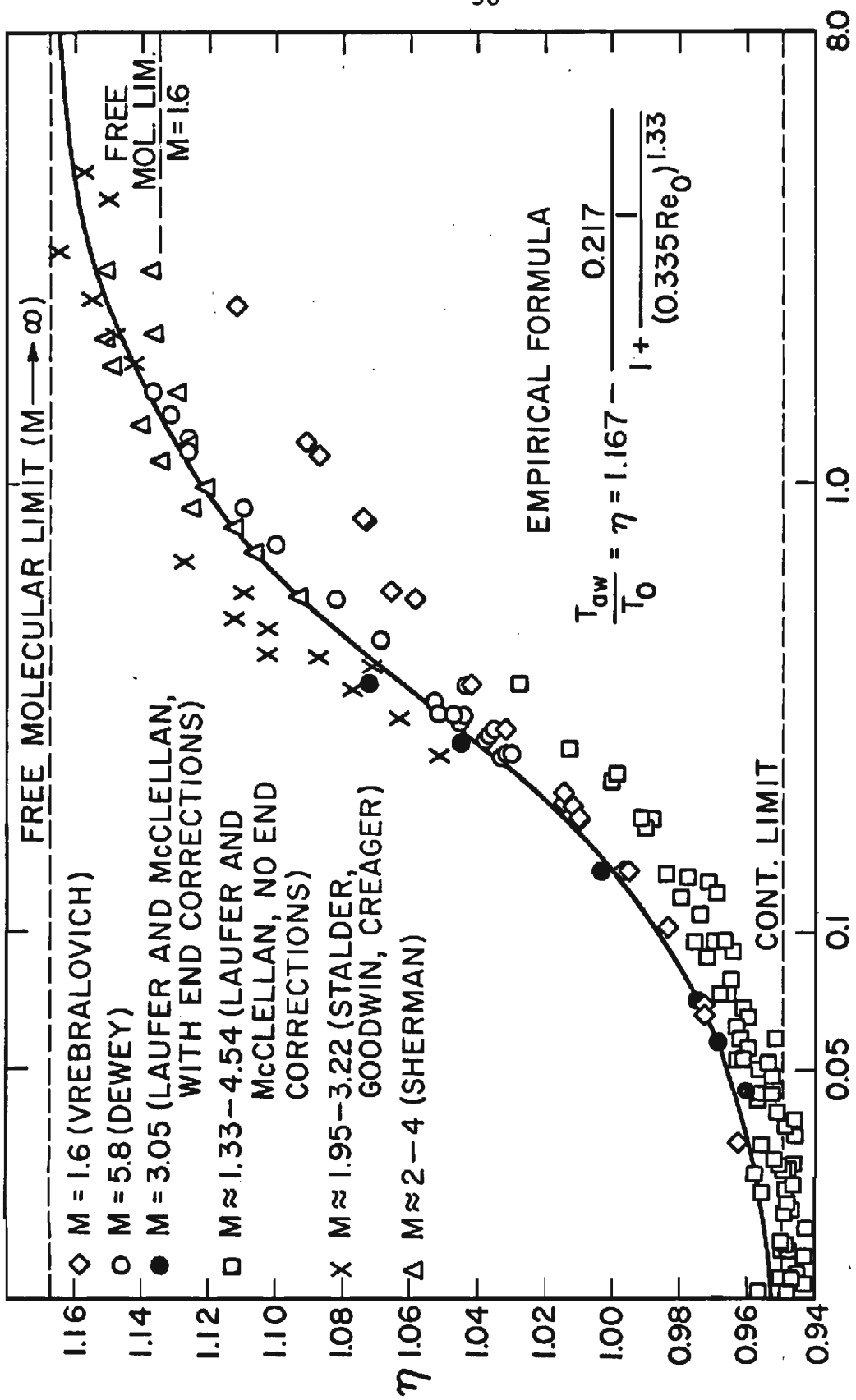

FIG.10 RECOVERY FACTOR VARIATION IN THE TRANSITION RANGE

TOP VIEW

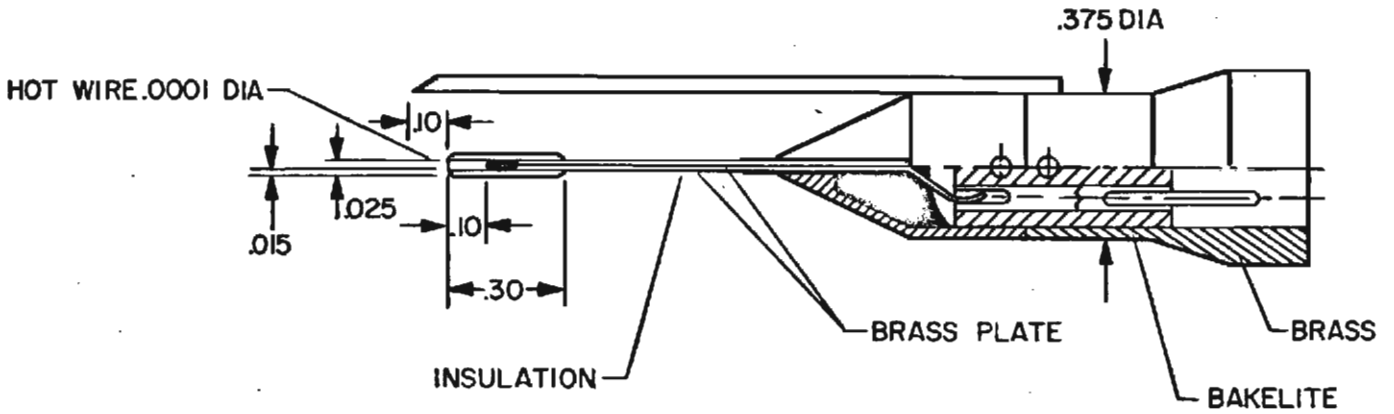

SIDE VIEW

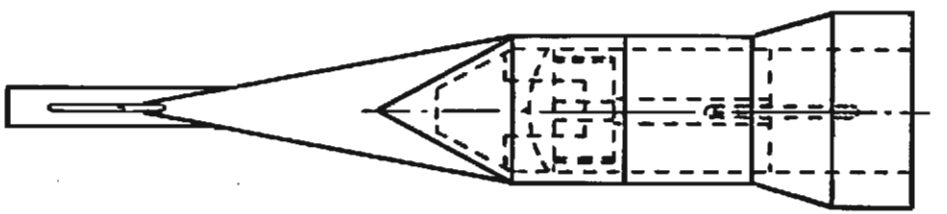

NOTE: DIMENSIONS ARE IN INCHES
SCALE 2:1

FIG. 11 HOT WIRE PROBE

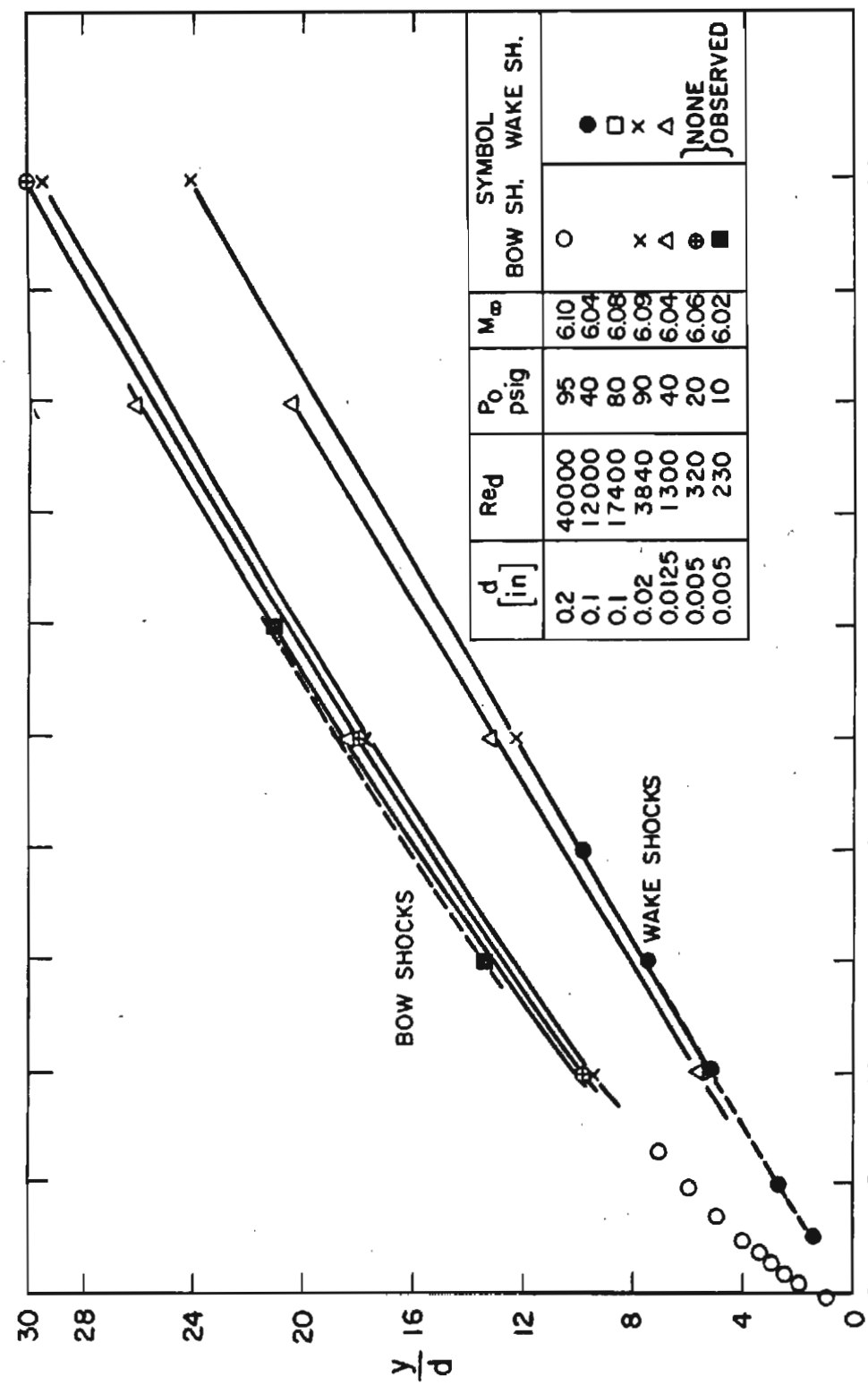

FIG. 12 BOW SHOCK-AND WAKE SHOCK-SHAPES

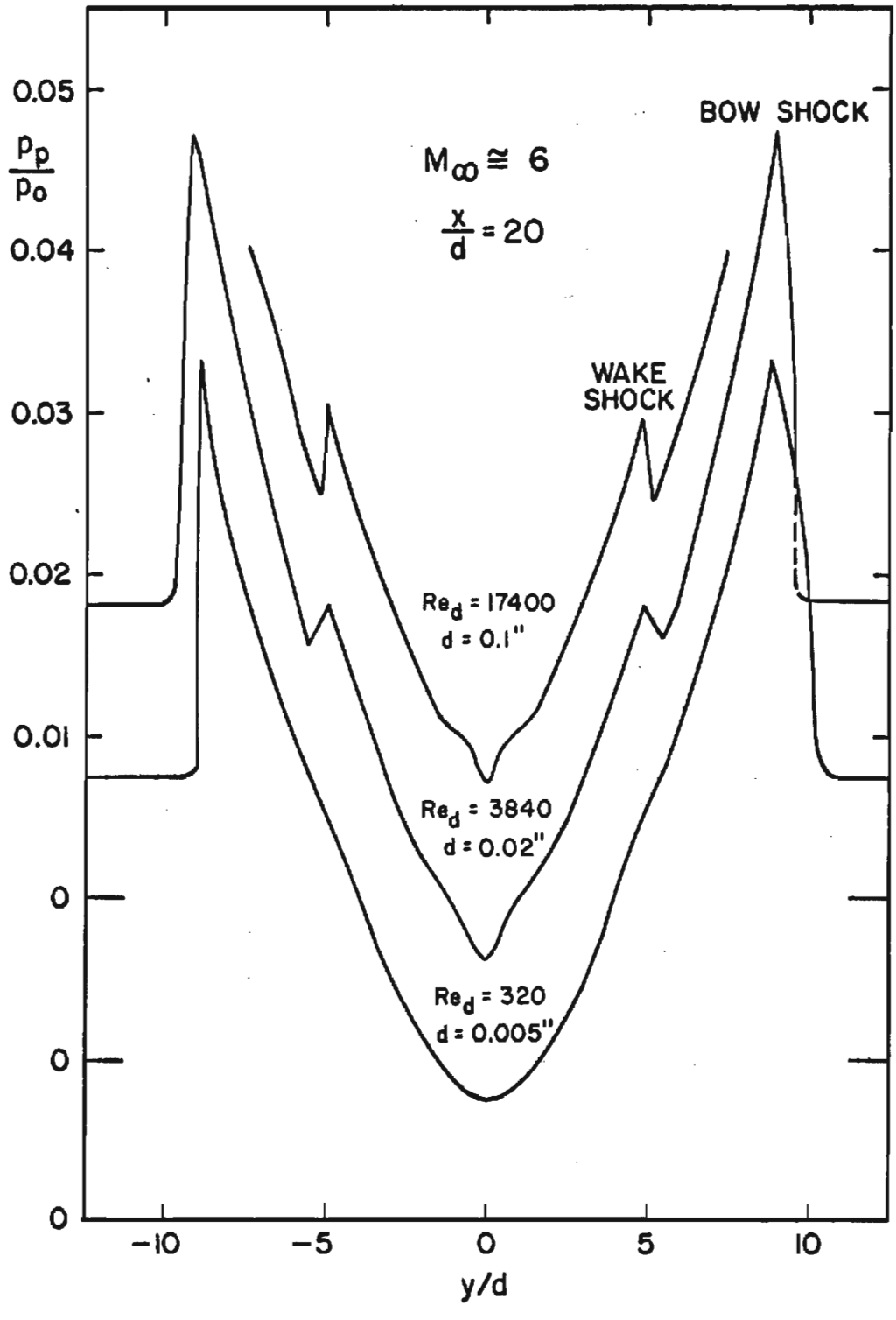

FIG. 13 PITOT PRESSURE TRACES AS A FUNCTION OF REYNOLDS NUMBER AT x/d = 20

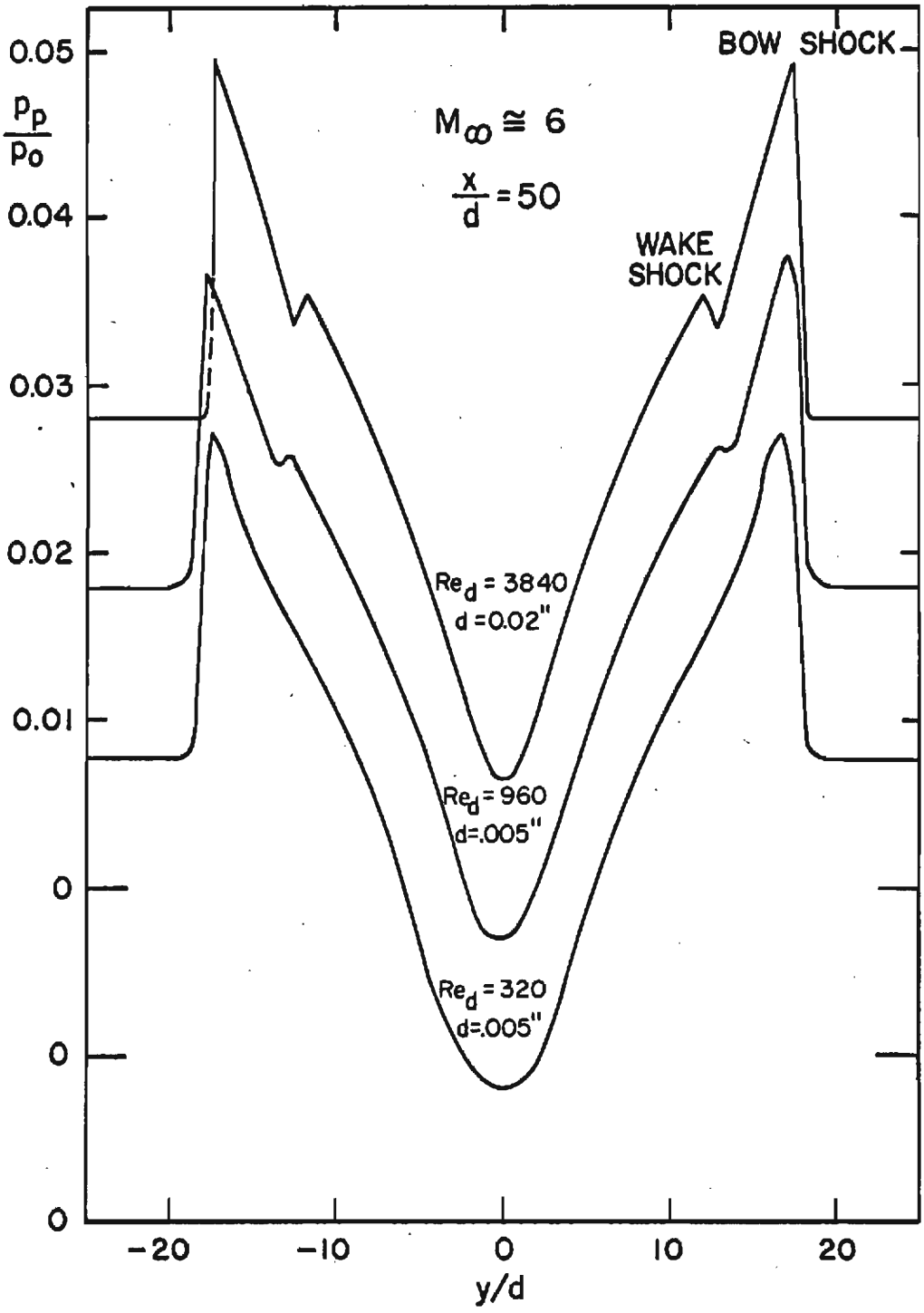

FIG. 14 PITOT PRESSURE TRACES AS A FUNCTION OF REYNOLDS NUMBER AT x/d = 50

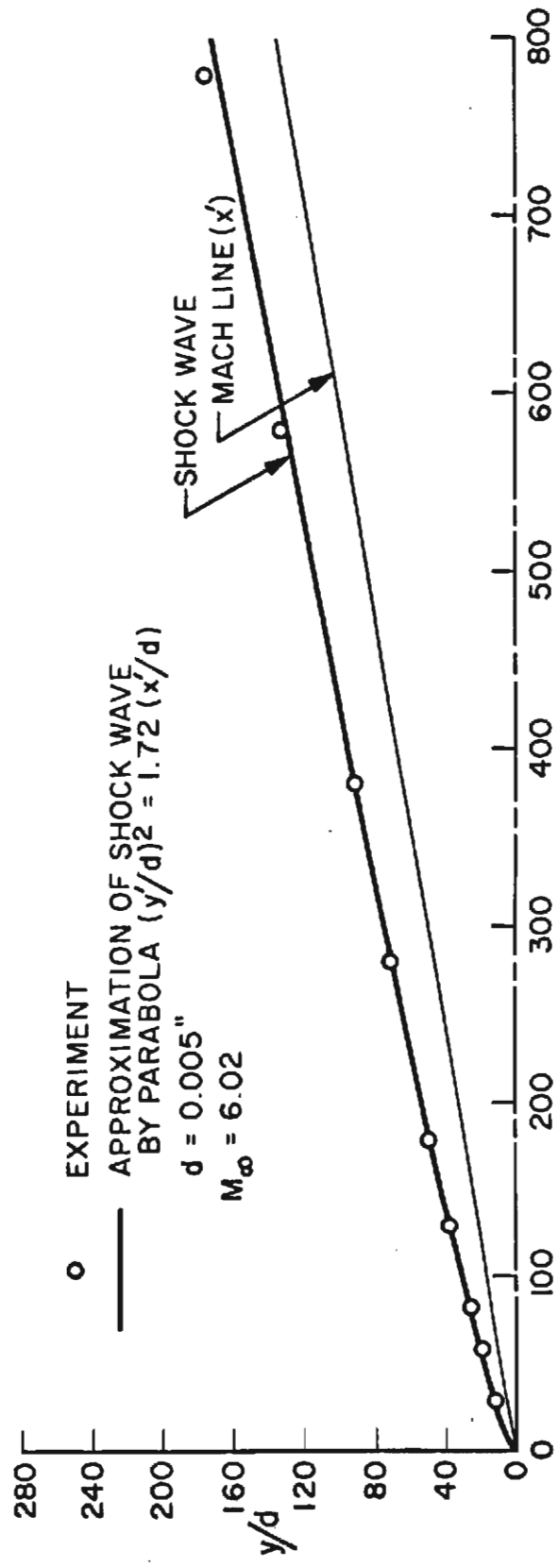

FIG. 15 SHAPE OF A BOW SHOCK ABOUT A CYLINDER

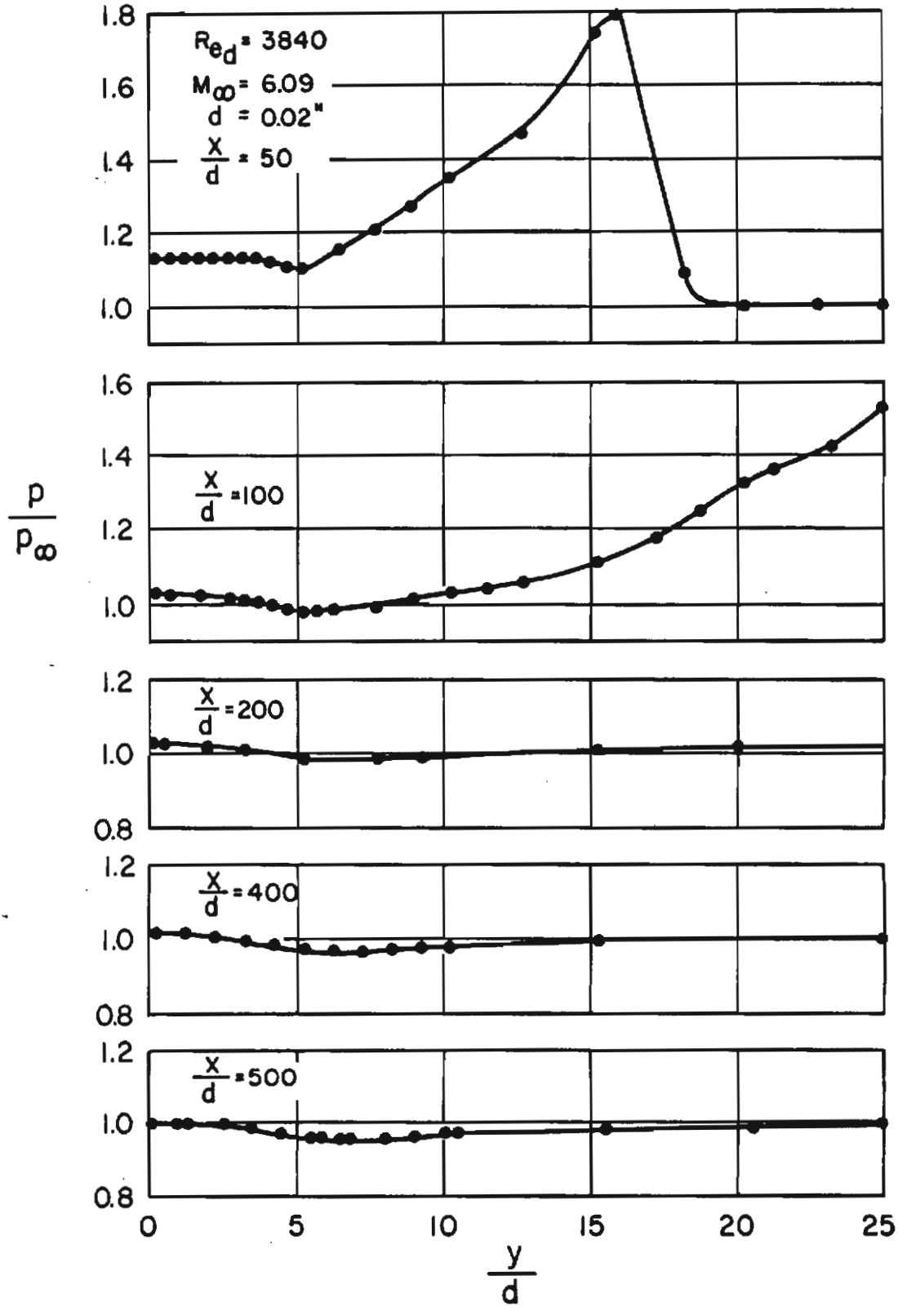

FIG. 16 STATIC PRESSURE DISTRIBUTION

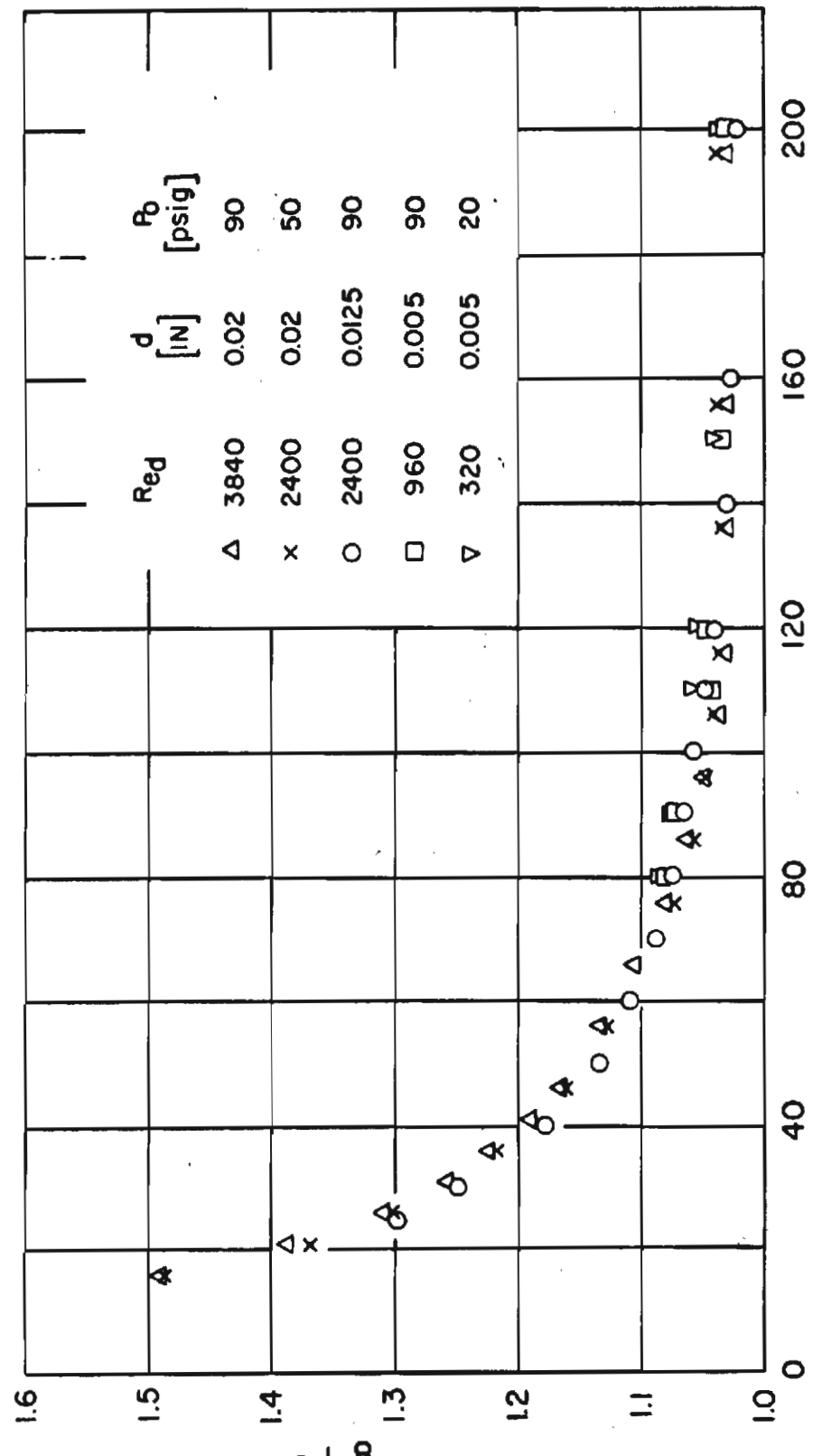

FIG. 17 STATIC PRESSURE VARIATION ON THE CENTERLINE OF THE WAKE

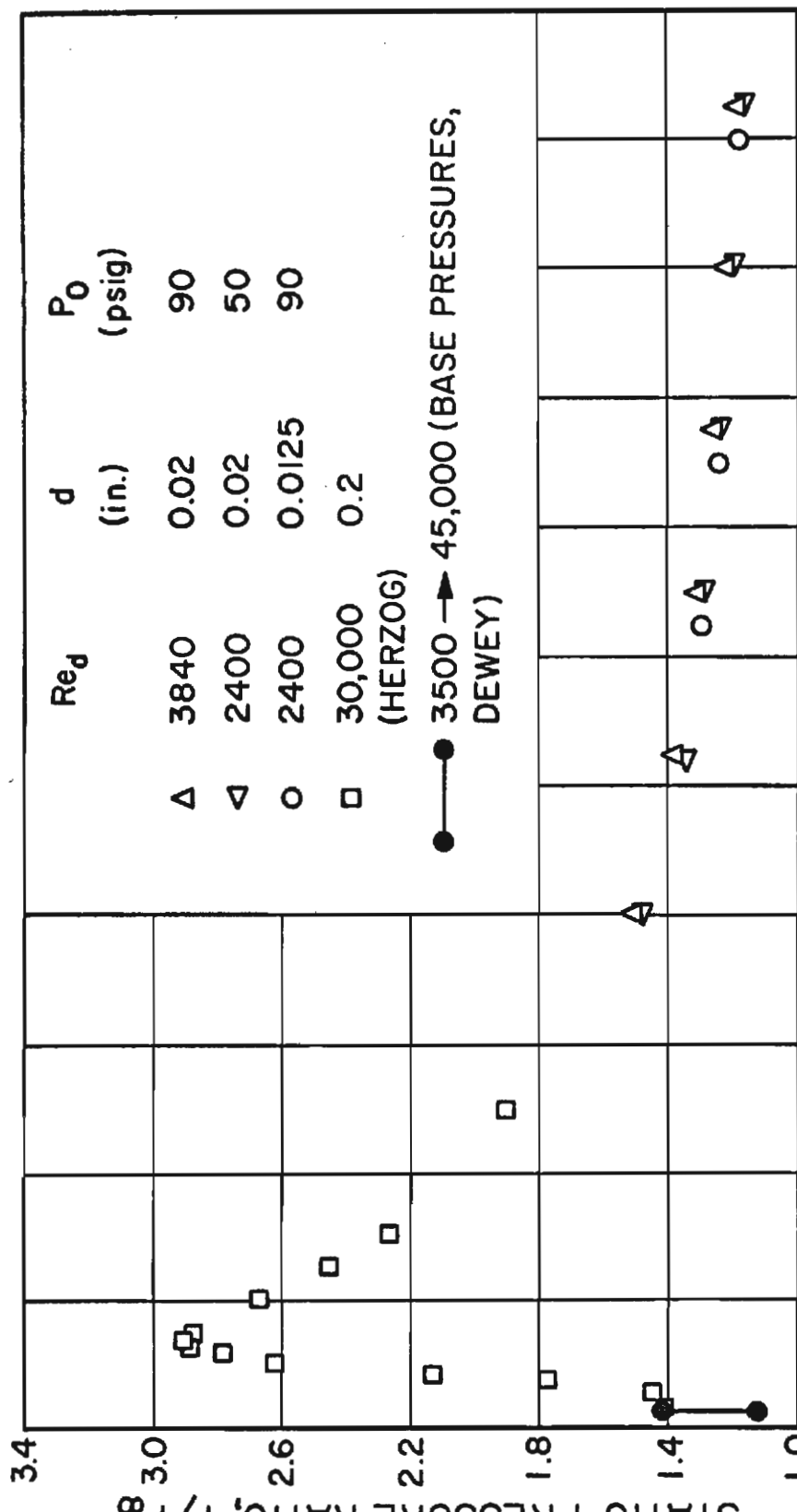

FIG. 18 STATIC PRESSURE ON THE CENTERLINE OF THE WAKE

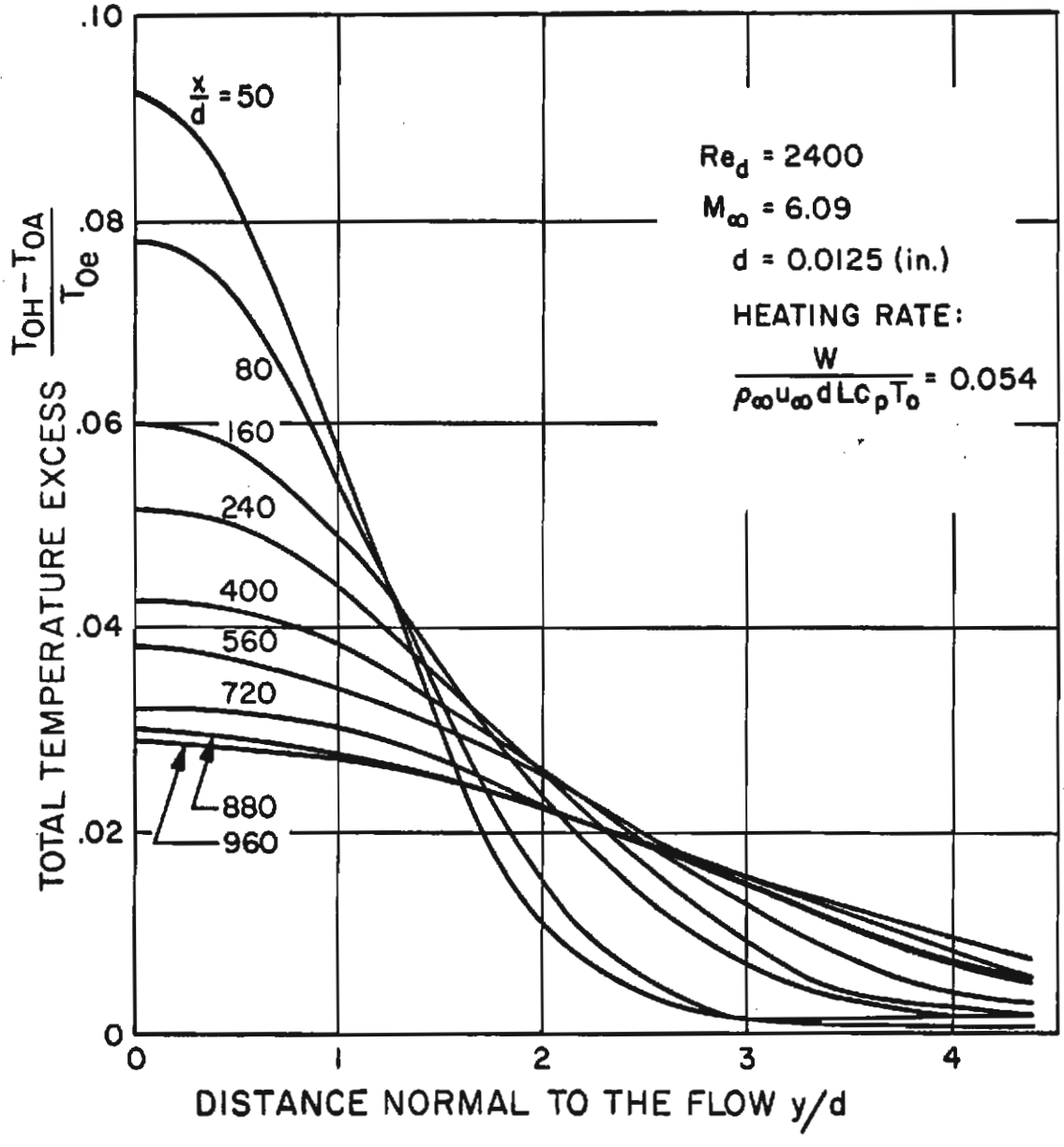

FIG.19 TOTAL TEMPERATURE EXCESS PROFILES OF HEATED OVER UNHEATED WAKE

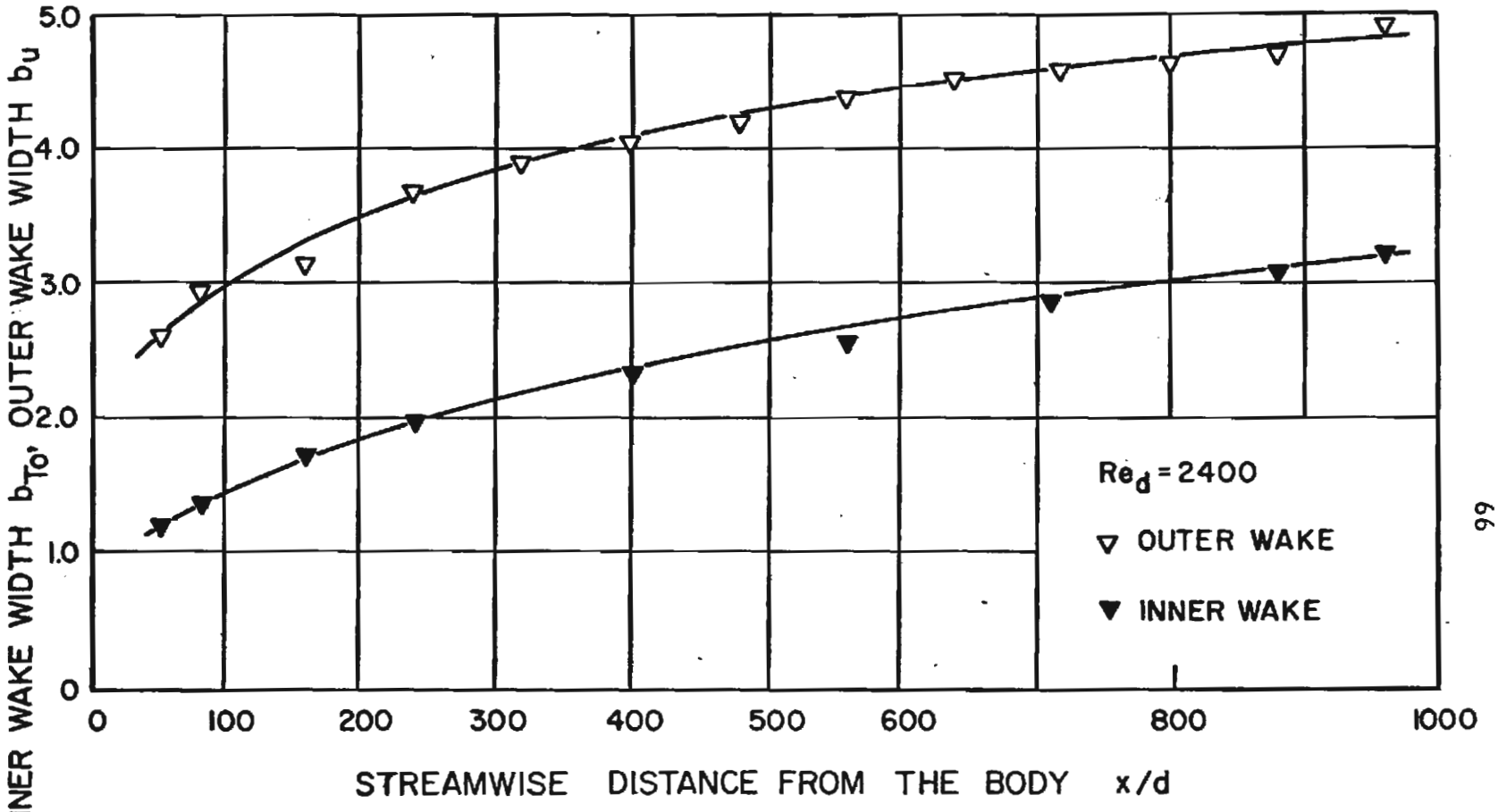

FIG.20 GROWTH OF INNER (TOTAL TEMP.) WAKE AND OUTER WAKE (VELOCITY)

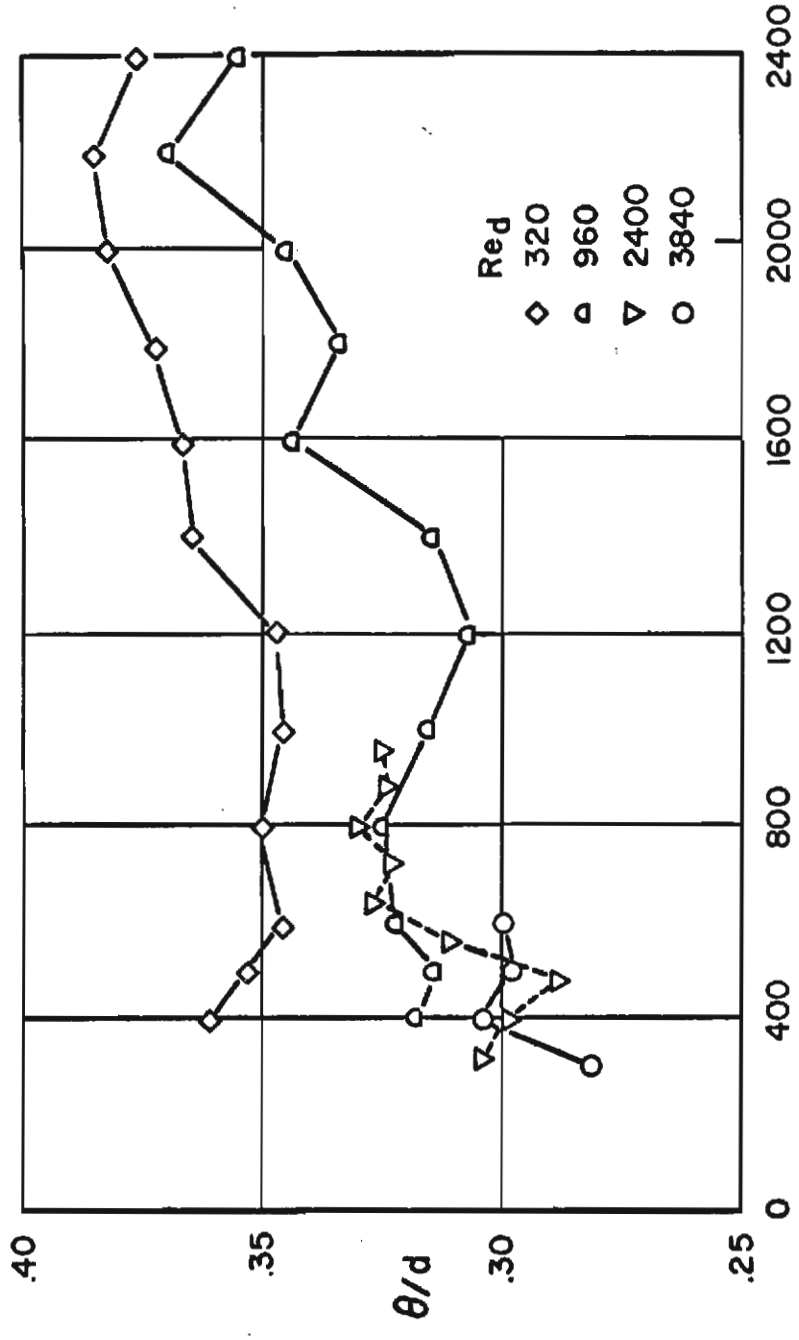

FIG. 21 LOCAL MOMENTUM THICKNESS CALCULATED FROM EXPERIMENTAL RESULTS

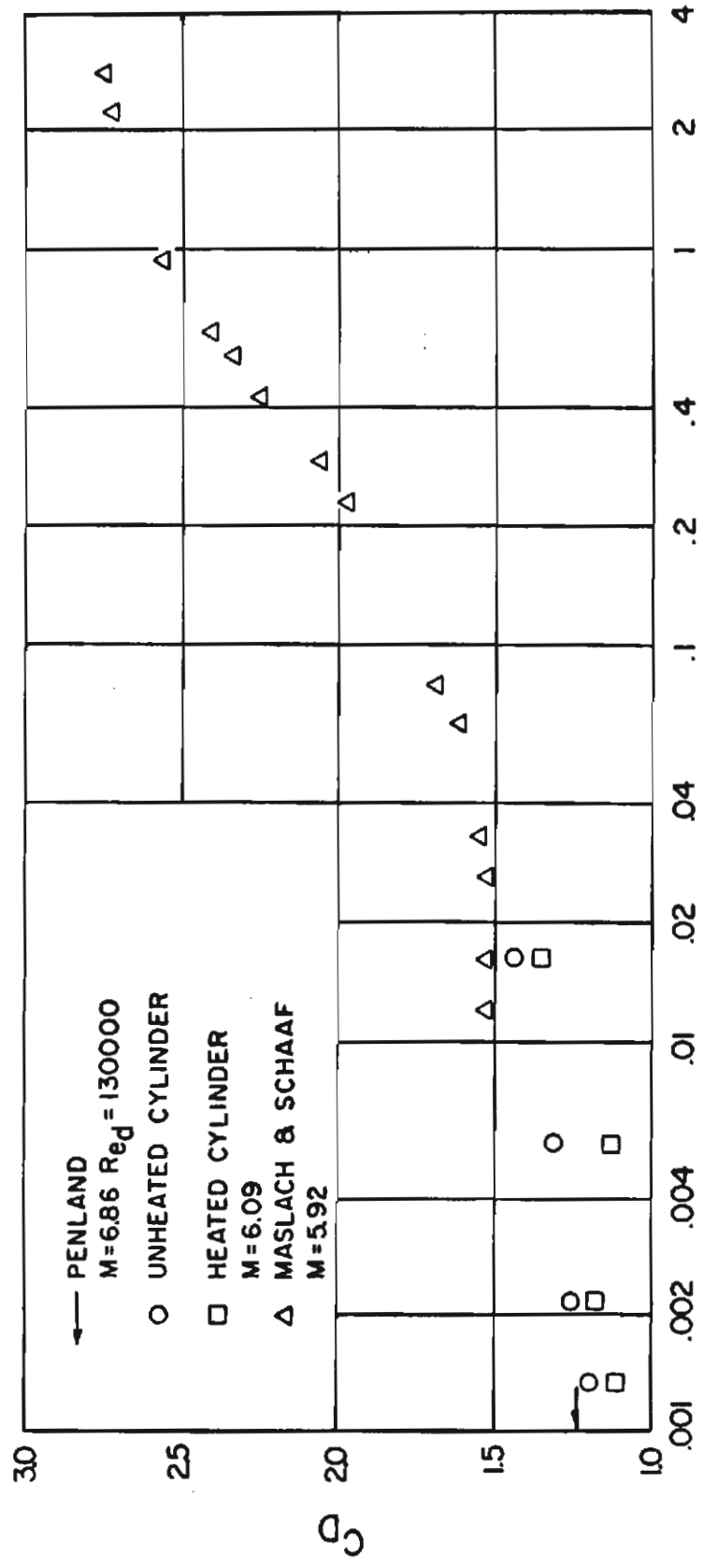

FIG. 22 DRAG COEFFICIENTS AS CALCULATED FROM MOMENTUM DEFECT

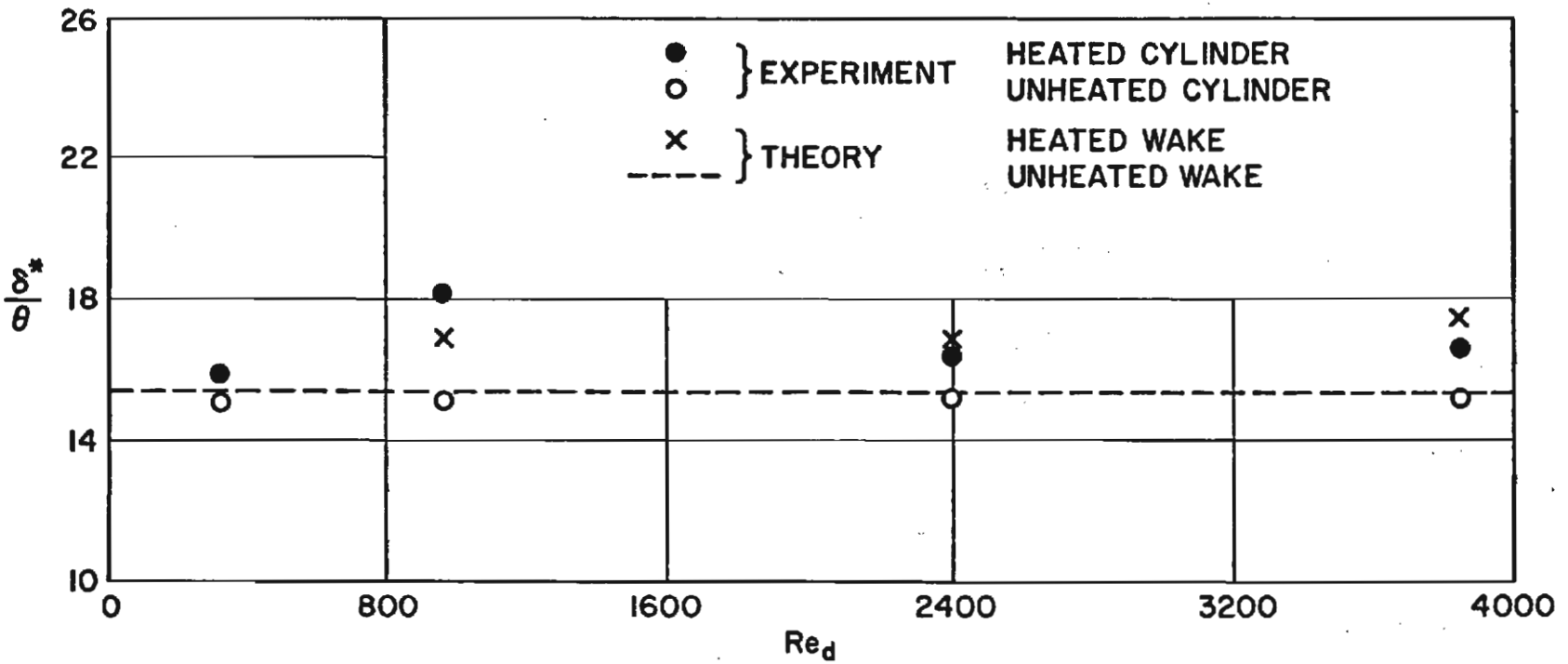

FAR WAKE: $\frac{\delta^*}{\theta} = 1+(\gamma-1)M_e^2+\left[1+\frac{\gamma-1}{2}M_e^2\right]\frac{(T_{o\mathbb{C}}-T_{oe})/T_{oe}}{(u_e-u_{\mathbb{C}})/u_e}$ (EQU. 4.3)

AT $M_e = 6.0$ $\left(\frac{\delta^*}{\theta}\right)_{UNH.W.} = 15.4$ $(\gamma = 1.4)$

FIG. 23 FORM-PARAMETER IN THE FAR WAKE AT SEVERAL REYNOLDS NUMBERS

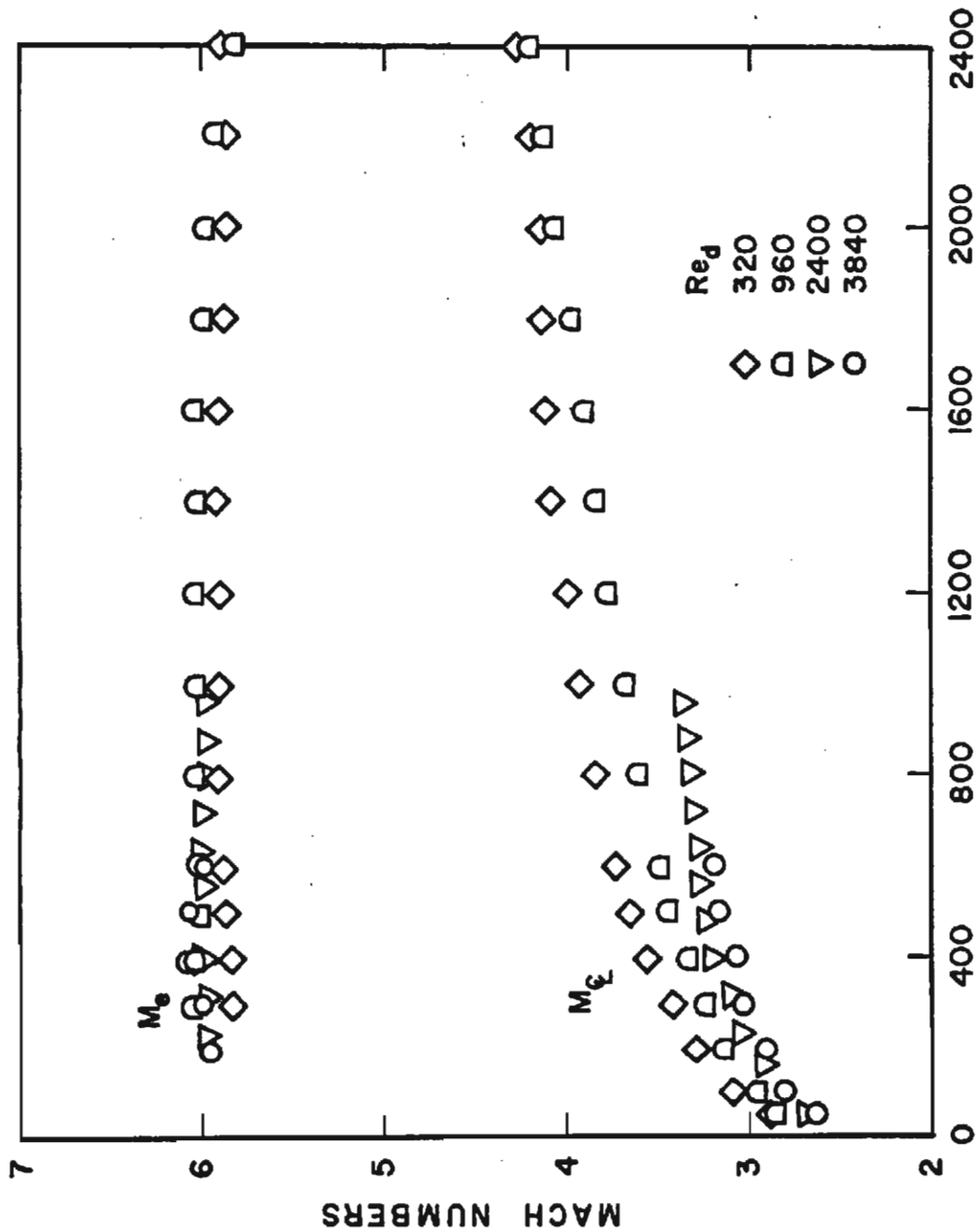

FIG. 24 MACH NUMBER ON THE CENTER LINE OF THE WAKE

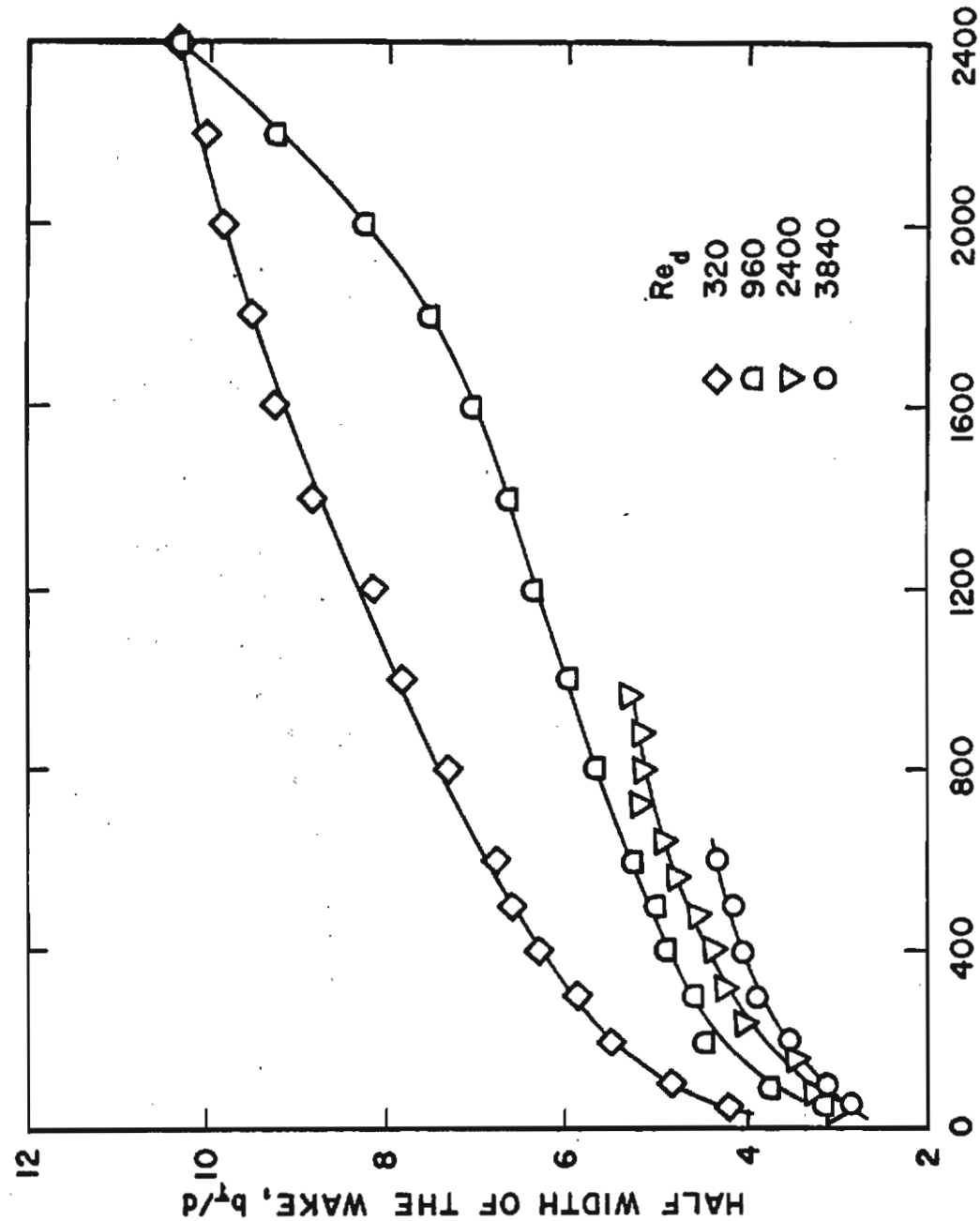

FIG. 25 WIDTH OF THE TEMPERATURE–WAKE

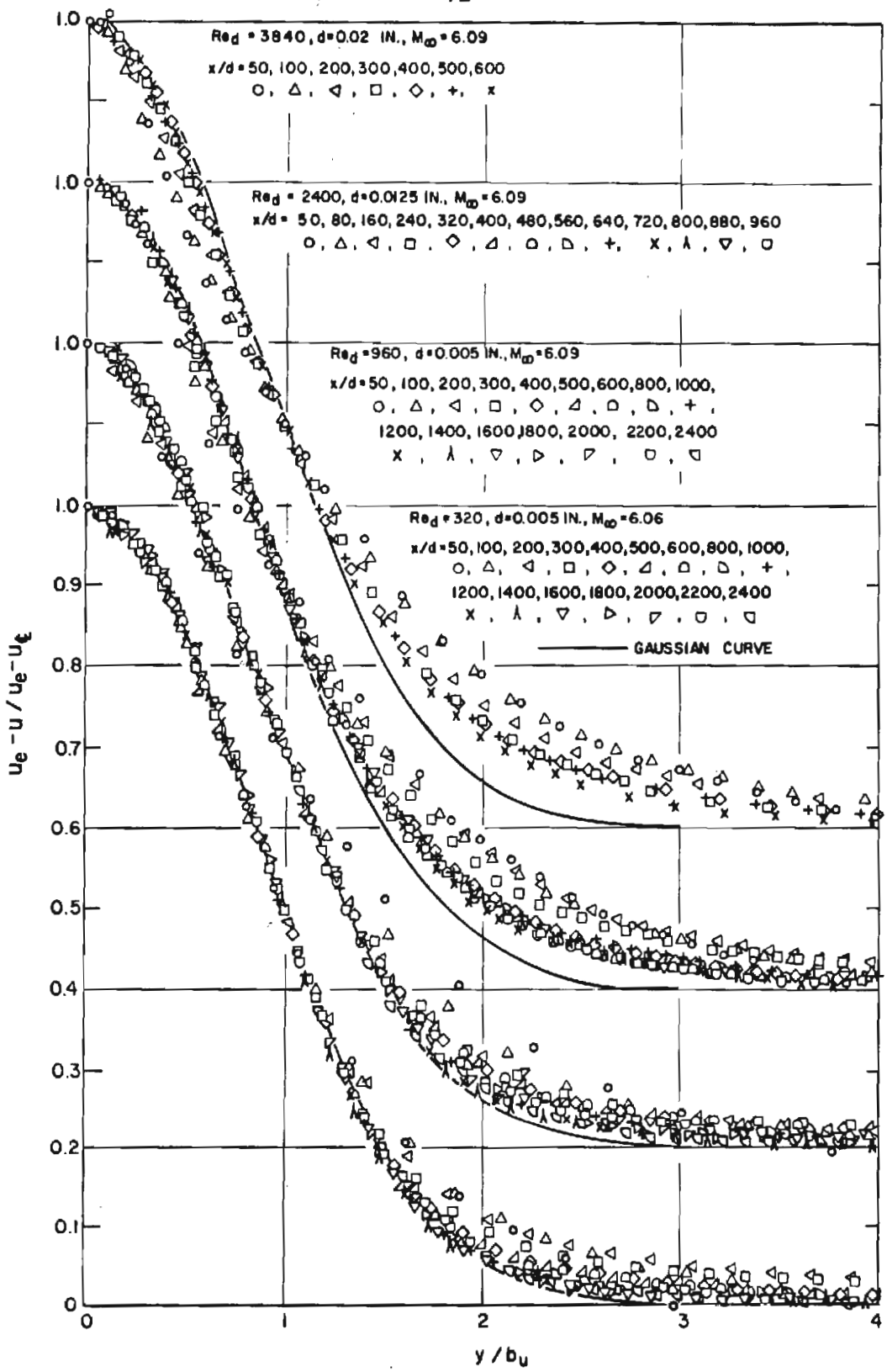

FIG.26 DEPENDENCE OF THE VELOCITY DEFECT PROFILES UPON REYNOLDS NUMBER AND DISTANCE FROM THE BODY

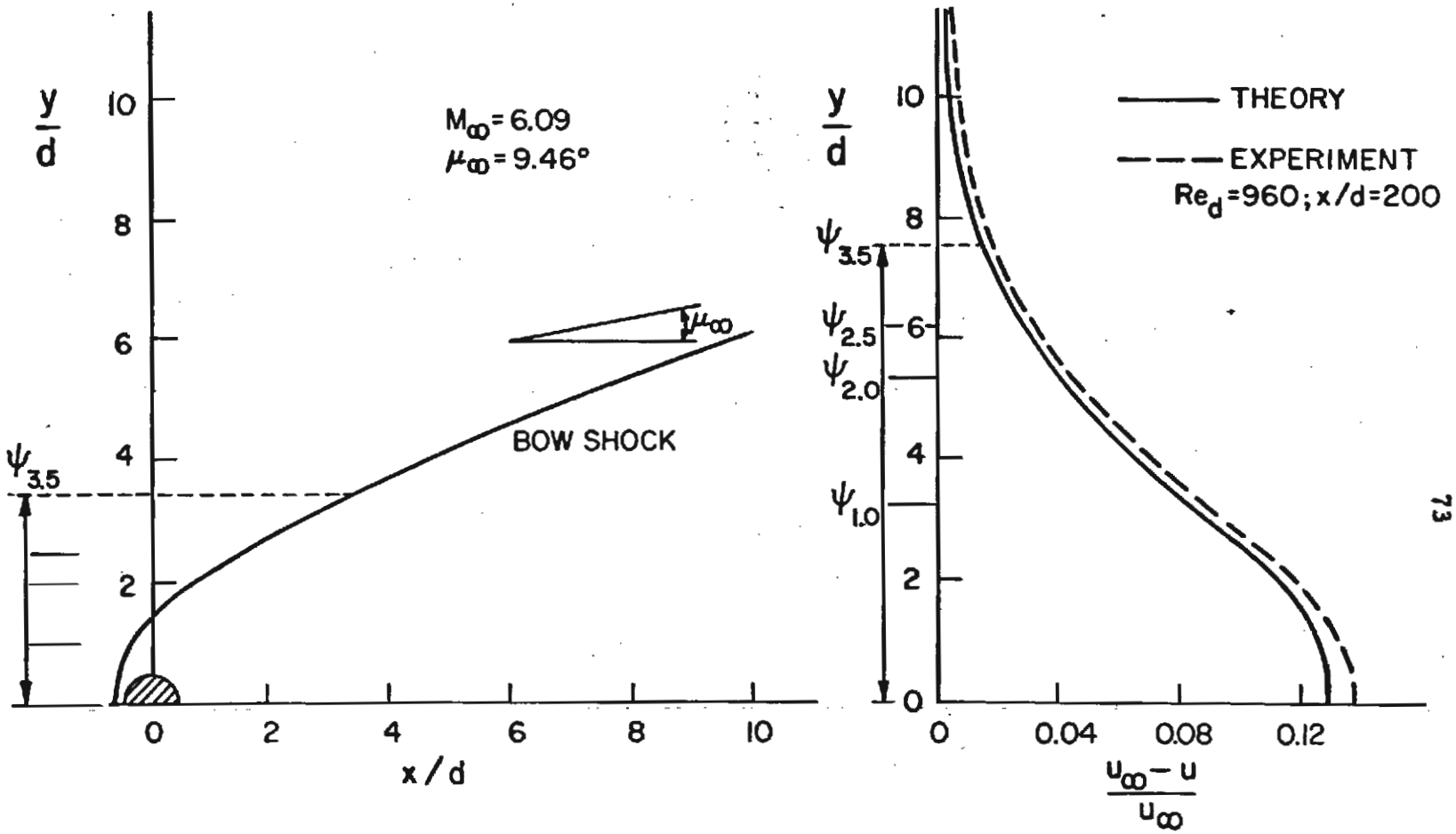

FIG. 27 VELOCITY PROFILE IN FAR WAKE GENERATED BY BOW SHOCK

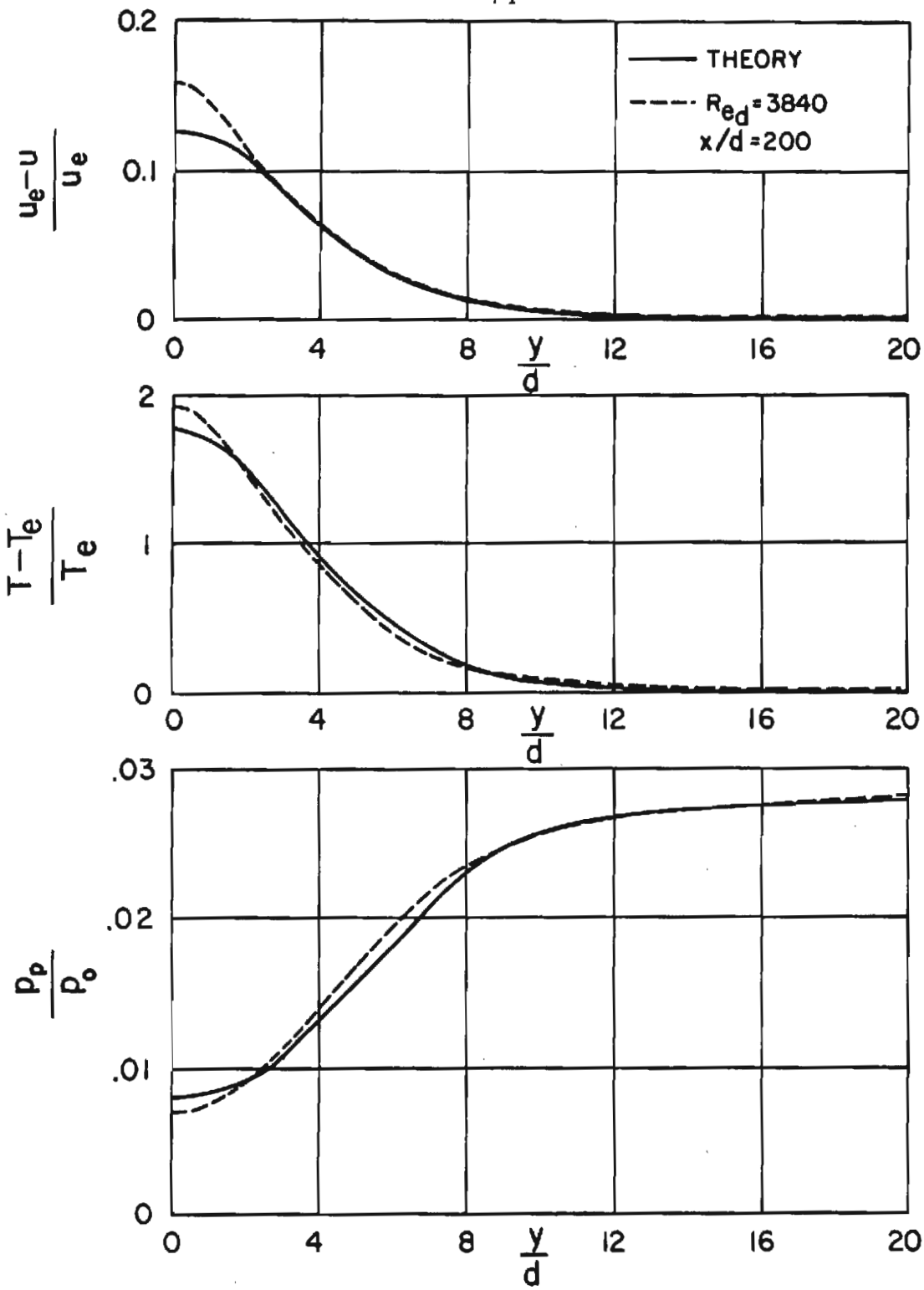

FIG. 28 FLOW PROPERTIES IN COMPARISON WITH A THEORETICAL CALCULATION

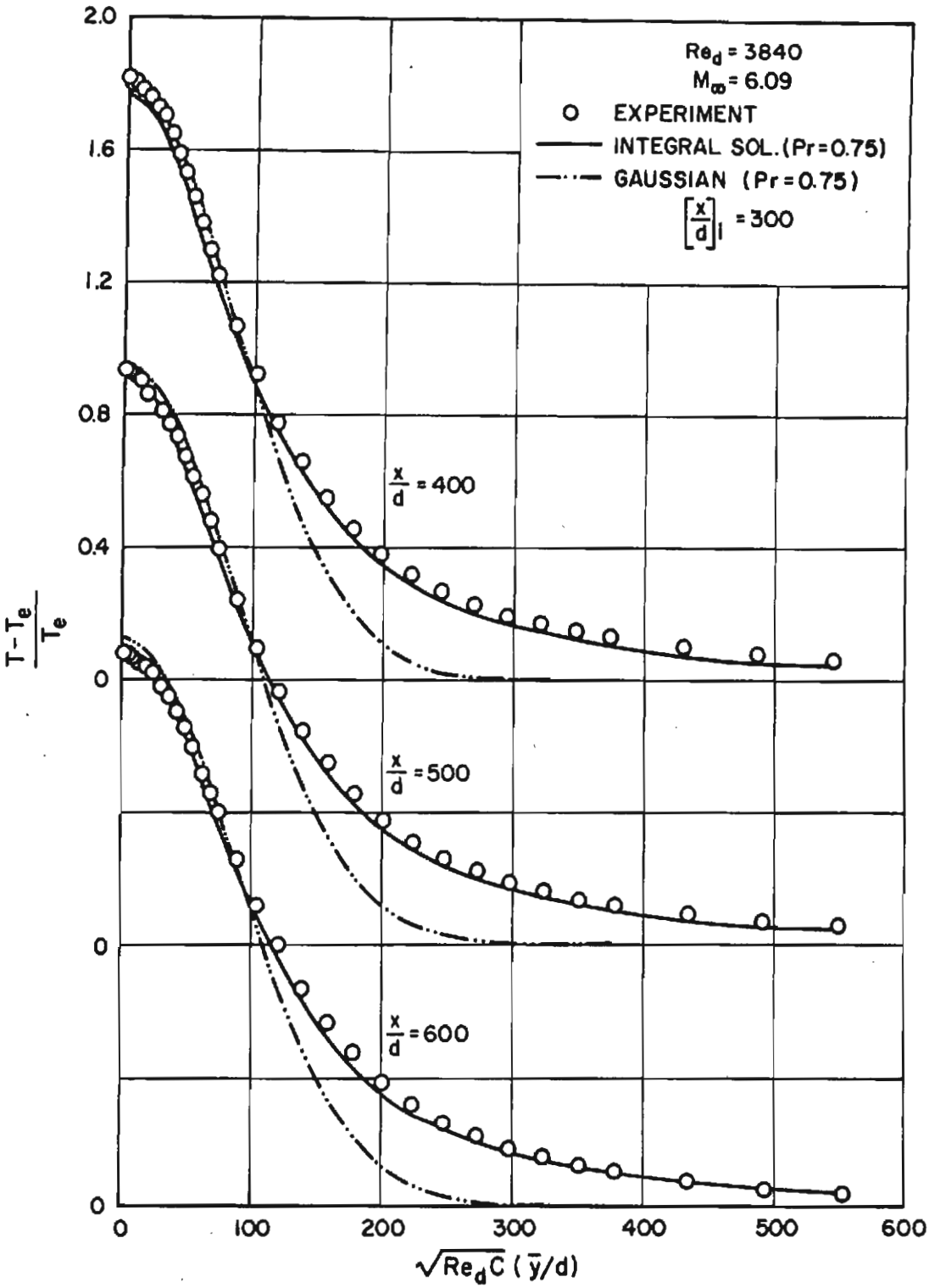

FIG. 29 TEMPERATURE PROFILES IN THE FAR WAKE AT Re_d=3840

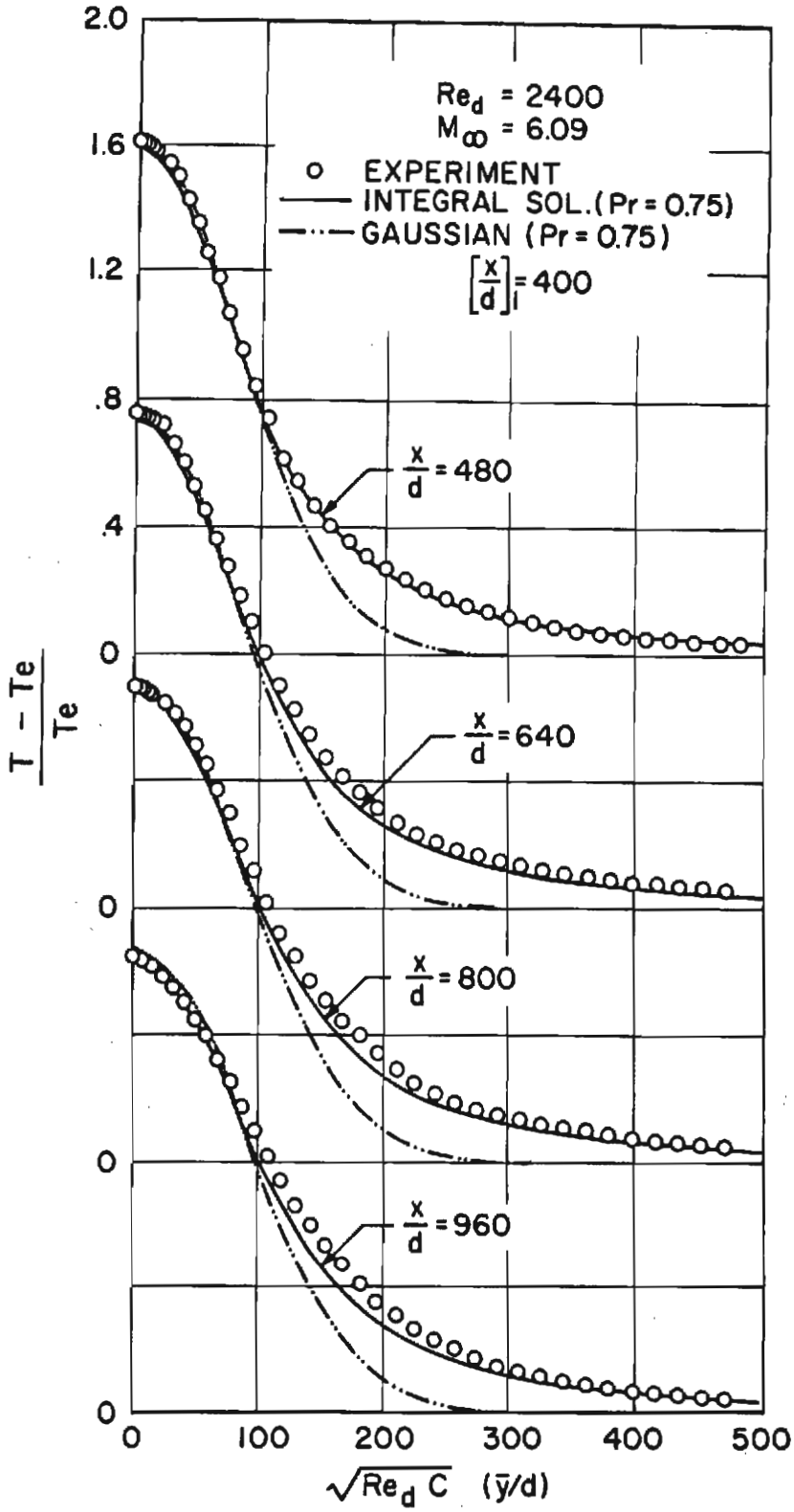

FIG. 30 TEMPERATURE PROFILES IN THE FAR WAKE AT Re_d = 2400

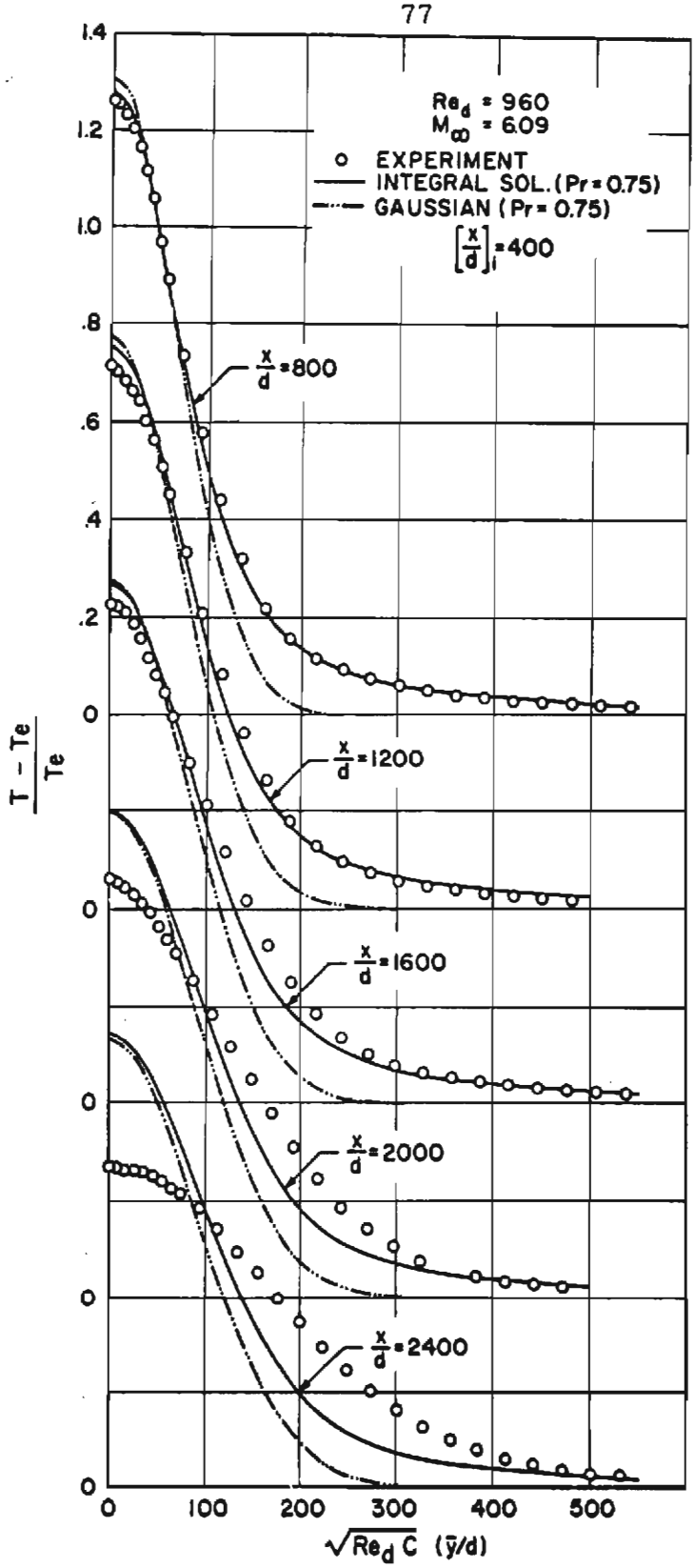

FIG. 31 TEMPERATURE PROFILES IN THE FAR WAKE AT Re_d = 960

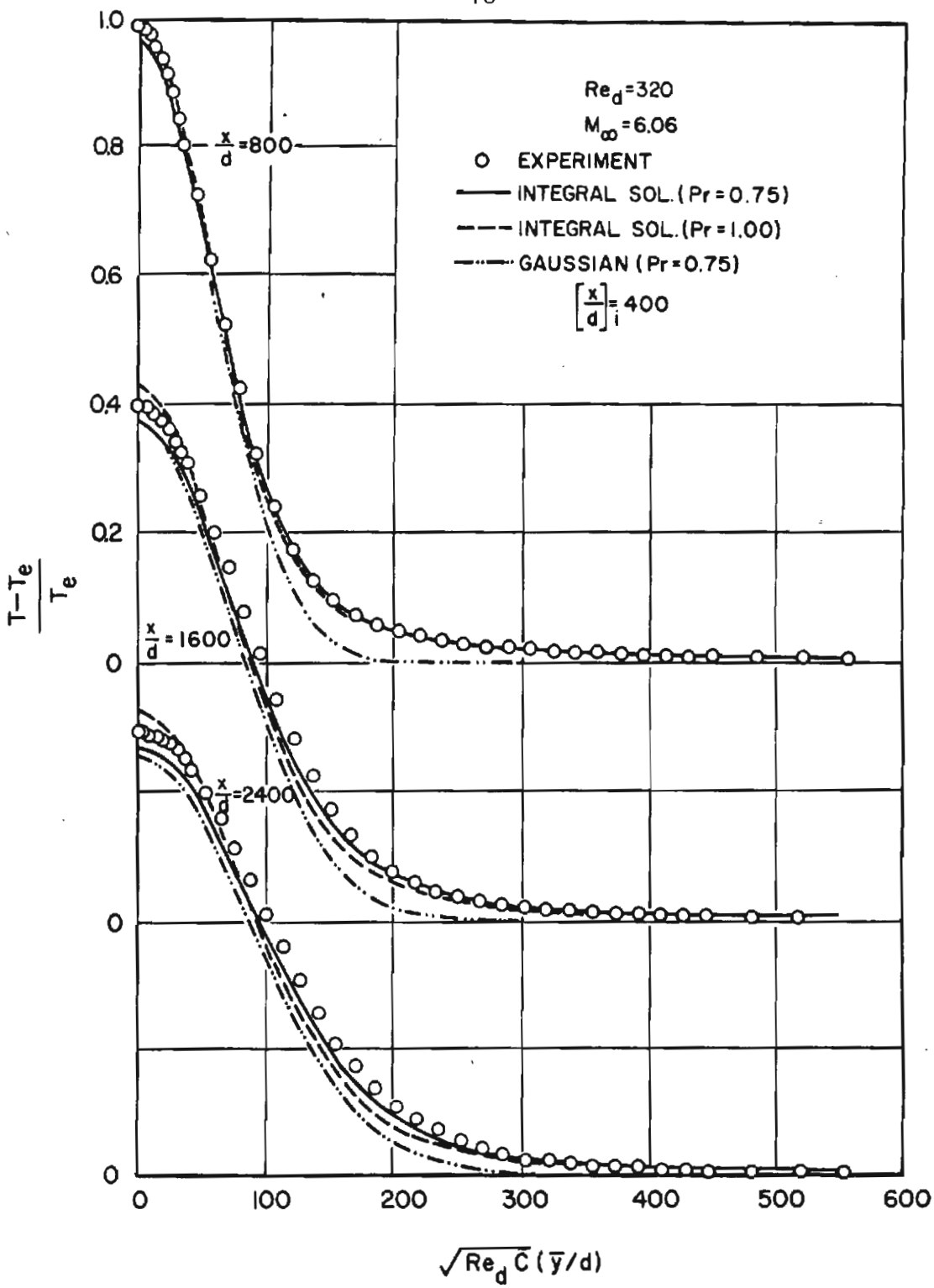

FIG. 32 TEMPERATURE PROFILES IN THE FAR WAKE AT Re_d = 320

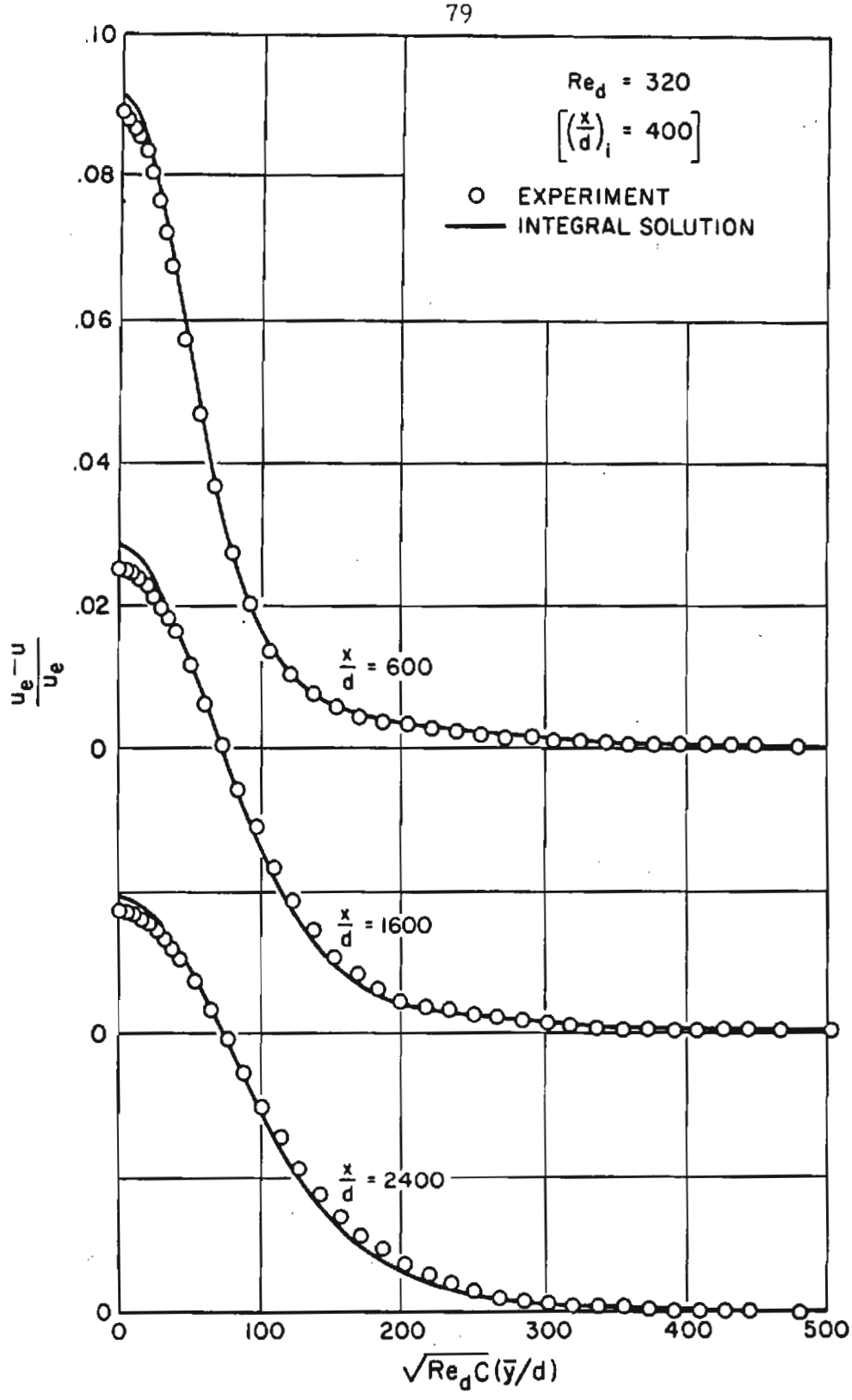

FIG. 33 VELOCITY-DEFECT DATA COMPARED TO RESULTS OF INTEGRAL-SOLUTION

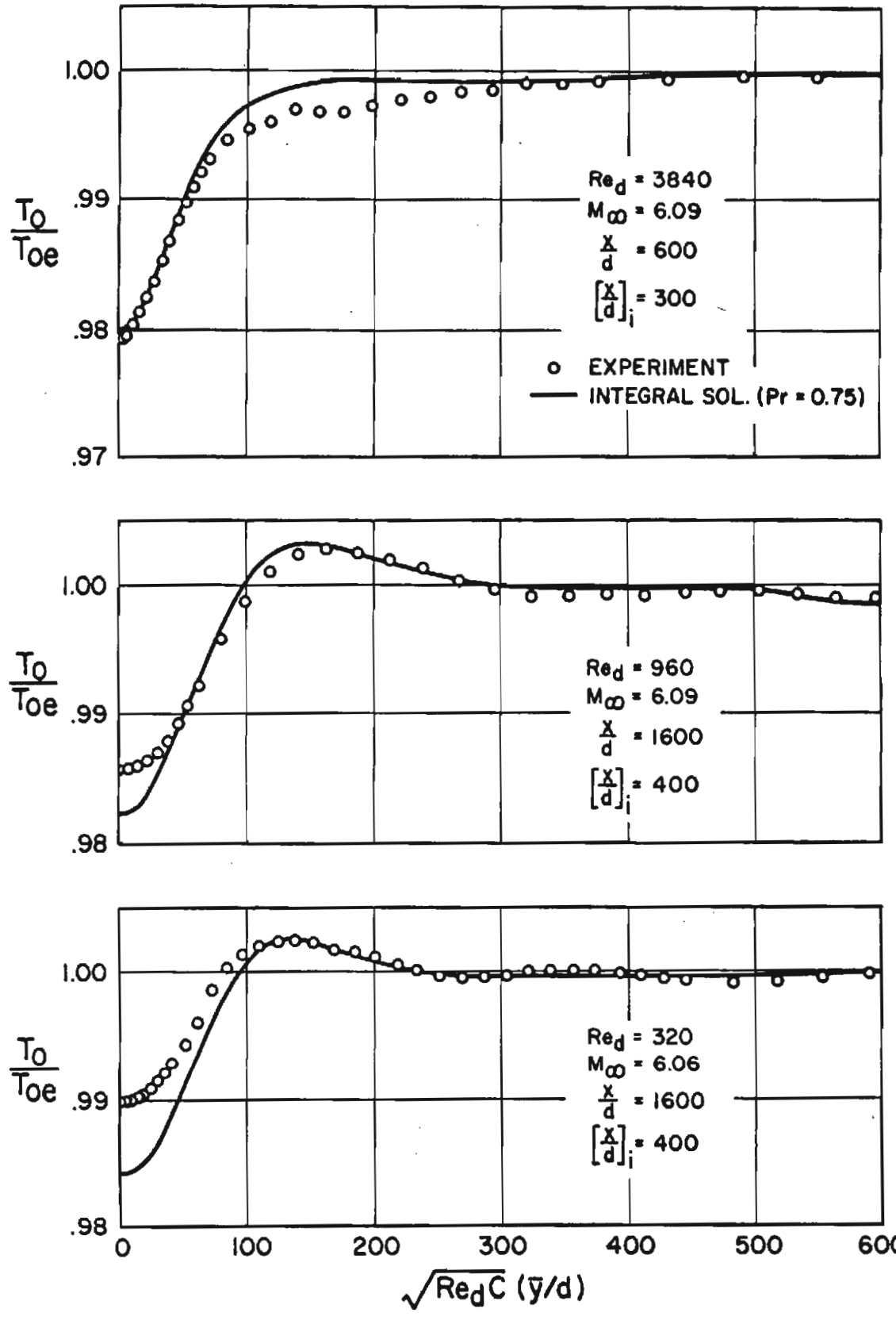

FIG. 34 TOTAL TEMPERATURE PROFILES IN WAKES

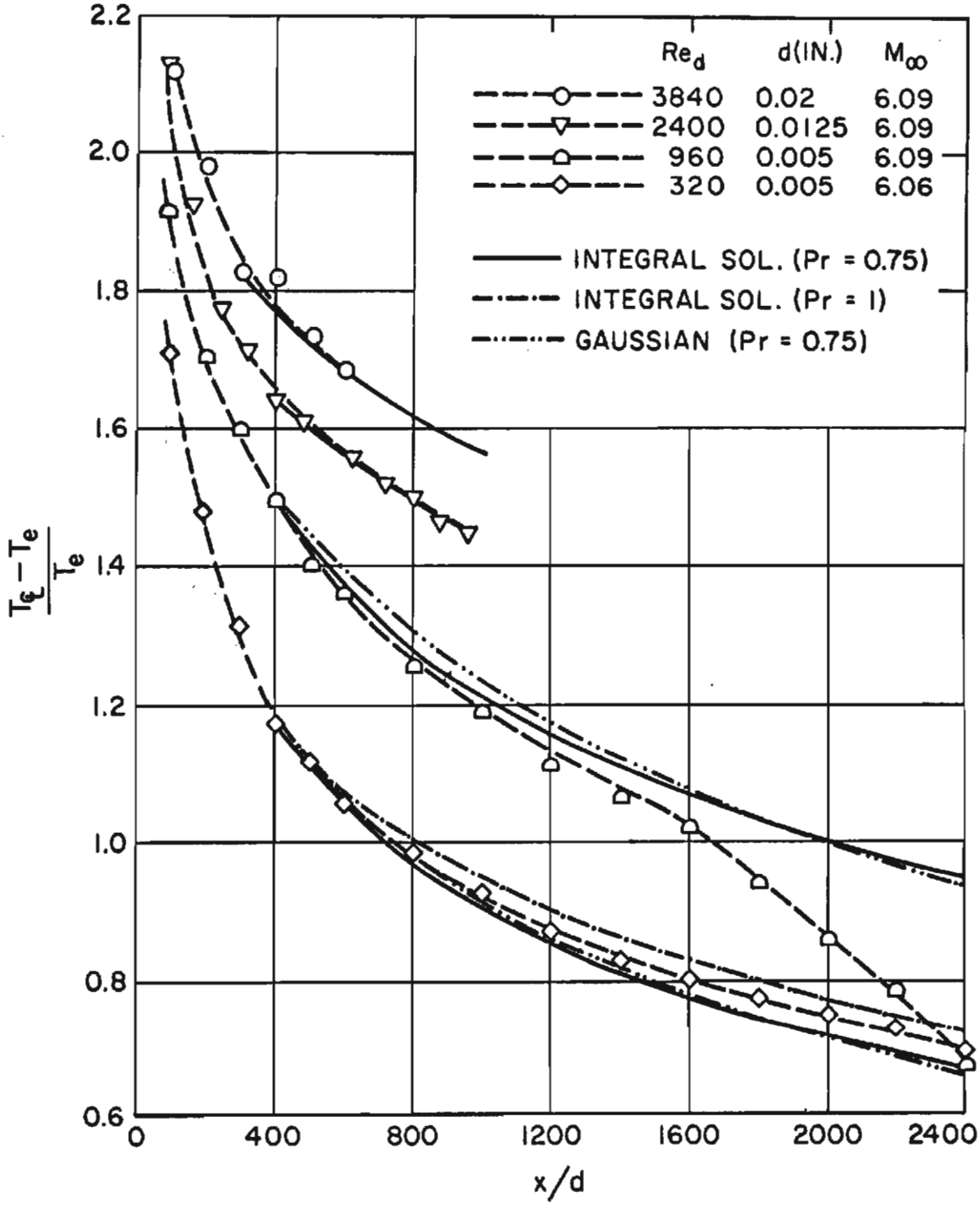

FIG.35 TEMPERATURE DECAY ALONG THE CENTERLINE OF THE WAKE

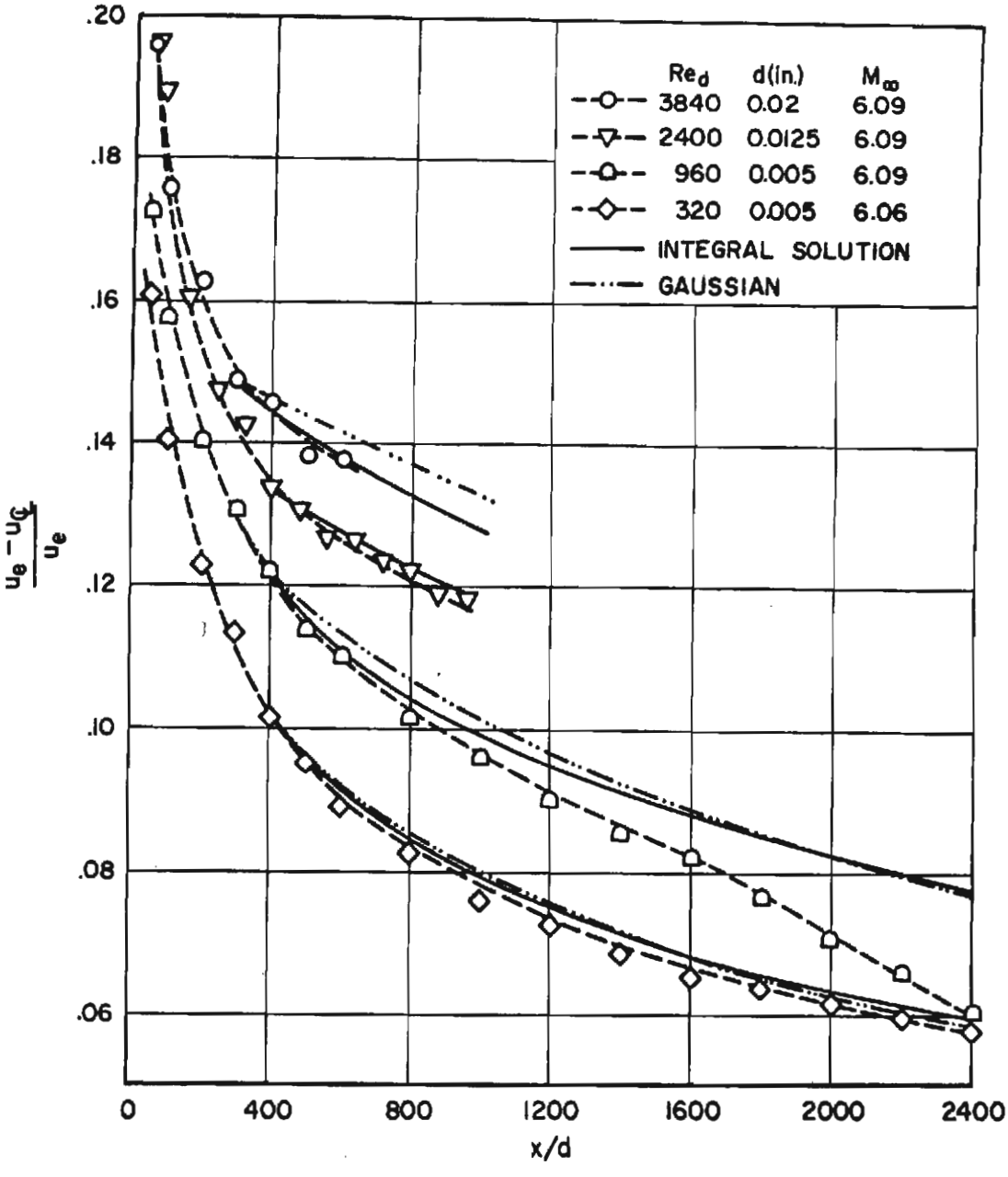

FIG. 36 VELOCITY DECAY ALONG THE CENTERLINE OF THE WAKE

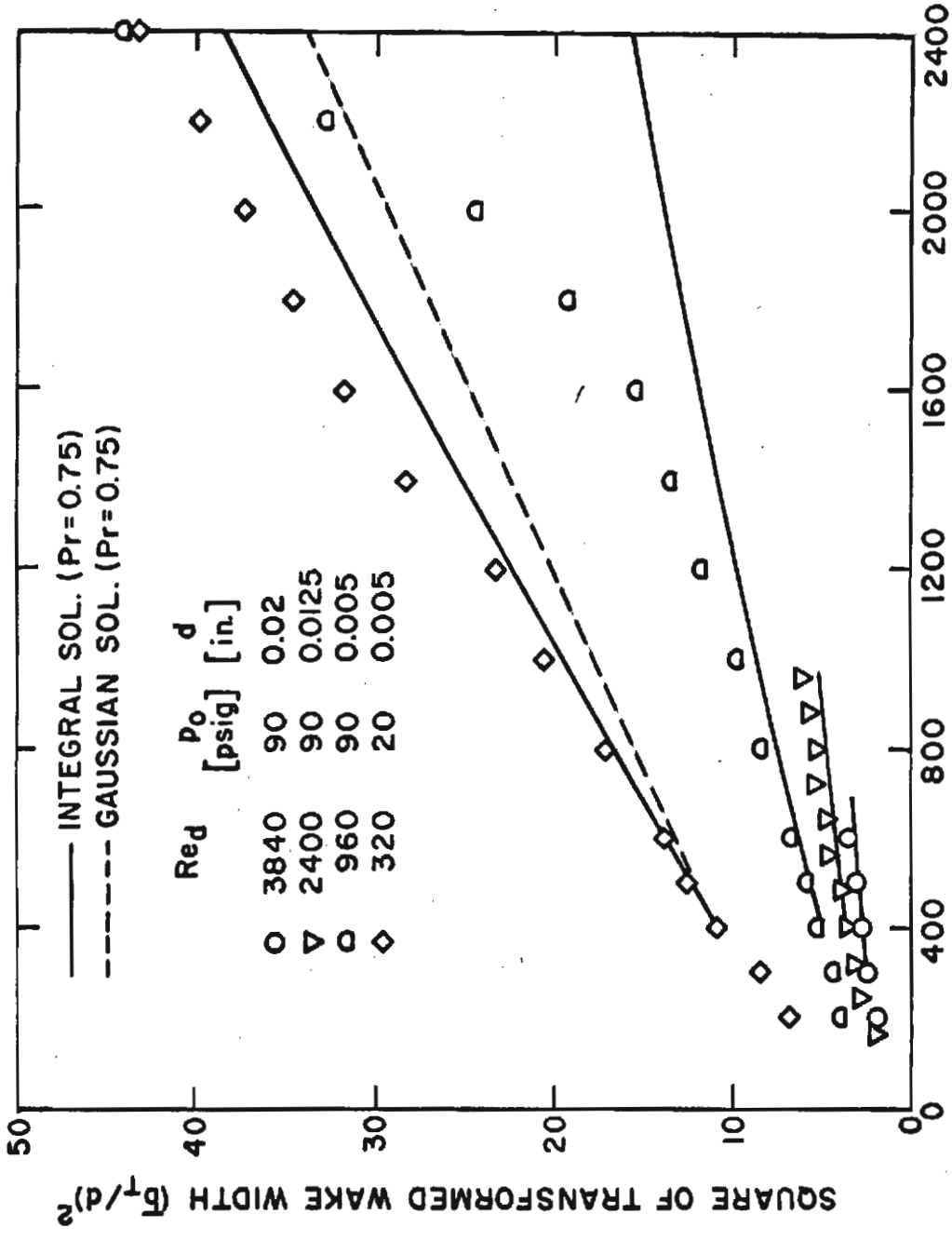

FIG. 37 EXPERIMENTAL GROWTH OF WAKES COMPARED WITH THEORY

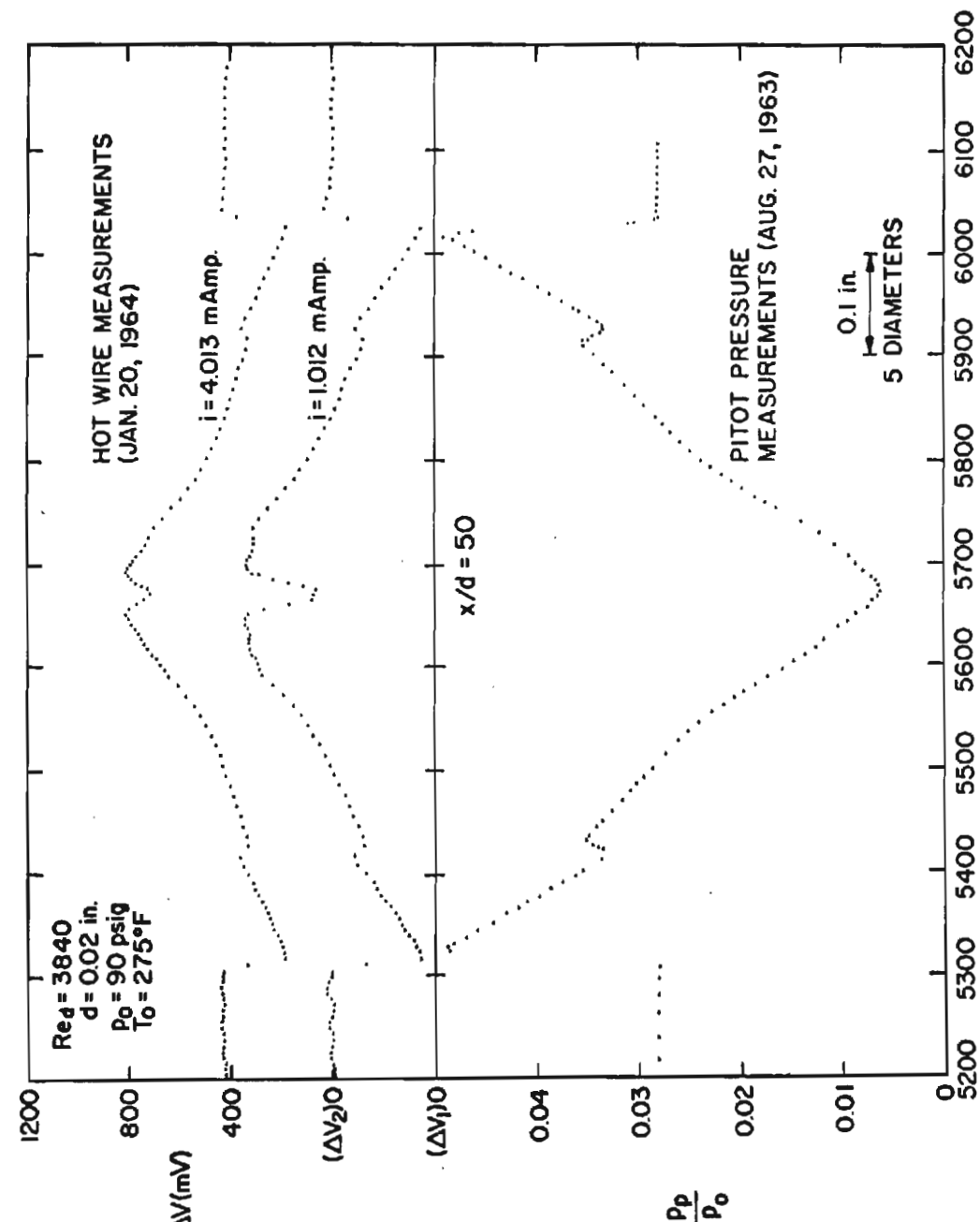

FIG. 38a RAW HOT WIRE AND PITOT PRESSURE PROFILES
AT ONE AXIAL STATION (x/d = 50)

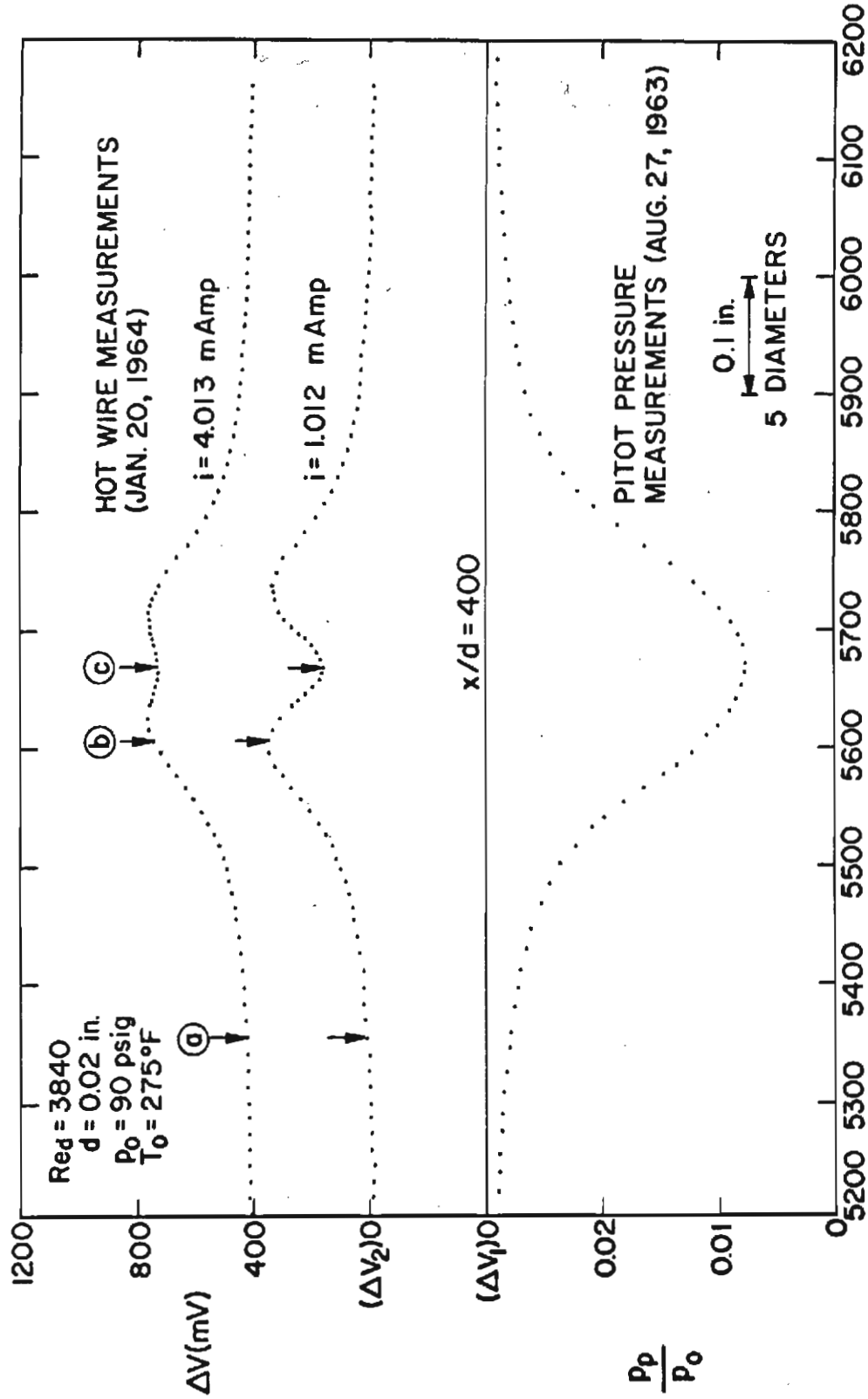

FIG. 38b RAW HOT WIRE AND PITOT PRESSURE PROFILES AT ONE AXIAL STATION (x/d=400)

DETERMINATION OF HOT WIRE RESISTANCE

GIVEN: $V_{B_1} = 25.90$ mV, $V_{B_2} = 102.50$ mV
$F_1 = 10^{-3}$, $F_2 = 8.013 \times 10^{-3}$
$i_1 = 1.0124$ m Amp, $i_2 = 4.0135$ m Amp
$R_L = 0.39$ Ohm, $R_L = 0.39$ Ohm

FIND: $$R_j = \frac{V_{B_j} + \Delta V_j \times F_j}{i_j} - R_L$$

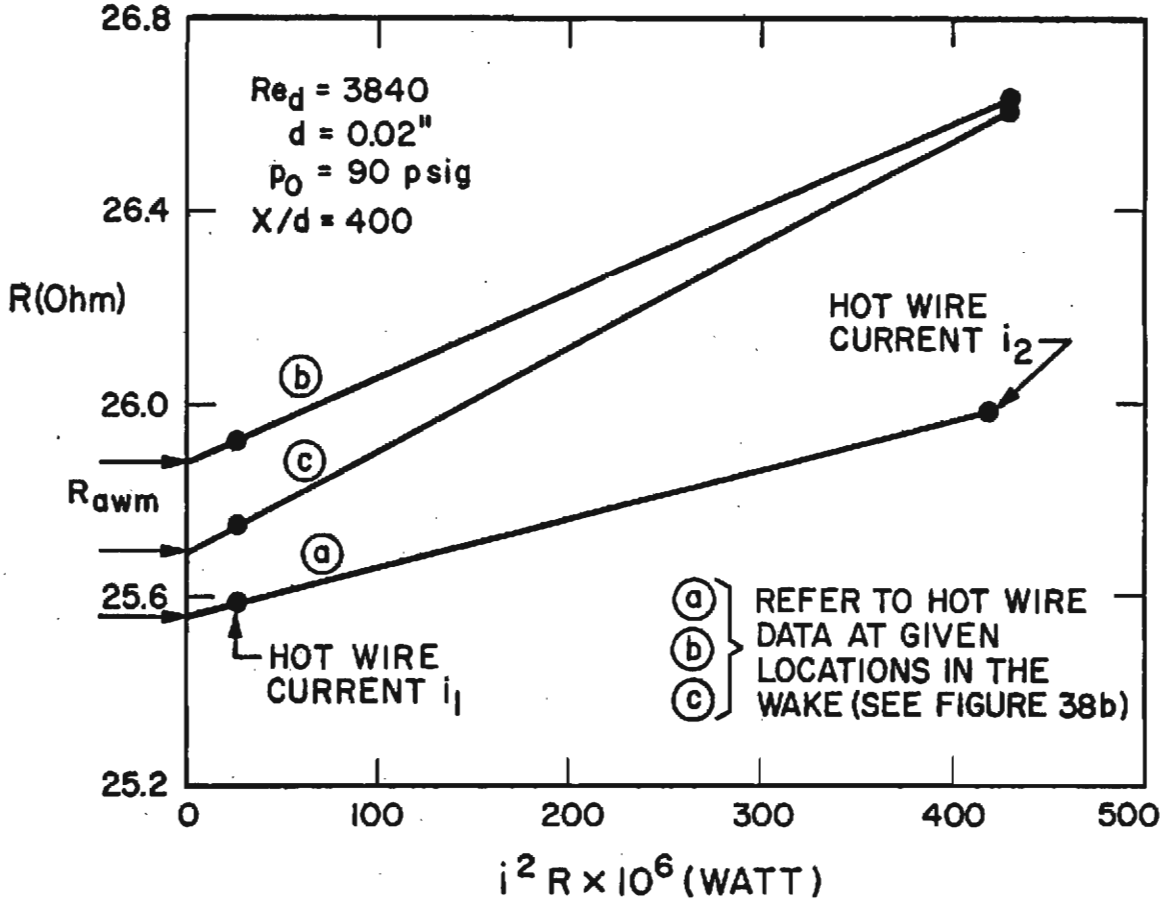

FIG. 39 ILLUSTRATION OF RAW DATA REDUCTION PROCEDURE

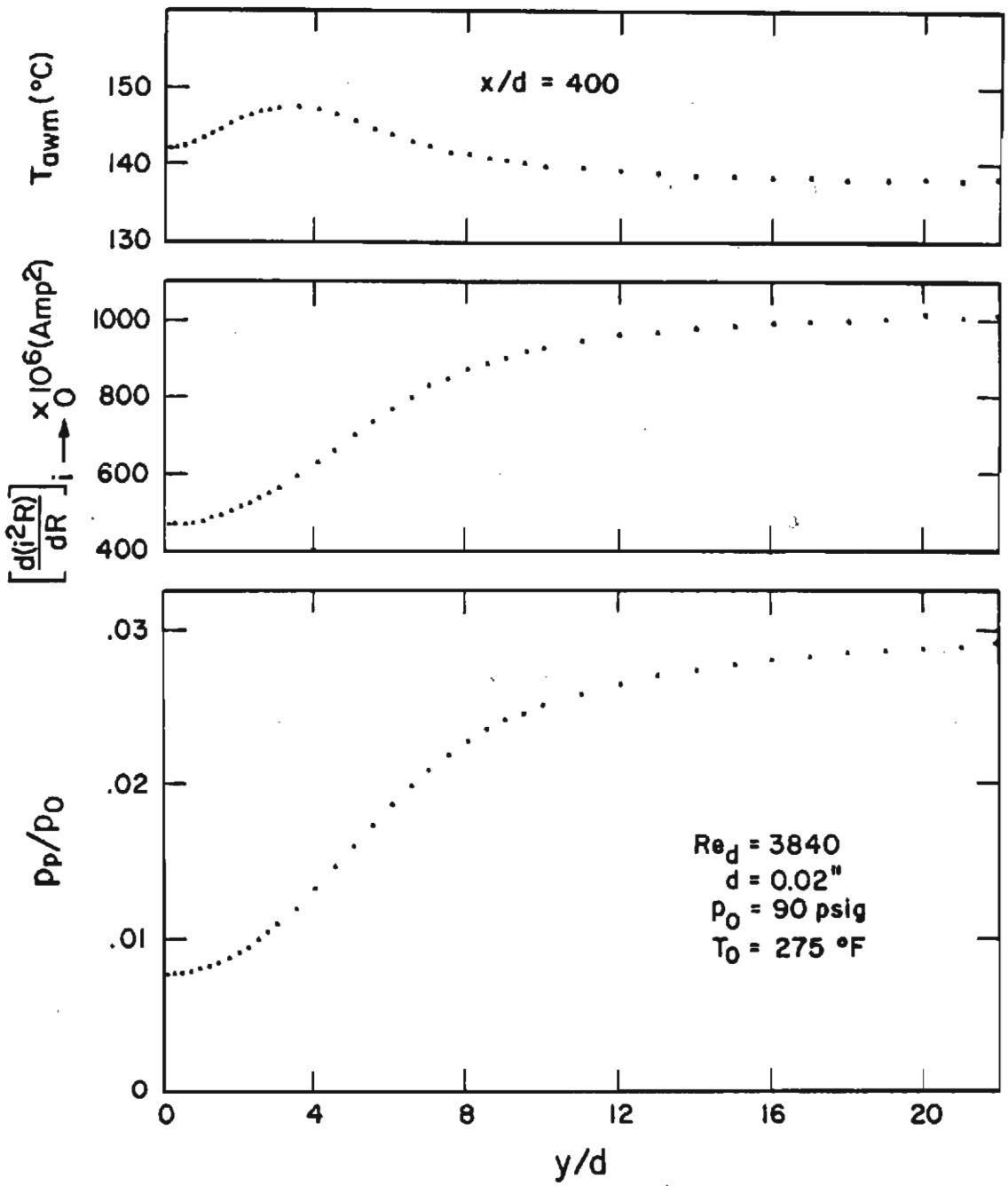

FIG. 40 OUTPUT OF THE RAW DATA REDUCTION, PROFILES AT ONE AXIAL STATION (X/d = 400)

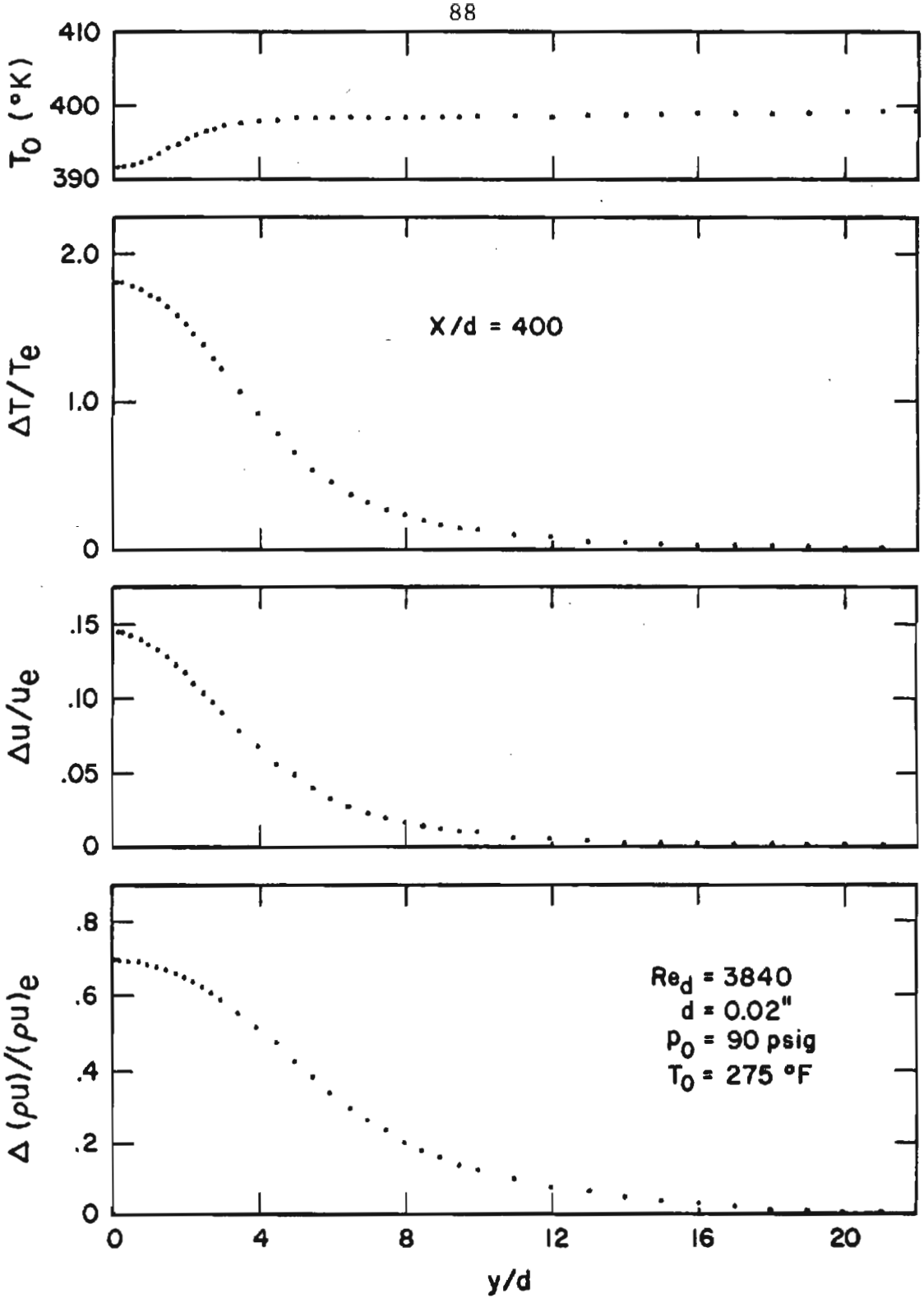

FIG. 41 SOME FINAL DATA, FLOW PROFILES AT ONE AXIAL STATION (X/d = 400)

PART II. STABILITY OF THE FAR WAKE BEHIND CYLINDERS AT HYPERSONIC SPEEDS

1. INTRODUCTION

The mean flow investigation (Part I) showed that at a certain axial station the far outer wake starts to grow more rapidly and the velocity defect and temperature excess decay at a higher rate than predicted by laminar steady theory. This phenomenon suggests a breakdown of the flow caused by strong non-linear oscillations in the far wake, as already pointed out in reference (1). This explanation implies that the whole wake is a laminar steady flow up to this point. However, from earlier measurements by Demetriades (2) and McCarthy (3) and others, it is known that transition occurs in the inner wake at certain Reynolds numbers, as shown in Figure 1. Yet, as pointed out by Lees (4) there is a minimum Reynolds number below which turbulence cannot maintain itself, thus transition is not possible anymore in the inner wake below this Reynolds number. As will be shown in Section 3.2 fluctuation measurements support this view. Below a certain Reynolds number ($Re_{d,\infty} \sim 10^4$ at M = 6 or in general $Re_{f,d} \sim 1.5 \times 10^3$), transition was not observed anymore in the inner wake. Thus if there is transition at these low Reynolds numbers, ($Re_{d,\infty} < 5000$), it can occur only in the outer wake.

Recall from Part I that the outer wake profiles are profiles with an inflection point. Lees and Lin (5) showed that these profiles are dynamically unstable. But as suggested by stability theory, the rate of amplification of disturbances $\frac{1}{Q'}\frac{dQ'}{d(x/d)} = \frac{\alpha c_I d}{c_g} \sim \frac{\Delta u_c}{u_e} \Big/ \frac{b}{d}$,

which means that this rate is very low compared to the rate of amplification in the inner wake (at higher Reynolds numbers), or in the low speed wake behind a flat plate [Sato and Kuriki (6)]. It takes many hundreds of cylinder diameters until the fluctuations become large enough to distort the mean flow drastically. As in the case of the inner wake, one expects that at some minimum critical Reynolds number characteristic for the outer wake the viscous damping becomes dominant.

Following these interpretations, the objectives of this investigation are:

(1) to establish the Reynolds number limit of laminar flow in the inner wake;

(2) to measure the spatially growing oscillations in the far "outer" wake (if they exist), and to delineate the linear and the non-linear growth regions of fluctuations;

(3) to measure the fluctuations in the linear region in detail and to relate the experimental results to the linear stability theory [Lees and Gold (7)];

(4) to study the non-linear wake region as compared to findings in the low speed wake behind a flat plate by Sato and Kuriki;

(5) to establish a minimum critical Reynolds number for the outer wake.

The experimental studies are made with a hot wire anemometer; the techniques and the data reduction are described in Section 2. In Section 3 some general results are discussed as well as the inner

wake fluctuation measurements and overall fluctuation measurements in the outer wake to establish the boundaries between the linear and non-linear region. The detailed fluctuation growth measurements in the linear region are compared with linear stability theory in Section 4. The experimental results in the non-linear region, as compared to low speed wakes behind flat plates, are discussed in Section 5. A tentative picture of the onset of non-linearity and/or transition in the inner and outer wakes behind blunt bodies at hypersonic speeds is given in the same Section. Finally, the results of the mean flow and stability study are summarized in Section 6.1, and some problems for future investigation suggested by the present work are given in Section 6.2.

2. EXPERIMENTAL TECHNIQUES AND DATA REDUCTION

2.1. Wind Tunnel and Models

The dimensions and mean flow properties of the GALCIT Leg 1 Hypersonic Wind Tunnel in which the oscillation measurements were done are described in Part I, Section 2 of this thesis.

As shown by Laufer's measurements (8, 9) the turbulence level of the free stream in a supersonic flow is determined mainly by radiation of sound from the turbulent boundary layer. In the GALCIT Leg 1 tunnel the wall boundary layers are laminar in the test section below a total pressure of 25 psig and turbulent above 40 psig. Most of the fluctuation energy lies in the portion of the spectrum below a frequency of 50 KC; the energy density decreases rapidly towards higher frequencies (Figure 2). As the supply pressure is decreased the fluctuation level also decreases. The relative intensity of fluctuations at supply pressures of 20 psig and 90 psig is shown in Figure 2. The free stream mass flux fluctuation level at the highest pressure (90 psig) was estimated to 1%. The effect of sound radiation from the boundary layers on the wake instability is discussed in Section 3.

The models were tungsten and steel cylinders of diameters ranging from 0.001 to 0.1 inch. The cylinders spanned the tunnel. Tension was applied by means of a spring outside the tunnel (see Part I, Section 2.1 and Figure 6).

2.2. Hot Wire Probe

The same type of hot wire probe was used as in the mean flow measurements (Part I, Section 2 and Figure 11). Absolute intensity of fluctuations was not measured; only the ratio of fluctuation amplitudes at two stations is of interest in order to measure the growth of fluctuations. The absolute level of the output signal changes somewhat from hot wire to hot wire. In order to obtain meaningful data, one wishes therefore to make a complete set of experiments for a given Reynolds number with one and the same hot wire. In order to avoid breakage the aspect ratio of the hot wire was taken to be $\ell/d \cong 100$. A comparison of measurements performed with hot wires of higher aspect ratio yielded good agreement. Thus, for the present fluctuation measurements, hot wire end effects are negligible down to an aspect ratio of 100.

Another reason for choosing a hot wire with such a low aspect ratio is the problem of natural vibration. In comparison to hot wires of higher aspect ratio, fewer hot wires had amplitudes of natural vibration large enough to be noticeable. In addition, in most measurements, the frequencies of natural vibration (of the order of 250 KC or higher) were high enough to be out of the range of the frequencies of flow fluctuations.

2.3. Electronic Instrumentation

Hot wire system

The hot wire anemometer system used in the experiments was a constant current set with a frequency response between 0.1 KC and

320 KC (Shapiro-Edwards Model 50B, Transmetrix Corp., Newport Beach, California). With the aid of a battery operated square wave generator the time constant, M_T, of the hot wire due to thermal lag could be measured. The "floor to ceiling ratio" of the compensation network is 500 for any setting of time constant.

The original hot wire signal was in general smaller than the electronic noise, which increases towards higher frequencies (at 300 KC it is almost 10 times as large as at 20 KC). In order to make quantitative measurements possible an input transformer was used to increase the signal by a factor of 5 ahead of the input to the amplifier.

Wave analyzers

For an immediate check of outstanding features of the power spectrum and of extraneous signals a panoramic ultrasonic wave analyzer was used (Panoramic Model SB-7bZ, Panoramic Radio Products, Inc., Mt. Vernon, N. Y.). This wave analyzer has a continuously variable sweep width from 0 KC to 200 KC within a frequency range from 1 KC to 300 KC. The spectrum is visible on a screen and pictures of it can be taken.

In order to obtain quantitative amplitude measurements of fluctuations in a narrow frequency band another wave analyzer was used (Model 310A, Hewlett-Packard Company, Palo Alto, California). It amplifies, filters and takes the root mean square of an incoming signal in a frequency range from 1 KC, 5 KC or 10 KC to 1500 KC within a constant band width of 0.2 KC, 1 KC and 3 KC, respectively.

The measurements were recorded on an X-Y Plotter (Model 2 DR-2A, F. L. Moseley Co., Pasadena, California) which measures signals down to 0.5 milliVolts per division.

A diagram (Figure 3) shows the electronic setup for the fluctuation measurements.

2.4. Measurement Technique

Before taking data the heated hot wire was checked for vibrations which were visible on the Panoramic screen as sharp peaks. Such hot wires were discarded. Thereafter the time constant of the hot wire was determined and compensated for in the free stream [Kovasznay (10)]. It varied little across the wake (< 10%) and was of the order of 0.2-0.3 millisec. for an overheat of $\frac{\Delta R}{R_{adiab.}} = 20\%$, measured in terms of the resistance, R, of the hot wire.

Two measurements were performed. The first one was the mean square fluctuation signal, $\overline{e'^2_T}$, in a frequency band of 1 KC - 320 KC. Here the hot wire signal was amplified and fed into a thermocouple; the thermocouple signal, which is proportional to the power of fluctuations, was plotted on an X-Y recorder. The signal, $\overline{e'^2_T}$, is composed of the mean square hot wire signal, $\overline{e'^2}$, and the noise, $\overline{e'^2_N}$, i.e. $\overline{e'^2} = \overline{e'^2_T} - \overline{e'^2_N}$. Traces of the mean square fluctuation signal across the wake taken at several axial stations yield the overall rise of disturbances and the growth of the wake width as the flow moves downstream. Examples are shown in Figures 4 a, b, c. An approximate quantitative view of the frequency spectrum is afforded by the panoramic wave analyzer.

In order to obtain the rate of amplification at a given frequency a second measurement was necessary. The root mean square signal for a given frequency at a bandwidth of 1 KC was measured with the aid of the Hewlett-Packard wave analyzer and plotted on an X-Y recorder. Traces were taken across the wake at several streamwise stations in the wake. Representative examples are shown in Figures 5 and 6.

Care was taken to minimize the electronic noise by shielding electronic equipment and lines. The noise level was checked for constancy before and after each trace by turning off the hot wire current and measuring the signal. This procedure does not take into account the thermal noise of the hot wire, which was measured without flow in the tunnel by keeping the wire temperature at a level corresponding to the mean value of the temperature experienced in the wake with flow.

2.5. Data Reduction

The rates of amplification are calculated from the root mean square fluctuation measurements. The total voltage signal, $\tilde{e}'_{fT}$, at a given frequency consists of the hot wire signal, $\tilde{e}'_{f}$, and the noise, $\tilde{e}'_{fN}$, i.e. $\tilde{e}'_{f} = \sqrt{\tilde{e}'^{2}_{fT} - \tilde{e}'^{2}_{fN}}$ (the noise and the hot wire signal are uncorrelated). From these signals the rate of amplification of disturbances are calculated.

Following linear theory, the properly normalized disturbance quantities in the wake are of the form

$$Q'_n = \frac{Q'}{\Delta \overline{Q}_{\ell}} = q' \left(\frac{y}{d}\right) e^{i\alpha(x-ct)}$$

→ b ?

where $\Delta\overline{Q}_{\ell}$ is the corresponding defect of the mean flow quantity and b the wake width. The spatial rate of amplification which one obtains from theory is

$$\frac{1}{Q'_n}\frac{dQ'_n}{dx} = \frac{1}{\tilde{Q}'_n}\frac{d\tilde{Q}'_n}{dx} = \frac{\alpha c_I}{c_g}$$

(Note that α, c_I and c_g are in dimensional form).

But the hot wire measurements yield the rate of amplification

$$\frac{1}{\tilde{e}'_f}\frac{d\tilde{e}'_f}{dx}$$

In order to obtain meaningful results $\frac{1}{\tilde{e}'_f}\frac{d\tilde{e}'_f}{dx}$ has to be related to $\frac{\alpha c_I}{c_g}$. The fluctuation of voltage across the hot wire is [Vrebalovich (11)]:

$$e' = -\Delta e_m \frac{m'}{\overline{m}} + \Delta e_T \frac{T'_o}{\overline{T}_o}$$

where Δe_m and Δe_T are the mass flux and total temperature sensitivity coefficients, respectively, and $\frac{m'}{\overline{m}}$ and $\frac{T'_o}{\overline{T}_o}$ the corresponding normalized flow disturbances at the given frequency. The mass flux fluctuation can be separated into the density and velocity fluctuations:

$$\frac{m'}{\overline{m}} = \frac{\rho'}{\overline{\rho}} + \frac{u'}{\overline{u}} \quad ,$$

and the total temperature fluctuation into the static temperature and velocity fluctuations:

$$\frac{T'_o}{\overline{T}_o} = a\frac{T'}{\overline{T}} + b\frac{u'}{\overline{u}}$$

Assuming isentropic relations between these variables

$$a = \left(1 + \frac{\gamma-1}{2} M^2\right)^{-1} ,$$

and $$b = (\gamma-1)\, a\, M^2$$

In order to obtain a relatively simple relation between $\frac{a c_I}{c_g}$ and $\frac{1}{\tilde{e}_f} \frac{d\tilde{e}_f}{dx}$ it is assumed that the voltage signal, $\tilde{e}'_f$, is proportional to the mass flux fluctuation only. This approach was suggested to the author by J. M. Kendall, Jr. (private communication). It is motivated by results of fluctuation measurements in boundary layers by Laufer and Vrebalovich (12), who found that the maximum mass flux fluctuations were an order of magnitude larger than the total temperature fluctuations at the same station. Demetriades (2) found similar results in the wake. The sensitivity coefficients at large overheats of the hot wire are of equal order. The hot wire relation becomes in this case:

$$e'_f = - \Delta e_m \frac{m'}{\overline{m}}$$

or in terms of the root mean square quantities

$$\tilde{e}'_f = \Delta e_m \frac{\tilde{m}'}{\overline{m}}$$

where $$\frac{\tilde{m}'}{\overline{m}} = \frac{\tilde{\rho}'}{\overline{\rho}} + \frac{\tilde{u}'}{\overline{u}}$$

assuming the fluctuations to be of the form of linear theory. Two different approaches can now be taken.

In the first approach it is assumed that

$$\frac{d}{dx}\left[\ell n \frac{\tilde{u}'}{\Delta u_\ell}\right] = \frac{d}{dx}\left[\ell n \frac{\tilde{T}'}{\Delta T_\ell}\right] = \frac{d}{dx}\left[\ell n \frac{\tilde{\rho}'}{\Delta \rho_\ell}\right] = \frac{a c_I}{c_g}$$

In this case the relation for the rate of amplification is:

$$\frac{1}{\tilde{e}'_f}\frac{d\tilde{e}'_f}{dx} = \frac{1}{\Delta e_m}\frac{d(\Delta e_m)}{dx} + \frac{\alpha c_I}{c_g} + \frac{\frac{\tilde{\rho}'}{\Delta\rho_{\ell}}\frac{d}{dx}\left(\frac{\Delta\rho_{\ell}}{\bar{\rho}}\right) + \frac{\tilde{u}'}{\Delta u_{\ell}}\frac{d}{dx}\left(\frac{\Delta u_{\ell}}{\bar{u}}\right)}{\tilde{m}'/\bar{m}}$$

Some further approximations are necessary to make this formula usable. For the present experiments the following approximations are justified:

$$\frac{d}{dx}\left[\ell n\left(\frac{\Delta\rho_{\ell}}{\bar{\rho}}\right)\right] \cong \frac{d}{dx}\left[\ell n\ \frac{\Delta u_{\ell}}{\bar{u}}\right]$$

and

$$\frac{d}{dx}\left[\ell n\,\bar{u}\right] << \frac{d}{dx}\left[\ell n\,\Delta u_{\ell}\right] \text{ since } \frac{\Delta u_{\ell}}{\bar{u}} << 1$$

where $\bar{u}$, $\bar{T}$ and $\bar{\rho}$ are the mean values at the position in the wake where the fluctuation signal is a maximum, and $\bar{m} = \bar{\rho}\,\bar{u}$. The rate of amplification is calculated at this station. The rate of change of the mass flux sensitivity coefficient was estimated to be

$$\frac{d}{dx}\left[\ell n\,(\Delta e_m)\right] \cong -\,1.25\,\frac{d}{dx}\left[\ell n\,(\bar{\rho}\,\bar{u})\right]$$

The final approximate formula for the rate of amplification which corrects for the change in the mean flow, is then:

$$\frac{\alpha c_I d}{c_g} \cong \frac{1}{\tilde{e}'_f}\frac{d\tilde{e}'_f}{d(x/d)} - \frac{1}{\Delta u_{\ell}}\frac{d(\Delta u_{\ell})}{d(x/d)} + \frac{1.25}{\bar{\rho}\,\bar{u}}\frac{d(\bar{\rho}\,\bar{u})}{d(x/d)} \qquad (2.1)$$

In the second approach it is assumed that

$$\frac{d}{dx}\left[\ell n\left(\frac{\tilde{m}'}{\Delta\bar{m}_{\ell}}\right)\right] = \frac{\alpha c_I}{c_g}$$

Making the same approximations as in the first approach the final relation becomes

$$\frac{\alpha c_I d}{c_g} \cong \frac{1}{\widetilde{e}'_f} \frac{d\widetilde{e}'_f}{d(x/d)} - \frac{1}{\Delta m_{\ell}} \frac{d(\Delta m_{\ell})}{d(x/d)} + \frac{2.25}{\overline{\rho}\,\overline{u}} \frac{d(\overline{\rho}\,\overline{u})}{d(x/d)} \qquad (2.2)$$

where

$$\Delta m_{\ell} = (\overline{\rho}\,\overline{u})_e - (\overline{\rho}\,\overline{u})_{\ell}$$

Both procedures yielded the same results within 4%. The mean flow "corrections" were within 25% at maximum amplification. The measured rates of amplification were "corrected" according to formula 2.1.

3. EXPERIMENTAL MEASUREMENTS OF WAKE INSTABILITIES

3.1. General Features

Several observations can be made directly from the representative hot wire traces in Figures 4 a, b, c to 6. The traces in Figure 5 represent the results of root mean square fluctuation measurements at a frequency (f = 50 KC) at which the disturbances experience maximum amplification in the far wake. In the first trace taken at a distance of 5 diameters from the cylinder 6 peaks appear. The two outermost are caused by the bow shock, the next two by the wake shock and the two innermost peaks [$(y/d) \sim 1$] are immersed in the inner wake. As the flow moves downstream, these peaks of the inner wake decrease; by $x/d = 100$ they have disappeared. Now new peaks appear further away ($y/d \cong 5$; Figure 5) from the center of the wake, which are caused by instabilities in the outer wake. As will be shown in Section 4 peaks of fluctuations occur close to the points in the wake at which the density-vorticity product of the mean flow has an extremum. The instability of the wake is indicated by the fluctuation amplitudes, which grow to very high levels, as shown by the signal at $x/d = 600$.

At a lower Reynolds number ($Re_d = 960$) and a supply pressure at which the tunnel boundary layer is laminar, the level of fluctuations is of the order of the noise or lower. Because of this low level of amplitudes quantitative amplification measurements are not possible (Figure 6). There is no sign of fluctuations in the inner wake (at $x/d \cong 25$). Peaks occur in the outer wake at a distance of 50 diameters,

and these peaks increase in amplitude downstream, indicating instability.

Large signals at the position of the bow and wake shocks were found also by Kovasznay (13) for very weak shocks. They were interpreted as random oscillations of the shock, such that the hot wire is upstream of the shock part of the time and downstream of the shock during the rest of the cycle. This explanation is supported by the following criteria: In the present experiments the diameter of the hot wire is of the order of the shock thickness, which suggests that relatively small amplitudes of oscillation of the shock would produce the observed result. The signal is increasing with shock strength, as it should if this explanation is correct. The randomness of the oscillations is supported by the fact that the signal is measured at all frequencies from 5 to 320 KC (with varying amplitude).

Another phenomenon apparent from these hot wire traces is that the signal in the wake near the body decreases steadily from the level in the freestream -- except of course for the shocks and peaks in the inner wake -- to a very low level at the center of the wake, even though the sensitivity of the hot wire increases as the hot wire current is constant. This decrease is observed no matter whether the boundary layers of the test section tunnel walls are laminar or turbulent, as shown in Figure 5 (turbulent boundary layer) and Figure 6 (laminar boundary layer). Note that the signal at the center of the wake (Figure 5) remains small at least up to 600 diameters, and is not affected by sound radiation from the turbulent tunnel wall boundary layer. There are several possible reasons for the damping of the

freestream disturbances in the flow about a cylinder, and for the apparently small effect of sound radiation on the wake fluctuation level (at least on the flow in the neighborhood of the wake center). Only a qualitative discussion can be given here.

As mentioned in Section 2, the freestream turbulence is mainly of the acoustic mode. Therefore, fluctuations are appreciable only when the boundary layer on the tunnel wall is turbulent. Yet, as seen from Figures 5 and 6 qualitatively the same damping occurs no matter whether the tunnel wall boundary layer is turbulent or laminar. Thus, the same physical mechanism should cause the damping. When fluctuations of acoustic mode encounter a shock, the interaction gives rise to all three modes (entropy, vorticity and acoustic) of comparable strength downstream of the shock (14, 15). The vorticity and entropy modes are convected with the mean flow. The mean flow expands rapidly about a cylinder behind the bow shock. As shown by several investigators (for instance 16, 17) the turbulence level is decreased appreciably by acceleration. This fact, together with the refraction on the shocks, might explain the sharp decrease of fluctuation level close to the cylinder. It also means that the bow and wake shocks partially shield the wake downstream of the body from turbulent boundary layer radiation.

At a Mach number of 6 the angle between the direction of the sound radiation from the boundary layer and the freestream is about 20°, according to Laufer's measurements (9). Upon encountering the shock the sound radiation is partially transferred into the vorticity

and entropy modes, which are swept downstream with the mean flow without disturbing the wake at all. Sound radiation is also partially refracted towards the shock, so that the refracted sound wave of reduced strength hits the wake at a very shallow angle, where it is likely to be reflected and/or refracted because of the velocity and temperature gradients. This explanation is suggested by experiments in a jet by Atvars et al (18). They put an omnidirectional sound source in the jet center. Downstream of the source a pronounced minimum occurred in the jet center indicating refraction of sound out of the jet. This effect, as well as the shock refraction, might cause the apparently small influence of sound radiation on the wake stability. This question requires further investigation.

It is assumed now that quantitative measurements of natural fluctuation are of general validity even when the tunnel boundary layers are turbulent. In fact, because of the initial strong damping of the freestream fluctuations and their consequent low rate of amplification in the wake, quantitative measurements of natural oscillations were possible only at pressures at which the tunnel wall boundary layers were turbulent.

3.2. Inner Wake

At Reynolds numbers above about 1.2×10^4 transition occurs in the inner wake behind cylinders, as found by Demetriades (2) and McCarthy (3). Mean square fluctuations measured in a frequency range of 0.2-30 KC at a Reynolds number of 13,500 are large compared to fluctuations outside the inner wake (Figure 7a), and the

inner wake width obtained from these fluctuation profiles increases rapidly at some axial station ($x/d \cong 30$). At about this station, according to McCarthy's mean flow data (3), the diffusivity starts to become large compared with laminar diffusivity, which is taken as a sign of transition (Figure 3). (Note that transition is used here as an indication of strong non-linear effects. It does not necessarily mean that the wake is fully turbulent beyond this point.)

At a lower Reynolds number ($Re_d = 8440$) the mean square fluctuation signals are very low (Figure 7b) compared to the signals measured at $Re_d = 13,500$, and the inner wake width does not increase suddenly at any station up to $x/d = 110$ (Figure 8). Thus, the inner wake at this Reynolds number is laminar up to $x/d = 110$. Because of the small mean flow gradients in the inner wake beyond this point it is expected that transition -- if it occurs -- encompasses the whole wake and not only the inner wake. Kendall (19) made fluctuation measurements behind cylinders at $M = 3.7$ up to $x/d = 140$ and found the inner wake to be laminar below $Re_d \cong 12,000$. Thus, the inner wake is certainly laminar in the Reynolds number range under consideration in the present investigation ($Re_d < 5000$).

As an added note, a comparison can be made between the inner wakes for a heated and unheated cylinder at a Reynolds number of 13,500 (Figure 8). In the unheated wake transition occurs at about 30 diameters downstream, but the heated wake is still laminar at 100 diameters. This result qualitatively confirms the linear stability theory prediction (7) that heating increases the wake stability.

There are still many questions unanswered with respect to inner wake instability. At the time the measurements described were done (1962) the experimental measuring instruments limited the study to mean square fluctuations in a frequency range of 0.2 to 30 KC. An investigation using the experimental set-up as described in Section 2 and Figure 3 is desirable to answer the following questions:

(1) Are there several regions of instability, as in the incompressible wake, namely linear; laminar, non-linear two dimensional; non-linear three dimensional; turbulent [Sato and Kuriki (6)]?

(2) If the inner wake becomes turbulent, are there non-linear "periodic" regions and what is their axial extension?

(3) Is there a Reynolds number range where the inner wake becomes non-linear but not fully turbulent?

(4) What is the role of longitudinal vortices measured by Kendall (19)?

3.3. Overall Fluctuation Intensity and Growth of Outer Wake

In the incompressible wake of a flat plate Sato and Kuriki (6) found that the mean wake starts to widen faster and the velocity decreases more rapidly than linear theory predicts at the position where non-linear effects become dominant. Kovasznay (20) made the same observation in the incompressible wake of a cylinder. This phenomenon occurred also in the present hypersonic "outer" wake experiments. First of all, one sees that the width of the wake as determined from the mean square fluctuation measurements compare well with the wake width as determined from the mean velocity profiles (Figure 9).

The wake width, b/d, based on the mean velocity profiles is the distance from the center of the wake to the point where $\frac{\Delta u}{\Delta u_{\mathbb{C}}} = 0.5$, whereas the wake width b_1/d, is the width of the fluctuation profile, as shown in Figure 9. These wake widths are normalized at one axial station, so that $b_{1\,\text{vel.}} = \left(\frac{b_1}{b}\right)_{x/d=400} b$, and are plotted in this form in Figure 9. The good correspondence between these two methods of measuring the wake width shows that the growth of the mean square fluctuation profile represents the growth of the mean wake itself. Deviation from the laminar mean flow theory is noticeable at x/d = 1400 and unmistakable at x/d = 1600. On the basis of the width of the mean square fluctuation profiles the linear and non-linear regions are delineated also for other Reynolds numbers (Figure 10). The sudden growth of the wake thickness is in all cases accompanied by a steep increase of the mean square fluctuation signal in the center of the wake (Figure 11).

At the two highest Reynolds numbers (Re_d = 3840, 2400) only the linear growth region was observed up to the maximum axial stations obtainable. The mean flow was found to correspond to laminar linear theory (Part I, Section 4). As shown in Figures 4a and 4b the mean square fluctuation signals on the wake centerline were both small and did not show any sudden increase up to the maximum axial stations attainable.

For the lowest Reynolds number (Re_d = 192) non-linear effects occur, if at all, beyond x/d = 12,000. There is no steep increase in the wake centerline fluctuation signal (Figure 11) and no sudden increase in the wake thickness (Figure 12). It should be noted that

Reynolds number similarity holds as long as the wake flow is laminar (Figure 12).

All wake measurements were made at the same tunnel supply pressure in the same test-section length of 12 inches. At the two highest Reynolds numbers (Re_d = 3840, 2400) only the linear growth region was observed, while at somewhat lower Reynolds numbers the linear and non-linear growth regions were measured, and at the lowest pressure again only the linear region was found. These results show that the phenomenon of non-linearity is not characteristic of the wind tunnel but is associated with the wake flow. It does not mean, however, that the frequency distribution and the level of freestream turbulence has no effect on the location of the onset of the non-linear phenomenon. As shown in Figure 13 mean square fluctuation signals at about the same Reynolds number are at different levels at different supply pressures, because the freestream fluctuation level is different at the two pressures.

On the basis of the mean square fluctuation measurements the locations of onset of non-linearity as a function of Reynolds number at one stagnation pressure (p_o = 90 psig) are given in the following table:

TABLE 1: Onset of Nonlinearity

Re_d	3840	2400	960	576	384	288	192
$(x/d)_{N.L.}$	>600	>960	1600	2400	3600	5000	>12000 (if at all)
d(in.)	0.02	0.0125	0.005	0.003	0.002	0.0015	0.001

At the Reynolds numbers of Re_d = 960, 576, 384 and 288 the Reynolds number based on the physical location of onset of non-linearity is about the same, namely $Re_x \cong 1.4 \times 10^6$. This observation is similar to results found in the inner wake, where $Re_{fxtr.} \cong 56,000$ in a certain Reynolds number range (4). A more detailed discussion of the onset of non-linearity and/or transition is given in Section 5. Here the purpose was to delineate the different regions in order to investigate their features separately in some detail.

4. LINEAR GROWTH REGION AND RELATION TO LINEAR STABILITY THEORY

4.1. Experimental Measurements of Amplification in Linear Growth Region

The question naturally arises as to the nature of the fluctuations of growing amplitude shown in Figures 4 a, b, c and Figures 11 and 12. One is especially interested in the existence of discrete frequencies in the energy spectrum. In this Section we examine the frequency spectrum in the linear growth region and in Section 5 we discuss the nonlinear region.

In Figure 14 the maximum amplitudes $\tilde{e}'_f$ of the fluctuation profiles for various frequencies at several axial stations are compared to their values at x/d = 400. A definite amplitude peak is found around 180 KC which, as we shall see later (Section 4.2), is very close to the value of the most unstable frequency determined theoretically. Unlike Sato and Kuriki's findings in the incompressible wake (6) sinusoidal oscillations at the most unstable frequency were not observed. This situation is similar to the one in boundary layers. Laufer and Vrebalovich (12), who measured fluctuations in a compressible boundary layer at M = 2.2, also found a definite peak in the fluctuation energy spectrum, but no monochromatic oscillations similar to those reported by Schubauer and Skramstad (21) at low speed.

The increase of fluctuation amplitude with respect to axial distance downstream is plotted for several frequencies in Figure 15.

From this data the rates of amplification were determined for two cases (Re_d = 960, x/d = 1000, and x/d = 1400). At these stations (and frequencies) the hot wire fluctuations are larger than the electronic noise and a reasonable accuracy is expected. (A quantitative error analysis was not possible, yet a comparison of measurements at 60 and 93 KC with and without the input transformer, which changes the total signal to noise ratio by roughly a factor of 3, yielded results which were less than 10% different from each other.) Results of the rates of amplifications are shown in Figure 16, with "corrections" applied as discussed in Section 2 (relation 2.1).

4.2. Theoretical Considerations and Numerical Stability Calculations

The occurrence of preferred frequencies and the existence of a nearly linear growth region (Figure 15) strongly suggest that these experimental results can be fitted into the framework of a wake stability theory with respect to small disturbances.

The theory of the inviscid stability of two-dimensional compressible wakes as formulated by Lees and Gold (7) is based on the following assumptions:

(1) Any flow quantity, Q, can be written as

$$Q(\vec{r}, t) = \overline{Q}(\vec{r}) + Q'(\vec{r}, t)$$

where

$$\frac{|Q'|}{|\overline{Q}|} << 1$$

The disturbance equations are linearized in Q', i.e., squares and products of Q' and its derivatives are neglected.

(2) The mean flow is quasi-parallel to order $(\alpha Re_b)^{-1}$. The wake profile considered is of the form $\overline{Q} = \overline{Q}(y)$, which is uniform in x from $-\infty$ to $+\infty$.

(3) The disturbance is also assumed to be two-dimensional and of the form

$$Q'(x, y, t) = q'(y)\, e^{i\alpha(x-ct)}$$

where $\alpha = \frac{2\pi}{\lambda}$ is the real wave number and $c = c_R + i\, c_I$; c_R is the phase velocity and c_I the temporal amplification factor.

(4) Only inviscid stability is studied. Wake profiles are dynamically unstable because at one point in the profile an extremum in the mean density-vorticity product occurs [Lees and Lin (5)]. Since compressible wake flow behaves in a manner analogous to incompressible free shear layers and wakes, viscosity acts as a damping mechanism only. The effect of viscosity starts to be felt only at fairly low Reynolds numbers.*

(5) The disturbances considered are subsonic, i.e. in the two-dimensional case which is considered here the relative phase velocity $u_e - c_R$ is smaller than the ambient speed of sound a_e,

$$\text{or} \qquad -\Delta c_R < \frac{1}{\Delta M}$$

$$\text{where} \quad \Delta c_R = \frac{c_R - u_e}{u_e - u_\ell} \qquad \text{and} \quad \Delta M = \frac{u_e - u_\ell}{a_e}$$

In the hypersonic far wake this condition is satisfied in general.

---

* Compare the free shear layer stability analysis by Betchov and Szewczyk (22), who found that the maximum rate of amplification was about 20% lower at a Reynolds number of 40 than in the inviscid case.

In order to compare theoretical rates of amplification with experimental results the rate of amplification which is calculated from theory, $\frac{1}{Q'} \frac{\partial Q'}{\partial t} = \alpha c_I$, has to be transformed into a spatial rate of amplification. If the mean flow does not change in the flow direction (x), then according to Whitham (23) the fluctuation energy propagates with the group velocity, i.e.

$$\frac{dx}{dt} = c_g$$

and

$$\frac{1}{Q'} \frac{\partial Q'}{\partial t} = \frac{1}{Q'} \frac{\partial Q'}{\partial x} \frac{dx}{dt}$$

The spatial rate of amplification is then:

$$\frac{1}{Q'} \frac{\partial Q'}{\partial x} = \frac{\alpha c_I}{c_g}$$

Recently the stability problem has been treated by calculating the spatial rate of amplification directly (24). The plane wave is of the form:

$$Q' = q'(y)\, e^{i(\alpha x - \beta t)}$$

where $\alpha = \alpha_R + i\alpha_I$ and β is real.

In this case, the spatial rate of amplification is

$$\frac{1}{Q'} \frac{\partial Q'}{\partial x} = -\alpha_I$$

Gaster (24) showed mathematically that to $0(\beta_{I\,max})$ the spatial rate of amplification can be transformed to the timewise rate of amplification, $\beta_I = \alpha c_I$, by means of the group velocity, provided that β_I is

appropriately normalized. He found that

$$\frac{\beta_I}{\alpha_I} = -\frac{\partial \beta_R}{\partial \alpha_R} = -c_g$$

Thus, as long as the rate of amplification is small the timewise and spatially growing disturbances are approximately equivalent.

Numerical stability calculations for temporally growing oscillations were performed using Gaussian profiles. The problem essentially is to find the eigenvalues c_I and c_R as functions of α, which was done by an iteration scheme devised by Gold (25). Gold transformed the equations by means of the Howarth-Dorodnitsyn transformation:

$$\bar{y} = \int_o^y \frac{\rho}{\rho_e}\, dy$$

The wake profiles are assumed Gaussian and are fitted to the actually measured profiles at the center and at the point where $\frac{\Delta u}{(\Delta u)_{\mathfrak{L}}} = 0.5$, which yields the wake half width. (Note that Gold measured the wake half width at the point where $\frac{\Delta u}{(\Delta u)_{\mathfrak{L}}} = \frac{1}{e}$ so that the present wake width, $\bar{b} = 0.833 L^*_{\underline{\text{Gold}}}$.) Only the eigenvalues for the antisymmetric disturbances are computed, since these are more unstable than the symmetric disturbances. Mean profiles at two Reynolds numbers, $Re_d = 960$ and 320, were considered at 4 axial stations each. The pertinent parameters of these cases are given in the table below.

TABLE 2: MEAN FLOW DATA FOR STABILITY CALCULATIONS

CASE	Re_d	$\frac{x}{d}$	$\frac{\Delta u_{\ell}}{u_e}$	$\frac{\Delta T_{\ell}}{T_e}$	$(\Delta M)^2$	$\frac{\bar{b}}{d}$	$\frac{b}{d}$
1	960	200	0.140	1.71	0.707	1.71	4.01
2	960	400	0.122	1.50	0.540	2.03	4.45
3	960	1000	0.096	1.19	0.334	2.79	5.44
4	960	1400	0.086	1.07	0.265	3.24	6.03
5	320	200	0.128	1.48	0.556	2.27	4.93
6	320	400	0.102	1.17	0.352	2.96	5.78
7	320	1000	0.076	0.93	0.201	4.10	7.46
8	320	1400	0.068	0.83	0.163	4.81	8.10

Local similarity was assumed in the sense that in the theory the profile is uniform from $x = -\infty$ to $+\infty$. The local rates of amplification were calculated for each profile and the increase of amplitude calculated by following one frequency. The eigenvalues $\Delta c_I = \frac{c_I}{u_e - u_{\ell}}$ and $-\Delta c_R = \frac{u_e - c_R}{u_e - u_{\ell}}$ are plotted as functions of the normalized wave number $\alpha \bar{b}$ in Figure 17 for a few representative cases.

Some conclusions are derived directly from the results. The rate of amplification, $\frac{1}{Q'} \frac{dQ'}{dx} = \frac{\alpha c_I}{c_g} \sim \frac{\Delta u_{\ell}}{b}$ decreases rapidly as the flow moves downstream. It also decreases at the same station in the wake as the Reynolds number decreases [Figures (18) and (19)]. The frequency of maximum rate of amplification decreases also as the flow moves downstream and for decreasing Reynolds number (when the diameter of the cylinder is kept constant). Consequently, the rate of amplification of a disturbance moving downstream

decreases more or less depending on the frequency (Figure 19). The amplitude of the disturbance at a particular station in the wake depends on its amplification and the magnitude at the "initial" upstream station. For simplicity the amplitude at x/d = 200 is set equal to 1. The frequency of maximum amplitude is obviously not equal but larger than the frequency of maximum rate of amplification at the same station. By plotting $\frac{1}{Q'}\frac{dQ'}{d(x/d)} = \frac{\alpha c_I d}{c_g}$ versus (x/d) as in Figure 19, the ratio of amplitudes for any frequency is obtained by determining the area under the curve (Figure 20). The strong dependence of amplitude of disturbance on Reynolds number is apparent from Figure 20. In other words the effect of viscosity on the laminar oscillations directly is negligible except at very low Reynolds numbers, but viscous diffusion strongly influences the rate of amplification through its effect on the <u>mean</u> wake flow, i.e. $\frac{d(\ell n Q')}{d\, x/d} = \frac{\alpha c_I d}{c_g} \sim \frac{\Delta u/u_e}{b/d} \sim \frac{Re_d}{x/d}$ for a given α d.

When the rates of amplifications are normalized according to theory (by means of the transformed wake half width) the normalized rates of amplification show a strong dependence on compressibility. Note also that the spatial rate of amplification for the incompressible wake as calculated by Davey [see Gaster (24)]* is reasonably close to the timewise rate of amplification calculated by Gold (Figure 21). However, if the wave number is made non-dimensional by using the

---

* Unfortunately, there is a numerical error in the timewise stability calculation by Sato and Kuriki (6); the proper comparison between spatial [Davey (24)] and timewise rates of amplification [Gold (5)] yield better agreement than reported by Gaster (24), who compared Davey's and Sato and Kuriki's results.

physical wake width, the normalized rates of amplification of incompressible and hypersonic wakes considered here agree in first approximation (Figure 22). This surprisingly simple result is equivalent to the findings on stability of boundary layers by Laufer and Vrebalovich (12). They compared their measurements in a compressible boundary layer at M = 1.6 and 2.2 with those of Schubauer and Skramstad (21) in a low-speed boundary layer and found that within experimental accuracy at a given Reynolds number the stability limits as well as the nondimensional rates of amplification are governed only by the local boundary layer thickness and are independent of Mach number. Comparing the amplification curves in detail (Figure 22) there appears to be an influence of the relative Mach number and the temperature excess, especially in the neighborhood of neutral stability, and on the value of the wave number of neutral stability itself. As shown in Figure 10 of reference (7), this effect is more pronounced as the temperature excess becomes large, which corresponds to very high Mach numbers. (It seems possible that this effect might also be present in the boundary layer, but is too small to be detected in the cases considered by Laufer and Vrebalovich.) Thus, within the limits of experimentally realized wakes ($M_\infty = 6$) the main parameters governing the instability of incompressible as well as compressible laminar wakes are the velocity defect and the physical wake width, while the compressibility enters only indirectly through these parameters. This result will be checked by experiments (Section 4.3).

4.3. Comparison Between Experiment and Inviscid Stability Theory

4.3.1. Amplification Rates

In order to compare the experimental with the theoretical rates of amplification at the same station, the data are normalized by the velocity defect and the physical wake width. The value of the most unstable wave number compares reasonably well in experiment and theory, yet the maximum rate of amplification is about 25% lower in the experiment (Figure 23). The relatively high value of rate of amplification at the highest wave number (at x/d = 1400) might be caused by the first effects of nonlinearity. The ratio of electronic noise to signal increases sharply as the frequency increases. For this reason it was not possible to measure the frequency of neutral stability.

In order to make sure that this phenomenon of amplification of fluctuations in a certain frequency range (in the foregoing example around 180 KC) is not a phenomenon associated with the tunnel but with the wake flow, fluctuation measurements were made in the wakes of cylinders of several other diameters. According to theory, the most unstable frequency changes with cylinder diameter and can be predicted. In each case, measurements were made at two axial stations in the wake; for instance at $Re_d = 960$ these stations were selected at x/d = 400 and x/d = 1400. The rate of amplification was calculated from the relation

$$\frac{\ell n\, \tilde{e}'_f [x/d = 1400] - \ell n\, \tilde{e}'_f [x/d = 400]}{\Delta(x/d)\ [= 1000]}$$

which is assumed to be the local rate of amplification at the axial station halfway between the stations at which the measurements were taken, i.e. in this example at $x/d = \frac{400 + 1400}{2} = 900$. For this case it was found that this procedure of calculating the rate of amplification yielded results which were 8% lower at the most unstable frequency than the results for the local rates of amplification, obtained by taking the slopes from the amplitude-frequency curves at x/d = 900 (Figure 15). On the average the difference for all points was only 4%. Considering the accuracy achievable in determining the slope from a curve faired through experimental points, this procedure seems to be justified. In fact, for the small cylinders (d = 0.002 in. and 0.003 in.) this method was the only feasible way to obtain rates of amplification. In the interesting range of frequencies (f = 200 to 300 KC) the signals are of the order of or only somewhat larger than the electronic noise, and the rate of amplification $\frac{d \ln \tilde{e}'_f}{d(x/d)}$ is small, so that only fluctuation measurements at two stations far apart ($\Delta x/d \geq 1000$) yield differences in the signals which are large compared to the scatter in repeated measurements.

The results for 5 different model diameters (Figure 24) indicate a pronounced increase of the most unstable frequency as the diameter of the models is decreased. This behavior corresponds <u>qualitatively</u> to linear stability theory, and it can now be stated that the amplification of fluctuations is caused by the instability of the wakes and is not associated with the wind tunnel. In order to make a <u>quantitative</u> comparison of the results with theory, the rates of

amplification $\frac{d\,\ell n\,\tilde{e}'_f}{d(x/d)}$ have to be "corrected" according to relation (2.1.) to obtain $\alpha c_I d/c_g$. For the three highest Reynolds numbers the mean flow data are available (Part I). For the two lowest Reynolds numbers (Re_d = 576 and 384) the rate of change of the mean velocity defect $\frac{1}{\Delta u_{\mathfrak{E}}} \frac{d\Delta u_{\mathfrak{E}}}{d(x/d)}$ could be calculated by extrapolation from the mean flow measurements at Re_d = 960 and Re_d = 320. The "corrected" data are also shown in Figure 24. At the most unstable frequency the rate of amplification, $\frac{\alpha c_I d}{c_g}$, is up to 25% higher than $\frac{1}{\tilde{e}'_f} \frac{d\tilde{e}'_f}{d(x/d)}$. These rates of amplifications, $\frac{\alpha c_I d}{c_g}$, are normalized with the mean flow velocity defect and the half width of the wake. The pertinent mean flow data are summarized in the table below.

TABLE 3: MEAN FLOW DATA FOR STABILITY EXPERIMENTS

Re_d	x/d	$\frac{\Delta u_{\mathfrak{E}}}{u_e}$	$\frac{b}{d}$	$\frac{b/d}{\Delta u_{\mathfrak{E}}/u_e}$	$\frac{\Delta T_{\mathfrak{E}}}{T_e}$
3840	400	0.146	3.75	25.7	1.82
2400	580	0.126	4.40	34.8	1.55
960	900	0.099	5.38	53.2	1.22
576	1800	0.074	7.42	100	0.91
384	2700	0.060	9.18	153	0.74

In order to calculate the normalizing quantities for the cases for which no mean flow data were available, the following empirical relations were used

$$\frac{\Delta u_{\mathfrak{E}}}{u_e} \frac{b}{d} \cong 0.55$$

$$b_1/b \cong 4.30$$

$$\frac{\Delta T_{\ell}}{T_e} \Big/ \frac{\Delta u_{\ell}}{u_e} \cong 12.3$$

which hold for Reynolds numbers $Re_d = 4000 \rightarrow 320$ and $x/d \geq 300$.

The normalized rates of amplification are compared with one another and with theory in Figure 25. The results at the three lowest Reynolds numbers ($Re_d = 960$, 576 and 384) correspond within experimental accuracy whereas the rates of amplification at the two higher Reynolds numbers and at smaller axial distances from the body are smaller.

In order to find the reasons for this discrepancy between theoretical and experimental amplification rates the assumptions of the stability theory have to be reexamined and the accuracy of the experimental data verified. As far as the disturbance measurements are concerned, it can only be pointed out that the data are consistent and that a variation of signal to noise ratio had no effect on the results. The real test, however, would be to measure the amplification of controllable artificial disturbances. Yet, it seems unlikely that the discrepancy between theory and experiment is entirely caused by experimental inaccuracy.

One significant difference between theoretical calculation and experiment is in the mean profile shape. For the theoretical calculations Gaussian profiles in the transformed Howarth-Dorodnitsyn coordinates are used, whereas the measured wake profiles are somewhat different, even at large distances from the body (Figure 26). An indication that the profile shape is of importance for its stability is given

by a comparison of the present results with Kendall's fluctuation measurements and Batt's flow measurements in the wake of a flat plate. Kendall [(26) and private communication] made "artificial" and in one case natural fluctuation measurements in the laminar wake of a flat plate at Mach number 3.7, and found agreement with linear stability theory within 10% at maximum amplification (the measured amplification rates were lower). Mean flow measurements by Batt (private communication) in the wake behind a flat plate at Mach number 6 revealed that the mean flow profiles were already very close to similar Gaussian profiles in terms of the transformed Howarth-Dorodnitsyn variables at a distance less than one plate length behind the plate. If one assumes that the wake profiles do not change appreciably from Mach number 3.7 to 6, then in the theoretical stability calculations the measured profiles are used for the comparison with wake fluctuation measurements. The good agreement between theoretical and experimental amplification rates (within $\sim 10\%$) as compared to the poorer agreement in the present investigation suggests that the wake profile is of importance.

A second argument for the influence of the wake profile shape on the wake stability is given by the solution for the amplification factor, c_I, at small α [Lees (private communication)]:

$$\left(\frac{c_I}{\Delta u_{\mathfrak{E}}}\right)^2 = \alpha b \int_0^1 \frac{\left(\frac{u-c_R}{\Delta u_{\mathfrak{E}}}\right)^2}{T/T_e} \, d\left(\frac{y}{b}\right)$$

For one example (Re_d = 3840, x/d = 600: Figure 26) the integral was evaluated for both the experimental and the theoretical Gaussian profile which was fitted to the experimental profile at two points, the centerline and the point where $\frac{\Delta u}{\Delta u_{\mathfrak{L}}} = 0.5$. In both cases, the integration was carried out to the point where $\frac{\Delta u}{\Delta u_{\mathfrak{L}}} = \underline{0.05}$ in the experimental profile. It yielded the following results:

$$\left(\frac{c_I}{\Delta u_{\mathfrak{L}}}\right)^2 a\, b = 0.243 \qquad \text{(measured profile)}$$

$$\left(\frac{c_I}{\Delta u_{\mathfrak{L}}}\right)^2 a\, b = 0.460 \qquad \text{(Gaussian profile)}$$

or $$\frac{\left[c_I/\Delta u_{\mathfrak{L}}\right]_{exp.}}{\left[c_I/\Delta u_{\mathfrak{L}}\right]_{Gauss.}} = 0.73 \quad \text{for equal wave numbers.}$$

Of course, this result is valid only for small a, but together with the experimental findings it suggests that there is an influence of the profile shape. However, only a stability calculation using the measured profile shapes can ultimately clarify this point.

Other possible influences on the stability are viscous effects. In the inviscid stability equations terms of the order of $\frac{1}{aRe_b}$ are neglected. In present experiments the Reynolds number was varied by a factor of 10 (from Re_d = 3840 to 384) and yet no Reynolds number effect is observed when the amplification rates are properly normalized.

The next assumption in the theory to be investigated is the assumption of one-dimensionality of the mean flow. The flow profile is considered to be independent of the axial distance and only a function of the normal coordinate. This assumption means that terms in

the stability equations accounting for the rate of change of the mean flow are neglected, namely $\frac{1\partial\overline{Q}}{\overline{Q}\partial x}$ is neglected as compared to $\frac{1\partial Q'}{Q'\partial x}$. This assumption is tested for the present experiments. A severe test is the rate of change of density along the centerline of the wake.

The results are compared with the maximum rate of amplification of fluctuation in the table below.

TABLE 4: MEAN FLOW AND RATE OF AMPLIFICATION DATA AT $Re_d = 960$

x/d	200	400	600	800	1000	1200	1400
$\frac{d[\ell n(\rho_\ell/\rho_e]}{d(x/d)}$	0.58	0.40	0.28	0.19	0.17	0.15	0.11×10^{-3}
$\left.\frac{d\left(\ell n\tilde{e}'_f\right)}{d(x/d)}\right]_{exp.}$					2.08		1.62×10^{-3}
$\left.\frac{\alpha c_I d}{c_g}\right]_{theor.}$	6.16	4.75	3.95	3.45	3.10	2.75	2.40×10^{-3}

This comparison shows that the rate of change of the mean flow is an order of magnitude lower than the maximum rate of amplification of small disturbances. It seems that the linear small disturbance equations are quite a good approximation. However, in the neighborhood of neutral disturbances the axial rate of change of the mean flow is of the order of the rates of amplification of disturbances, so that in this region there should be some difference between theory and experiment.

4.3.2. Neutral Phase Velocity and Fluctuation Profiles

Lees and Lin (5) showed that for neutral inviscid subsonic disturbances the wave speed must equal the mean velocity at the point in the wake profile where the density-vorticity product has an extremum, namely

$$c_R = u \quad \text{at} \quad \frac{d}{dy}\left[\frac{T_e}{\Delta T}\frac{d}{dy}\left(\frac{\Delta u}{\Delta u_{\ell}}\right)\right] = 0$$

Because of this condition the phase velocity of neutral disturbances can be calculated from the mean profile. The relative phase velocity determined from measured profiles is somewhat larger than the theoretical value obtained from the Gaussian profile, i.e.

$$\left[\frac{\Delta c_R}{\Delta u_{\ell}}\right]_{exp.} = 0.40 \quad \text{and} \quad \left[\frac{\Delta c_R}{\Delta u_{\ell}}\right]_{theor.} = 0.34 \text{ at } Re_d = 960,$$

$x/d = 1400$. This difference is expected because the measured profile is not Gaussian. It should be noted that maximum of the profile of mean square fluctuations over all frequencies (f = 1-320 KC) is very close to the theoretically determined critical point, i.e. the point where the density-vorticity product has an extremum, and $u = c_R$ for neutral disturbances (Figure 27). Note also that the peak of the fluctuation profiles is the closer to the center of the wake the higher the frequency, and the thickness of the fluctuation profile also decreases with increasing frequency (Figure 28). Comparative theoretical amplitude distributions are not available.

5. NON-LINEAR REGION

5.1. Instability Regions in the Low Speed Wake Behind a Flat Plate

As pointed out in the Introduction, there are certain similarities between the stability of the low speed wake behind a flat plate and the hypersonic wake. In order to make a comparison between these wakes some significant stability features of the low speed wake behind a flat plate as found by Taneda (27) and Sato and Kuriki (6) are briefly discussed. There are five possible stability regions: (1) for a sufficiently low Reynolds number ($Re_{\ell} \leq 700$) the whole wake is laminar without laminar oscillations; (2) at somewhat higher Reynolds numbers a linear growth region of laminar oscillations is observed, but the rate of growth is too small to form a non-linear region because of viscous diffusion of the mean flow; (3) raising the Reynolds number further, a non-linear two-dimensional fluctuation region is observed downstream of the linear region, which develops into a double row vortex street; further downstream it decays by viscous action or, at sufficiently high Reynolds number, is distorted into (4), a three dimensional periodic region; (5) finally, the wake becomes turbulent.

Sato and Kuriki found that the change from the linear growth region to the non-linear region is characterized by several phenomena. First, the mean velocity defect starts to decay much faster than steady laminar theory predicts, reaches a relative minimum, becomes larger and then slowly decays again. Second, the amplitude of the fundamental frequency increases in the linear region and in the very first part of the

non-linear region, reaches a peak and then decays in the second part of the non-linear region. The amplitude distribution across the wake shows two peaks at/or close to the position where $\frac{d^2u}{dy^2} = 0$, which develop into four peaks as the double row vortex street is formed. Third, the first harmonic (double frequency of fundamental component) is very small in the linear region, grows in the non-linear region to a maximum a little upstream of the point where the mean velocity defect reaches a minimum, and thereafter starts to decay slowly. The amplitude distribution of the first harmonic shows three peaks right after the beginning of the non-linear region, the largest one being on the wake axis. Further downstream the signals decrease and the off-axis peaks disappear completely once the double row vortex street is formed.

In this context, the experimental investigation of J. Kendall, Jr. (private communication) should be noted. He "artificially excited" the wake behind a flat plate at a Mach number of 3, 7. From schlieren-photographs it appears that a linear growth region is followed by a non-linear region with a persisting double row vortex array.

5. 2. Non-linear Region in the Far Hypersonic Wake Behind Cylinders

5. 2. 1. Low Frequency Components

One important factor in the present experiments is the relatively high energy content of the low frequencies in the free stream (Figure 2). This frequency distribution (with some distortion) is qualitatively the same in the wake close to the body. The low frequency component, even though it is not amplified much, is still

dominant when flow non-linearities first appear in the wake. As an example, the fluctuation signals are shown as functions of frequency in Figures 29a and 29b for the case of Re_d = 960 at several axial stations. At the beginning of the non-linear region (x/d = 1600) the maximum signal of the fluctuation profile at the most unstable frequency (about 180 KC) is still much smaller than the signal at 20 KC, even though the experimentally determined amplification of disturbances at 180 KC is higher by a factor of 23 than the amplification of disturbances at 20 KC, as the flow moves from x/d = 400 to x/d = 1600 (Figure 29a). However, at the largest axial distance attainable in the experiment (x/d = 2400) the signal in the most unstable frequency band is larger than at low frequencies. The frequency distribution of fluctuation amplitudes measured on the wake axis is also shown (Figure 29b). Thus, in the present experiments, the axial position of the onset of non-linearity might be somewhat influenced by the low frequency component, and some interaction with the high frequency components should take place in the non-linear region. In spite of this unwanted low frequency component, there are noteworthy observations in the non-linear region, some of which are analogous to Sato and Kuriki's findings in the incompressible wake.

5.2.2. Most Unstable Frequency Components

There are no theoretical treatments for the non-linear instability region, so the interpretations of the experimental observations are only qualitative.

The fluctuation profiles measured at the largest axial distance

attainable in the experiment (x/d = 2400) indicate several interesting phenomena (Figure 30). There are the relatively large triple peak signals at the low frequencies (f = 6-60 KC) as discussed in the previous section. Basic significance is not attributed to them. Fluctuation profiles in the most unstable frequency band (at about 140 KC because of the increase in wake width) still show the typical double peak profiles already observed in the linear region. At about twice the fundamental frequency (f = 303 KC) a triple peak fluctuation profile appears. The signal at this frequency is so small in the linear region that it cannot be measured at all. Then, at x/d = 1400, a small double peak fluctuation profile appears which grows at a fast rate to the triple peak signal measured at x/d = 2400 (Figure 31). The appearance of a triple peak in the first harmonic amplitude profile* may be explained in terms of the oscillation of the wake in the antisymmetric mode [F. Hama (28)]. Since the hot wire is fixed in space, the transverse oscillation of the wake at the fundamental frequency produces a signal at twice this frequency on the wake axis. The amplitude of this signal is roughly proportional to the curvature of the mean flow profile, which is a maximum on the wake axis, and to the square of the amplitude of oscillation. In addition, the transverse oscillation of the wake means that the lateral distribution of amplitude of the fundamental frequency also oscillates past the fixed hot wire. The "beat" between these two

---

* In the hypersonic wake presently under consideration the terms "fundamental frequency" and "1st harmonic" mean maxima of instability at these frequencies. It does not mean that monochromatic periodic oscillations are observed as in the low speed wakes of Sato and Kuriki.

produces a signal at twice the fundamental frequency, with a maximum on each side of the axis lying between the point of maximum curvature of the amplitude profile for the fundamental frequency, and the maximum amplitude. Thus three peaks are expected at the double frequency.

The increase of fluctuation amplitudes up to the frequency band of the first harmonic could be measured in only one case ($Re_d = 960$, $d = 0.005$ in.). For the wakes of smaller cylinders, $d = 0.003$ in. and $d = 0.002$ in., the first harmonic frequencies were higher than could be detected with the hot wire set, which measures fluctuations up to a frequency of 320 KC. Yet, in all cases the signals still grow in the non-linear region (Figure 32). The rate of amplification of the fluctuations in the non-linear region was calculated from the data shown in Figure 32 in the same way as described in Section 4 for linear fluctuations, and then normalized by mean flow quantities. The following empirical relations were used to obtain the mean quantities:

$$b_1/b \cong 4.30 ;$$

$$\frac{\Delta u_{\mathfrak{L}}}{u_e} \frac{b}{d} \cong 0.55.$$

Since the wake width b_1/d is known from the mean square fluctuation profiles, the quantities $\frac{b/d}{\Delta u_{\mathfrak{L}}/u_e}$ and b/d can be determined. The rates of amplification calculated are assumed to be those at the axial position, $(x/d)_m$, halfway in between the two measuring positions at

the beginning of the non-linear region $(x/d)_i$, and at the maximum position attainable $(x/d)_e$. The results (Figure 33) indicate that the normalized rates of amplification and the most unstable (fundamental) normalized frequencies agree with each other within experimental accuracy, and are also close to the most unstable normalized frequency measured in the linear region. In a rough way the logarithmic rate of growth of the double-frequency component should be just about double the logarithmic rate of growth of the fundamental, because $A^2 \sim A_i^2 \, e^{2\alpha c_I t}$ and the double-frequency (1st harmonic) $\sim A^2$. As shown in Figure 33 ($Re_d = 960$) the rate of amplification at $\alpha b = 2.2$ is not quite 2 times the rate of amplification at $\alpha b = 1.1$. The experimental results as compared with the measurements of Sato and Kuriki (6) in the incompressible wake suggest that the phenomena observed are characteristic of the first stage of the non-linear region.

The main features of the onset of non-linearity are summarized in Figure 34, which shows the deviation of the mean temperature excess and wake width from steady laminar behavior, the relatively rapid increase of the maximum signal of the fluctuation profile at the first harmonic frequency, and also of the fluctuation signals on the wake axis, especially again at the 1st harmonic frequency. Furthermore, the frequency distribution of the fundamental component shows a double peak profile and the first harmonic a triple peak profile. These results, particularly the lack of "saturation" of the fundamental and the first harmonic amplitude, suggest that it might take many more cylinder diameters at $M_\infty = 6$ until the wake becomes fully turbulent, if turbulence occurs at all. Because $\frac{1}{Q'} \frac{dQ'}{d(x/d)}$ is much lower

than in the low speed wake of Sato and Kuriki (effect of $\frac{\Delta u}{b}$) the instability and flow breakdown process is "stretched out" in space, in terms of cylinder diameters.

5.3. Tentative Picture of Onset of Non-Linearity and/or Transition

On the basis of measurements in the inner wake by Demetriades (2) and McCarthy (3) and the present outer wake experiments (Section 3, Table 1) a tentative picture can now be sketched of the onset of non-linearity in wakes behind cylinders at Mach number $M_\infty \cong 6$ as a function of Reynolds number.

At very low Reynolds numbers the entire wake is laminar. According to Lees' argument (4) the minimum critical Reynolds number is reached when the effective turbulent diffusivity falls below the appropriate laminar diffusivity. For two dimensional blunt bodies

$$\frac{\tilde{\epsilon}_T}{\nu} \cong 0.015\, C_D\, Re_d$$

where for the outer wake we must use the total C_D. Since $C_D \cong 1.30$ for a circular cylinder and Re_d is the free stream Reynolds number based on cylinder diameter $\left(Re_{d,\infty}\right)_{min,\,crit} \cong 50$. This value is a lower limit and the actual minimum critical Reynolds number might be somewhat larger ($Re_d \leqslant 150$). It should be noted that in the present experiments at a Reynolds number of $Re_d = 192$ the wake was still laminar at a distance of 12,000 diameters from the cylinder. As the Reynolds number is increased "transition" moves towards the body until it approaches (for example) $x/d = 1000$ at $Re_d = 4000$, and would continue to move slowly towards the body if only the outer wake were involved.

However, instability of the laminar flow in the inner wake leads to non-linear effects and/or transition at $Re_d \sim 10^4$, so the transition location suddenly "jumps" forward to the vicinity of $x/d \sim 100$ at this Reynolds number. As the Reynolds number is increased further transition continues to move towards the body. Figure 35 shows this trend of the onset of non-linearity and or transition.

Following Lees and Gold (7) this trend of transition indicated by experiments can be explained qualitatively by results of linear stability theory. Linear theory does not predict transition, but if one assumes that after a certain amplification of linear disturbances non-linearities occur, the distance from the body to the onset of non-linearities can be estimated. The ratio of amplitudes at two axial stations is:

$$\frac{Q'}{Q_i'} = \exp \int_{x_i}^{x} \frac{\alpha c_I}{c_g} \, dx \qquad (5.1)$$

From this relation, the axial distance x at which the fluctuation amplitude is Q' was evaluated by Lees and Gold (7) in the inner wake for the most unstable frequency; it is given by

$$\frac{x}{d} = \frac{x_N}{d} + \frac{(x_i - x_N)}{d} \left(\frac{Q'}{Q'}\right)^{D/\sqrt{Re_{f,d}}} \qquad (5.2)$$

$Re_{f,d}$ is the Reynolds number based on inner wake edge conditions. For a comparison with outer wake results $Re_{d,\infty}$ is determined from $Re_{f,d}$ using McCarthy's mean flow results (3). Some approximations

are made to obtain this relation [see (7)]. The most important one is that the maximum value of the rate of amplification of disturbances at a given frequency is chosen, ignoring its streamwise variation for a fixed frequency. This procedure underestimates the distance necessary to obtain a certain amplitude as indicated in Section 4.2.

The same calculation is now carried out for the outer wake. Empirical relations obtained from the present mean flow measurements are used to simplify the equations, and maximum amplification was assumed to hold along the wake axis, again ignoring the streamwise dependence for a fixed frequency.

The ratio of amplitudes (5.1) becomes

$$\ell n \left(\frac{Q'}{Q_i'}\right) = ab \frac{c_I}{\Delta u_{\ell}} \frac{1}{0.55} \int_{(x/d)_i}^{(x/d)} \left(\frac{\Delta u}{u_e}\right)^2 d\left(\frac{x}{d}\right)$$

where

$$\frac{\Delta u_{\ell}}{u_e} \frac{b}{d} \cong 0.55 \qquad \text{(empirical relation)}$$

$$\left(ab \frac{c_I}{\Delta u_{\ell}}\right)_{max} \cong 0.168 \quad \text{and} \quad c_g \cong u_e$$

Assuming the wake profile to be Gaussian and laminar linear theory (29) to hold, then one obtains for the velocity defect of the outer wake (Eq. 4.1)

$$\frac{\Delta u_{\ell}}{u_e} = \left(\frac{\Delta u_{\ell}}{u_e}\right)_o \sqrt{\frac{A}{A+4X}}$$

where

$$X = \frac{x-x_o}{d}$$

and

$$A = \frac{\left(\overline{b}/d\right)_o^2 \left(Re_d C\right)}{\ell n\, 2}$$

$$C \cong 1$$

The subscript "o" indicates some axial position at which A and $(\Delta u_{\ell} / u_e)_o$ are evaluated. The empirical relations for A and $(\Delta u_{\ell} / u_e)_o$ are as follows:

$$A = 34.6\ Re_d^{0.66} + 800$$

$$\left(\frac{\Delta u_{\ell}}{u_e}\right)^2 = 0.00524\, Re_d^{0.194}$$

where

$$\frac{x_o}{d} = 200$$

The final formula for the outer wake becomes then

$$\frac{x}{d} = \left(\frac{x_o}{d} - \frac{A}{4}\right) + \left(\frac{x_i - x_o}{d} + \frac{A}{4}\right)\left(\frac{Q'}{Q_i'}\right)^{\frac{1}{C_1}} \qquad (5.3)$$

and with $\frac{x_i}{d} = 200$ and $\frac{x_o}{d} = 200$, it is

$$\frac{x}{d} = \left(200 - \frac{A}{4}\right) + \frac{A}{4}\left(\frac{Q'}{Q_i'}\right)^{\frac{1}{C_1}}$$

where

$$C_1 = \left(a\, b\, \frac{c_I}{\Delta u_{\ell}}\right)_{max} \frac{A(\Delta u_{\ell}/u_e)_o^2}{2.20}$$

The results of the linear stability calculation for an amplitude ratio of $Q'/Q_i' = 100$ are shown as solid lines in Figure 35. Qualitatively

the trend of "transition" as the Reynolds number decreases is verified by linear stability theory. The effect of viscosity will be to damp laminar oscillations; at sufficiently low Reynolds number the curves will approach vertical asymptotes.

6. SUMMARY OF RESULTS AND SUGGESTIONS FOR FUTURE WORK

6.1. Summary of Results

A detailed flow field and stability study has been carried out in the wake of circular cylinders at a Mach number of 6 in a Reynolds number range Re_d = 200 - 4000. Mean flow measurements were done up to axial distances x/d = 2400 and fluctuation measurements up to x/d = 12,000.

Mean Wake Flow

At these low Reynolds numbers the inner viscous wake stemming from the cylinder boundary layer is laminar and loses its identity within 60 diameters or less, depending on the Reynolds number. The outer wake caused by the bow shock expands back to free stream pressure in the first 100 diameters and is effectively inviscid in this region, compared to the inner viscous wake. Further downstream ($x/d \geq 100$) the wake is viscous. Experimental results agree with steady laminar linear theory for the Reynolds number cases Re_d = 3840, Re_d = 2400 and Re_d = 320 up to the respective maximum axial distances attainable, i.e. $(x/d)_{max.}$ = 600, 960 and 2400, and at Re_d = 960 up to $x/d \sim 1400$. Even at the lowest Reynolds number (Re_d = 320) the wake profiles are not yet similar at the maximum axial station, x/d = 2400. At Re_d = 960, 576, 384 strong deviations from steady laminar behavior are observed starting at $x/d \sim 1600$, 2400, 3600 respectively, suggesting laminar instabilities of the flow upstream of these points, a breakdown of laminar steady flow and a

non-linear nonsteady behavior which increases the "effective diffusivity" of the mean flow.

Stability of the Outer Wake

In a certain Reynolds number range, a linear growth region is followed by a non-linear region. Small disturbances over a wide frequency band are amplified, with a distinct peak at the most unstable frequency, but no monochromatic periodic signals are detected such as those found in the low speed wakes behind a flat plate.

In the linear growth region the most unstable frequencies are very close to the ones predicted by linear stability theory; the measured rates of amplification are somewhat lower than predicted by theory, and the difference is attributed to the difference between the experimentally measured mean wake profiles and the ones used in theory (Gaussian).

To first approximation the normalized rates of amplification are correlated by one curve for both incompressible and hypersonic wakes at $M_\infty = 6$; i.e. in terms of $\alpha b \frac{c_I}{\Delta u_{\mathfrak{L}}}$ versus αb (where b is the physical wake width) one curve is obtained. Thus, the rate of amplification, $\frac{1}{Q'} \frac{dQ'}{d(x/d)} \left(= \frac{\alpha c_I d}{c_g}\right)$ is indirectly influenced by viscosity (Reynolds number) through its effect on the mean flow.

In the non-linear region the mean flow decays faster than predicted by steady laminar theory and the wake width increases more rapidly. This mean flow behavior is associated with a further increase of the amplitude of the fundamental instability component and the appearance of the first harmonic, which increases rapidly to a

triple peak fluctuation profile. "Saturation" of these two components does not occur within a non-linear region 800 cylinder diameters in length at $Re_d = 960$ indicating a long "stretched-out" non-linear region in comparison with the low speed wake.

From these far wake fluctuation measurements together with earlier inner wake investigations, a tentative picture of the onset of non-linearity and/or transition is given for the cylinder wake at $M_\infty = 6$. At very low Reynolds numbers, $Re_d \leqslant 150$, the whole wake is laminar. When the Reynolds number is increased above this level the onset of strong non-linear effects occurs several thousand diameters downstream of the cylinder; it moves toward the body at higher Reynolds numbers until it reaches, for example, $x/d \sim 1000$ at $Re_d = 4000$. Then the onset of non-linearity and/or transition "jumps" at $Re_d \sim 10^4$ to the inner wake in the vicinity of $x/d \sim 100$ and continues to move forward as the Reynolds number is increased still further.

6.2. Suggestions for Future Work

On the basis of the present study several related investigations of interest are suggested:

(1) An experimental investigation of the near wake region to find the shear layer and near wake structure, the wake shocks (if there are any) and the base pressure behavior in the range of Reynolds numbers considered in the present study; and also at still lower Reynolds numbers in order to find the limits of continuum flow.

(2) Study of the damping of fluctuations experienced in moving from the free stream to the near wake, and the influence of radiation from the turbulent boundary as it interacts with the shocks and wake.

(3) Inner wake stability studies along the lines suggested in Section 3.2; especially a frequency analysis of fluctuations.

(4) Studies in the linear region of the far "outer" wake with artificial disturbances of controlled frequency and amplitude to find their influence on the extent of this region, and to compare the results with the natural fluctuation measurements.

(5) Investigation of the non-linear wake region using controlled artificial disturbances to move the onset of non-linearity further upstream than observed with natural fluctuations. In that case the wake might become turbulent, within the available test section length (12"), so that the whole transition region could be studied and the turbulent wake as well.

REFERENCES

1. Behrens, W. and L. Lees: "Technical Comment," AIAA J. 3, 991-992 (1965).

2. Demetriades, A.: "Some Hot-Wire Anemometer Measurements in a Hypersonic Wake," Proc. 1961 Heat Transfer and Fluid Mechanics Institute.

3. McCarthy, J. F. Jr.: "Hypersonic Wakes," GALCIT Hypersonic Research Project, Memorandum No. 67 (1962). Also, McCarthy, J. F. Jr. and T. Kubota: "A Study of Wakes Behind a Circular Cylinder at M = 5.7," AIAA J. 2, 629-636 (1964).

4. Lees, L.: "Hypersonic Wakes and Trails," AIAA J. 2, 417-428 (1964).

5. Lees, L. and C. C. Lin: "Investigation of the Stability of the Laminar Boundary Layer in a Compressible Fluid," NACA TN 1115 (1946).

6. Sato, H. and K. Kuriki: "The Mechanism of Transition in the Wake of a Thin Flat Plate Placed Parallel to a Uniform Flow," J. Fluid Mech. 11, 321-352 (1961).

7. Lees, L. and H. Gold: "Stability of Laminar Boundary Layers and Wakes at Hypersonic Speeds. Part I. Stability of Laminar Wakes," Fundamental Phenomena in Hypersonic Flow, ed. by J. Gordon Hall, Cornell Univ. Press, 310-342 (1966).

8. Laufer, J.: "Aerodynamic Noise in Supersonic Wind Tunnels," J. Aero. Sci. 28, 685-692 (1961).

9. Laufer, J.: "Some Statistical Properties of the Pressure Field Radiated by a Turbulent Boundary Layer," Phys. Fluids 7, 1191-1197 (1964).

10. Kovasznay, L. S. G.: "Hot Wire Method," High Speed Aerodynamics and Jet Propulsion, Vol. IX, Section F.2, Princeton University Press (1954).

11. Vrebalovich, T.: "Application of Hot-Wire Techniques in Unsteady Compressible Flows," California Institute of Technology, JPL TR 32-229 (May, 1962). Presented at ASME Hydraulic Division Conference, May 21-23, 1962.

REFERENCES (Cont'd)

12. Laufer, J. and T. Vrebalovich: "Stability and Transition of a Supersonic Laminar Boundary Layer on an Insulated Flat Plate," J. Fluid Mech. 9, 257-299 (1960).

13. Kovasznay, L. S. G.: "Turbulence in Supersonic Flow," J. Aero. Sci. 20, 657-674 and 682 (1953).

14. Ribner, H. S.: "Shock-Turbulence Interaction and the Generation of Noise," NACA TR 1233 (1955).

15. Johnson, W. R. "The Interaction of Plane and Cylindrical Sound Waves with Stationary Shock Waves," University of Michigan, Technical Report 2539-8-T (1957).

16. Morkovin, M.: "Effects of High Acceleration on a Turbulent Supersonic Shear Layer," The 1955 Heat Transfer and Fluid Mechanics Institute IV, 1-17.

17. Launder, B. E.: "Laminarization of the Turbulent Boundary Layer by Acceleration," Mass. Inst. of Tech., Gas Turbine Laboratory Report No. 77 (1964).

18. Atvars, J., L. K. Schubert, E. Grande and H. S. Ribner: "Refraction of Sound by Jet Flow or Jet Temperature," UTIAS Technical Note No. 109 (1965).

19. Kendall, J. M. Jr.: "Experimental Study of Cylinder and Sphere Wakes at a Mach Number of 3.7," Technical Report No. 32-363, Jet Propulsion Laboratory, California Institute of Technology, Pasadena, Calif. (1962).

20. Kovasznay, L. S. G.: "Hot-Wire Investigation of the Wake Behind Cylinders at Low Reynolds Numbers," Proc. Royal Society, A, 19B, 174-189 (1949).

21. Schubauer, G. B. and H. K. Skramstad: "Laminar Boundary Layer Oscillations and Transition on a Flat Plate," NACA TR 909 (1948).

22. Betchov, R. and A. Szewczyk: "Stability of a Shear Layer Between Parallel Streams," Physics of Fluids 6, 1391-1396 (1963).

23. Whitham, G. B.: "Group Velocity and Energy Propagation for Three-Dimensional Waves," Communications on Pure and Applied Math, 14, 675-691 (1961).

REFERENCES (Cont'd)

24. Gaster, M.: "The Role of Spatially Growing Waves in the Theory of Hydrodynamic Stability," Progress Aero. Sci. 6, 251-270 (1965).

25. Gold, H.: "Stability of Laminar Wakes," California Institute of Technology, Ph. D. Thesis (1963).

26. Kendall, J. M. Jr.: "Stability of a Supersonic Wake Flow, Part II," Jet Propulsion Laboratory, California Institute of Technology, Space Programs Summary No. 37-34, Vol. IV (1965).

27. Taneda, L.: "Oscillations of the Wake Behind a Flat Plate Parallel to the Flow," J. Phys. Soc. of Japan, 13, 418-425 (1958).

28. Hama, F. R.: "An Interpretation of the Laminar-Wake Development Behind a Flat Plate," Jet Propulsion Laboratory, California Institute of Technology, Space Programs Summary No. 37-28, Vol. IV (August 31, 1964).

29. Kubota, T.: "Laminar Wake with Streamwise Pressure Gradient," GALCIT Hypersonic Research Project, Internal Memorandum No. 9 (April 1962).

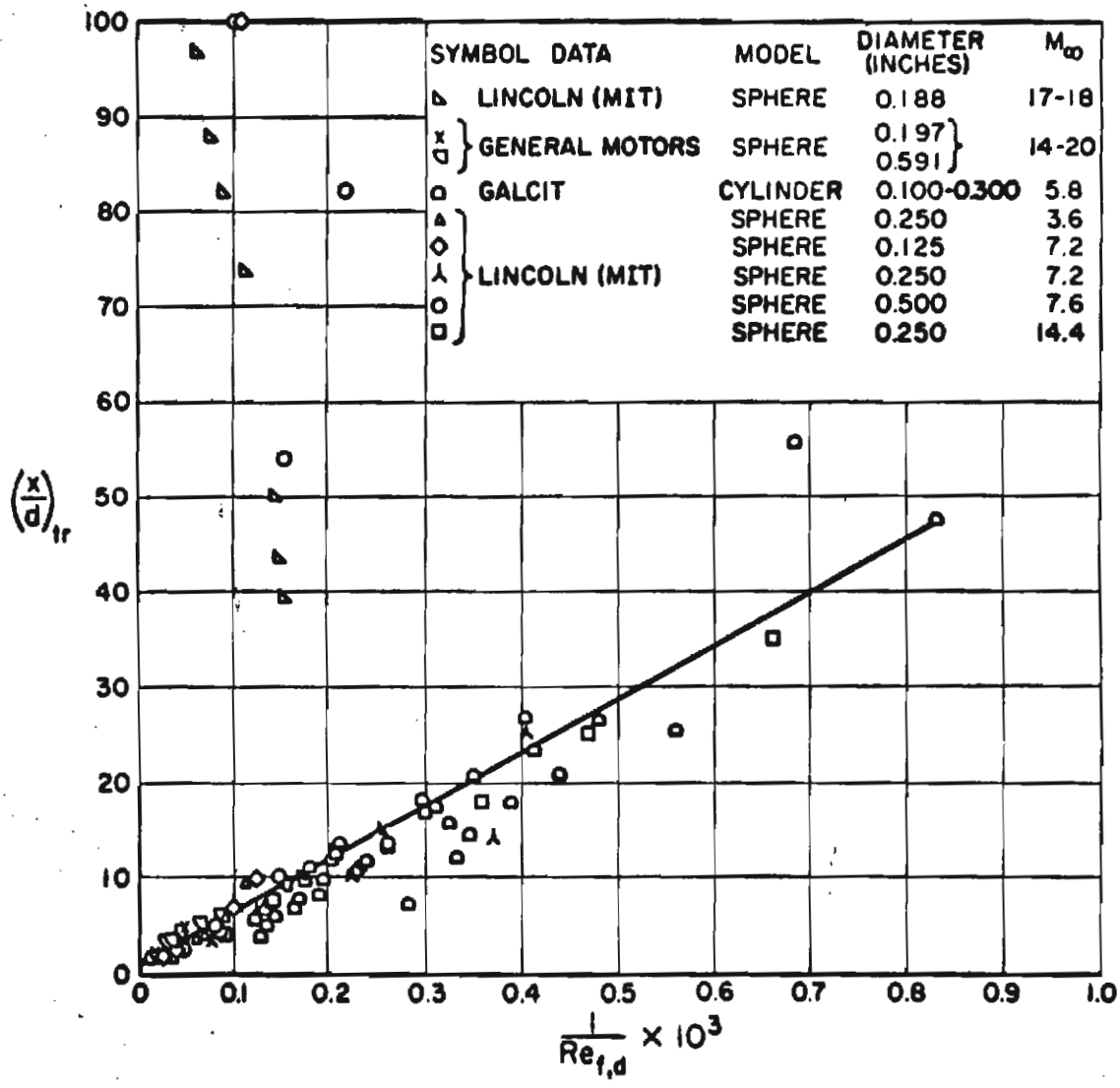

FIG. 1 CORRELATION OF TRANSITION TO TURBULENT FLOW IN THE HYPERSONIC INNER WAKE BEHIND BLUNT BODIES

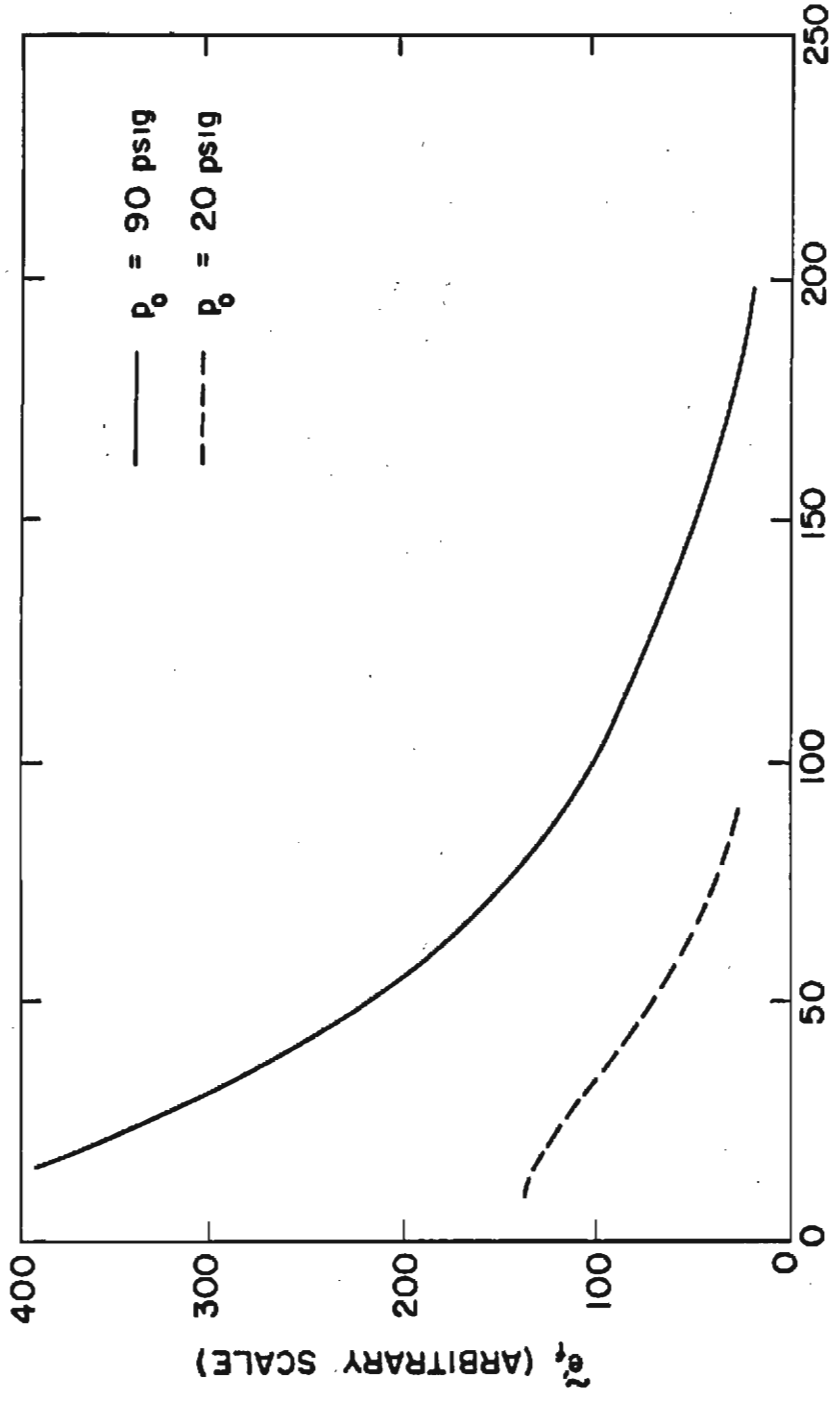

FIG. 2 FREQUENCY DISTRIBUTION OF FLUCTUATIONS IN THE FREE STREAM

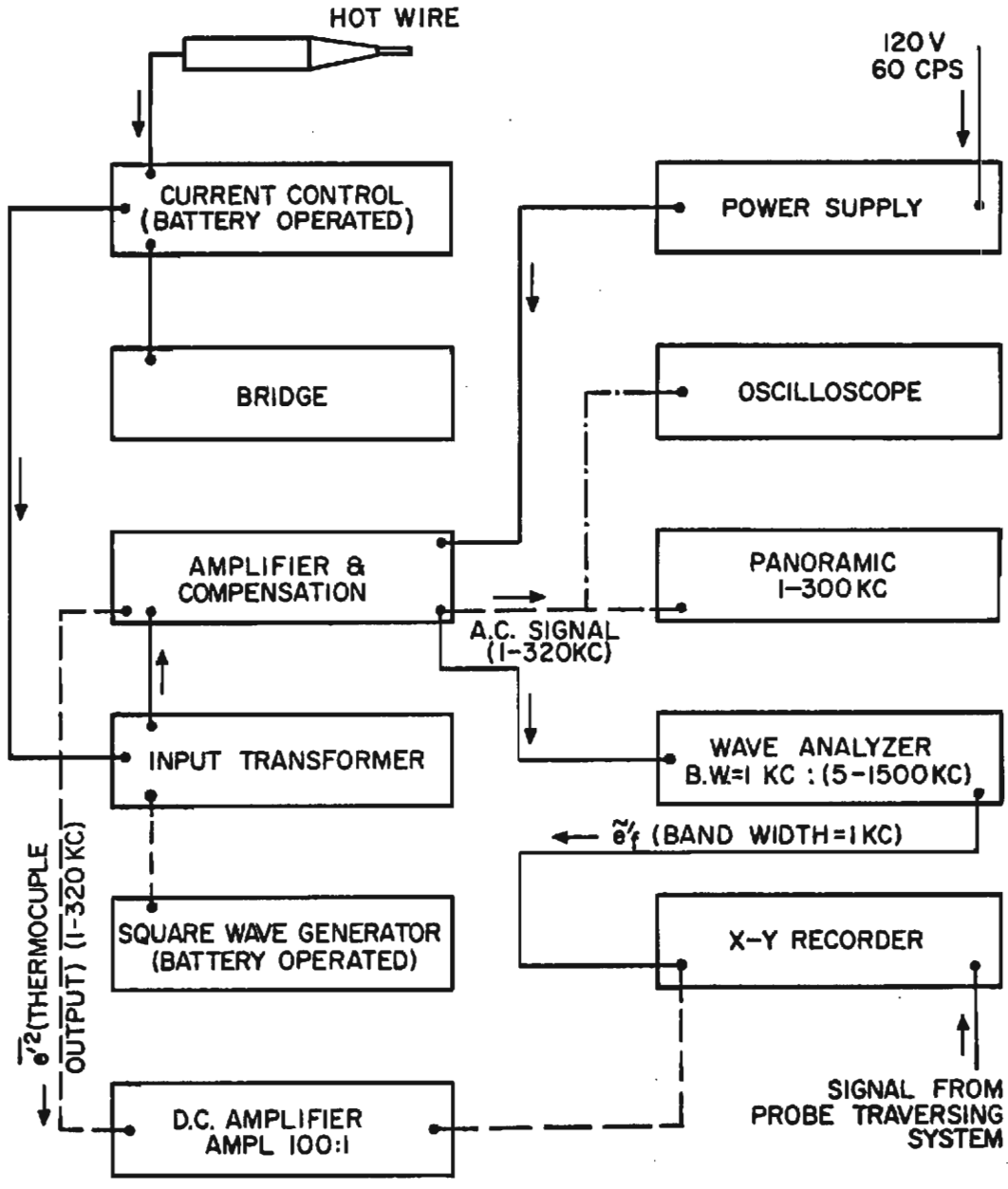

—·—·— COMPENSATION PROCEDURE

– – – – MEAN SQUARE MEASUREMENT ($\overline{e'^2}$)

——— ROOT MEAN SQUARE MEAS. AT PARTICULAR FREQUENCY ($\tilde{e}'_f$)

——— CONNECTIONS FOR ALL THREE MEASUREMENTS

FIG. 3 HOT WIRE FLUCTUATION MEASUREMENT SET-UP

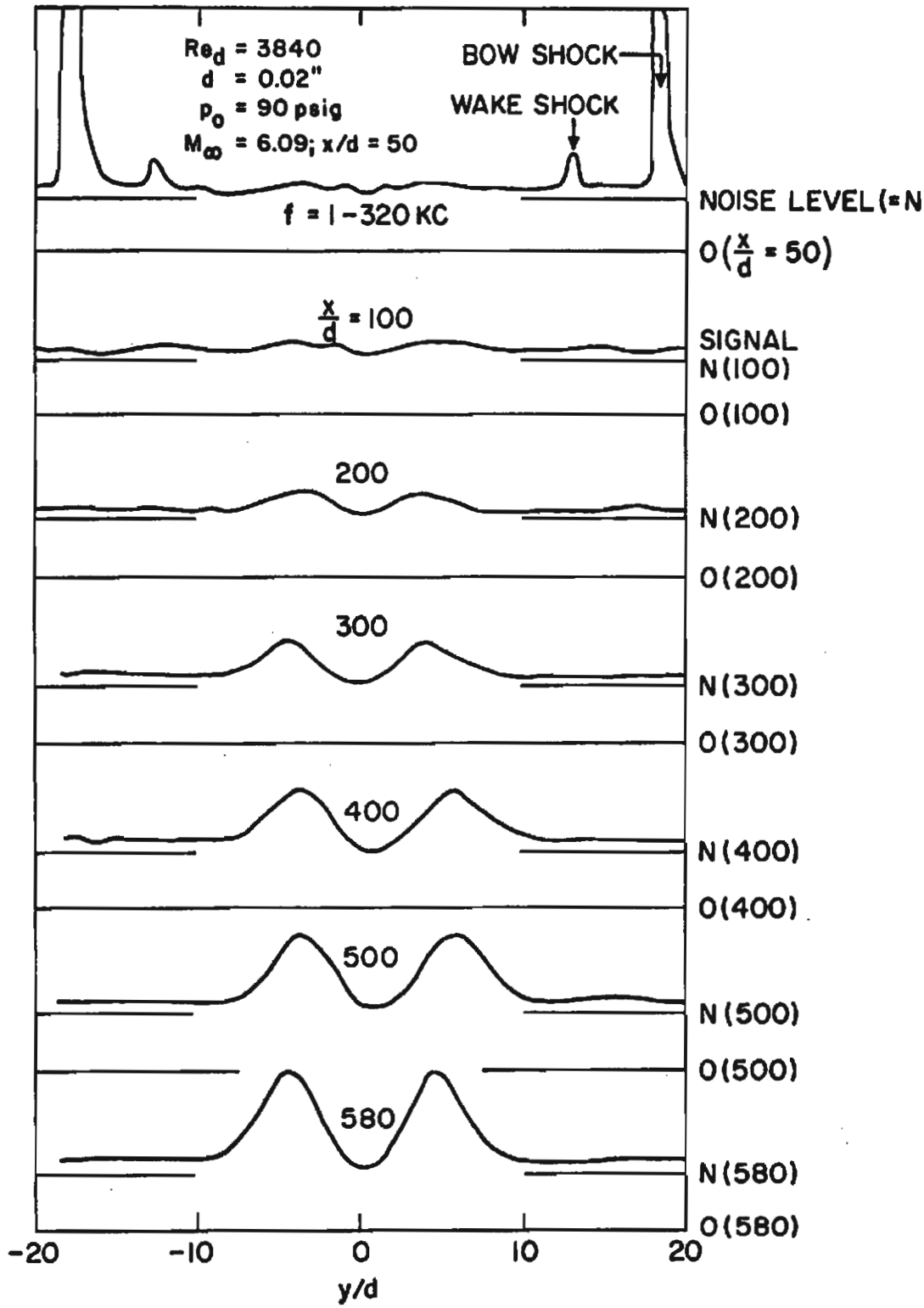

FIG.4a MEAN SQUARE FLUCTUATION MEASUREMENTS IN THE WAKE OF A CYLINDER AT Re_d = 3840

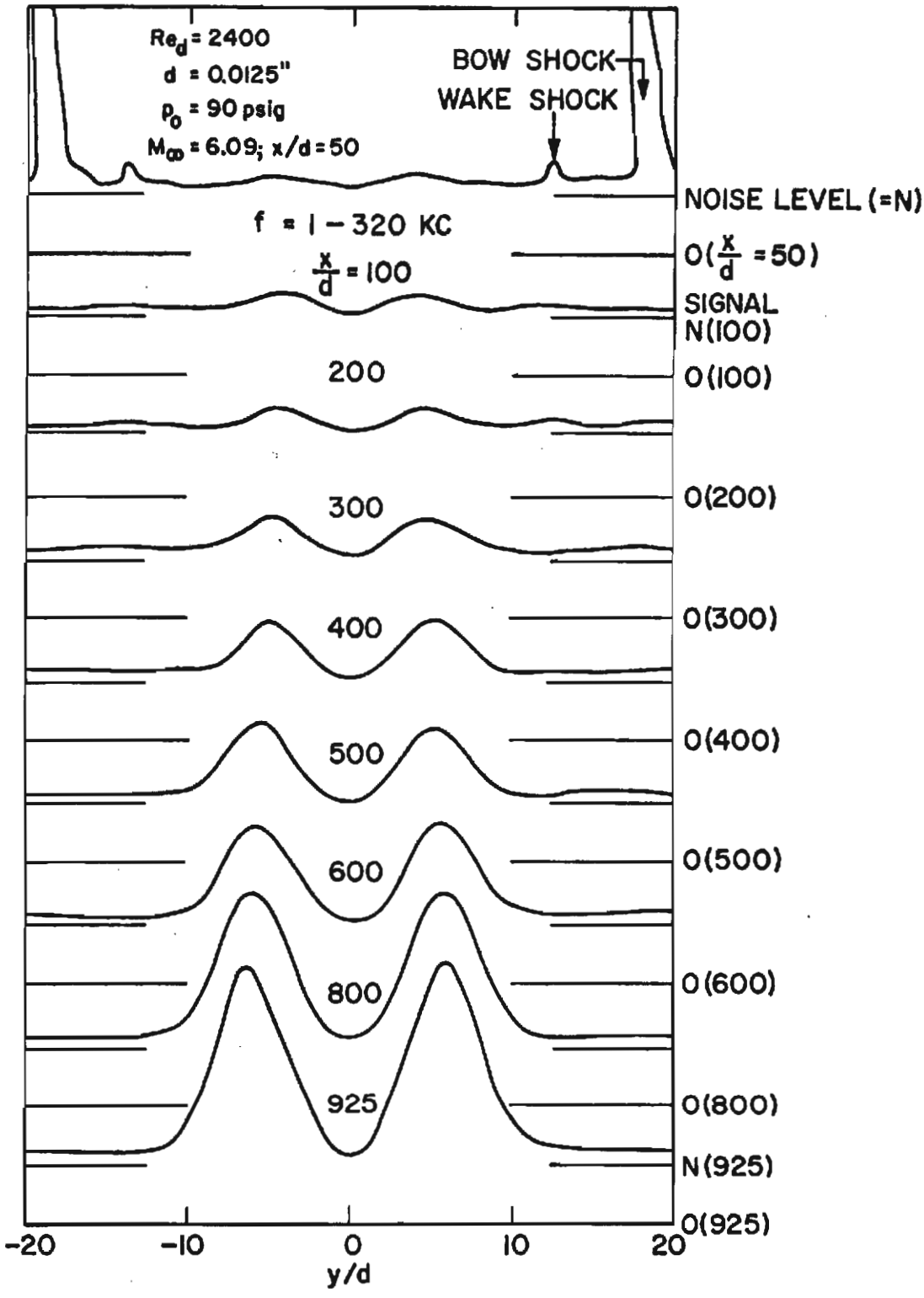

FIG. 4b MEAN SQUARE FLUCTUATION MEASUREMENTS IN THE WAKE OF A CYLINDER AT $Re_d = 2400$

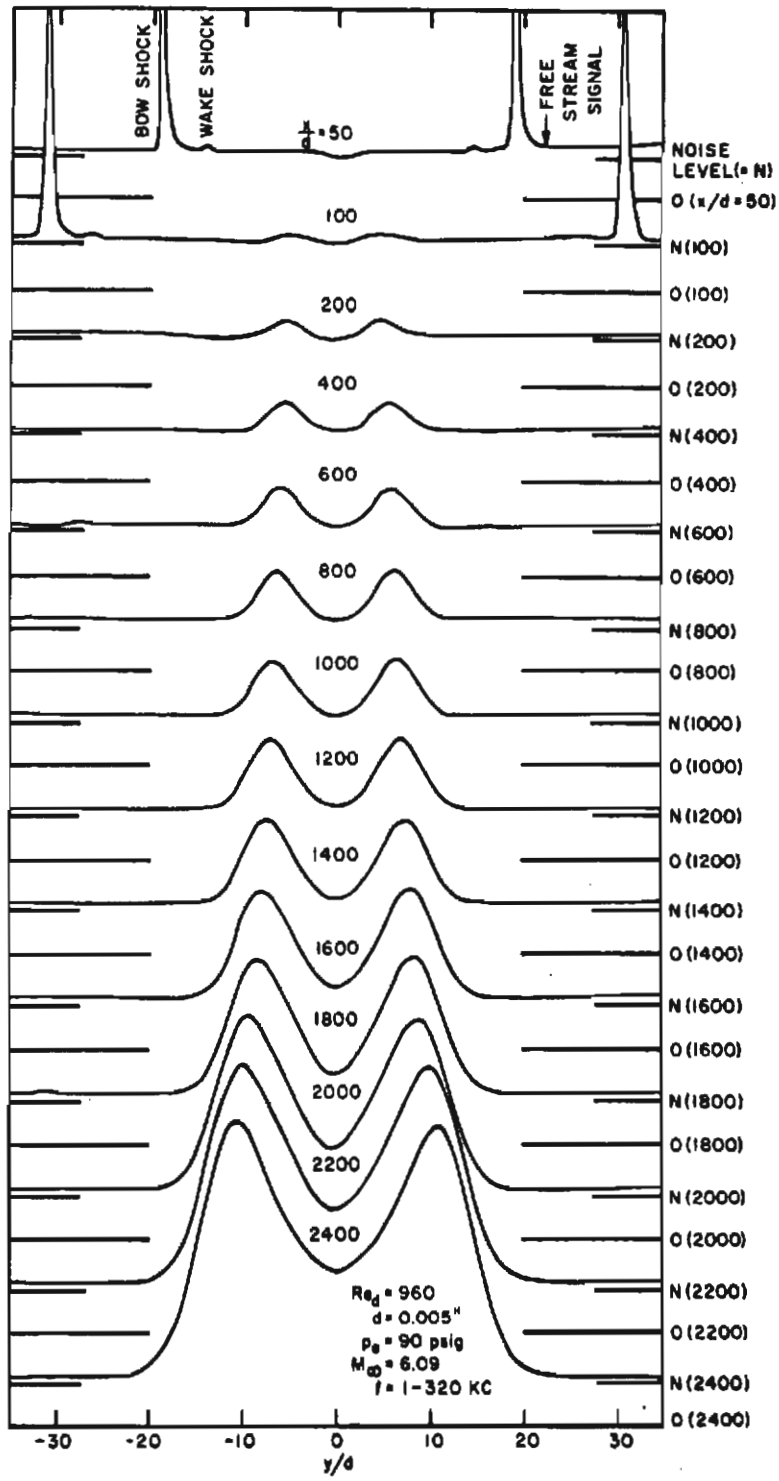

FIG. 4c MEAN SQUARE FLUCTUATION MEASUREMENTS IN THE WAKE OF A CYLINDER

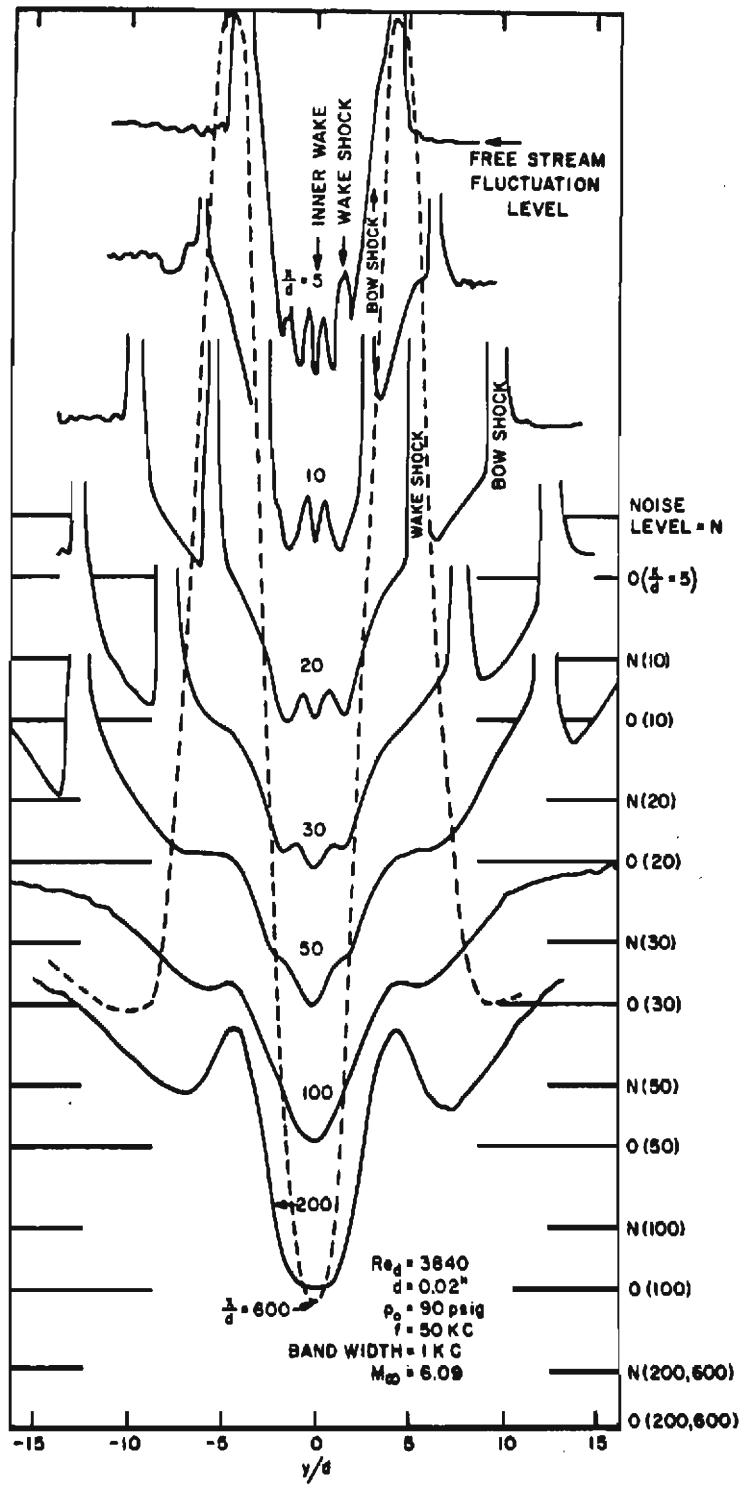

FIG. 5 HOT WIRE RMS-FLUCTUATIONS
IN THE WAKE OF A CYLINDER

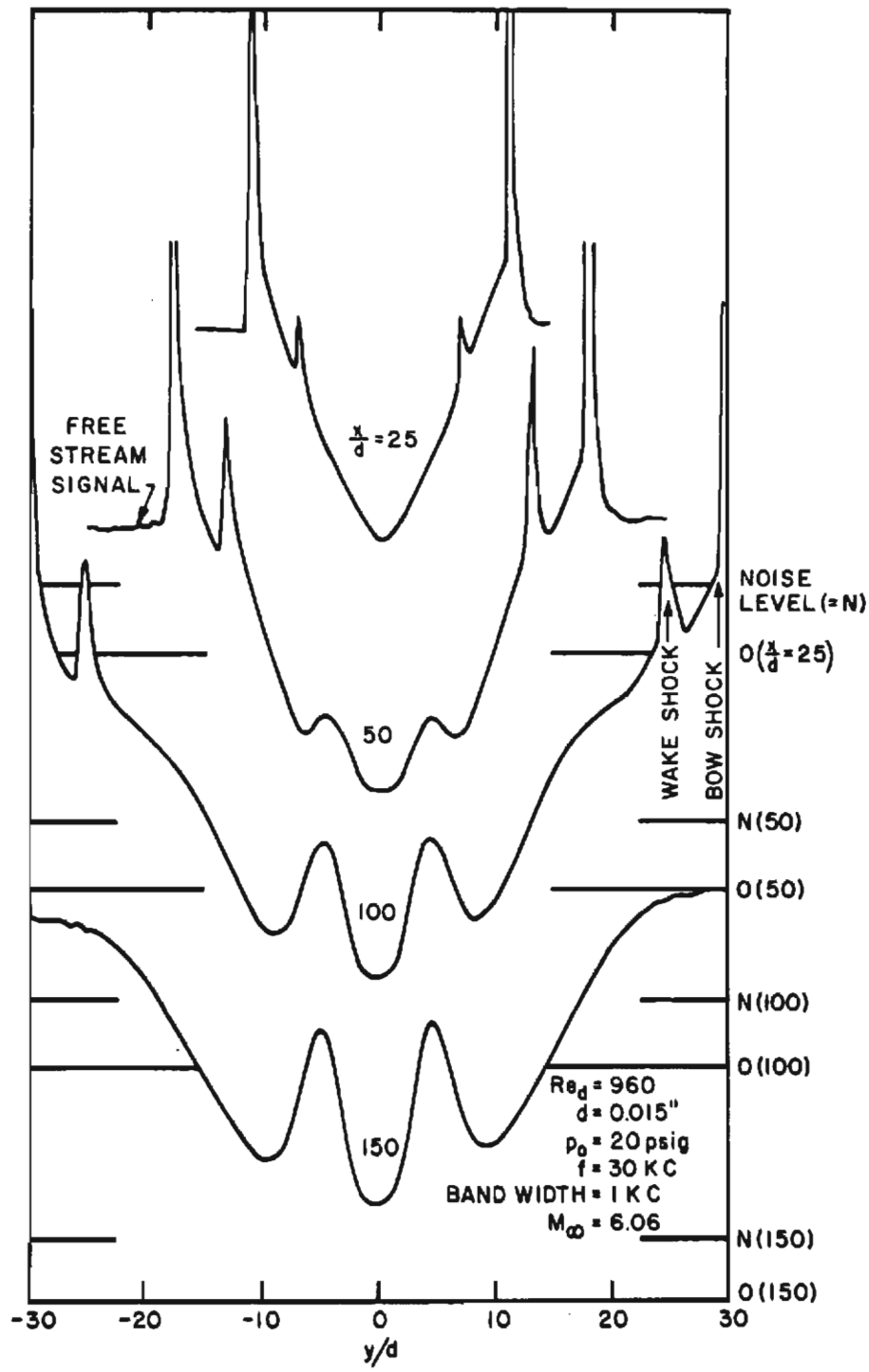

FIG.6 HOT WIRE RMS FLUCTUATIONS
IN THE WAKE OF A CYLINDER

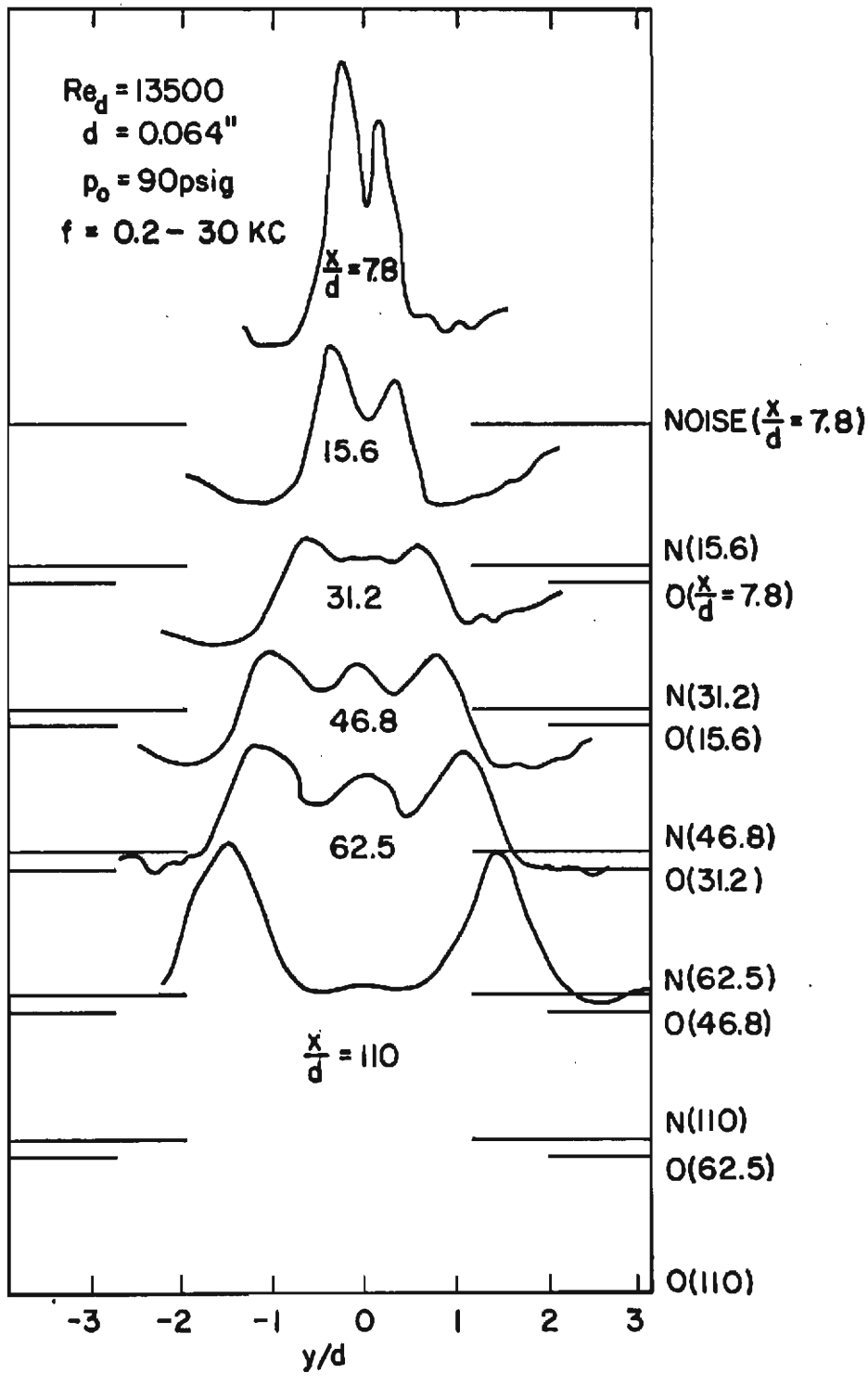

FIG.7a MEAN SQUARE FLUCTUATION MEASUREMENTS IN THE INNER WAKE AT Re_d = 13500

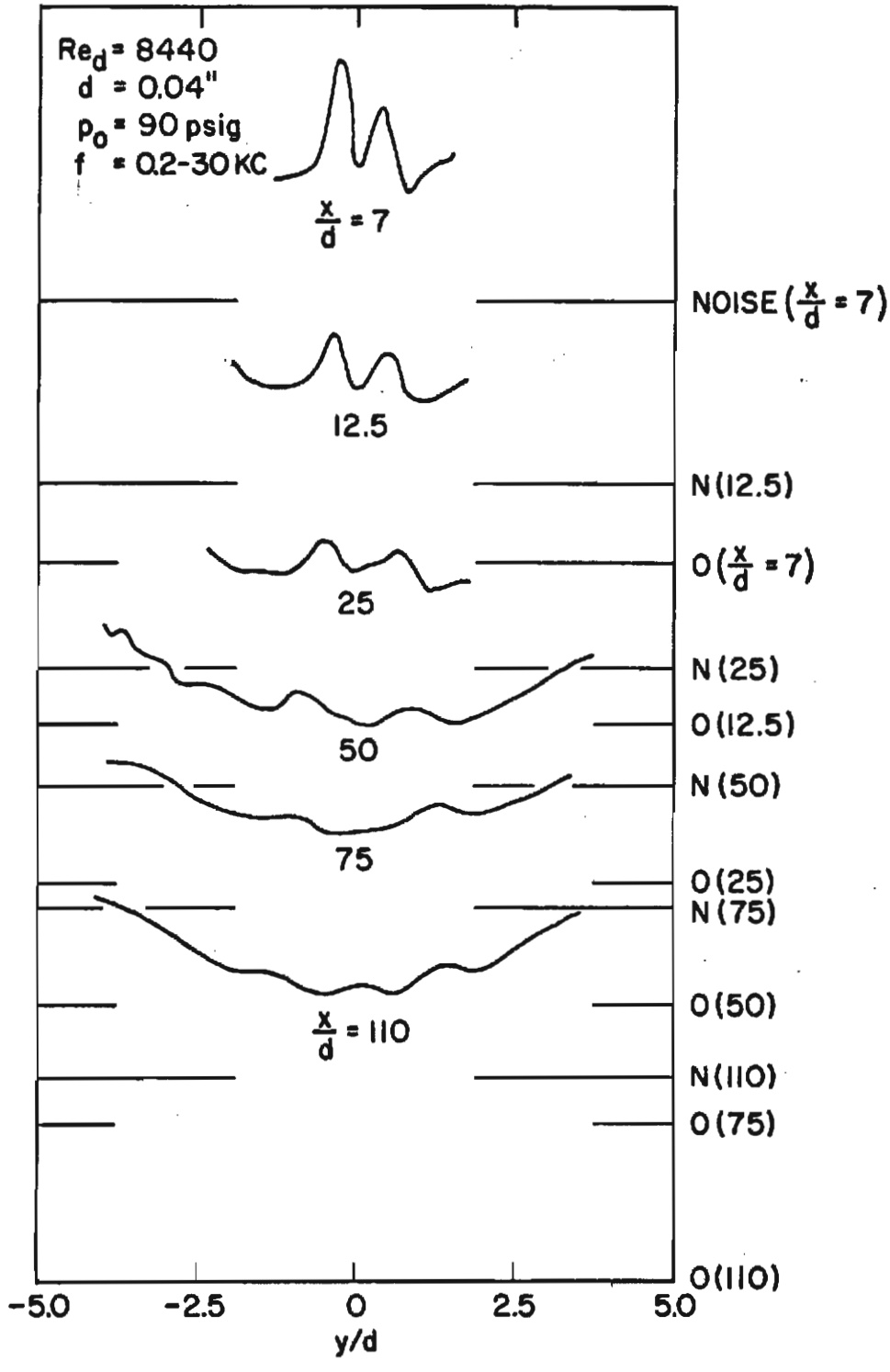

FIG.7b MEAN SQUARE FLUCTUATION MEASUREMENTS IN THE INNER WAKE AT Re_d = 8440

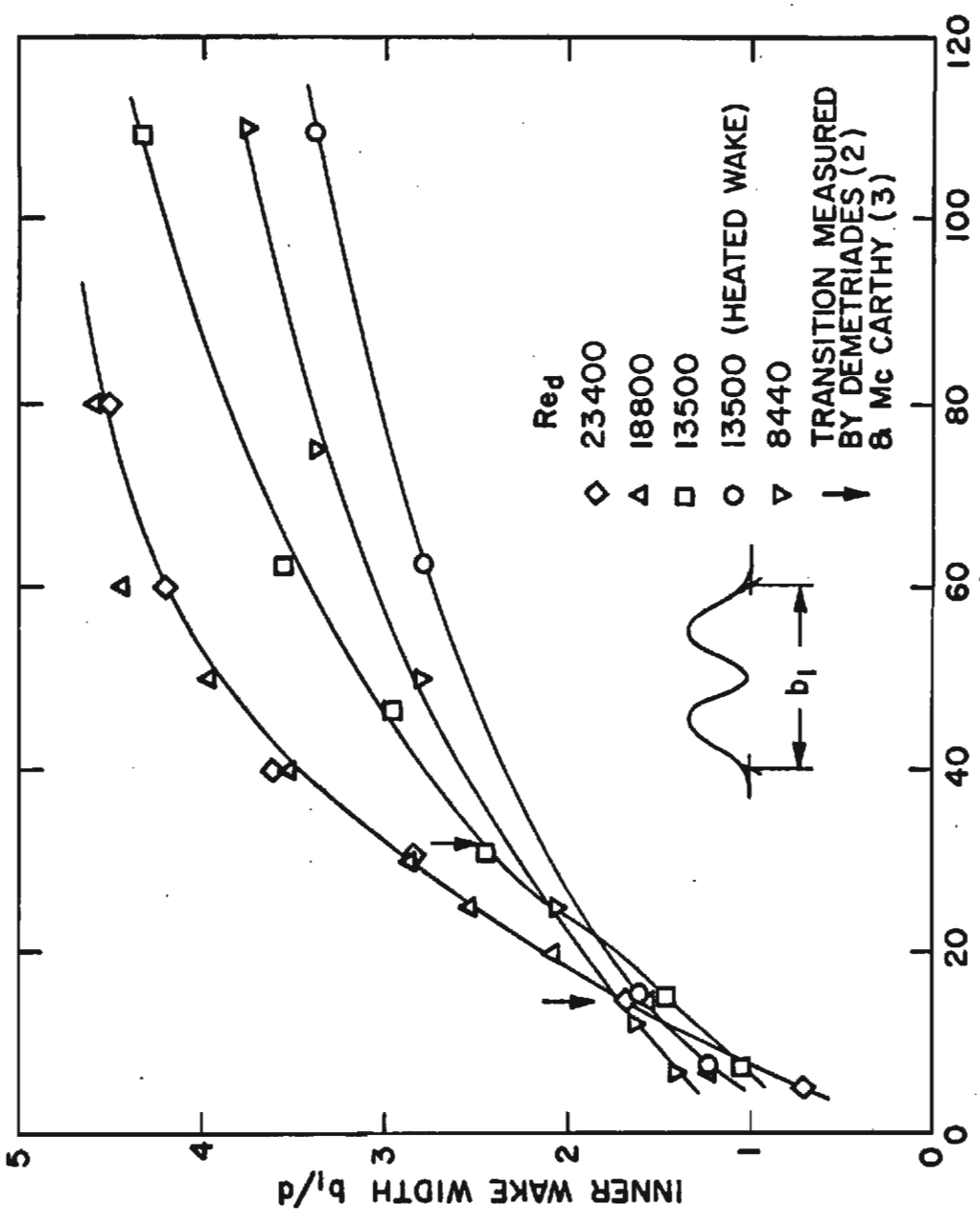

FIG.8 INNER WAKE WIDTHS AS OBTAINED FROM MEAN SQUARE FLUCTUATION MEASUREMENTS

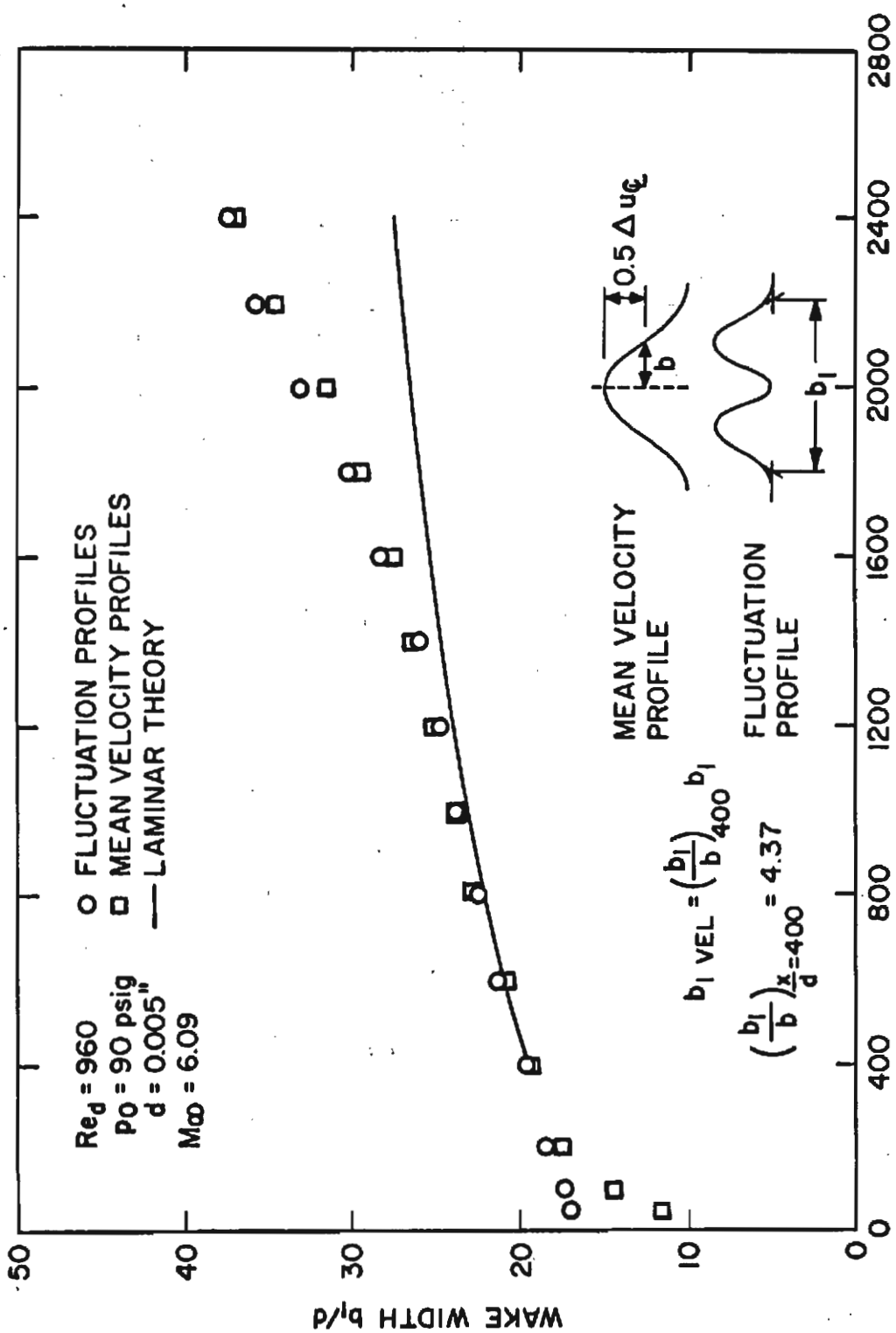

FIG. 9 WAKE WIDTH COMPARISON AS DETERMINED FROM MEAN FLOW AND M.S. FLUCTUATION PROFILES

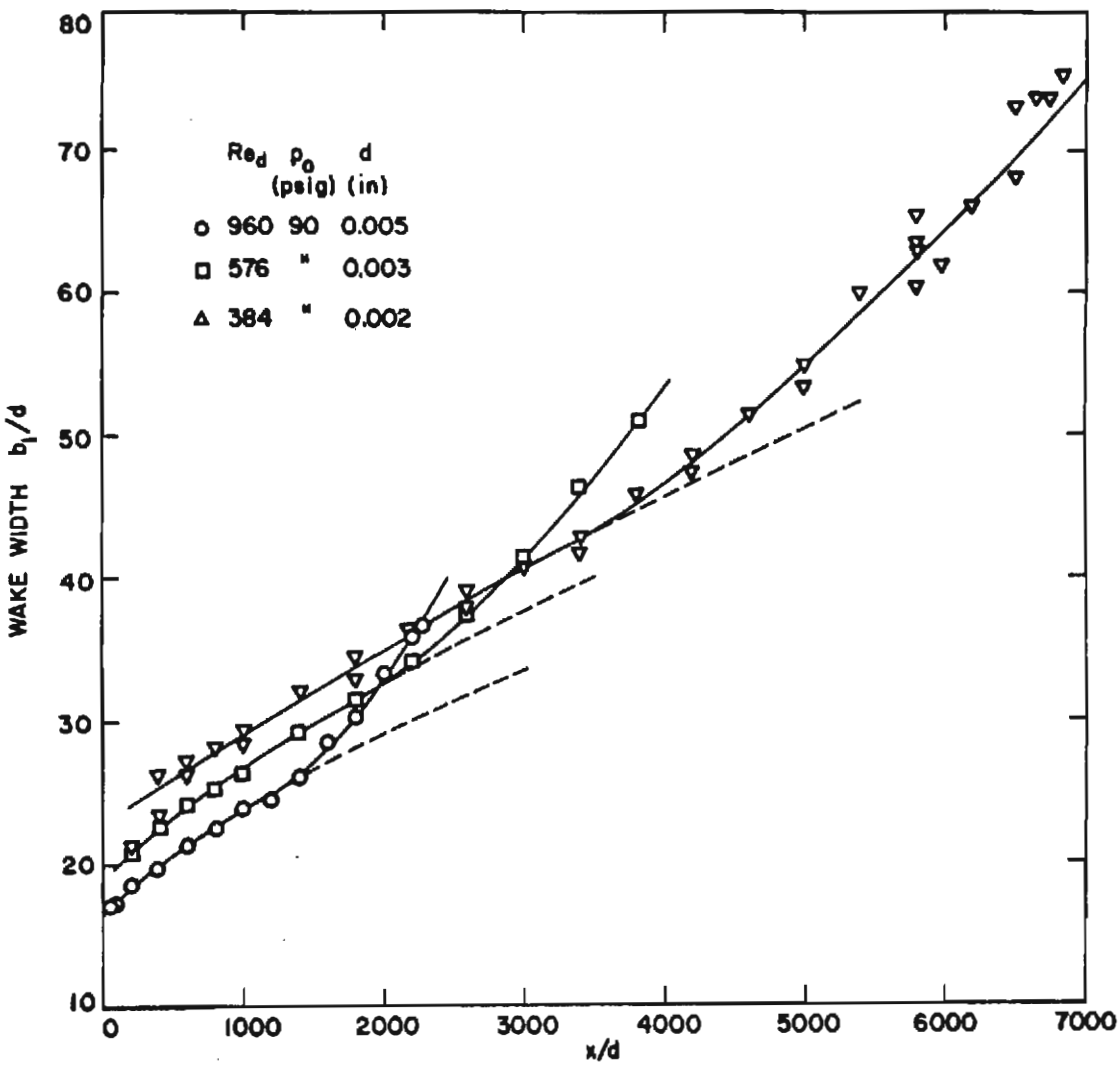

FIG.10 WAKE GROWTH AT SEVERAL REYNOLDS NUMBERS

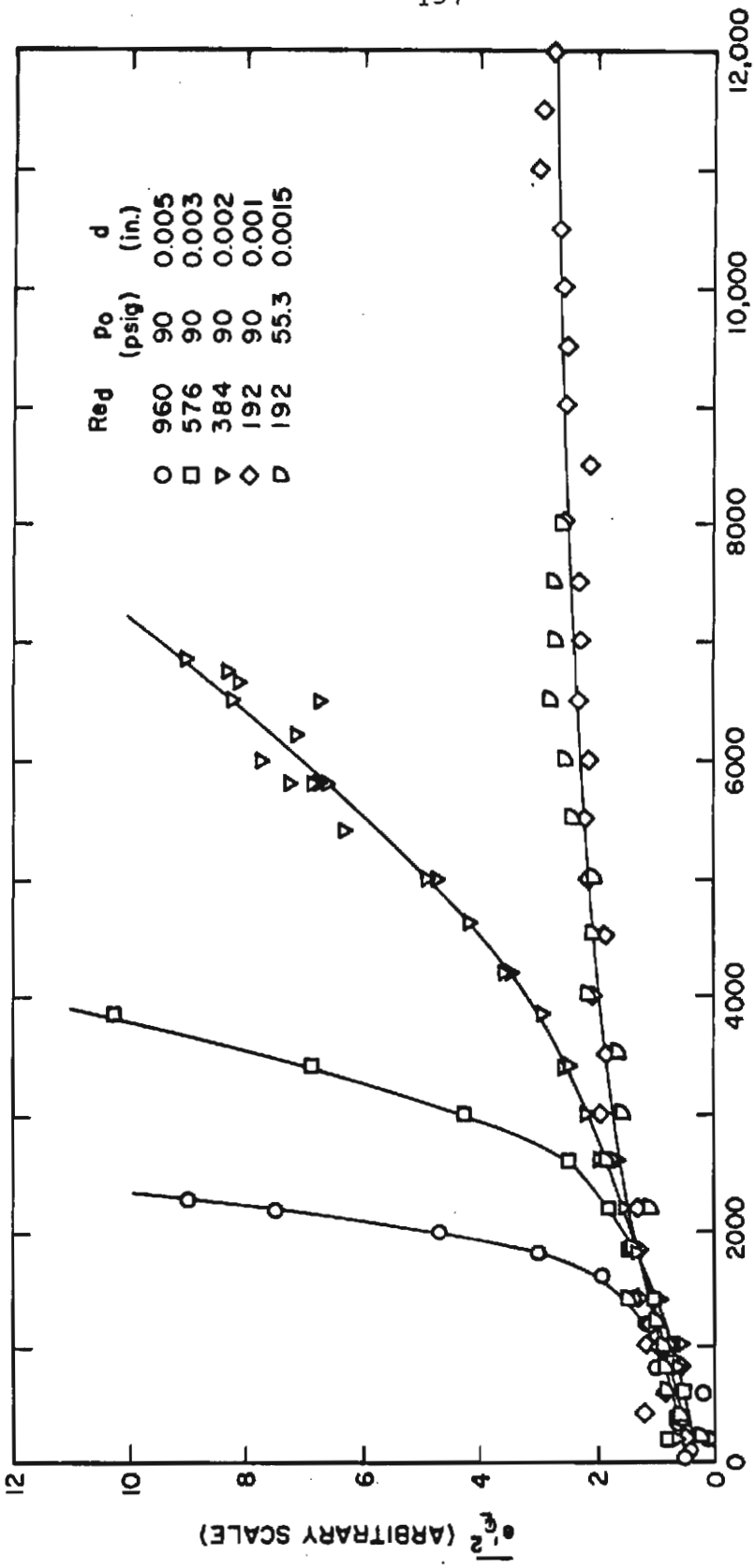

FIG. 11 MEAN SQUARE FLUCTUATION SIGNAL AT WAKE CENTER LINE

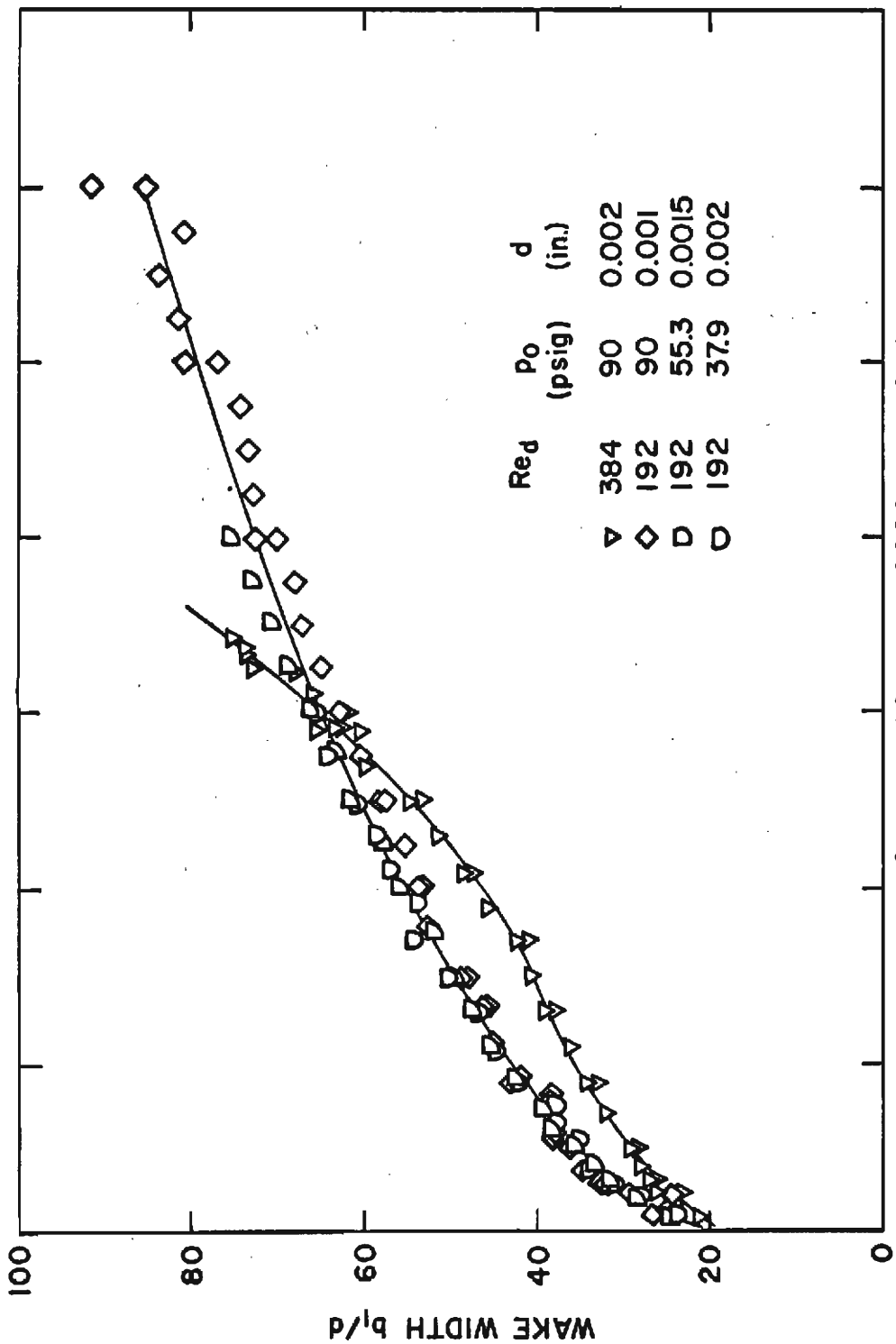

FIG.12 REYNOLDS NUMBER SIMILARITY IN LAMINAR WAKES

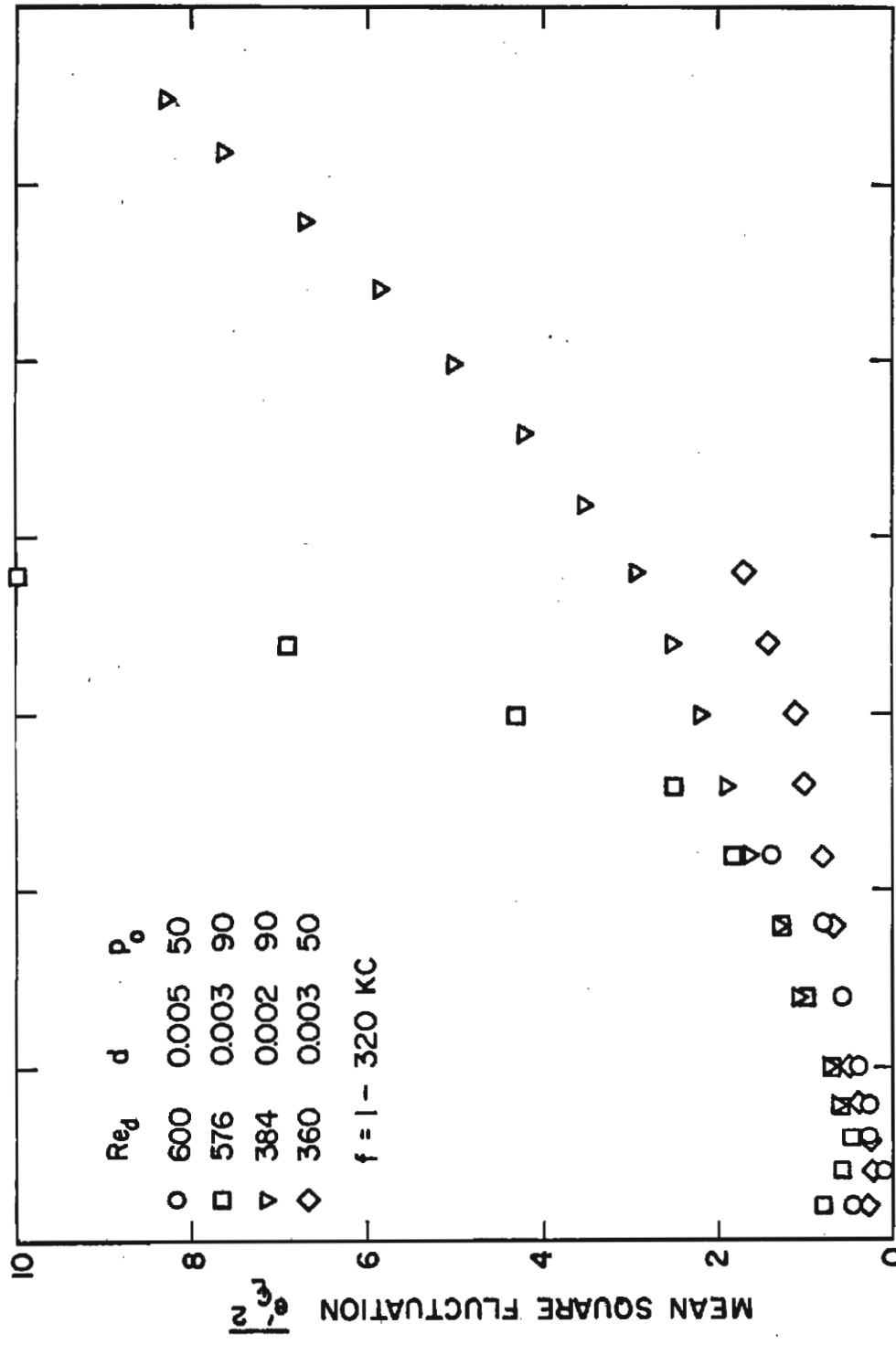

FIG.13 MEAN SQUARE FLUCTUATION SIGNALS ON THE WAKE CENTERLINE

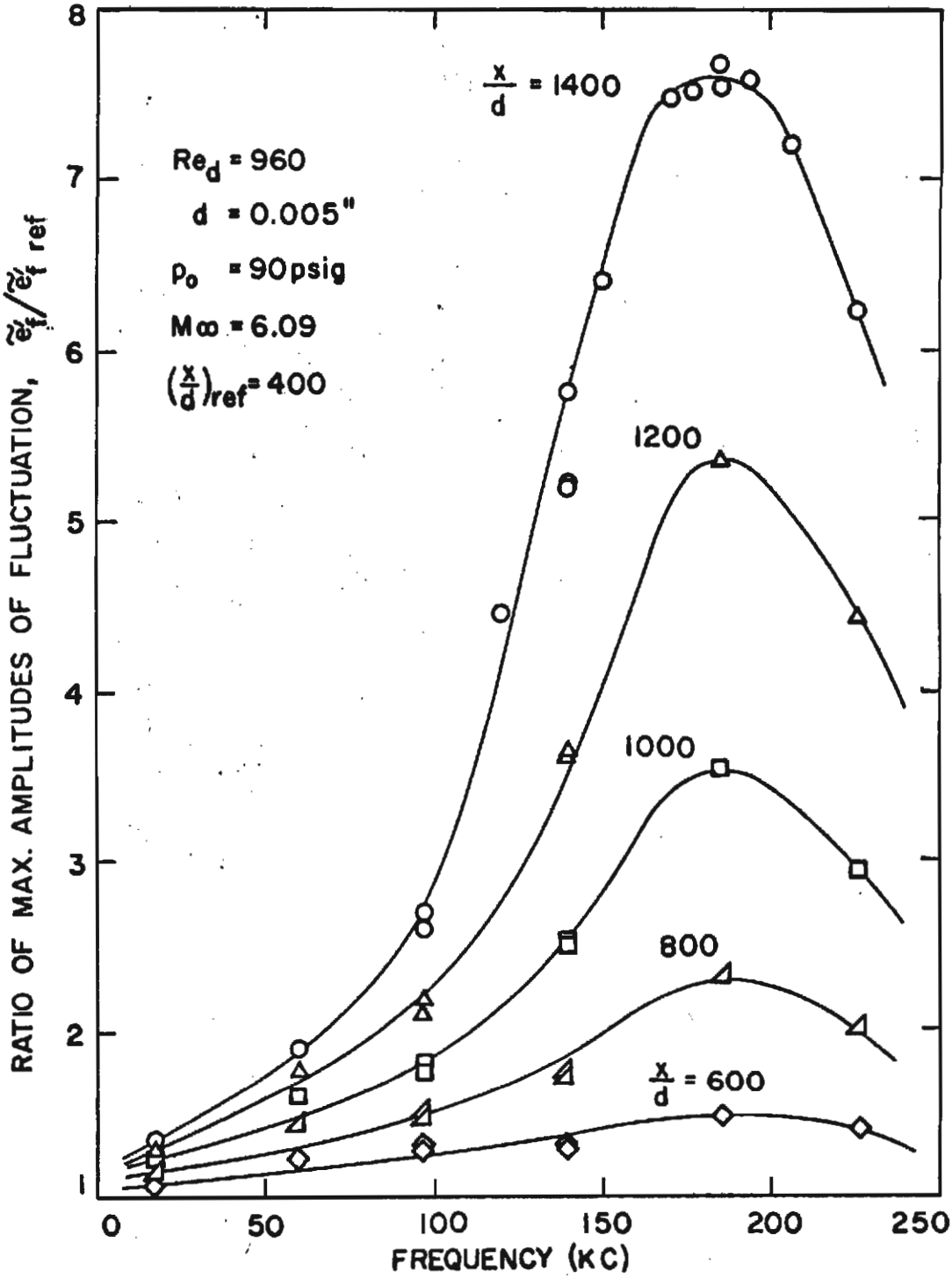

FIG. 14 GROWTH OF FLUCTUATIONS IN THE WAKE

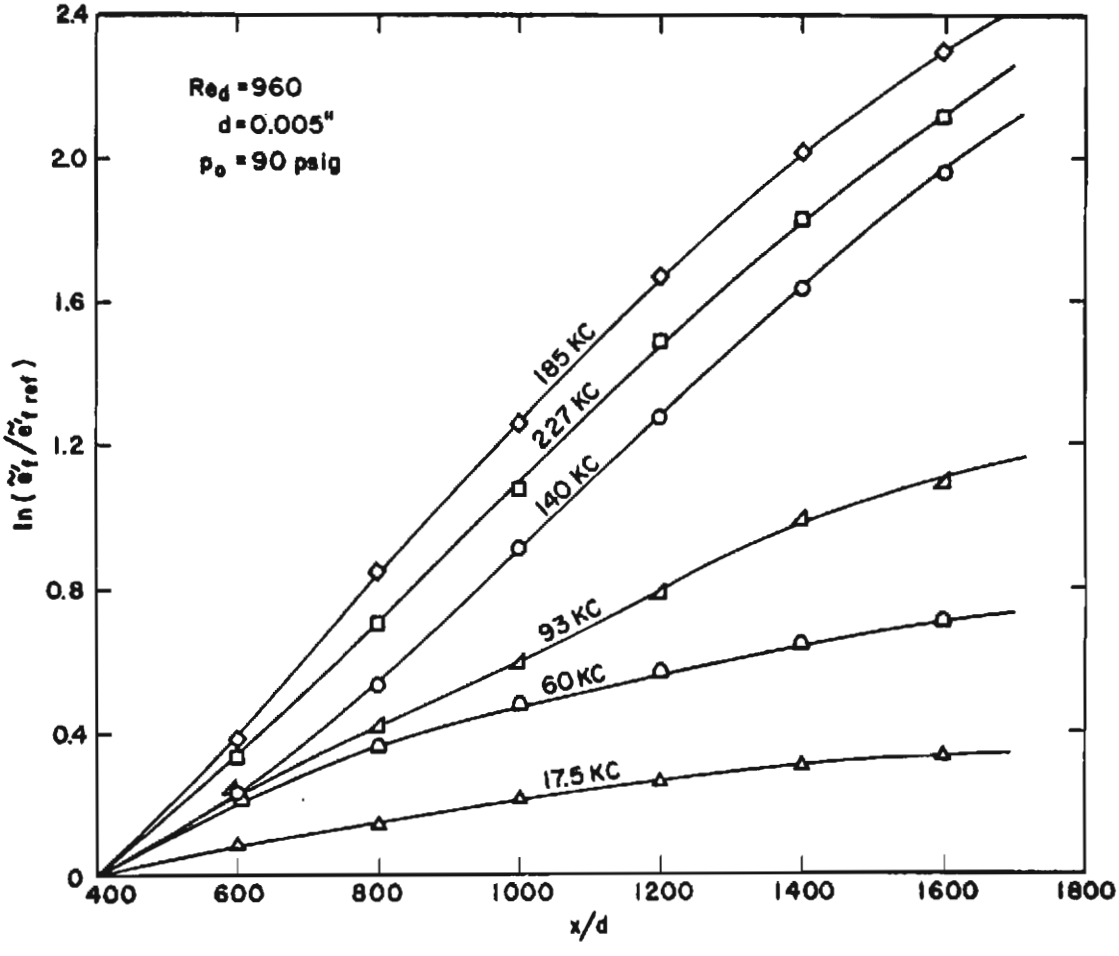

FIG. 15 GROWTH OF FLUCTUATIONS IN THE WAKE

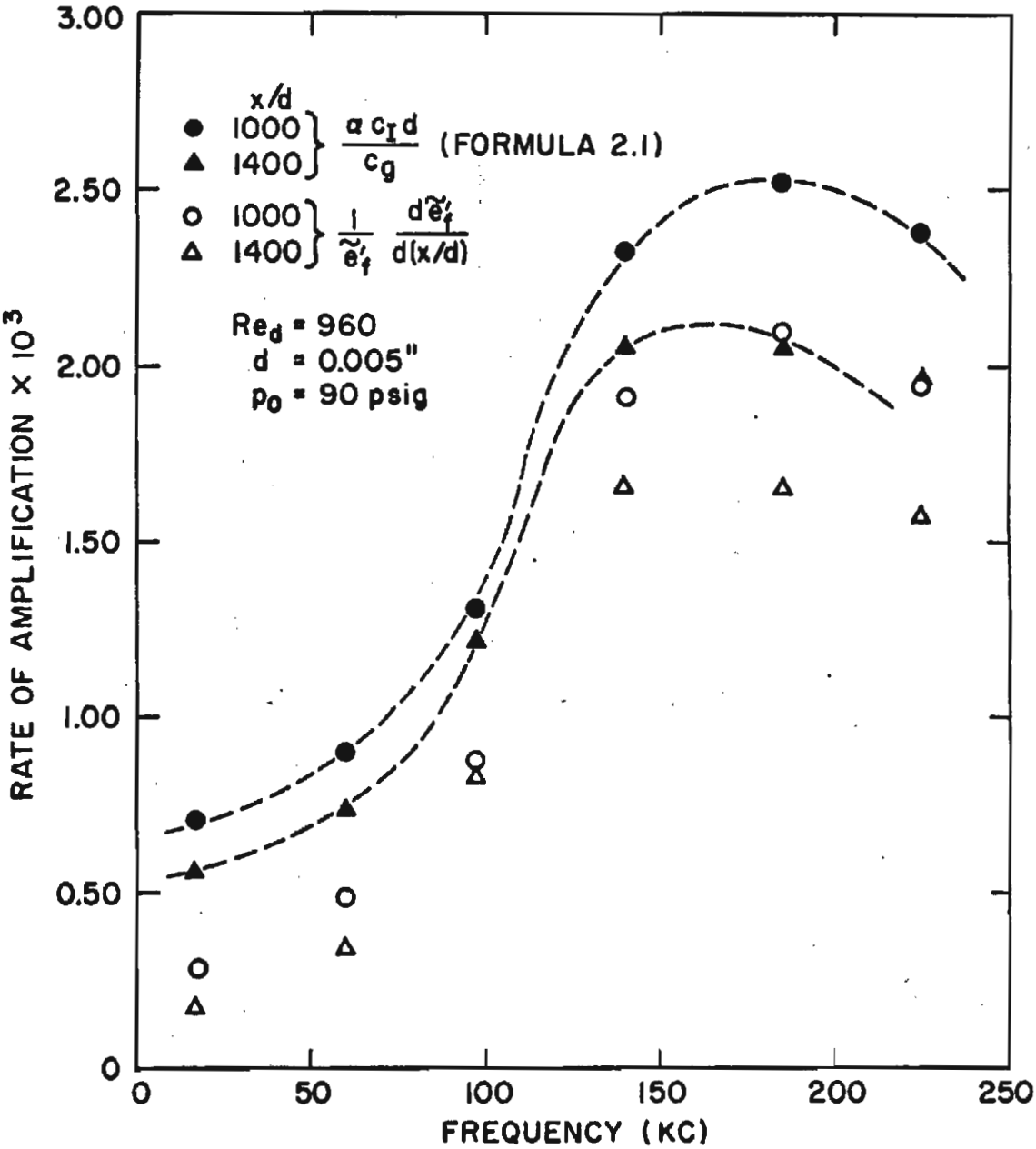

FIG. 16 LOCAL RATES OF AMPLIFICATION OF FLUCTUATIONS

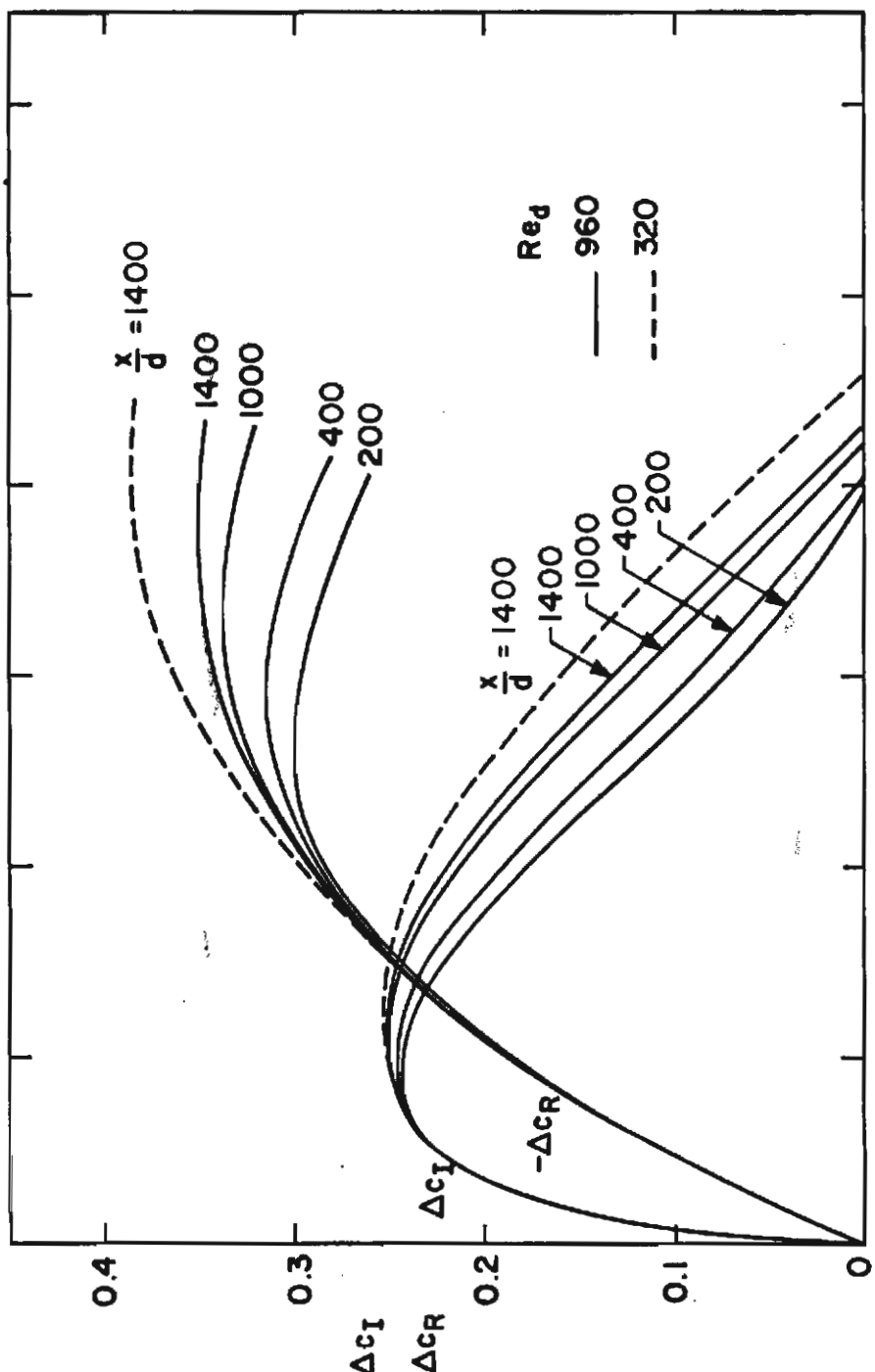

FIG.17 EIGENVALUES OF HYPERSONIC WAKE STABILITY PROBLEM

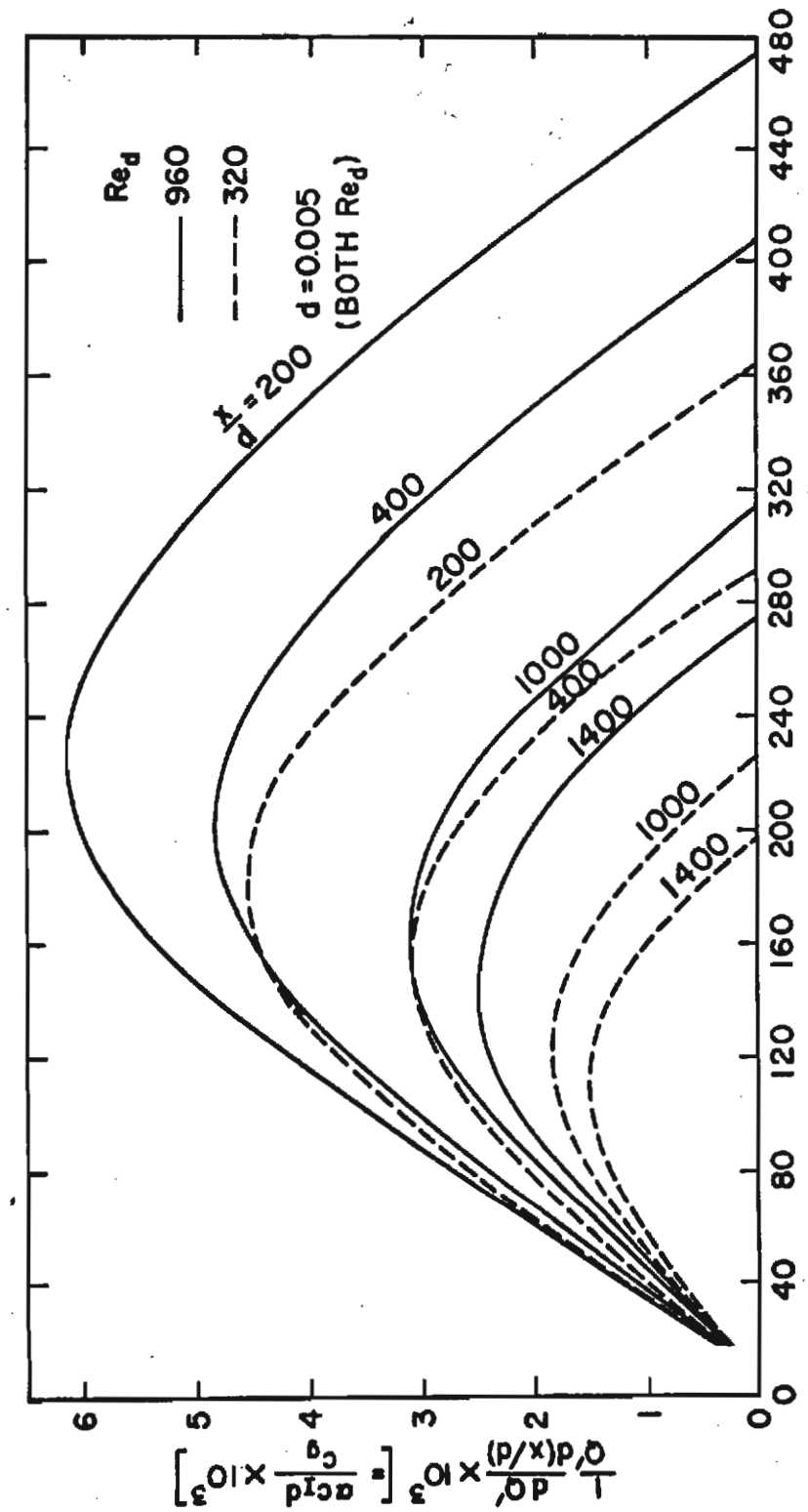

FIG. 18 RATE OF AMPLIFICATION AT SEVERAL STATIONS IN THE WAKE AS FUNCTION OF THE FREQUENCY

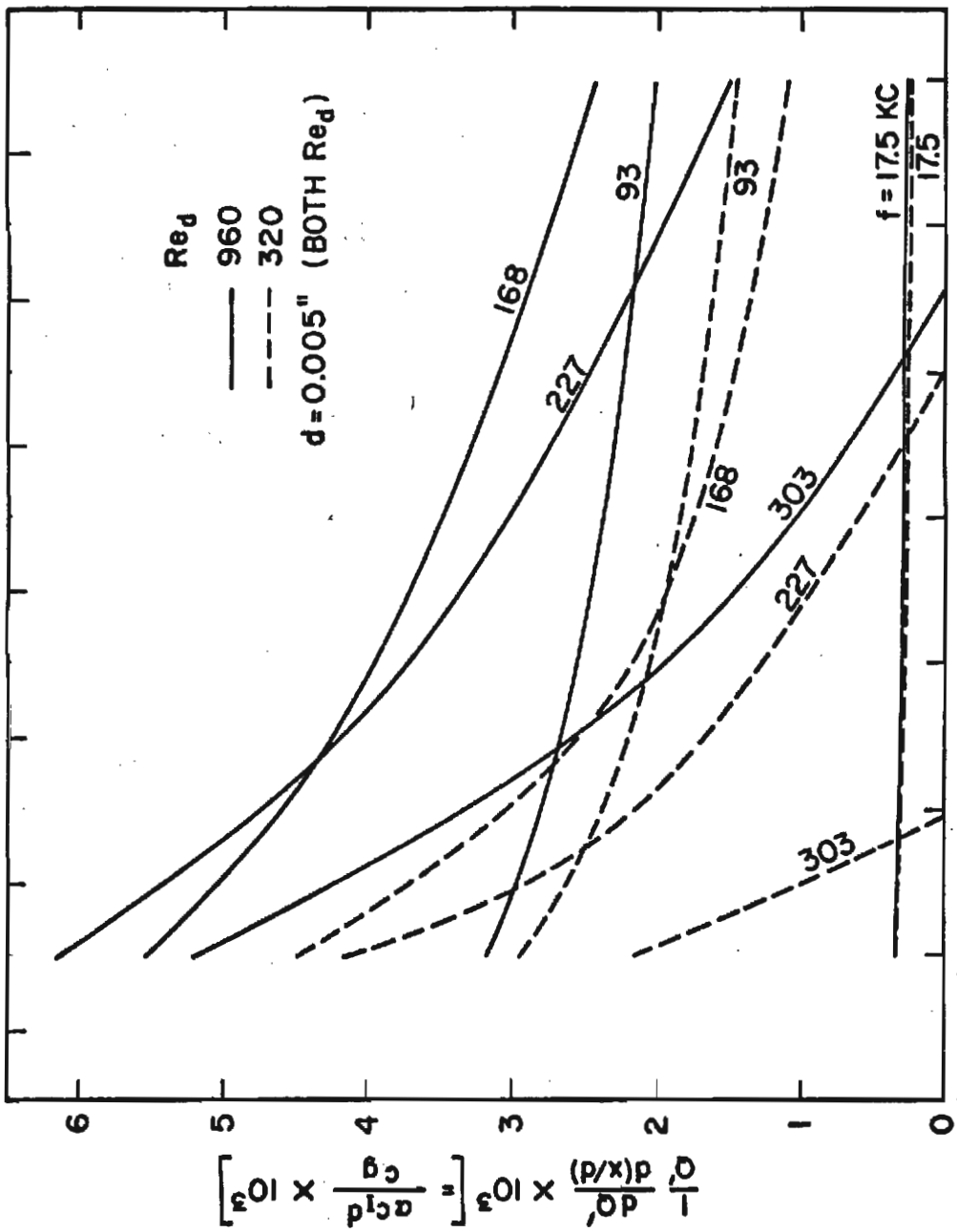

FIG. 19 RATE OF AMPLIFICATION FOLLOWING A GIVEN FREQUENCY DOWNSTREAM

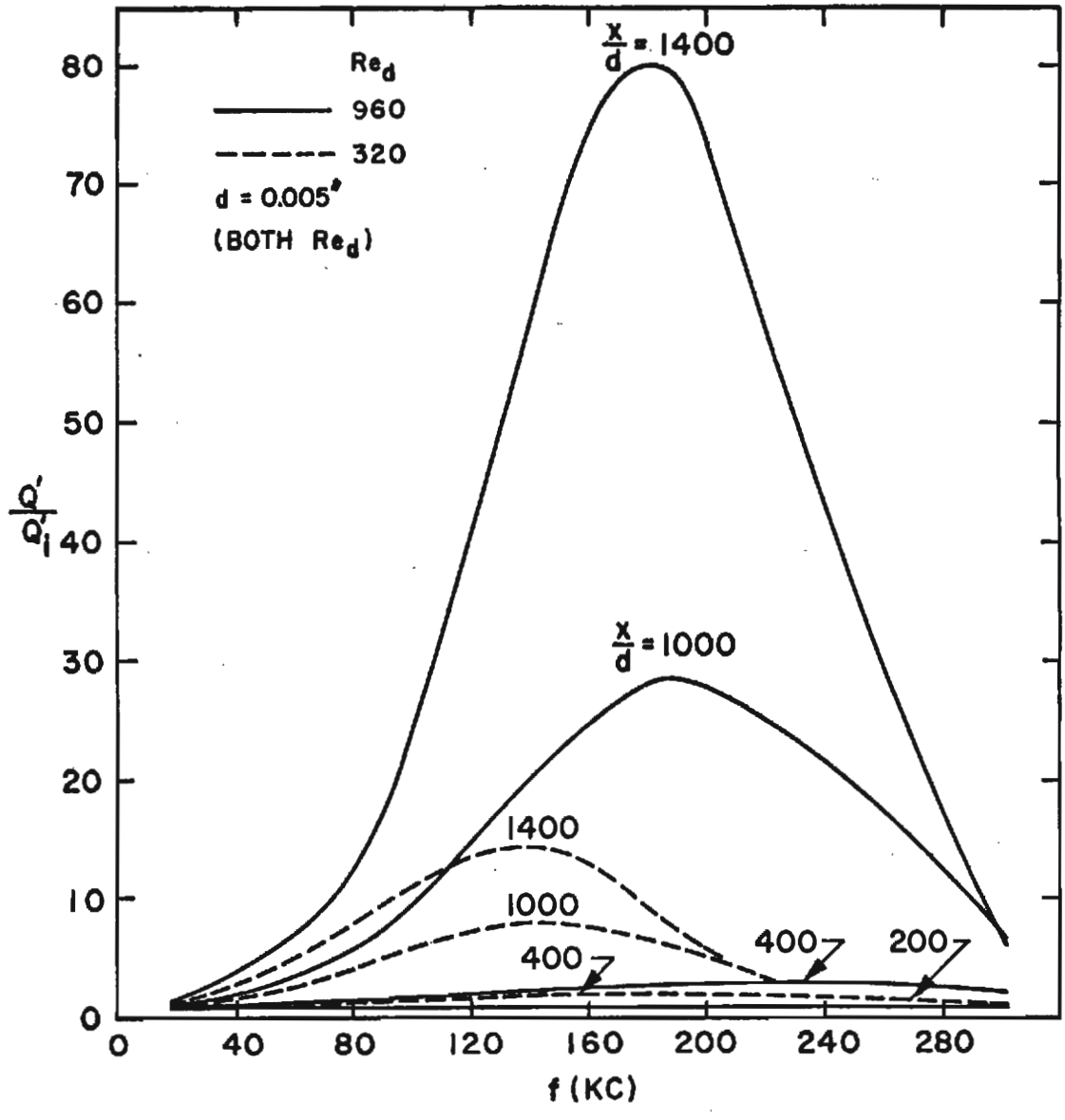

FIG.20 RATIO OF AMPLITUDES OF DISTURBANCE vs. FREQUENCY ($Q'/Q'_i = 1$ AT $x/d = 200$)

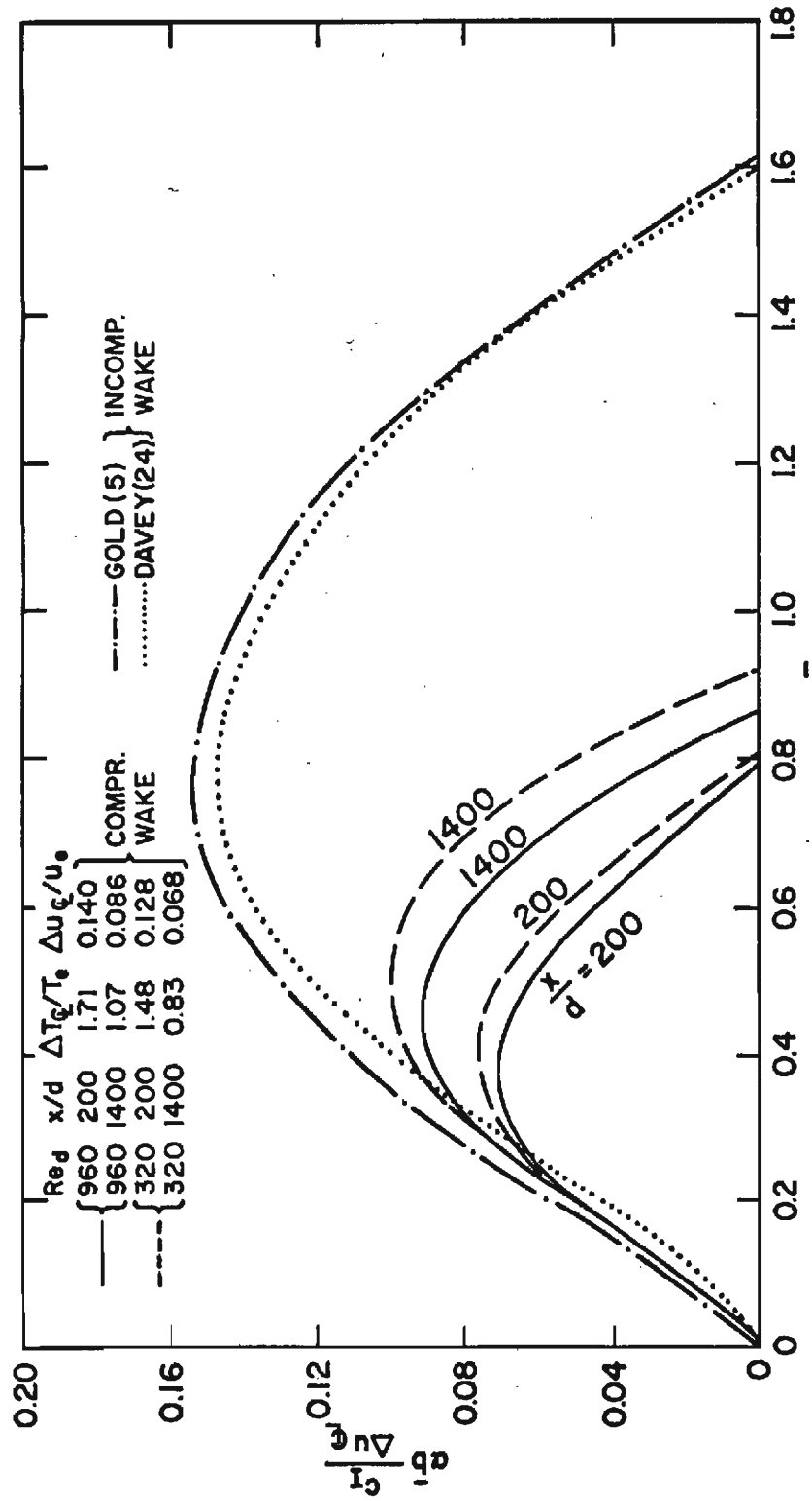

FIG.21 COMPARISON OF RATES OF AMPLIFICATION IN COMPRESSIBLE AND INCOMPRESSIBLE WAKES (NORMALIZED BY TRANSFORMED WAKE WIDTH)

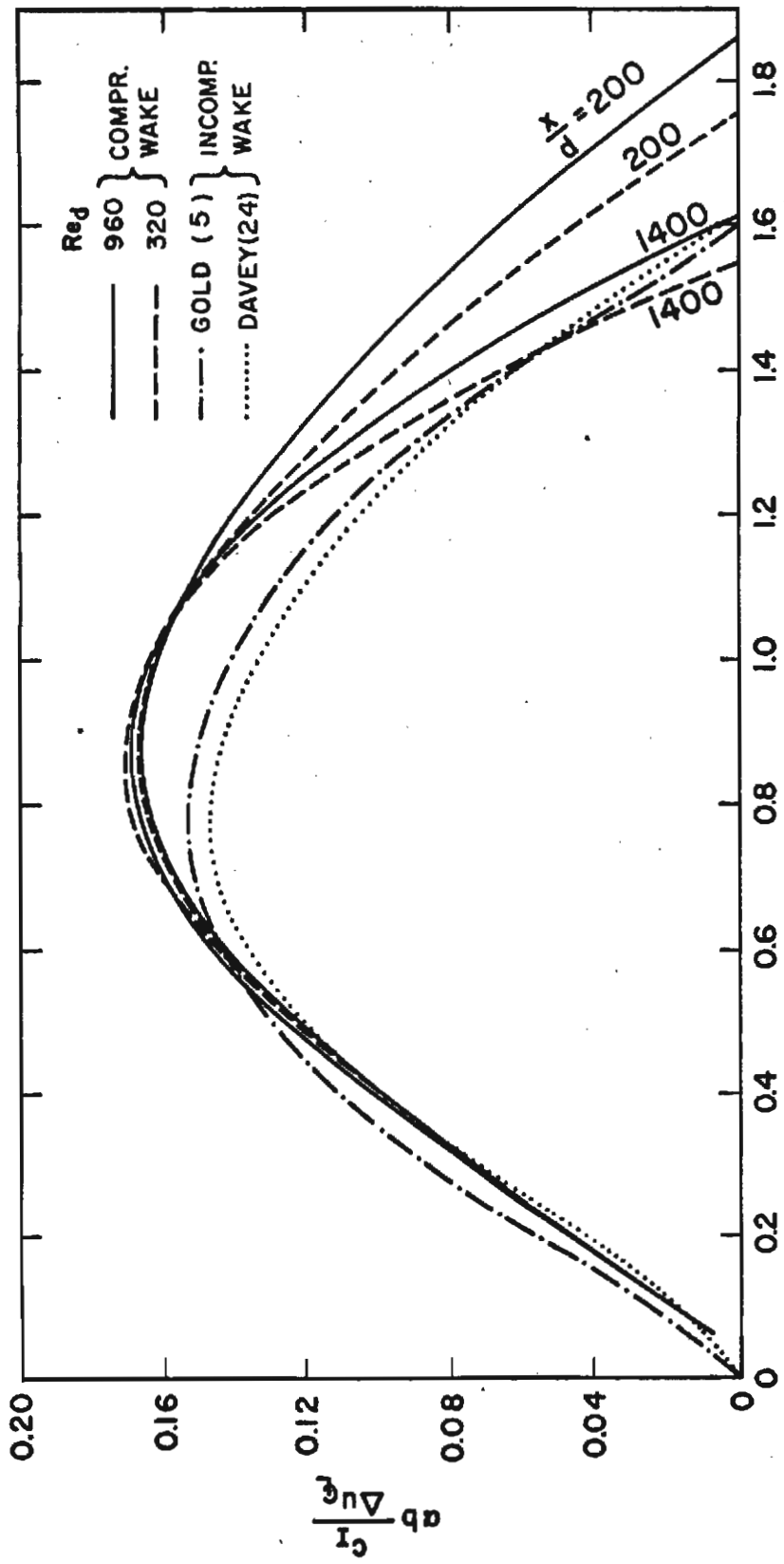

FIG. 22 COMPARISON OF RATES OF AMPLIFICATION IN COMPRESSIBLE AND INCOMPRESSIBLE WAKES (NORMALIZED BY PHYSICAL WAKE WIDTH)

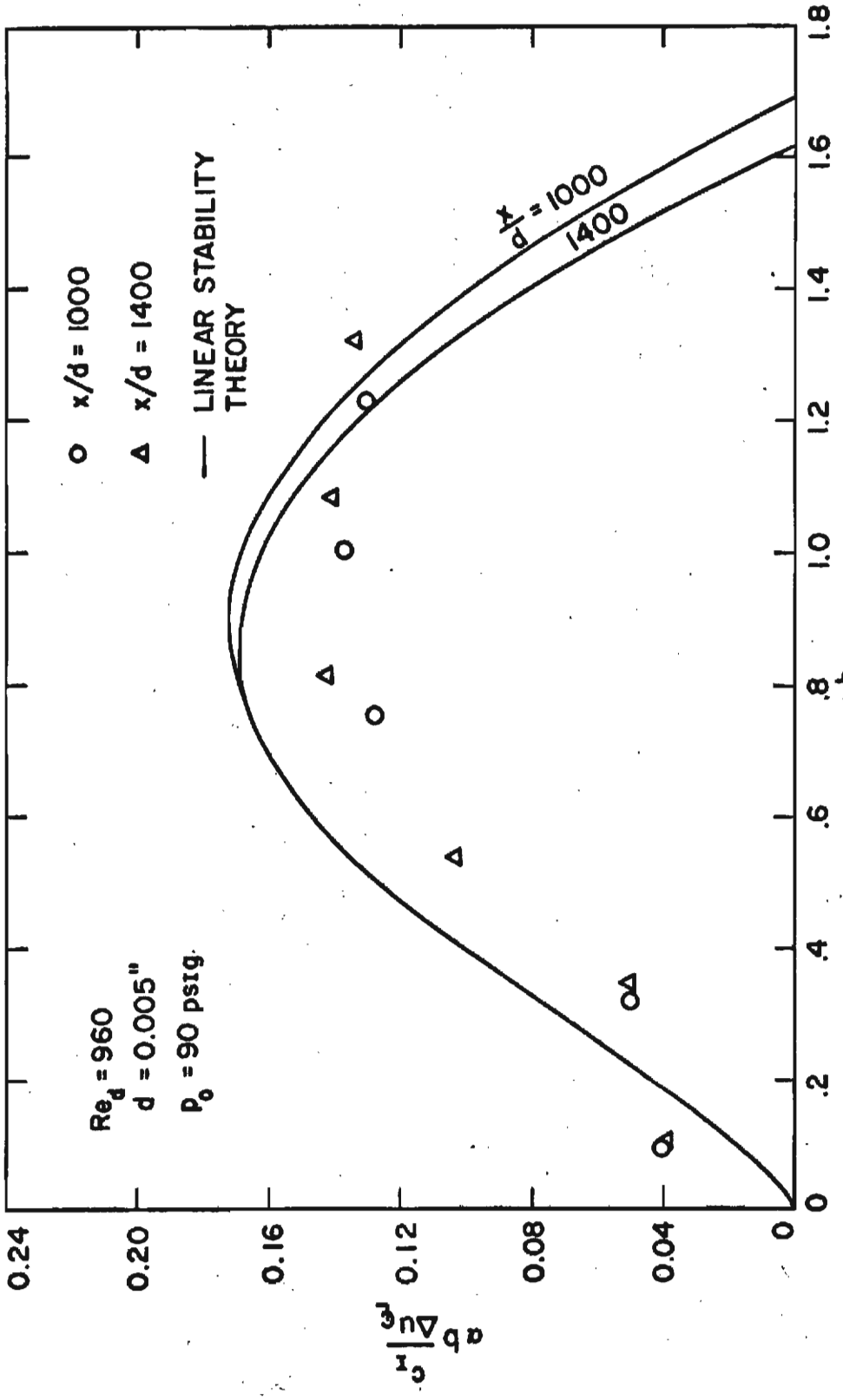

FIG.23 NORMALIZED RATES OF AMPLIFICATION COMPARED WITH LINEAR STABILITY THEORY

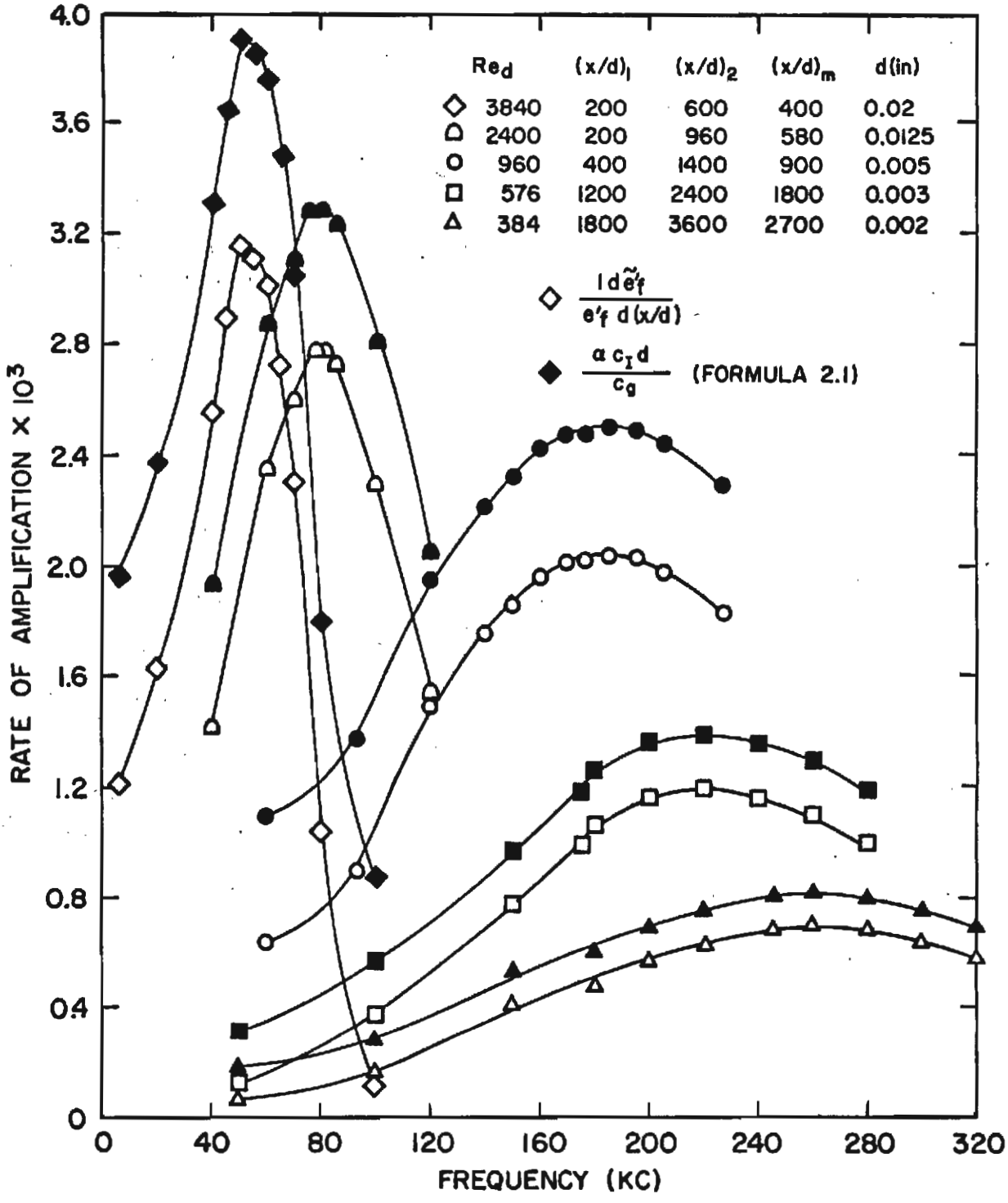

FIG.24 AMPLIFICATION OF FLUCTUATIONS FOR SEVERAL CYLINDER DIAMETERS

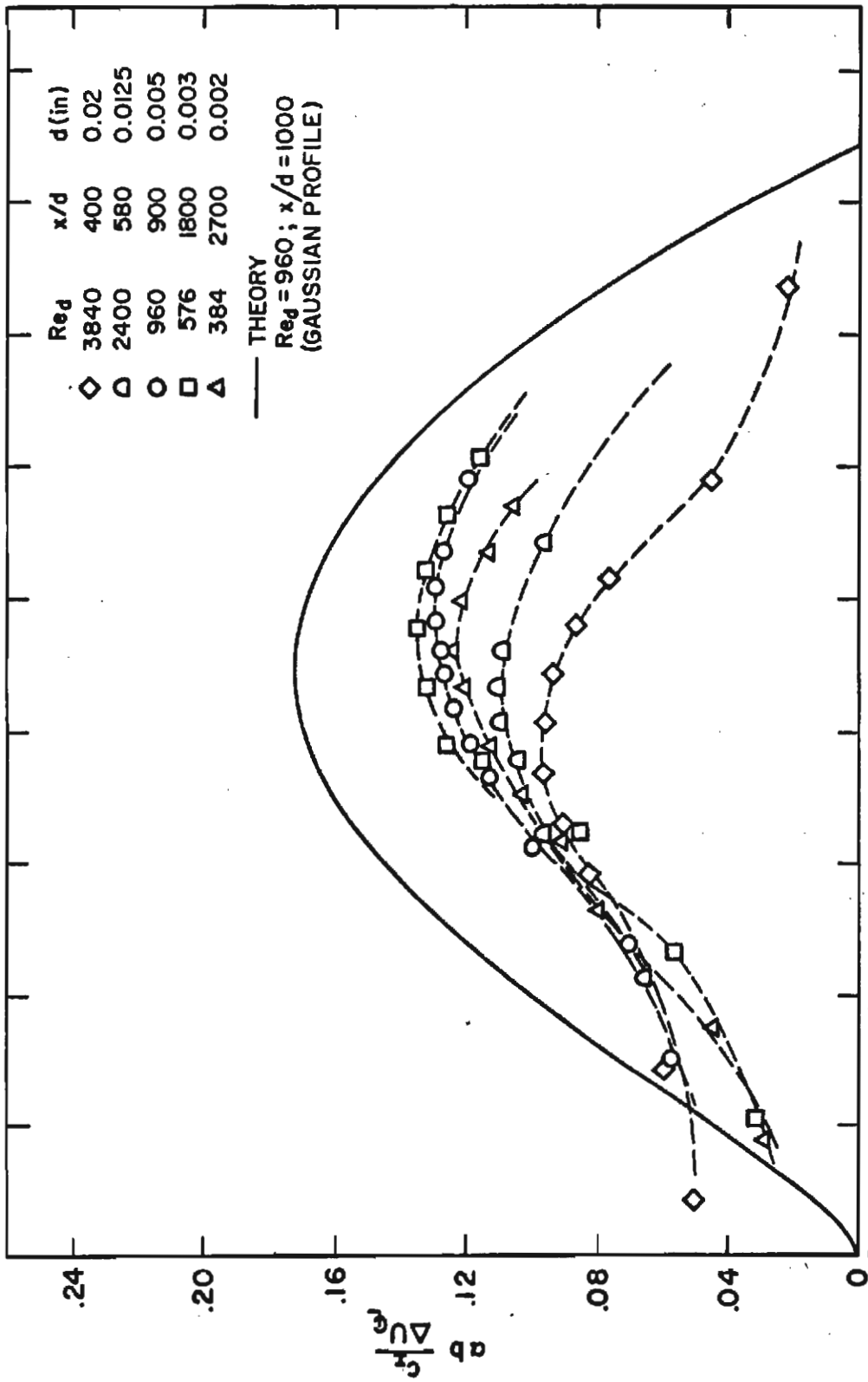

FIG.25 NORMALIZED RATES OF AMPLIFICATION AT SEVERAL REYNOLDS NUMBERS IN COMPARISON WITH THEORY

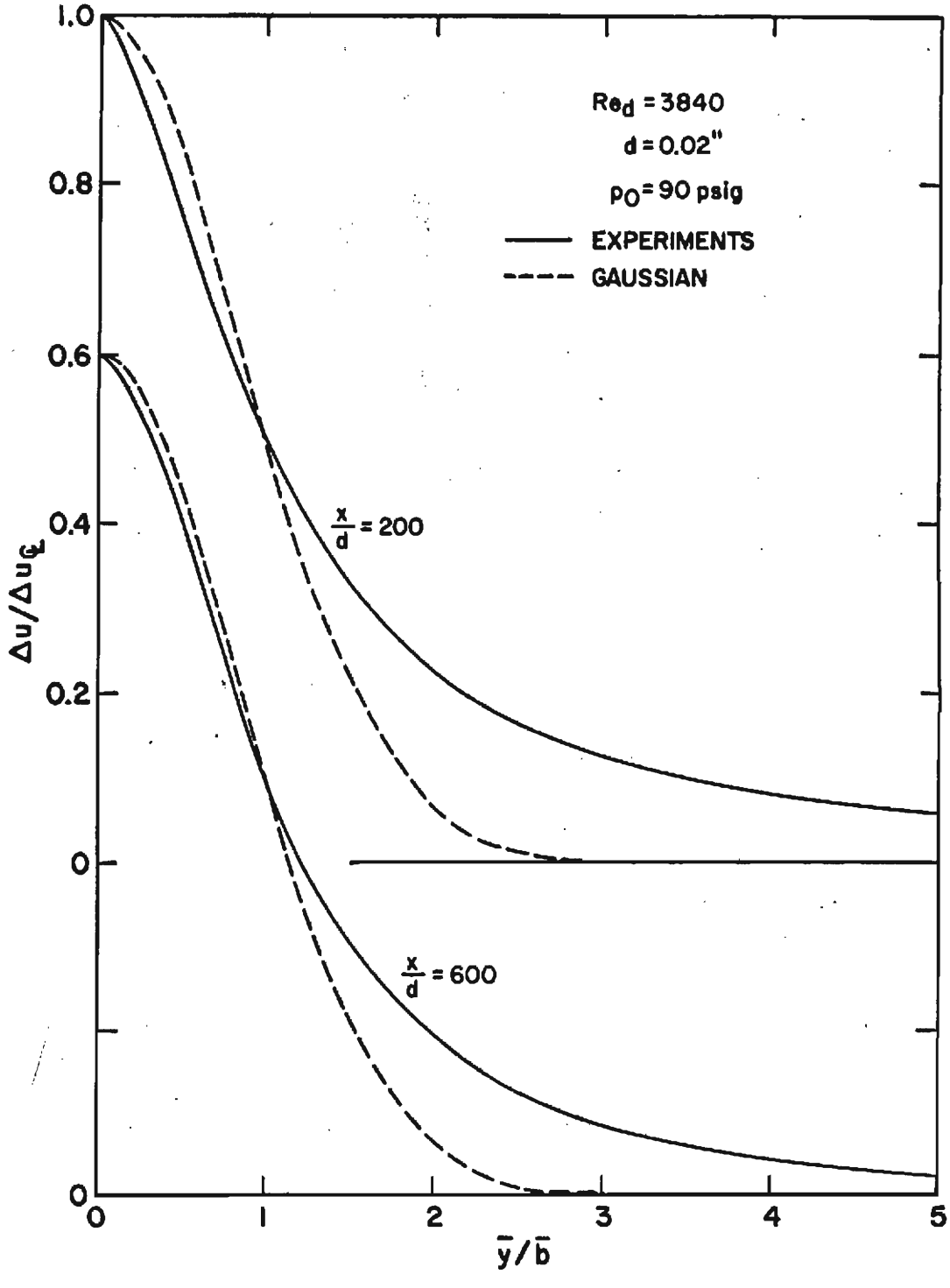

FIG.26 COMPARISON OF MEASURED WAKE PROFILES WITH A GAUSSIAN IN HOWARTH-DORODNITSYN COORDINATES

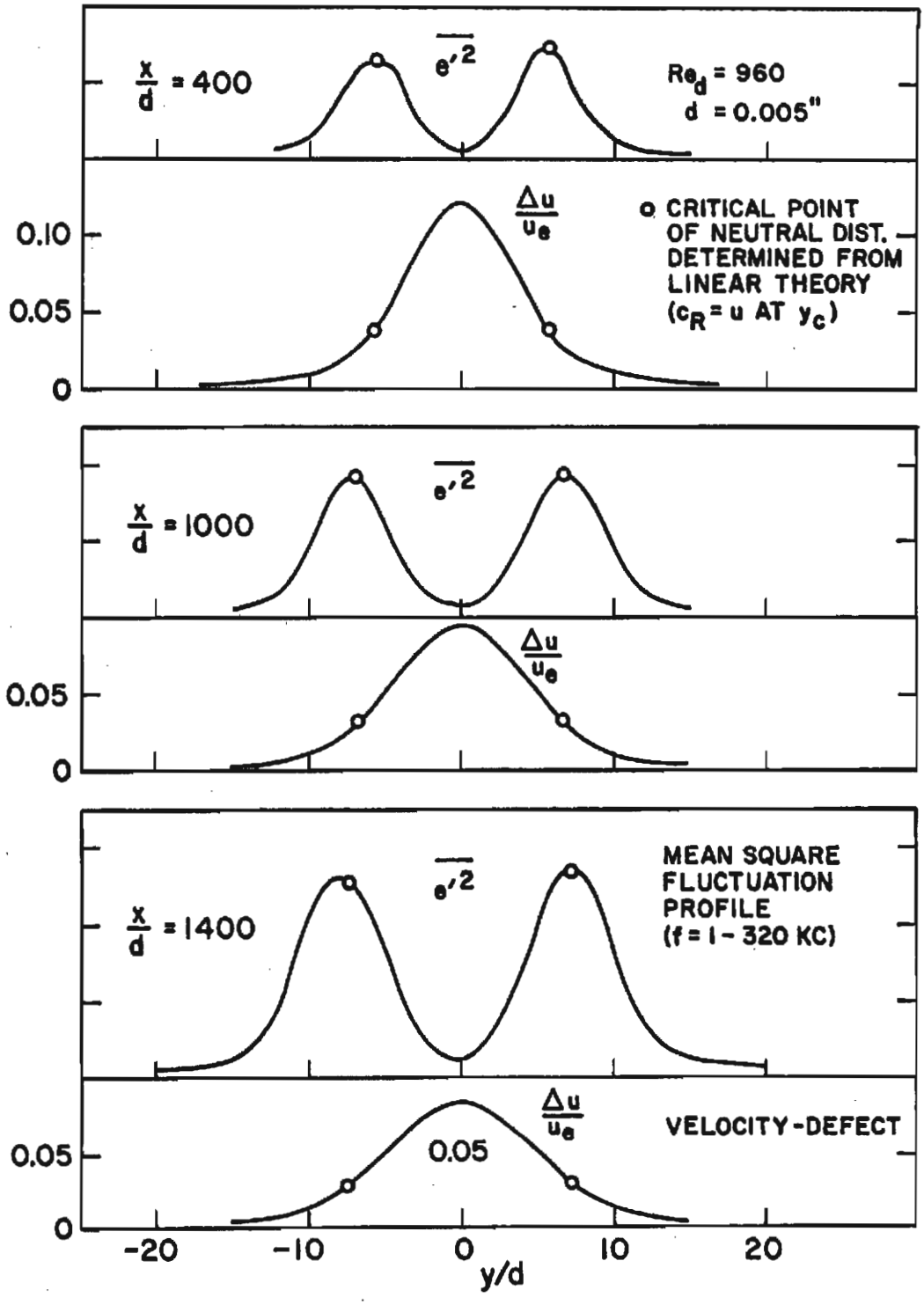

FIG.27 LOCATION OF CRITICAL POINT

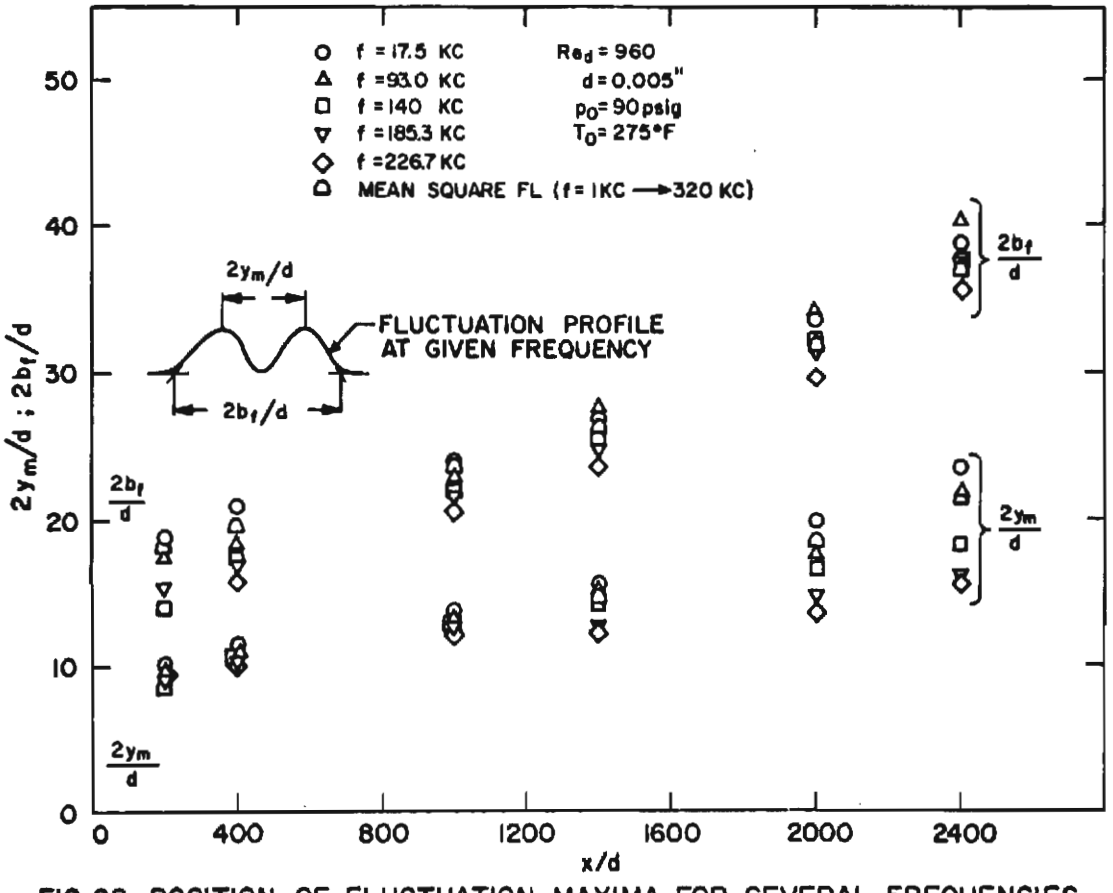

FIG. 28 POSITION OF FLUCTUATION MAXIMA FOR SEVERAL FREQUENCIES AND WIDTH OF FLUCTUATION PROFILES

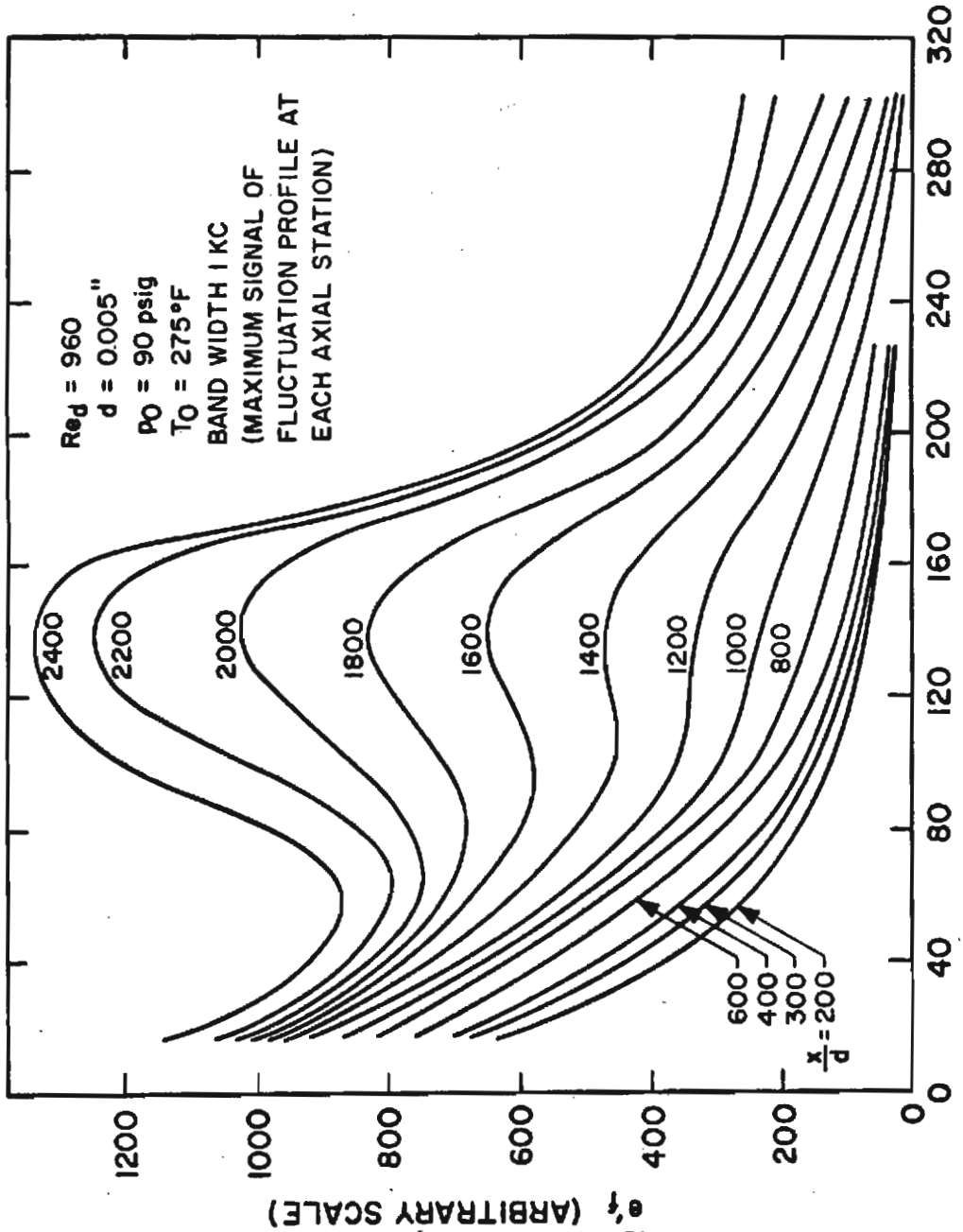

FIG.29a MAXIMUM FLUCTUATION AMPLITUDES AT SEVERAL AXIAL DISTANCES

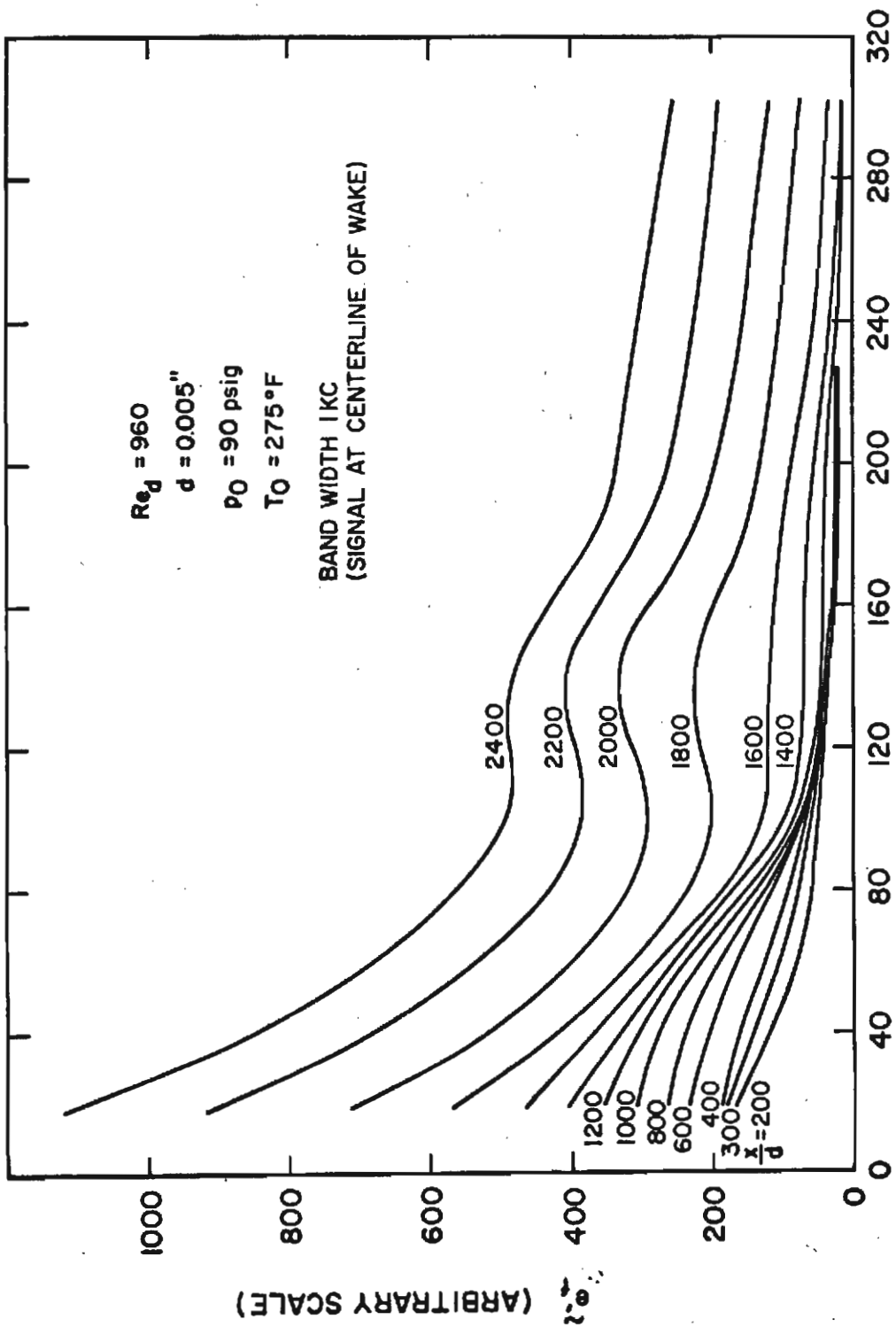

FIG.29b FLUCTUATION AMPLITUDES AT CENTERLINE OF WAKE

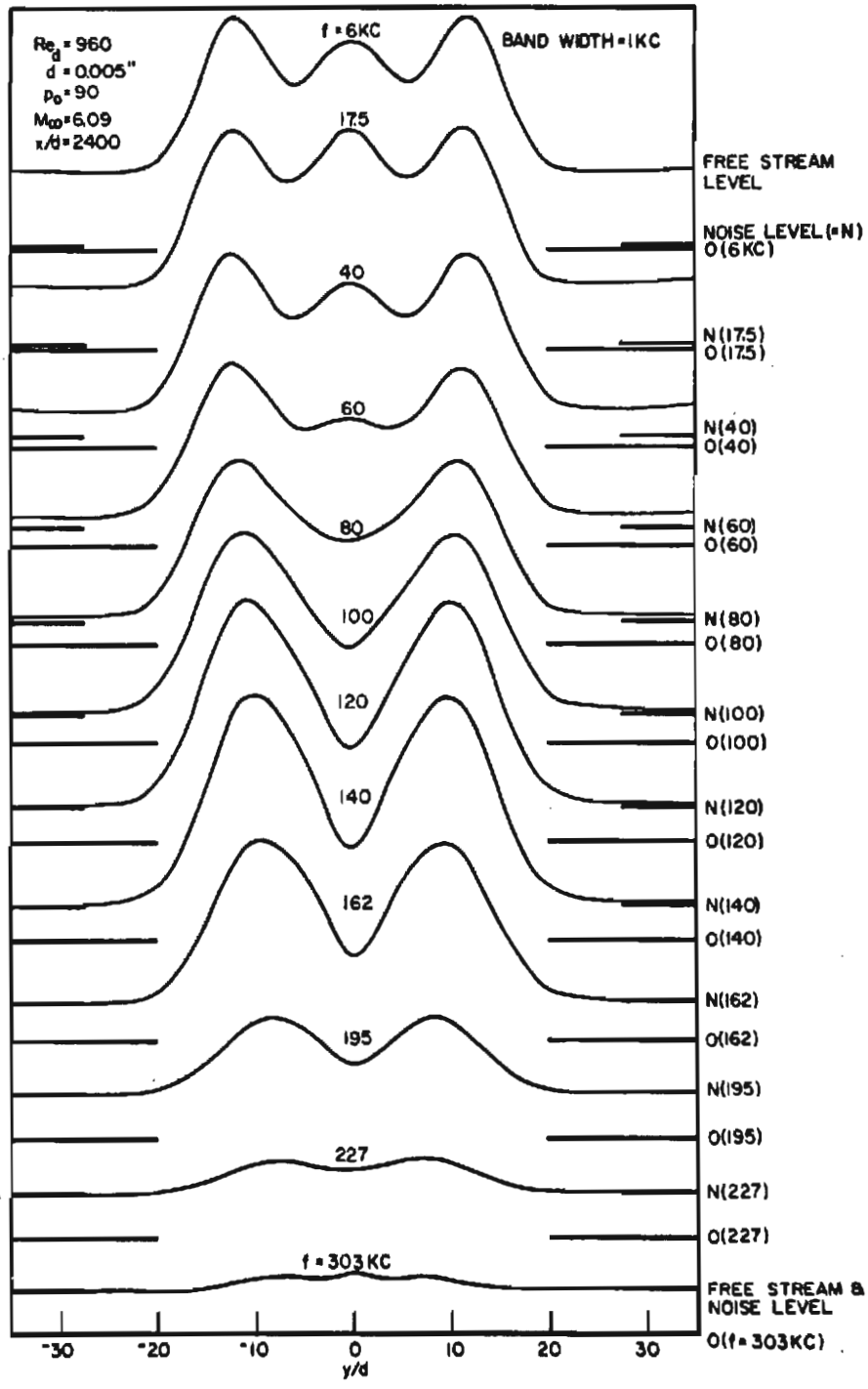

FIG.30 HOT WIRE RMS FLUCTUATIONS IN THE WAKE OF A CYLINDER AT x/d = 2400

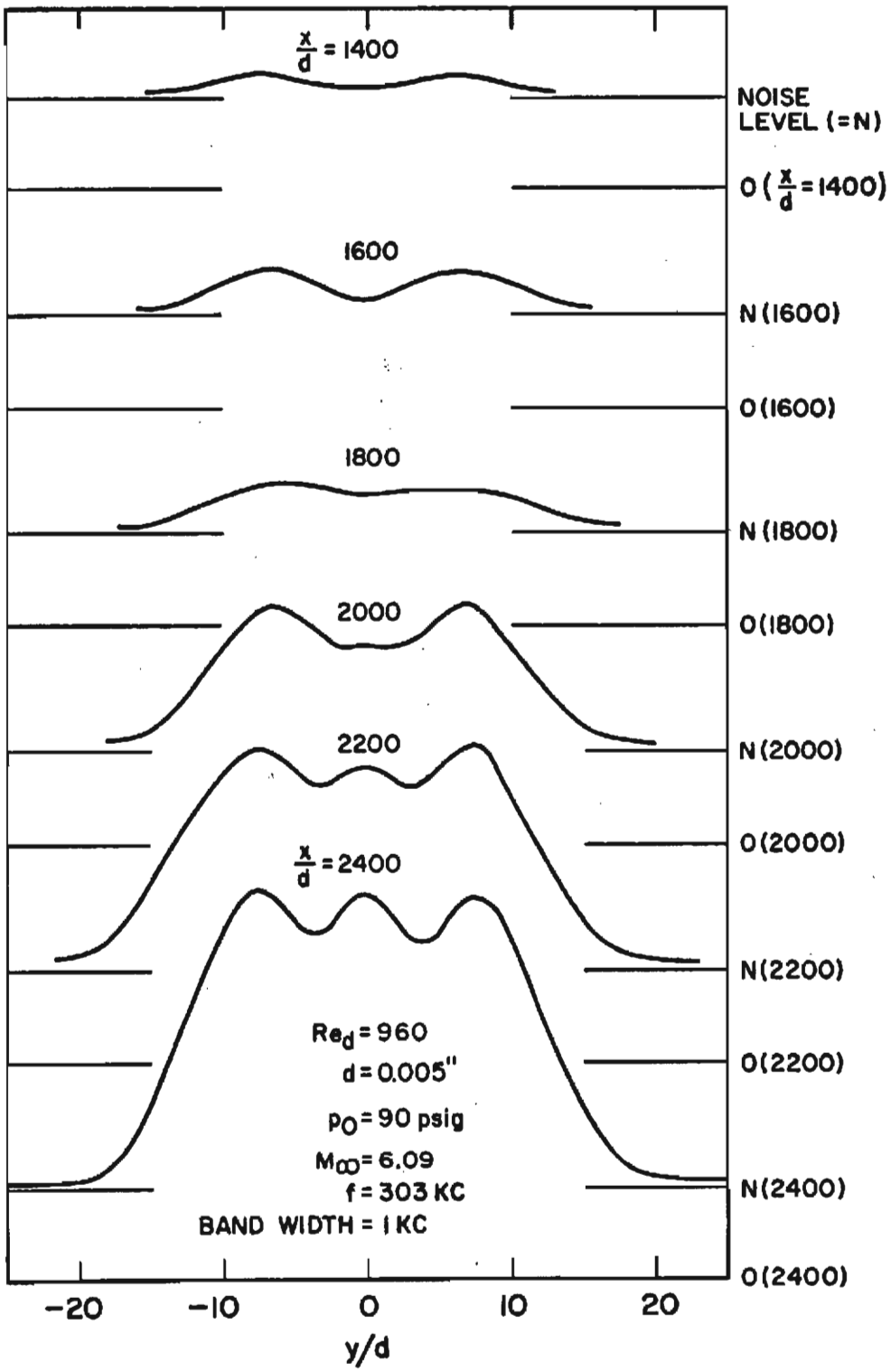

FIG. 31 INCREASE IN THE HOTWIRE RMS SIGNAL AT THE FIRST HARMONIC FREQUENCY

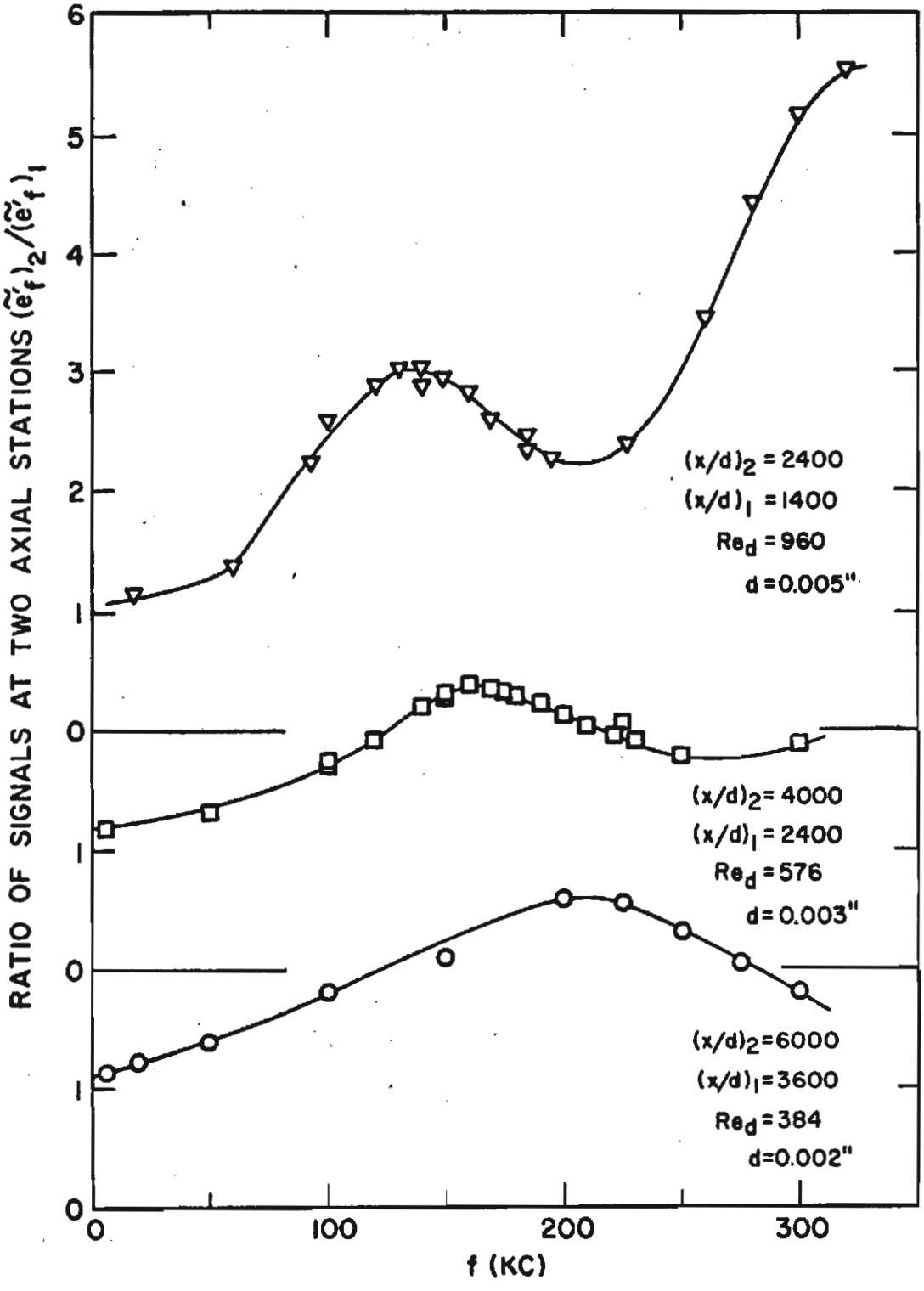

FIG. 32 RATIO OF AMPLITUDES OF FLUCTUATION IN THE NONLINEAR REGION

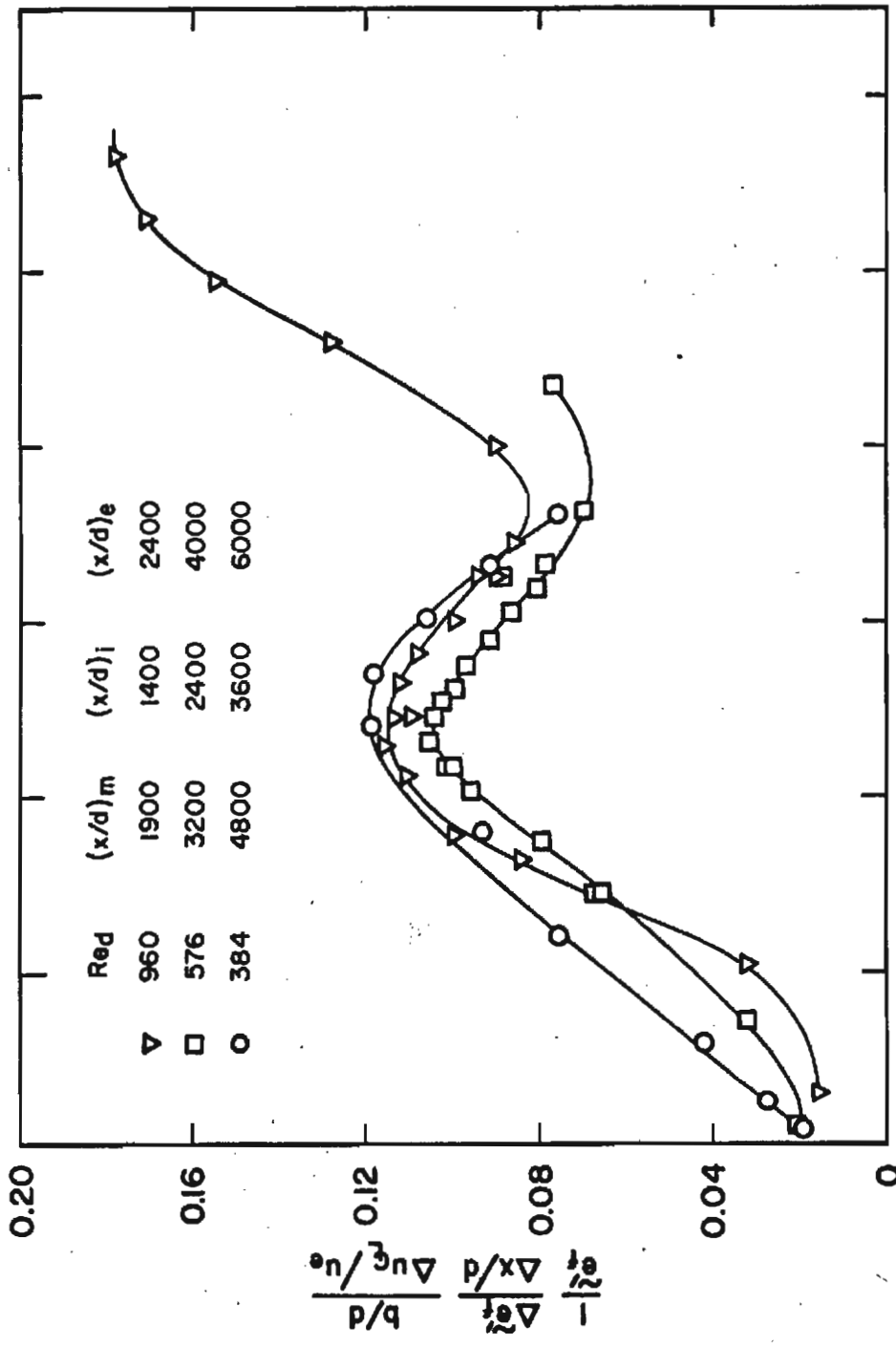

FIG.33 RATE OF AMPLIFICATION IN THE NONLINEAR REGION

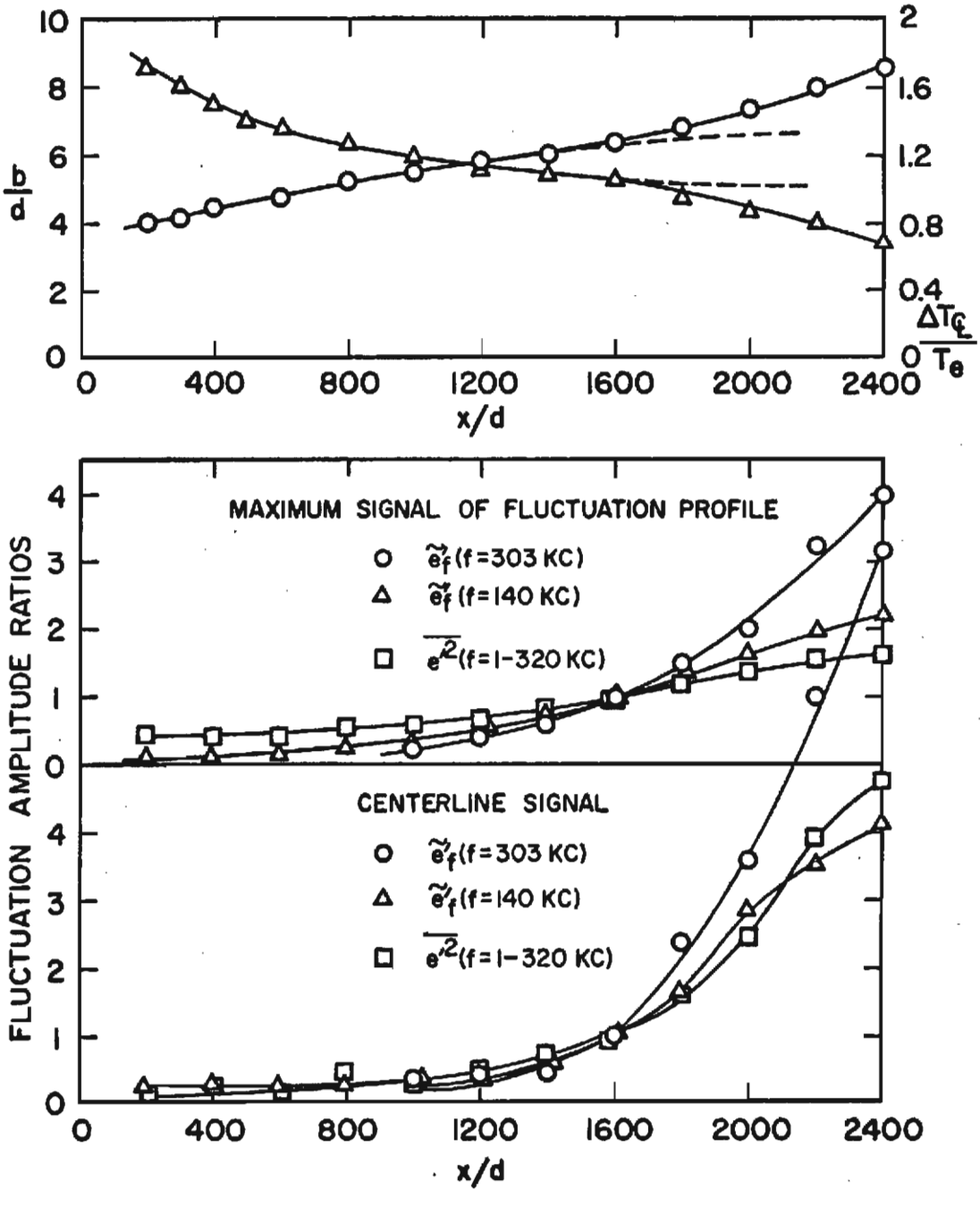

FIG.34 INDICATIONS OF NONLINEARITIES

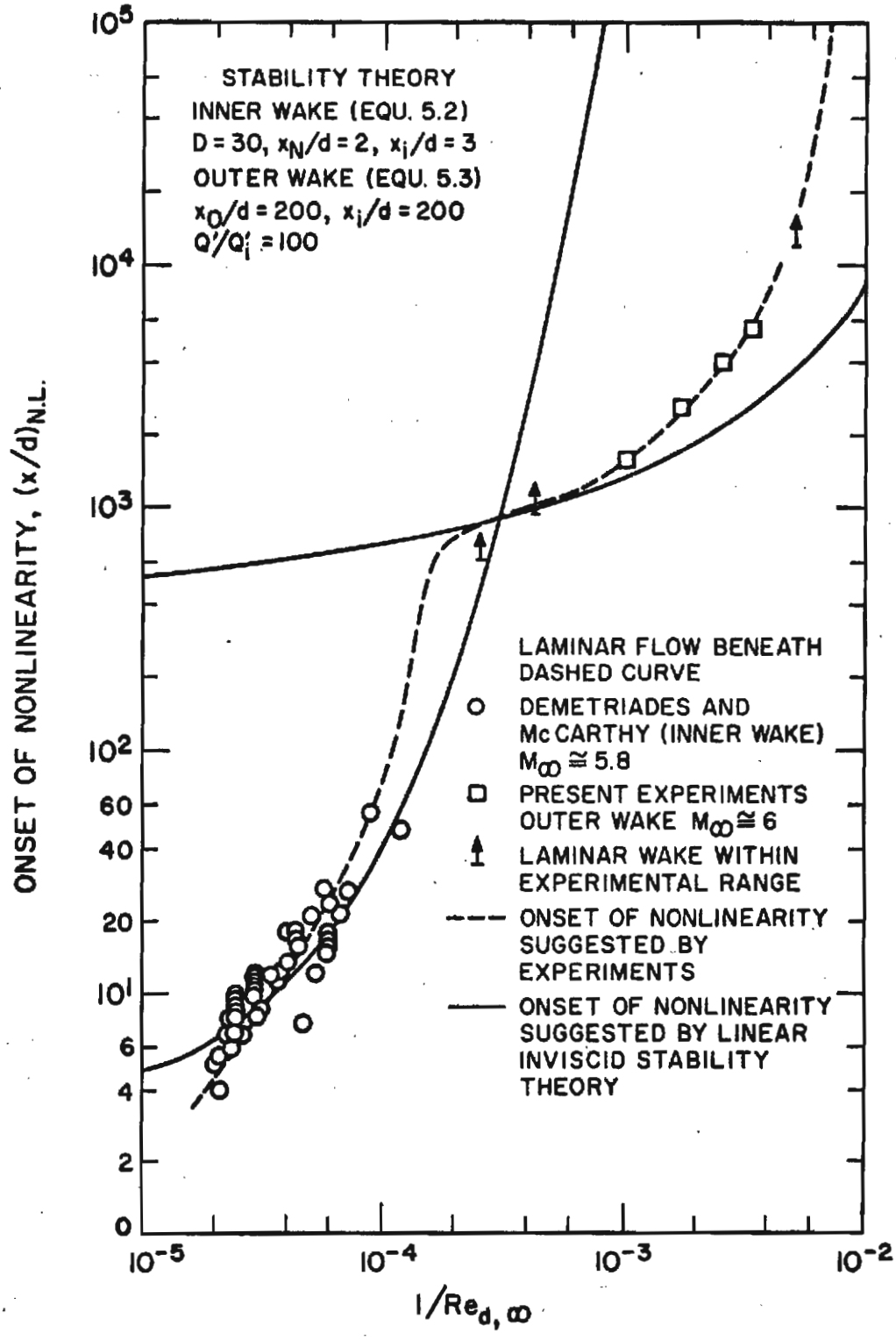

FIG. 35 ONSET OF NONLINEAR EFFECTS IN HYPERSONIC WAKES BEHIND CYLINDERS ($M_\infty \cong 6$)